REPORT NO.
UCB/EERC-97/07
JULY 1997

EARTHQUAKE ENGINEERING RESEARCH CENTER

PB99-107484

ANALYSIS OF THE NONLINEAR RESPONSE OF STRUCTURES SUPPORTED ON PILE FOUNDATIONS

by

DEEPAK BADONI
NICOS MAKRIS

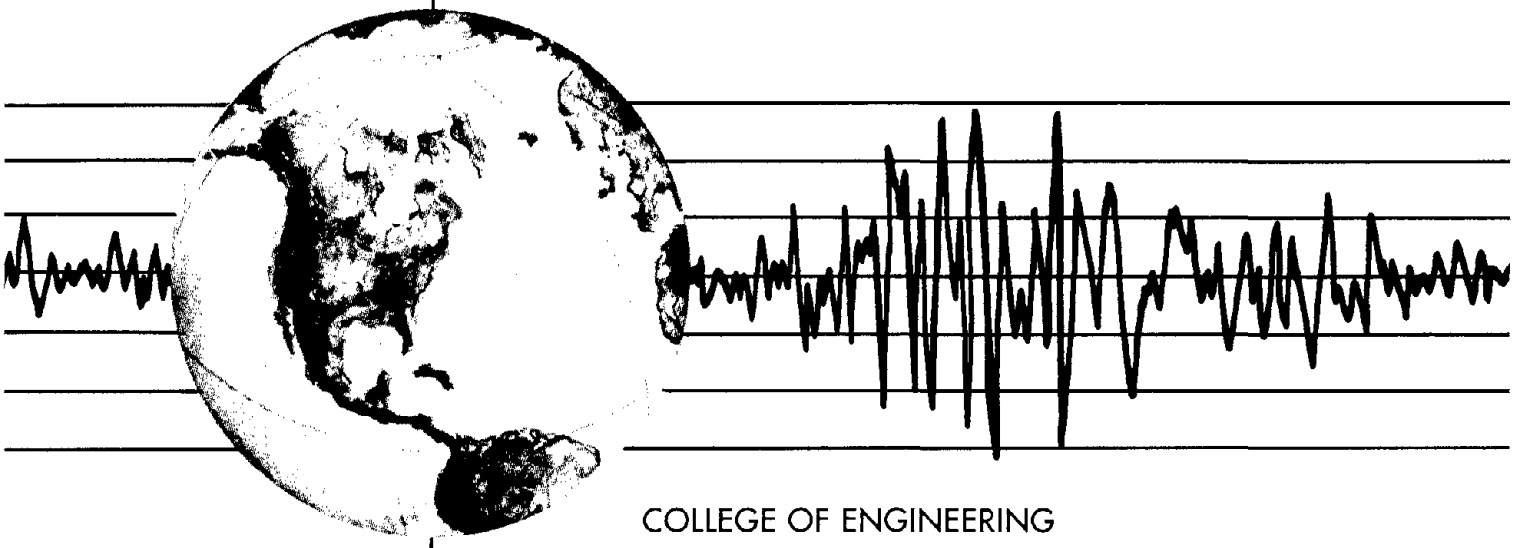

COLLEGE OF ENGINEERING

UNIVERSITY OF CALIFORNIA AT BERKELEY

For sale by the National Technical Information Service, U.S. Department of Commerce, Springfield, Virginia 22161

See back of report for up to date listing of EERC reports.

ANALYSIS OF THE NONLINEAR RESPONSE OF STRUCTURES SUPPORTED ON PILE FOUNDATIONS

by

Deepak Badoni

Nicos Makris

Report No. UCB/EERC-97/07
Earthquake Engineering Research Center
College of Engineering
University of California at Berkeley

July 1997

ANALYSIS OF THE NONLINEAR RESPONSE OF STRUCTURES SUPPORTED ON PILE FOUNDATIONS

by

Deepak Badoni[1] and Nicos Makris[2]

ABSTRACT

In this research, the problem of nonlinear pile foundation-superstructure interaction is addressed by adopting a substructure approach and developing appropriate time-domain methodologies for the analysis of each subsystem, as well as procedures to analyze the global system response. The need for nonlinear modeling and the importance of foundation dynamics to overall system response is established first by studying the response of the Painter Street bridge excited by the Petrolia Earthquake of 1994. Subsequently, the problem of a yielding superstructure on a linear foundation is studied. The superstructure is modeled by a two degree-of-freedom system that involves a Bouc-Wen model to simulate nonlinear behavior. Two different solution methods are developed to obtain the system response. The first method models the restoring force from the foundation by means of a convolution of the velocity history of the pile-cap relative motion and the dynamic relaxation stiffness of the pile foundation, while the second utilizes a state-space representation. Both methods are validated at the linear limit by comparing time with frequency domain analyses.

A time-domain procedure is then presented to compute nonlinear axial dynamic response of pile groups under inertial loading using a nonlinear winkler foundation model for the soil-pile interface and utilizing linear wave propagation theory to compute pile-to-pile interaction. The model is calibrated using two sets of field data obtained for single piles and is subsequently used to provide equivalent linear stiffnesses and damping for pile-groups. It is found that there is a significant deviation from linear behavior for single piles and pile-groups at high load amplitudes. The effect of pile yielding on overall system behavior is studied with the help of a new model which incorporates a bilinear hysteretic moment curvature relationship for the pile cross-section into a nonlinear soil-pile interaction model for lateral motion. This one-dimensional finite element model is shown to be a promising tool in analyzing foundation-structure interaction under earthquake strong motion, especially for drilled shaft foundations.

---

[1] Engineer, Impact Forecasting, L.L.C, 230 W. Monroe St., Chicago, IL 60606. Formerly, Graduate Research Assistant, Department of Civil Engineering and Geological Sciences, University of Notre Dame, Notre Dame, IN 46556.

[2] Assistant Professor, Civil and Environmental Engineering, University of California, Berkeley, CA 94720.

TABLE OF CONTENTS

LIST OF FIGURES

ACKNOWLEDGEMENTS

This report is based on the Ph. D. dissertation submitted by Deepak Badoni to the Graduate School of the University of Notre Dame. Financial support for this research was provided by the National Science Foundation, Grant No. BCS 9300827 and Shimizu Corporation, Japan, with Grant No. NCEER/RF 150-7014A to NCEER and Grant No. ND 42550 to the University of Notre Dame.

CHAPTER 1

INTRODUCTION

Pile foundations are widely used for both inland and offshore structures, especially under adverse soil conditions. Of particular interest is the case of bridges which are structurally simple, yet highly response-sensitive to soil-structure interaction effects. The structural simplicity also implies increased sensitivity to design flaws making it critical to have accurate structural analysis tools. In most cases, the center bents and end abutments of such elevated structures are supported either on pile groups or on a single pile-column. The seismic performance of these structural systems has been the subject of considerable attention in recent years, particularly after the numerous failures of pile-supported bridges during the 1994 Northridge earthquake in California (Moehle 1994, Housner 1995), and, more recently, after the Hyogo-Ken Nanbu earthquake in Kobe, Japan, which devastated the transportation network in the city causing considerable economic losses to add to the severe human costs. The literature is also rich in the documentation of pile distress and failure during earthquakes. Mizuno (1987) has reported 28 cases involving seismic pile failure in Japan, CNEL-ENEL (1976) documents pile rupture under two bridges during the 1976 Fruili, Italy earthquake and Ross *et al.* (1969) describe numerous failures of piles supporting bridges in the 1964 Alaska earthquake. Therefore, there is a considerable need to improve the state-of-the-practice in the seismic response analysis and design of pile-supported bridges.

1.1 Background

In the last two decades several researchers have developed numerical and analytical methods to analyze the response of pile foundations accounting for pile-soil-pile interaction. A recent comprehensive review on the subject has been presented by Novak (1991). This pile-to-pile interaction is frequency-dependent, resulting from waves that are emitted from the periphery of each pile and propagate to "strike" the neighboring piles. At the same time, the software for structural analysis has been considerably developed and expanded so that complex structures with sophisticated behavior can be rigorously analyzed. Despite these advances, very little is known about the significance of pile-foundation-superstructure interaction, even for important structures like bridges. For instance, the sweeping assumption of the pile foundation behaving as a fixed monolithic support is still widely used. Among possible reasons for the lack of established procedures in analyzing these structures is that most research results published on the dynamic response of pile foundations are scattered and presented in a form that is of little use to the structural engineer. Also, some of the most reliable methods to analyze the response of pile foundations rely on proprietary computer codes which cannot be easily incorporated into existing analysis methodologies.

Figure 1.1 illustrates the basic problem at hand. Clearly, a holistic analysis of the entire system involving discretization of the superstructure, piles and surrounding soil is highly computationally intensive. Hence the popularity of the substructure approach to solve this problem. According to this approach, which assumes linear soil-foundation-superstructure response, the system analysis under seismic excitation can be performed in three consecutive steps: (1) obtain the motion of the foundation in the absence of the superstructure the so-called "foundation input motion", which includes translational as well as rotational components; (2) determine the dynamic impedances ("springs" and

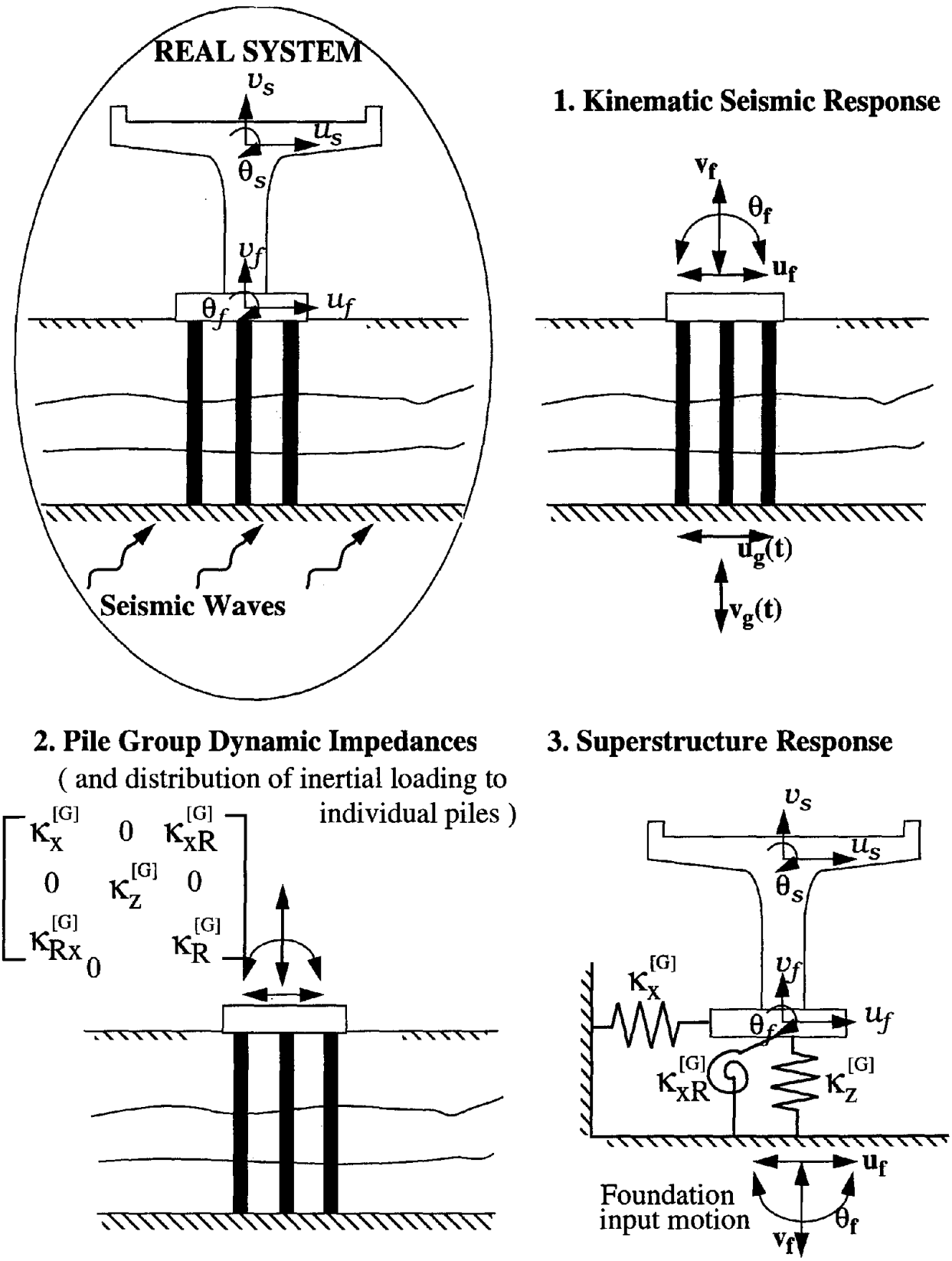

Figure 1.1: Schematic of 3-step procedure used to solve the soil-pile-superstructure interaction problem.

"dashpots") associated with swaying, rocking and cross-swaying-rocking oscillations of the foundation; (3) compute the seismic response of the superstructure supported on the "springs" and "dashpots" of step 2 and subjected at ground base to the "foundation input motion" of step 1.

For the first two steps, several alternative frequency domain formulations have been developed and published in the literature including finite-element (Blaney *et al.* 1976, Gazetas 1984, Kagawa and Kraft 1982, Kaynia and Kausel 1982), boundary-element (Banerjee and Sen 1987, Fan *et al.* 1991, Kaynia 1980, Waas and Hartman 1984, Kaynia and Novak 1992), semi-analytical type methods (Tajimi 1977, Kobori *et al.* 1991, Nogami 1983), and a number of simplified solutions (Dobry and Gazetas 1988, Makris and Gazetas 1992, Makris and Gazetas 1993, Makris and Badoni 1995). With this formulation, step 3 becomes a straightforward dynamics problem.

However, most modern structures, especially bridges, are designed to resist severe loading conditions for which inelastic action is an inherent component of the system response. Hence there is an urgent need to develop soil-structure interaction analysis methods which can account for inelastic behavior. Clearly, the origin of nonlinearity can be in either the superstructure or the foundation depending upon the system properties. Furthermore, foundation nonlinear behavior can originate from the phenomenon of nonlinear soil-pile interaction or yielding of the piles themselves. Presently, most models of pile supported structures used in design practice use single valued linear springs and dashpots, and the influence of soil nonlinearity is incorporated by choosing effective values for modulus of elasticity and frequency independent damping. Investigations of soil-structure interaction effects in the presence of a yielding superstructure are scarce, if they exist at all. It has been contended that yielding is essentially an energy dissipation process, and therefore tends to decrease soil-structure interaction effects, which might be a valid argu-

ment for classical structures. However, with the introduction of isolation and hysteretic energy dissipation devices in bridge superstructures, as well as the increased popularity of retrofit technology, which is inherently dependent on accurate modeling of damaged structural response, it is imperative to incorporate nonlinear models in the analysis of overall system behavior.

The objective of this research is to develop simple yet accurate methodologies to address the issue of nonlinear response analysis of pile-supported structures. To this end, the nonlinear behavior in different components of the system are analyzed separately, and the substructure approach is modified for a nonlinear time-domain analysis. This is also the basis for the organization of the chapters, as is presented in the next section.

1.2 Organization

Chapter 2 provides a background to the overall problem of soil-pile-superstructure interaction as applied to a linear analysis. It serves to illustrate the implementation of the substructure approach to a real problem and establishes the importance of modeling foundation dynamics to overall system response.

Chapter 3 tackles the problem of a nonlinearly behaving superstructure resting on a linear foundation and establishes the convolution integral method as a credible approach to solving the problem while also considering an alternative approach based on a state-space formulation. In both cases, the Bouc-Wen model is utilized to model nonlinear behavior. The versatility of this model in capturing the behavior of a variety of real systems is qualitatively demonstrated.

Chapter 4 describes a novel approach to the time-domain analysis of nonlinear pile-soil-pile interaction using a nonlinear Winkler foundation model for the soil-pile interface in conjunction with a time-domain formulation for the wave attenuation function

that governs pile-to-pile interaction. The model is used to predict dynamic field test data for a single pile, and subsequently to calculate equivalent linear dynamic stiffnesses of pile groups.

In Chapter 5, a nonlinear model for reinforced concrete piles is presented to be used in conjunction with nonlinear soil models so as to account for pile yielding in the analysis of nonlinear soil-pile-structure interaction for lateral quasistatic loading. It is applied to an example of a viaduct resting on a single pile-column, and the influence of pile yielding to the overall system response is studied.

Chapter 6 presents a summary of the proposed nonlinear analysis techniques and a discussion of the important results obtained. Several areas requiring further investigation are identified.

CHAPTER 2

A CASE STUDY OF LINEAR PILE FOUNDATION-SUPERSTRUCTURE INTERACTION

This chapter describes a simple integrated procedure to analyze the problem of linear soil-pile-foundation-superstructure interaction in the seismic response assessment of a bridge. The method employs existing theories for the computation of dynamic impedances and kinematic-seismic-response factors for pile foundations. It serves to establish the significance of considering the frequency dependence of pile-foundation impedances in estimating the response of the superstructure and identifies possible locations of nonlinear behavior. It follows closely the paper by Makris, Badoni, Delis and Gazetas (1994), and is primarily meant to illustrate the different substructure analyses and overall system response of a real structure under realistic loading conditions.

2.1 Model description

The Painter Street bridge, located near Rio Dell in northern California, is a continuous, two-span, cast-in-place, prestressed post-tensioned concrete, box-girdered, bridge. It is a typical concrete bridge constructed in 1973, and spans a four-lane highway. The structure has one span of 146 ft. (44.5 m) and one of 119 ft. (36.3 m). It is 52 ft. (15.8 m) wide. The two end abutments and the two-column "bent" are skewed at 39 degrees. The columns are approxi-

mately 20 ft. (6.0 m) high. The "bent" is supported by two pile groups, each consisting of twenty (4x5) driven concrete friction-piles. An elevation and plan view of the Painter Street bridge showing the location of the accelerometers is presented in figure 2.1. The cross-section of the bridge and a plan-view of the pile-group are presented in figure 2.2.

The Painter Street bridge was instrumented in 1977 by the California Division of Mines and Geology. Several earthquakes from 1980 to 1987, ranging in magnitude from $4.4 M_L$ to $6.9 M_L$, have produced significant accelerograms, the peak values of which are summarized by Maroney *et al.* (1990), who utilized these records in conjunction with a number of finite-element and lumped parameter ("stick") models of the entire bridge. However, none of these models accounted for soil-foundation-superstructure interaction. At each abutment, soil-wall interaction was modeled through a single real-valued transverse spring, the stiffness of which was backfigured from the interpreted fundamental natural period, $T \approx 0.30$ seconds, in lateral vibration.

On April 25, 1992, the bridge was severely shaken by the Petrolia Earthquake (Magnitude M_L=7.1, distance to fault R =18 km). Motions were recorded in all accelerographs, including one at the free field (Channels 12, 13, 14), one atop the footing of a pier (Channels 1, 2, 3), and one at the underside of the bridge girder directly above the pier (Channel 7). The locations of all accelerometers is depicted in figure 2.1, together with the peak recorded acceleration (PRA) for each channel. Of particular interest in this analysis are the records of channel 3 (PRA=0.48 g) and 7 (PRA=0.92 g). Despite the very high levels of accelerations, the bridge suffered only minor damage. The N-S (Channel 14), E-W (Channel 12) and vertical (Channel 13) free-field records of the Petrolia Earthquake are shown in Figure 2.3.

An interesting study of the response of the Painter Street bridge to the Petrolia earthquake was presented by Sweet (1993), who developed a finite-element model

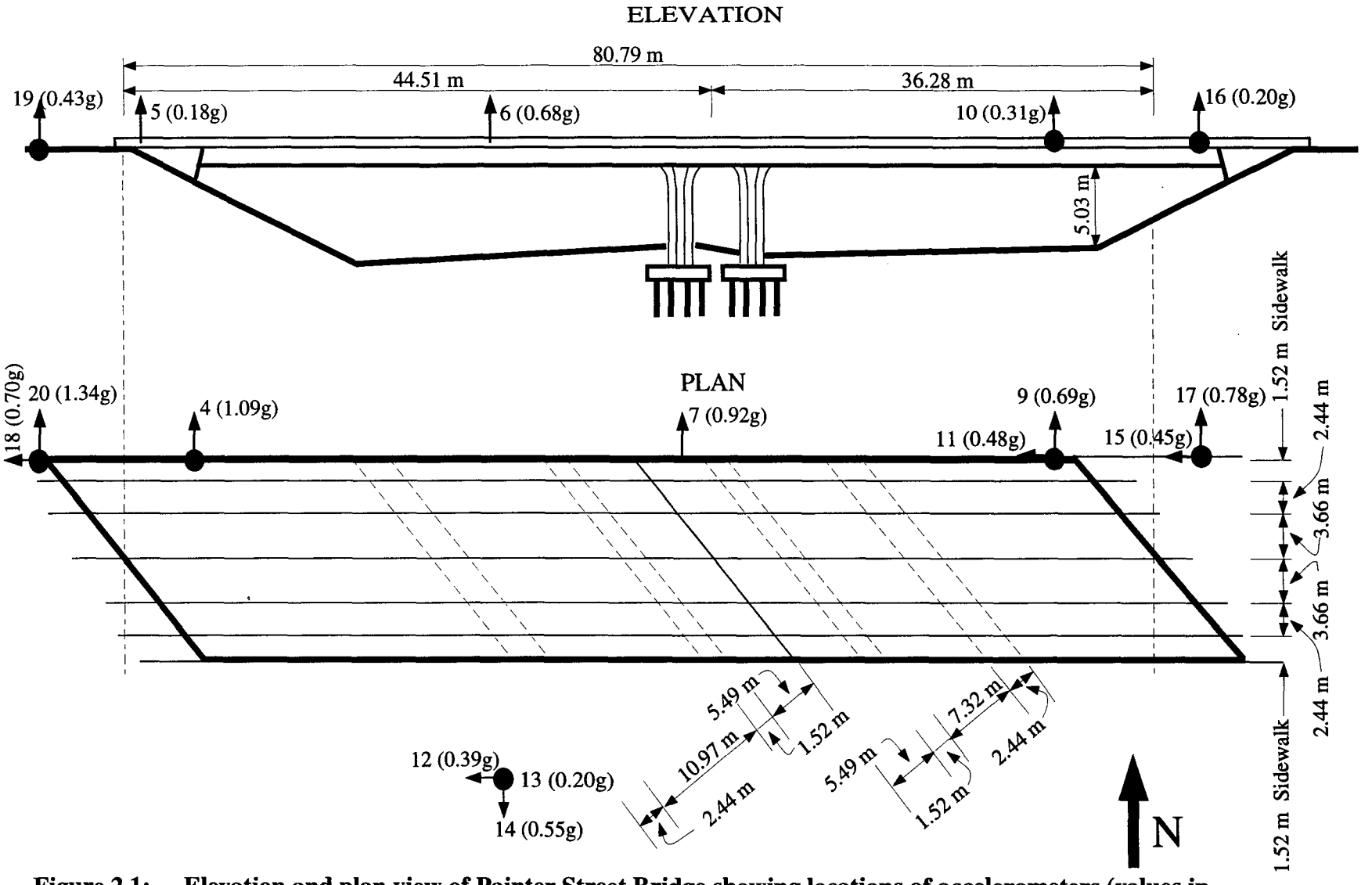

Figure 2.1: Elevation and plan view of Painter Street Bridge showing locations of accelerometers (values in parentheses indicate peak recorded acceleration at that location).

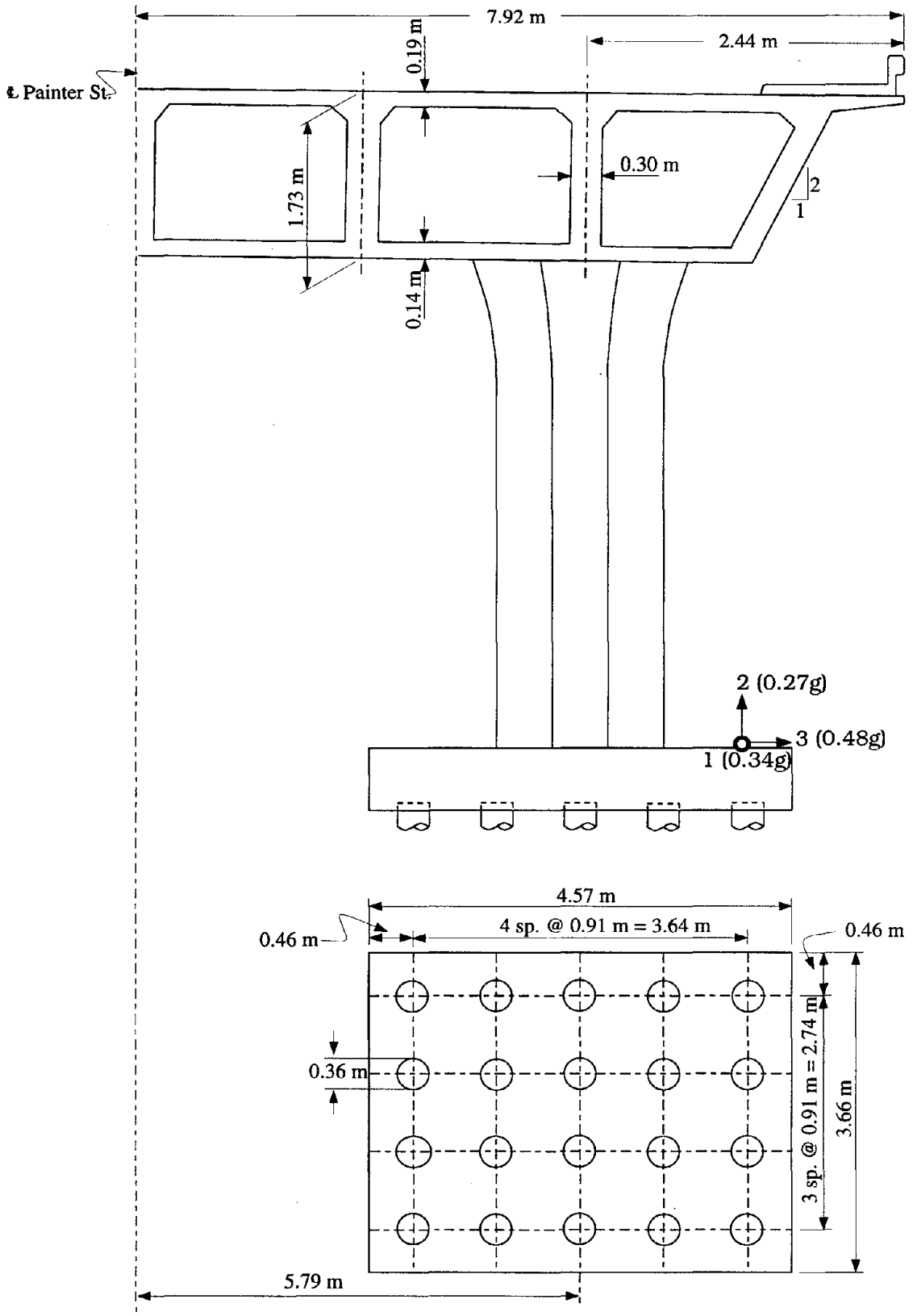

Figure 2.2: Cross-Sectional view of Painter Street Bridge and Plan View of Pile-Group.

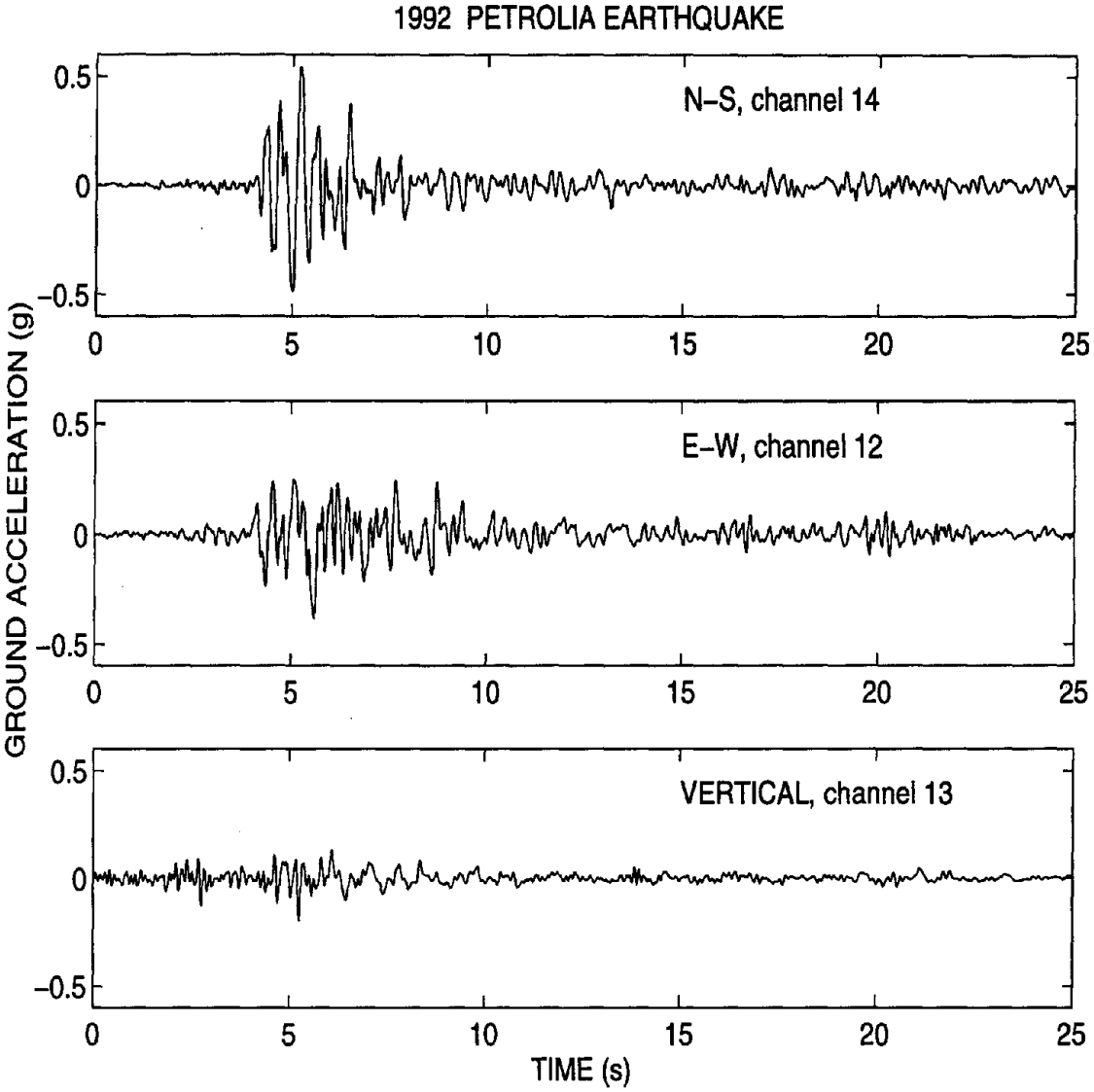

Figure 2.3: Recorded free-field acceleration time histories for the Petrolia earthquake, April 25, 1992.

encompassing the whole bridge and a large volume of surrounding and supporting soil. Inelastic soil behavior was modeled using an incremental plasticity model developed by the author. However, all this sophistication was inconsistent with the modeling of the pile group behavior, which was based on the sweeping assumption that no pile-soil-pile interaction occurs at the 3-foot spacing, and accordingly, the 20-pile group behavior was assumed to be merely 20 times that of a single pile. In fact, pile-to-pile interaction is expected to play a very substantial role in pile group response, given the very close rela-

tive spacing of the piles ($S/d \approx 2.60$).

The philosophy behind the model used herein is opposite to that of Sweet (1993) in that the simplest possible model of the pier-deck system is studied. The pile-group foundation is represented with a set of "springs" and "dashpots". However, the frequency-dependent values of these "springs" and "dashpots" are computed in a rational, physically motivated manner, accounting fully for pile-to-pile interaction.

The bridge is idealized as depicted in figure 2.4, with a plane 6-dof lumped-parameter mode in which m_s, m_f, I_s and I_f are the masses and moments of inertia of the superstructure and the foundation. In the case of a multi-span bridge, m_s and I_s are the mass and moment of inertia of the deck corresponding to one span plus some contribution from the bridge-pier. K_X^s, K_z^s, K_R^s and K_{XR}^s are the horizontal, vertical, rotational and cross horizontal-rotational stiffnesses of the superstructure. For the section of the superstructure considered, these are combinations of the stiffnesses of the bridge-pier and the bridge-deck. This is a reasonable approximation in the case where the abutments of the bridge and the foundation of the bridge-pier experience the same input motion, a condition that holds true for relatively short bridges. For long bridges, the abutment-motion might be incoherent, and a more sophisticated model would be more appropriate. However, for bridges with very long spans, the contribution from the deck stiffness might be negligible and the model would then become valid, since the entire horizontal stiffness of the superstructure is essentially due to the bridge-pier only. C_X^s and C_Z^s are the damping constants of the superstructure, and are assumed to be linear-viscous. $\mathcal{K}_X^{[F]}$, $\mathcal{K}_Z^{[F]}$, $\mathcal{K}_R^{[F]}$ and $\mathcal{K}_{RX}^{[F]}$ are the horizontal, vertical, rocking and cross horizontal-rocking stiffnesses of the pile-foundation and are complex valued quantities. It is to be noted that the presented procedure is not restricted to the simple structural model described above. Additional degrees of freedom for the structure could be incorporated to account for the motion of end-abut-

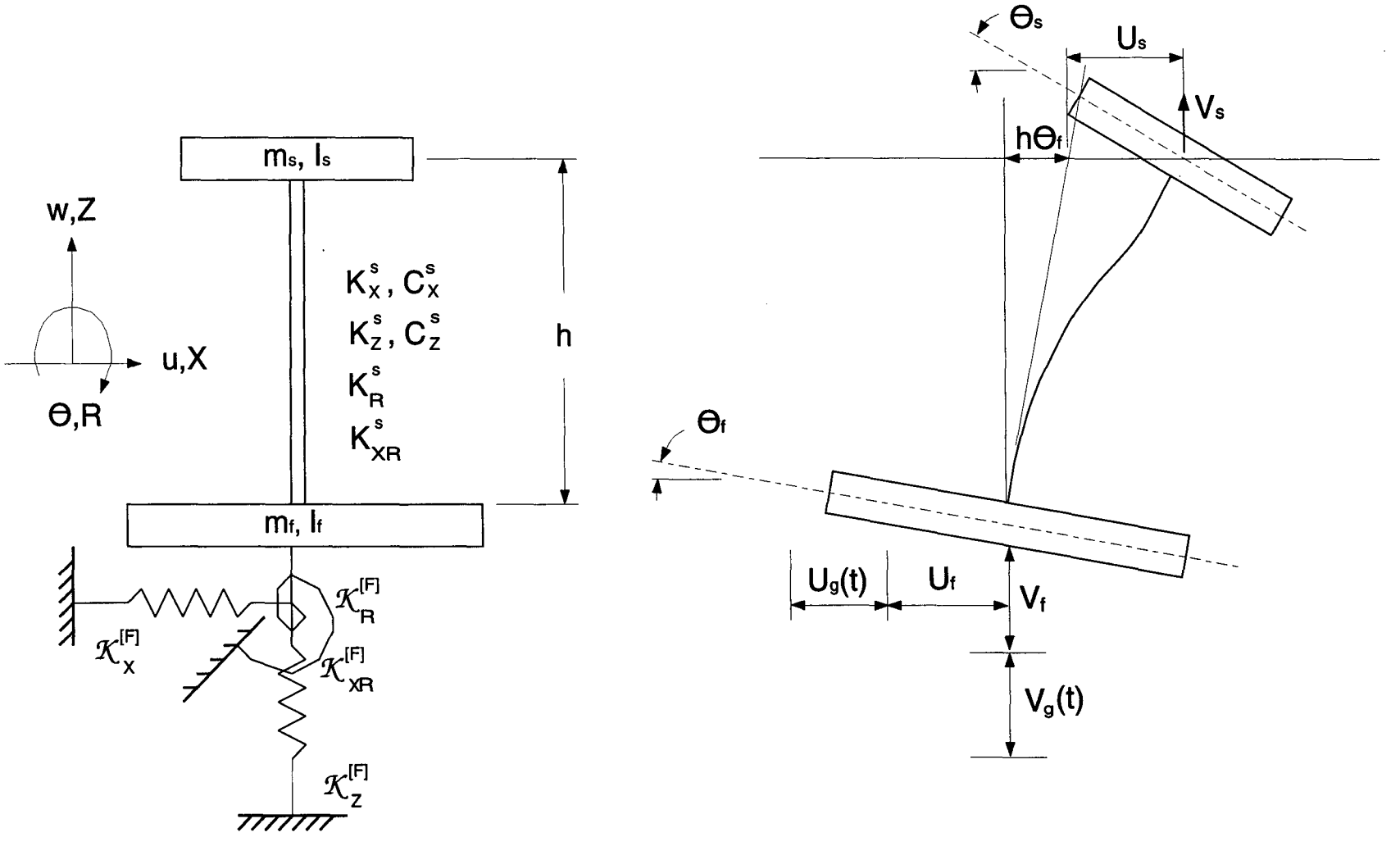

Figure 2.4: Pile foundation - superstructure idealization for the Painter Street Bridge response analysis.

ments and the torsional vibration of the bridge about the vertical axis.

2.2 Proposed analysis method

Assuming linear soil-foundation-superstructure response, the system analysis under seismic excitation can be performed in three consecutive steps, as mentioned in Chapter 1. These are discussed in the subsections that follow.

2.2.1 Foundation Input Motion: Step 1

The input motion to the system is induced at the foundation. In general, the support motion induced to the foundation is different than the "free-field" seismic motion. This difference is due to the "scattered wave field" which is generated between soil- and pile-displacement. Nevertheless, for motions that are not rich in high frequencies, the "scattered field" is weak, and the support motion can be approximately considered equal with that of the "free-field" (Fan *et al.* 1991).

In the case of the Painter Street bridge, the soil deposit has an average shear velocity $V_s \approx 200$ m/s (Heuze and Swift 1991) and the pile diameter d=0.36 m. Accordingly, even for the high frequency content of the input motion ($f \approx 10$ Hz), the dimensionless frequency $a_0 = 2\pi f d / V_s$ is only of the order of 0.1, and, therefore, the kinematic-seismic-response factors (head-group displacement over free-field displacement) in all vibration modes are very close to one (Gazetas *et al.* 1992). Based on the above supporting evidence, the excitation input motion on the pile-foundation of the bridge was assumed equal to that of the free-field motion.

2.2.2 Dynamic Impedances of Pile-Foundations: Step 2

The dynamic stiffness of a pile group, in any vibration mode, can be computed using the dynamic stiffness of the single pile in conjuction with dynamic interaction factors. This method, originally introduced for static loads by Poulos (1968), and later vali-

dated for dynamic loads by Kaynia and Kausel (1982), Sanchez-Salinero (1983), and Roesset (1984), can be used with confidence, at least for groups not having a large number of piles (such as less than 50). Dynamic interaction factors for various modes of loading are available in the form of ready-to-use non-dimensional graphs (Gazetas *et al.* 1991), or as closed-form expressions derived from a beam on a Winkler foundation model in conjuction with simplified wave propagation theory (Makris and Gazetas 1992). As an example, the horizontal and vertical dynamic interaction factor for two fixed-head piles in a homogeneous stratum takes the form:

$$\alpha_X(S,\theta) = \frac{3}{4}\psi(S,\theta)\frac{k_X(\omega)+i\omega c_X(\omega)}{k_X(\omega)+i\omega c_X(\omega)-m\omega^2} \tag{2.1}$$

$$\alpha_Z(S) = \left(\frac{d}{2S}\right)^{1/2} exp\left[-(\beta_s+i)\frac{\omega\left(S-\frac{d}{2}\right)}{V_s}\right] \tag{2.2}$$

where k_X, c_X are distributed "spring" and "dashpot" coefficients, and $\psi(r,\theta)$ is an approximate attenuation function proposed in the above mentioned reference. Furthermore, $i = \sqrt{-1}$; S = the axis-to-axis distance between two piles, θ is the angle between the direction of loading and the line connecting the axis of the two piles, β_s = hysteretic damping in the soil and V_s = shear wave velocity of the soil.

Knowledge of the dynamic stiffnesses of the single pile and the dynamic interaction factors between any two piles allows the computation of the dynamic stiffnesses of a group of piles using the concept of superposition. Let y_i be the horizontal displacement of pile i belonging to a group of N piles. Superposition of displacements leads to:

$$y_i = \sum_{j=1}^{N} \alpha_{X(i,j)} y_j \tag{2.3}$$

where $\alpha_{X(i,j)}$ is given from (2.1). Of course if $j = i$, then $\alpha_{X(i,i)} = 1$. y_j, the displacement of a single (solitary) pile is obtained as

$$y_j = \frac{F_j}{\mathcal{K}_X^{[1]}} \tag{2.4}$$

where F_j is the force that this pile carries, and $\mathcal{K}_X^{[1]}$ is the horizontal dynamic stiffness of the single "fixed-head" pile. Note that $\mathcal{K}_X^{[1]}$ is a function of ω, but this is not explicitly depicted here for brevity. Since all piles are connected with a rigid cap, the displacement of the group, $y^{[G]}$, is equal to y_i for all i. Substitution of (2.4) into (2.3) gives

$$y^{[G]}\mathcal{K}_X^{[1]} = \sum_{j=1}^{N} \alpha_{X(i,j)} F_j \tag{2.5}$$

Repeating equation (2.5) for all N piles of the pile group, one obtains the matrix equation

$$\begin{bmatrix} \alpha_{X(11)} & \alpha_{X(12)} & \cdots & \alpha_{X(1N)} \\ \alpha_{X(21)} & \alpha_{X(22)} & \cdots & \alpha_{X(2N)} \\ . & . & . & \\ . & . & . & \\ \alpha_{X(N1)} & \alpha_{X(N2)} & \cdots & \alpha_{X(NN)} \end{bmatrix} \begin{bmatrix} F_1 \\ F_2 \\ . \\ . \\ F_N \end{bmatrix} = y^{[G]}\mathcal{K}_X^{[1]} \begin{bmatrix} 1 \\ 1 \\ . \\ . \\ 1 \end{bmatrix} \tag{2.6}$$

Equation (2.6) can be solved for the force vector:

$$F_i = y^{[G]}\mathcal{K}_X^{[1]} \sum_{j=1}^{N} \varepsilon_{X(i,j)} \tag{2.7}$$

where $\varepsilon_{X(i,j)}$ is an element of the inverse of the matrix $[\alpha_{X(i,j)}]$. Since $P_x^{[G]} = \mathcal{K}_X^{[G]} y^{[G]} = \sum_{i=1}^{N} F_i$, the dynamic stiffness of the pile-group for the horizontal mode is simply

$$\mathcal{K}_X^{[G]} = \mathcal{K}_X^{[1]} \sum_{i=1}^{N} \sum_{j=1}^{N} \varepsilon_{X(i,j)} \tag{2.8}$$

The vertical dynamic stiffness of the group is also given by an equivalent analysis, where

index X is replaced by Z. Accordingly,

$$\mathcal{K}_Z^{[G]} = \mathcal{K}_Z^{[1]} \sum_{i=1}^{N} \sum_{j=1}^{N} \varepsilon_{Z(i,j)} \tag{2.9}$$

where $[\varepsilon_{Z(i,j)}]$ is the inverse of matrix $[\alpha_{Z(i,j)}]$ obtained from (2.2).

The rocking group-dynamic stiffness can be derived by an analysis similar to the one presented above (Dobry and Gazetas 1988, Makris *et al.* 1993).

$$\mathcal{K}_R^{[G]} = \mathcal{K}_Z^{[1]} \sum_{i=1}^{N} x_i \sum_{j=1}^{N} x_j \varepsilon_{Z(i,j)} \tag{2.10}$$

where x_i is the distance of pile i from the axis about which the rotation occurs.

For the cross-horizontal-rocking interaction factors, it has been found (Gazetas *et al.* 1991) that the following approximation proposed by Randolph (1977) for statically loaded piles is also valid for dynamic loads:

$$\alpha_{XR(i,j)} \approx \alpha_{X(i,j)}^2 \tag{2.11}$$

Accordingly, the cross-horizontal-rocking group stiffness is:

$$\mathcal{K}_{XR}^{[G]} = \mathcal{K}_{XR}^{[1]} \sum_{i=1}^{N} \sum_{j=1}^{N} \varepsilon_{XR(i,j)} \tag{2.12}$$

where $\varepsilon_{XR(i,j)}$ is the element of the inverse of matrix $\alpha_{XR(i,j)}$ given by (2.11).

2.2.3 Equation of Motion and Solution: Step 3

The degrees of freedom of the structural model depicted in Figure 2.4 are: $<u_s,\ v_s,\ h\theta_s,\ u_f,\ v_f,\ h\theta_f>$. Within the linear range and for small rotations, the equations of motion of the system subjected to a ground acceleration are:

Horizontal equilibrium of the superstructure:

$$m_s(\ddot{u}_g + \ddot{u}_f + h\ddot{\theta}_f + \ddot{u}_s) + C_X^s \dot{u}_s + K_X^s u_s + K_{XR}^s(\theta_s - \theta_f) = 0 \tag{2.13}$$

Vertical equilibrium of the superstructure:

$$m_s(\ddot{v}_g + \ddot{v}_f + \ddot{v}_s) + C_Z^s \dot{v}_s + K_Z^s v_s = 0 \tag{2.14}$$

Rotational equilibrium of the superstructure:

$$I_s \ddot{\theta}_s = -K_R^s(\theta_s - \theta_f) - K_{XR}^s u_s \tag{2.15}$$

Horizontal equilibrium of the entire system:

$$m_s(\ddot{u}_g + \ddot{u}_f + h\ddot{\theta}_f + \ddot{u}_s) + m_f(\ddot{u}_g + \ddot{u}_f) = -P_X^{[F]} \tag{2.16}$$

Vertical equilibrium of the entire system:

$$m_s(\ddot{v}_g + \ddot{v}_f + \ddot{v}_s) + m_f(\ddot{v}_g + \ddot{v}_f) = -P_Z^{[F]} \tag{2.17}$$

Rotational equilibrium of the entire system:

$$I_f \ddot{\theta}_f - K_R^s(\theta_s - \theta_f) - K_{XR}^s u_s + m_s(\ddot{u}_g + \ddot{u}_f + h\ddot{\theta}_f + \ddot{u}_s)h = -M_R^{[F]} \tag{2.18}$$

where $P_X^{[F]}$, $P_X^{[F]}$ and $M_R^{[F]}$ are the horizontal, vertical, and rocking reactions of the pile foundation.

The linearity of the governing differential equations allows for solution in the frequency domain. Applying the Fourier transform to the system of equations (2.13) to (2.18), the equations of motion can be written in a matrix form

$$[S(\omega)]\{U(\omega)\} = \{F(\omega)\} \tag{2.19}$$

in which $\{U(\omega)\}$ is the Fourier transform of the response vector $\{u_s,\ v_s,\ h\theta_s,\ u_f,\ v_f,\ h\theta_f\}^T$, $\{F(\omega)\}$ is the Fourier transform of the excitation vector $\{-\ddot{u}_g,\ -\ddot{v}_g,\ 0,\ -(1+\mu)\ddot{u}_g,\ -(1+\mu)\ddot{v}_g,\ -\ddot{u}_g\}^T$, with $\mu = m_f/m_s$, and $[S]$ is the frequency dependent dynamic stiffness matrix of the soil-pile-foundation superstructure system. The Fourier transform of the reactions from the pile-foundation are given by

$$\mathcal{F}\{P_X^{[F]}(t)\} = \mathcal{K}_X^{[F]}(\omega)u_f(\omega) + \mathcal{K}_{XR}^{[F]}(\omega)\theta_f(\omega) \tag{2.20}$$

$$\mathcal{F}\{P_Z^{[F]}(t)\} = \mathcal{K}_Z^{[F]}(\omega)v_f(\omega) \tag{2.21}$$

$$\mathcal{F}\{M_R^{[F]}(t)\} = \mathcal{K}_{RX}^{[F]}(\omega)u_f(\omega) + \mathcal{K}_R^{[F]}(\omega)\theta_f(\omega) \tag{2.22}$$

where $\mathcal{K}_X^{[F]}$, $\mathcal{K}_Z^{[F]}$, $\mathcal{K}_R^{[F]}$ and $\mathcal{K}_{RX}^{[F]} = \mathcal{K}_{XR}^{[F]}$ are the horizontal, vertical, rocking and cross-horizontal-rocking impedances of the pile-foundation.

The parameters appearing in the dynamic stiffness matrix $[S]$ are:

$$\Omega_{Xs} = \left(\frac{K_X^s}{m_s}\right)^{1/2}, \quad \Omega_{Zs} = \left(\frac{K_Z^s}{m_s}\right)^{1/2}, \quad \Omega_{Rs} = \left(\frac{K_R^s}{m_s h^2}\right)^{1/2}, \quad \Omega_{XRs} = \left(\frac{K_{XR}^s}{m_s h}\right)^{1/2} \tag{2.23}$$

$$\xi_{Xs} = \frac{C_X^s}{2m_s\Omega_{Xs}}, \quad \xi_{Zs} = \frac{C_Z^s}{2m_s\Omega_{Zs}} \tag{2.24}$$

$$\Omega_{Xf} = \left(\frac{K_X^{[F]}}{m_s}\right)^{1/2}, \quad \Omega_{Zf} = \left(\frac{K_Z^{[F]}}{m_s}\right)^{1/2}, \quad \Omega_{Rf} = \left(\frac{K_R^{[F]}}{m_s h^2}\right)^{1/2}, \quad \Omega_{XRf} = \left(\frac{K_{XR}^{[F]}}{m_s h}\right)^{1/2} \tag{2.25}$$

$$\rho_s = \left(\frac{I_s}{m_s}\right)^{1/2}, \rho_f = \left(\frac{I_f}{m_f}\right)^{1/2} \tag{2.26}$$

The system response in the time domain is obtained by the inverse Fourier transform of the response vector $\{U(\omega)\}$ (Clough and Penzien 1993).

$$\{U(t)\} = \frac{1}{2\pi}\int_{-\infty}^{\infty}[H(\omega)]\{F(\omega)\}e^{i\omega t}d\omega \tag{2.27}$$

where $[H(\omega)]$ is the inverse of the matrix $[S(\omega)]$. Relative velocities and acceleration responses are obtained from equation (2.27) after having premultiplied the matrix $[H(\omega)]$ by $i\omega$ and $-\omega^2$, respectively. Numerical solutions are then derived by the Discrete Fourier Transform (DFT) method.

2.3 Model Parameters

2.3.1 Superstructure parameters

Even for a simplified model like the one presented herein, several uncertainties are involved in determining the parameters that govern structural stiffness, structural damping, mass distribution, foundation stiffness and pier-foundation-soil interaction. The model presented herein is a simplification of the "stick" model discussed by Maroney *et al.* (1990) in that the longitudinal and torsional modes are not considered. For the stick model, the first transverse period of the superstructure was determined by iteration, and reported to be 0.28 s during the 1982-87 seismic events which had produced less intense shaking of the bridge than the Petrolia earthquake. Accordingly, following our notation, $\Omega_{Xs} = 2\pi/0.28\,\text{s} = 22.4$ rad/s. The calibrated (back-calculated) horizontal stiffness of the superstructure is reported to be $K_X^s = 39,000$ kips/ft. $= 5.69x10^5$ kN/m (Maroney *et al.* 1990). As given by equation (2.25), the mass of the superstructure is $m_s = 1130$ Mg. The value of m_s, when estimated by taking the weight of half the deck plus the weight of the top half of the piers, was of the order of 1000 Mg, which is in agreement with the previously mentioned value. Furthermore, using stress-strain laboratory tests on core samples from existing bridges, Maroney *et al.* (1990) reported the Young's modulus of the concrete to be $E_c = 3800$ ksi $= 2.6x10^7$ kN/m^2. This value is approximately 80% less than the value of E_c resulting from empirical expressions. Under the stronger shaking of the Petrolia earthquake, more cracking is expected to have occurred, and thus the value of E_c should be further reduced in an equivalent linear dynamic analysis. In this study, the value of E_c reported by Maroney *et al.* (1990) is reduced by 15%. With this reduction, $E_c \approx 22$ GPa, which is a generally accepted value for moderately cracked concrete. Based on this assumption, the vertical stiffness of the bridge-pier, K_Z^c, can be approximated by

$$K_Z^c = \frac{E_c A_c}{h_c} \approx \frac{(2.2x10^7 \text{kN/m}^2)(1.19\text{m}^2)}{(6\text{m})} \approx 4.4X10^6 \text{kN/m} \qquad (2.28)$$

where A_c and h_c are the bottom cross-section area and net-height of the pier.

The vertical stiffness of the superstructure is approximately

$$K_Z^s = 2K_Z^c \approx 8.8X10^6 \text{ kN/m} \qquad (2.29)$$

and from equation (2.23), $\Omega_{Zs} = 96$ rad/s. If l is the projection to the N-S axis of the center-to-center distance between the two piers ($l \approx 9.5$ m), the rotational stiffness of the superstructure can be approximated by

$$K_R^s = \frac{K_Z^c l^2}{2} \approx \frac{(4.4X10^6 \text{kN/m})(90\text{m})^2}{2} \approx 2.0X10^8 \text{kNm/rad} \qquad (2.30)$$

and from equation (2.23), $\Omega_{Rs} \approx 60$ rad/s. The moment of inertia of the deck is estimated to be $I_s \approx 20,000$ Mg-m^2 and from equation (2.26), the radius of gyration of the superstructure is $\rho_s = 4.2$ m. It should be mentioned that sensitivity studies showed that the deck response was not altered by varying the modulus of concrete in the range $20\text{GPa} < E_c < 26\text{GPa}$. Rather, it is much more sensitive to the values of the foundation stiffnesses.

2.3.2 Soil Profile and Foundation Parameters

Prior to construction, a geotechnical exploration at the location of the piers had been conducted. With Standard Penetration Test (SPT) measurements from the ground surface down to a depth of about 10 m, moderately stiff/dense soil layers were identified, consisting of clayey sand, silty sand, sandy silt, and gravelly sand. STP blowcounts varied from 8 near the surface to 34 at 10m depth. The underlying stratum was a very dense gravelly and silty sand, with blowcounts exceeding 100 blows/ft.

A geophysical exploration was also conducted by Heuze & Swift (1991). Six so-

called "seismic refraction surveys" have been reported, along four lines parallel to the highway. Evidently, the differences in the S-wave velocities and shear moduli among the soil-profiles below the location of the lines are rather substantial, given that they are located 20 to 30 meters apart from each other. For instance, the resulting low-strain shear modulus from the data along line 2 (G_s = 100 MPa) has twice the value of that resulting from the data along line 1. It is quite possible that some of these differences merely reflect inadequacies (general and specific) of the "seismic" refraction technique. Herein, the dynamic analysis of the pile-foundation-bridge system was based on the values extracted from the data along line 2, which is adjacent to the pier ($V_s \approx 250$ m/s, $\rho_s \approx 1.6$ Mg/m^3, $\nu_s = 0.48$).

Closed form expressions for the static stiffnesses of a single pile have been derived by fitting finite-element results of the static problem (Gazetas 1984). The accuracy of these expressions has been verified by comparing their results with the solution of Blaney *et al.* (1976) for lateral and vertical pile-motion in homogeneous soil, and the solution of Randolph (1981) for lateral pile-motion in nonhomogeneous soil with modulus proportional to depth. Using the expressions derived by Gazetas, alongwith the soil data along line 2 (G_s = 100 MPa, ν_s = 0.48), pile diameter, d = 0.36 m, pile length, L = 7.62 m, and Young's modulus of pile E_p = 22,000 MPa, the static stiffnesses of the single "fixed-head" pile are approximated by:

$$K_X^{[1]} \approx E_s d\left(\frac{E_p}{E_s}\right)^{0.21} \approx 260 \text{ MN/m} \tag{2.31}$$

$$K_Z^{[1]} \approx 1.9 G_s d\left(\frac{L}{d}\right)^{2/3} \approx 520 \text{ MN/m} \tag{2.32}$$

$$K_R^{[1]} \approx 0.15 E_s d^3\left(\frac{E_p}{E_s}\right)^{0.75} \approx 50 \text{ MNm/rad} \tag{2.33}$$

$$K_{XR}^{[1]} \approx -0.22 E_s d^2 \left(\frac{E_p}{E_s}\right)^{0.5} \approx -75 \text{ MN/rad} \tag{2.34}$$

The horizontal, $K_X^{[1]}$, and vertical, $K_Z^{[1]}$, static stiffnesses of the single pile were also computed with a nonlinear analysis procedure developed by Trochanis *et al.* (1991). The method is based on a one-dimensional analysis that utilizes a realistic hysteretic model, which has been calibrated using a three-dimensional finite-element analysis of the soil-pile system. This procedure was originally developed to produce load controlled force-displacement curves, and had to be adapted to a displacement controlled formulation. Figure 2.5 shows the resulting head-force versus head-displacement curves. The resulting horizontal static stiffness of the pile is the slope of the force-displacement curve, which at small deflections has a value of approximately 200 MN/m. This value is indeed close to the value given by (2.31). Also, the initial vertical stiffness shown is approximately 450 MN/m, a value which is also very close to the result of (2.32).

All the aforementioned pile-stiffness values were computed using the small-strain value $G_s(\gamma_s < 10^{-5}) = G_{\max} = 100$ MPa. However, under the Petrolia seismic excitation the level of soil-strain is estimated to have been as large as $\gamma_s \approx 10^{-3}$, and occasionally reaching the neighborhood of $\gamma_s = 10^{-2}$. At this strain level, the soil-shear modulus is substantially reduced, and can be as low as five times less than the small-strain value $G_{\max}$ (Tatsuoka *et al.* 1979). Accordingly, the average realistic values for the horizontal, vertical and cross-horizontal-rocking static stiffnesses of the single pile were selected to be: $K_X^{[1]} = 65$ MN/m, $K_Z^{[1]} = 200$ MN/m, $K_{XR}^{[1]} = -20$ MN/rad, and the rocking stiffness of the individual piles is neglected, since it is negligible compared to the large rotational stiffness of the foundation system resulting from the axial vibration of piles. These stiffnesses are approximately two to four times smaller than the values obtained with the small-strain value of the soil shear modulus (equations (2.31) to (2.34)). The reason why

the horizontal and cross-horizontal rocking stiffnesses are reduced more than the vertical stiffness is because the soil strains near the soil surface which primarily influence the horizontal pile motion, are larger that the strains at larger depths on which the vertical stiffness depends.

Using the procedure described earlier (step 2), the group stiffnesses are computed with equations (2.8), (2.9), (2.10), and (2.12). For instance, the horizontal and vertical dynamic stiffness-coefficients for the 4x5 pile group are plotted in Figure 2.6 as a function

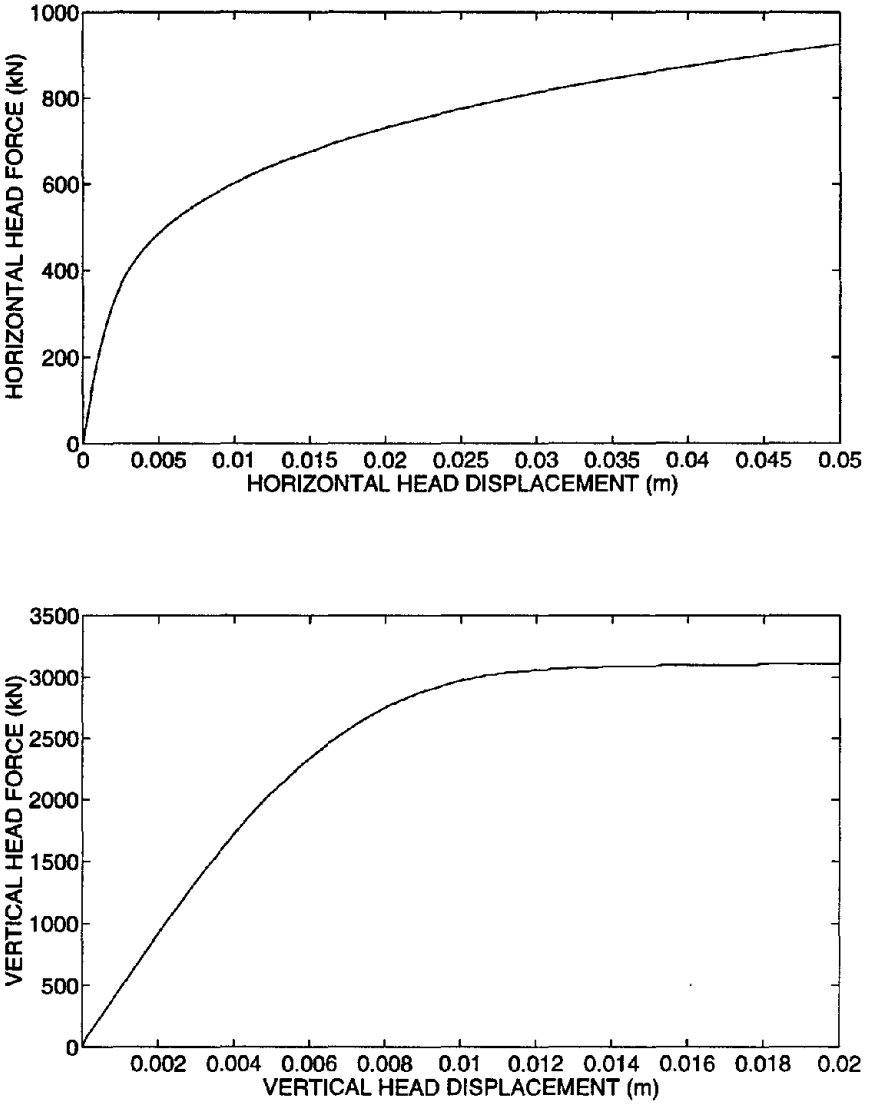

Figure 2.5: Computed head force-displacement curves for single pile (d = 0.36m, L = 7.62 m, G_s=100 MPa, S_u= 400 kPa, ν_s = 0.48).

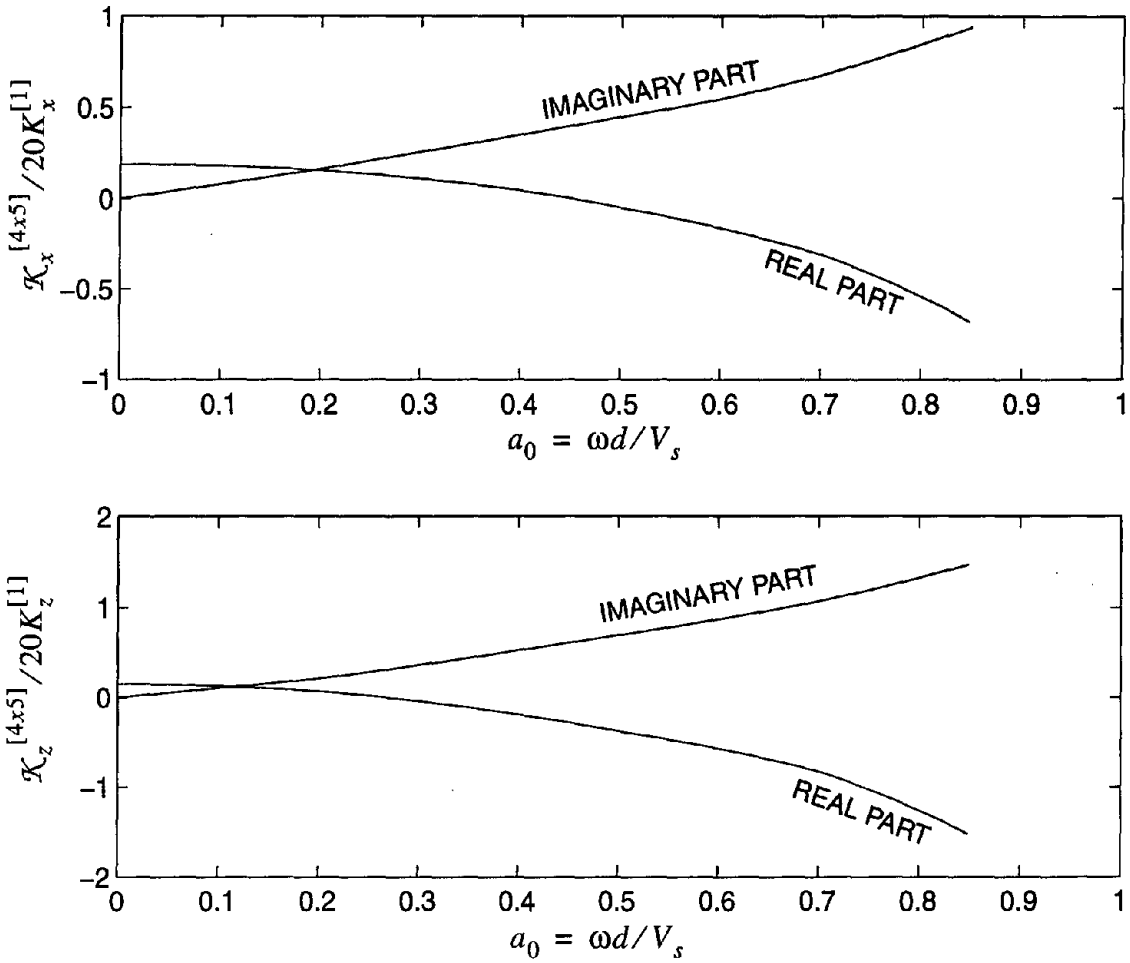

Figure 2.6: Storage (real part) and loss (imaginary part) stiffness factors for 4x5 pile-group with rigid pile cap for horizontal (top) and vertical (bottom) motions in a homogeneous half space (E_p/E_s = 75, ρ_p/ρ_s = 1.5, β_s = 0.05, ν_s = 0.48).

of the dimensionless frequency $a_0 = \omega d/V_s$. It is interesting to note that the normalized value of the real part at the zero frequency limit reaches the value of 0.19 for the horizontal and 0.16 for the vertical mode. These values are close to 1/5, which is the value that one obtains using the "flexibility" ratios provided in classical foundations textbooks (*e.g.* Fleming *et al.* 1984). The resulting static stiffnesses for the 4x5 group are: $K_X^{[4x5]} \approx 250$ MN/m, $K_Z^{[4x5]} \approx 600$ MN/m, $K_{XR}^{[4x5]} \approx 300$ MN/rad.

In order to compute the foundation-stiffnesses of the Painter Street bridge, it is assumed that the motion of a pile belonging to one pile-group does not affect the motion

of a pile belonging to the other. The minimum distance between two piles belonging to different pile-groups is S = 8 m = 26 ft., resulting in an $S/d > 22$. Although for such a high value of S/d no interaction is expected between two piles, the motion of the entire pile-group, which has an equivalent diameter $d_e \approx 4.6$ m, might influence the motion of the neighbor pile-group since $l/d_e \approx 2.5$. Nevertheless, for lack of other evidence, it is assumed that no such interaction occurs. To this end, the horizontal, vertical, rocking, and cross-horizontal-rocking stiffnesses of the foundation of the Painter Street bridge are estimated to be

$$K_X^{[F]} \approx 2K_X^{[4x5]} \approx 500 \text{ MN/m} \tag{2.35}$$

$$K_Z^{[F]} \approx 2K_Z^{[4x5]} \approx 1200 \text{ MN/m} \tag{2.36}$$

$$K_R^{[F]} \approx \frac{K_Z^{[4x5]} l^2}{2} \approx 27000 \text{ MNm/rad} \tag{2.37}$$

$$K_{XR}^{[F]} \approx 2K_{XR}^{[4x5]} \approx 600 \text{ MN/rad} \tag{2.38}$$

For the values above and an approximate value of h = 7 m, equation (2.25) gives $\Omega_{Xf} \approx 21$ rad/s, $\Omega_{Zf} \approx 32.5$ rad/s, $\Omega_{Rf} \approx 22$ rad/s and $\Omega_{XRf} \approx 9$ rad/s. The mass of the foundation was estimated to be $m_f \approx 225$ Mg, and the moment of inertia $I_f \approx 8000$ Mg-m^2. From equation (2.26), ρ_f = 5.96 m and $\mu = m_f/m_s$ = 0.2.

2.4 Response prediction

The response of the bridge-foundation system is computed using equation (2.27) and compared against the recorded motion. Three different predictions are shown. Prediction (A) is the result when the entire frequency dependence of the foundation impedance is considered. Prediction (B) is the result when the stiffness and damping of the foundation are computed at the predominant frequency of the input motion (f_p = 2.32 Hz, ω_p = 14.57 rad/s) obtained from the Fourier spectrum of channel 14. At this frequency,

the horizontal and vertical dynamic stiffness coefficients are $k_{X1}(14.57) + ik_{X2}(14.57) = 0.970 + i0.331$ and $k_{Z1}(14.57) + ik_{Z2}(14.57) = 0.903 + i0.545$, respectively. Prediction (C) is the result when the foundation is considered as a fixed, monolithic support.

Figure 2.7 presents the horizontal (N-S) motion of the pile-cap of the bridge foundation. The results of prediction (A) are indeed in very good agreement with the records. Notice that the peak values of both acceleration and displacement are very accurately predicted. The result for the displacement history from prediction (B) are also in very good agreement with the records, although the acceleration history is somewhat underestimated. Similar predictions are offered from prediction (C) where the acceleration history is overestimated.

Figure 2.8 presents the vertical motion of the pile cap. Again, the results of prediction (A) are most favorable for the peak acceleration values, whereas the total displacement histories of the three predictions are almost identical.

Finally, Figure 2.9 presents the horizontal (N-S) deck acceleration and the deck-drift relative to the pile-cap level. The results of prediction (A) for the deck-drift are good, but the acceleration is underestimated by approximately 30%. Several reasons might be responsible for this discrepancy between recorded and predicted motion, such as neglecting the torsional motion of the bridge about the vertical axis, yielding of bridge pier, yielding of pile-heads and so forth. Such effects are not captured with this simple model. For instance, the deck acceleration response is very sensitive to the value of the cross-horizontal-rocking stiffness of the pile foundation. As the absolute value of the cross-horizontal-rocking stiffness decreases, the predicted deck acceleration becomes more and more pronounced, reaching the recorded values when the cross-horizontal-rocking stiffness is assumed to be zero. Such reduction in the value of the cross-horizontal-rocking stiffness might result from yielding of the pile heads. However, if one decides to compute the

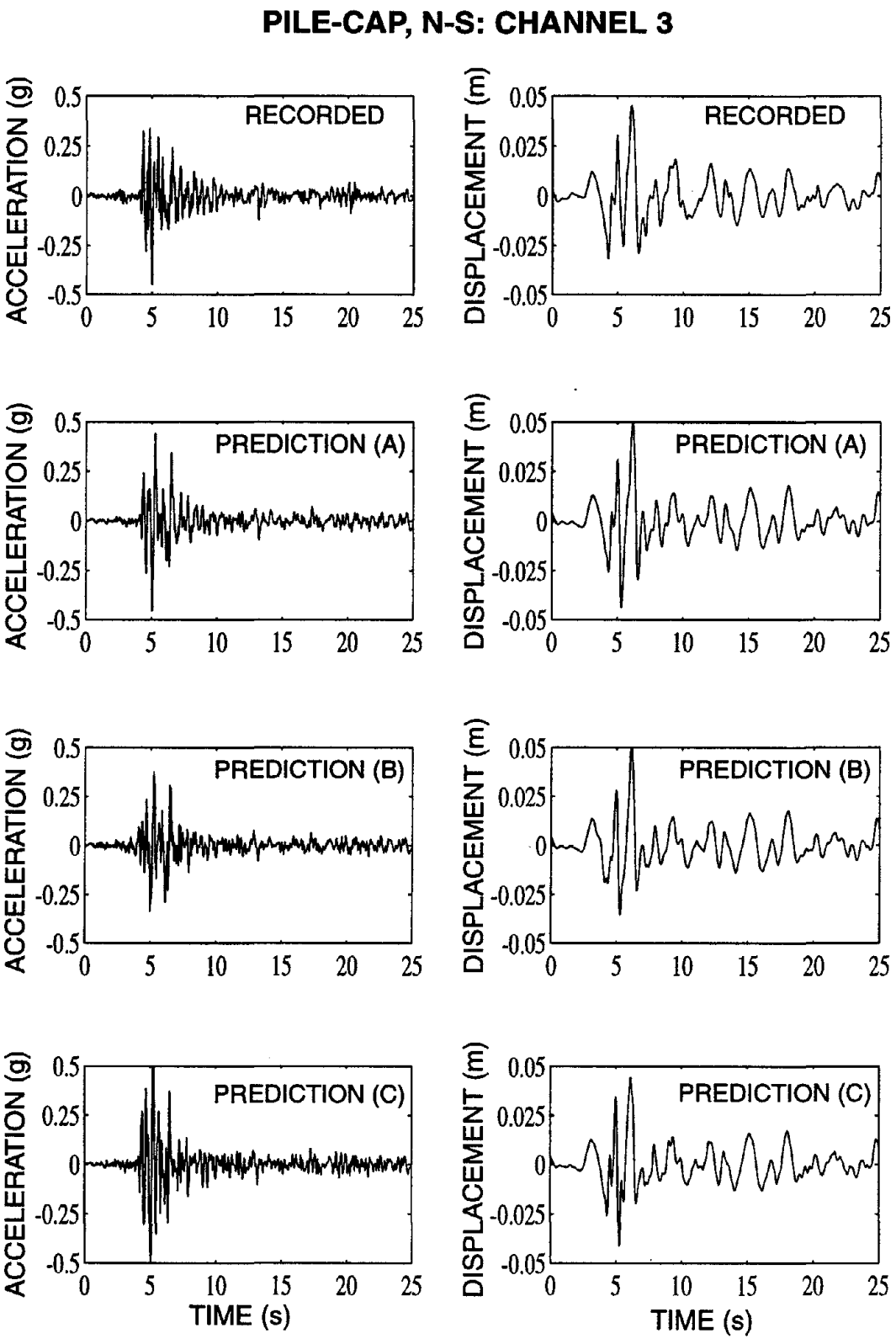

Figure 2.7: **Comparison of recorded N-S pile-cap acceleration- and displacement- time histories with model predictions.**

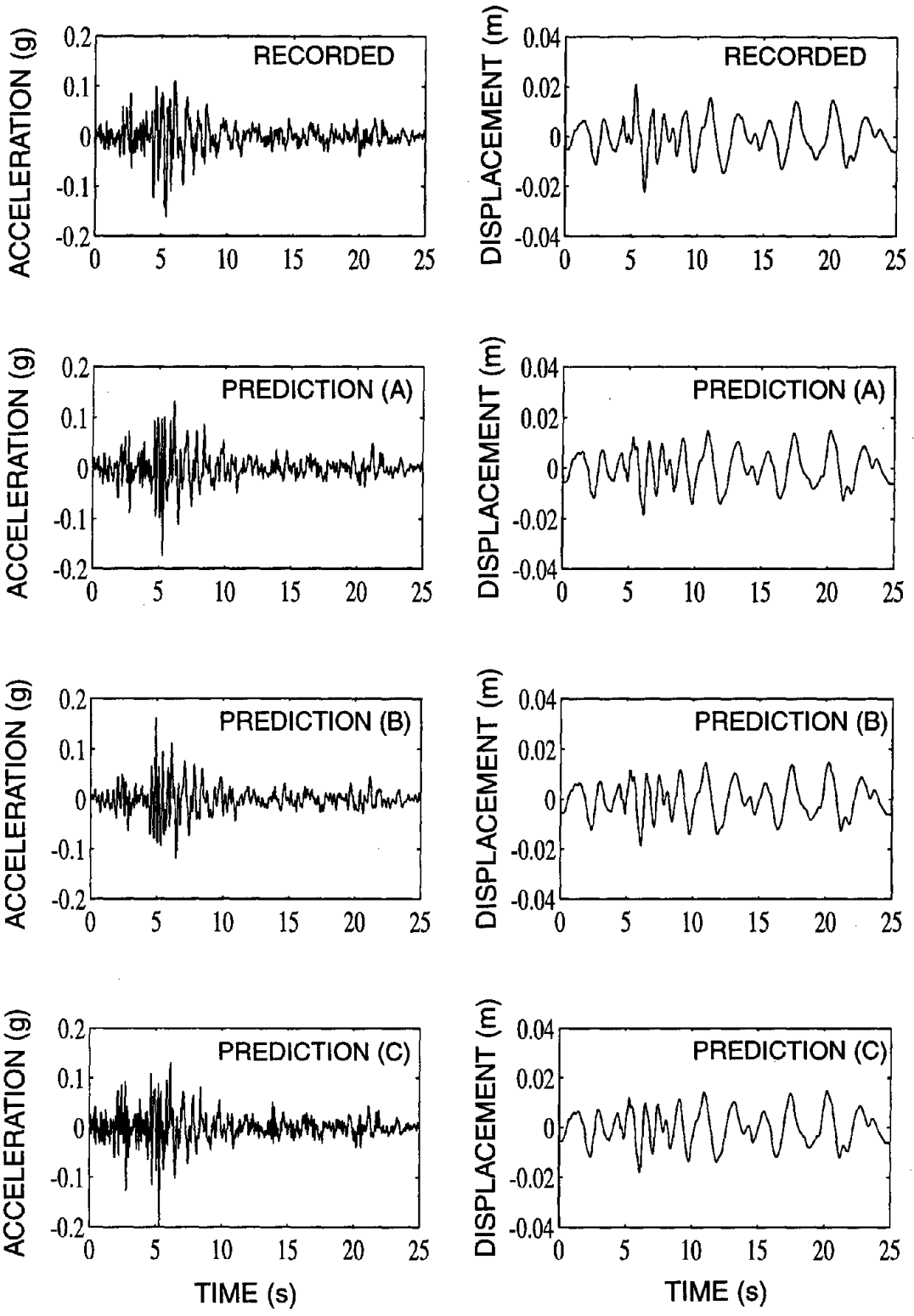

Figure 2.8: **Comparison of recorded vertical pile-cap acceleration- and displacement- time histories with model predictions.**

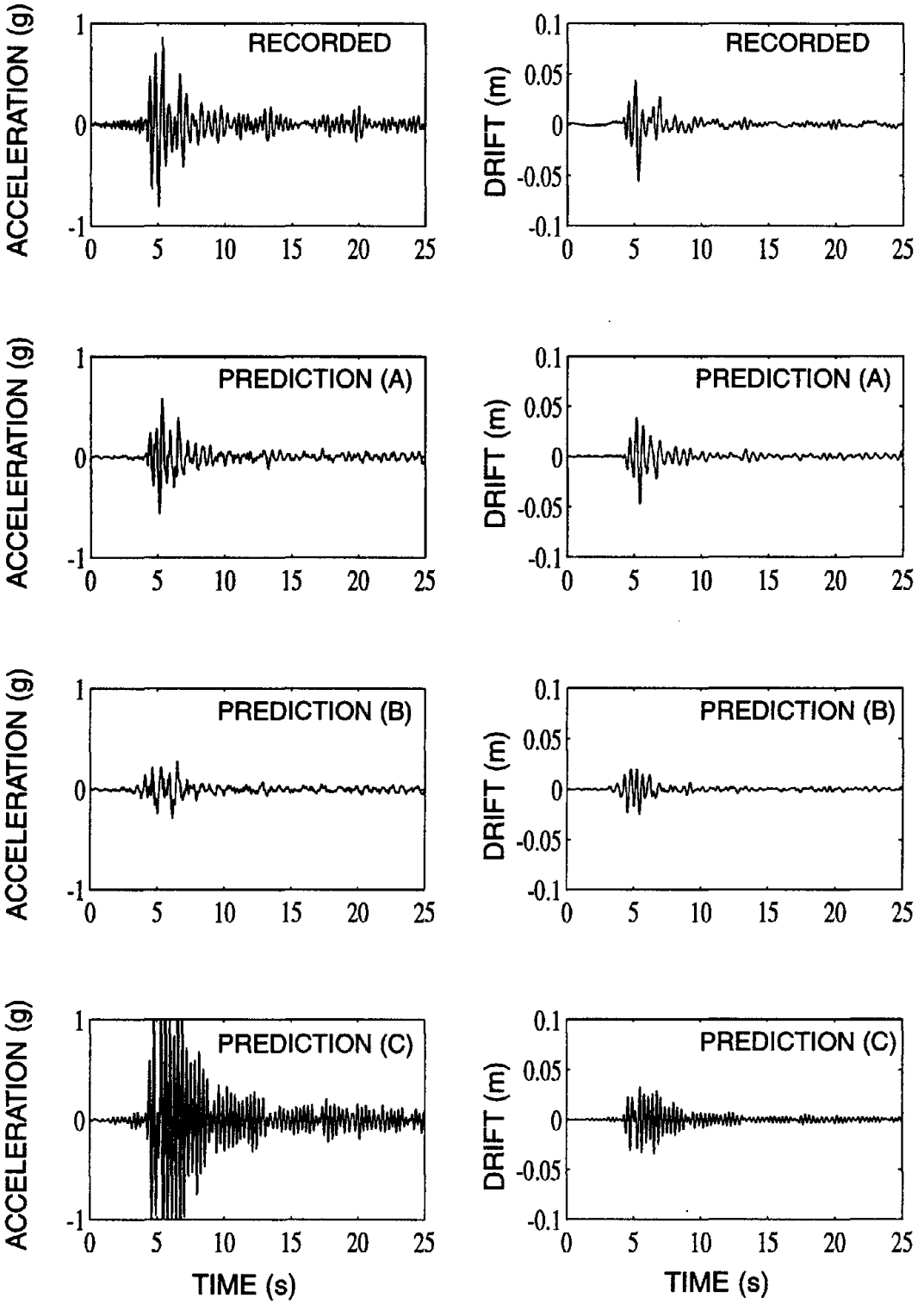

Figure 2.9: **Comparison of recorded N-S deck acceleration- and displacement-time histories with model predictions.**

bridge response by neglecting the moment transmitted at the pile-heads, the entire analysis should be redone, starting from the interaction factors given by (2.1) which have to be modified for free-head piles. The results offered by prediction (B) are less favorable, since the response is underestimated by 60%. An interesting result of this study is prediction (C), where the results offered are erroneous. The acceleration of the deck is substantially overestimated (more that 100%), and high frequencies are present. It is a notable example of poor modeling of the foundation drastically affecting the response of the superstructure. The origin of this poor prediction is the omission of foundation damping in the analysis. By assuming a fixed, monolithic foundation, no energy dissipation is allowed through the foundation (*i.e.* zero radiation damping), and all the induced seismic energy is trapped in the superstructure and is eventually dissipated only by structural damping.

Another interesting observation is that the ratio of the deck-drift to the height of the bridge pier is of the order of $\delta_r \approx 1\ \%$. Although there is no precise value of that ratio which indicates the level of nonlinearities in the structural response, structures with moderate ductility are expected to experience some nonlinear behavior for $\delta_r \approx 1\ \%$.

2.5 Concluding remarks

This chapter presented a simple integrated procedure to incorporate the existing theories for the computation of dynamic pile-foundation impedances and kinematic seismic response factors into a complete foundation-superstructure interaction problem. The method was shown to be capable of estimating system response fairly well within the limits of a linear analysis. The importance of modeling foundation dynamics was established. The possibility of nonlinear behavior was identified for the superstructure. The analysis of such a system is the subject of the next chapter.

CHAPTER 3

TIME-DOMAIN ANALYSIS OF PILE FOUNDATION-SUPERSTRUCTURE INTERACTION

The substructure method to solve the linear foundation-superstructure interaction problem is usually performed in the frequency domain because of the inherent computational simplicity as well as the ease of formulation. However, when nonlinear behavior is encountered, time-domain analysis becomes a much more viable option. Macroscopic time-domain models, which describe the response of the substructures at the force-displacement level, are of particular interest to structural engineers, since they allow for nonlinear modeling and are also easily incorporated into existing computer codes. In the specific problem of pile foundation-superstructure interaction, the two important stages involved in a time-domain substructure approach are: i) to obtain an appropriate macroscopic model for the foundation response; and ii) to devise a link between the simplified foundation model and the superstructure model.

In the last 25 years, several researchers have proposed various models for foundation response. Pioneering work in this field was done by Veletsos and Verbic (1974) who presented analytical models for the response of circular footings resting on the surface of a viscoelastic halfspace. They proposed a simple real parameter Kelvin model with frequency dependent coefficients for the horizontal, vertical and rocking modes. In the case of pile foun-

dations, several formulations for dynamic stiffnesses of piles and pile-groups have been developed and published in the literature including finite-element (Blaney et al. 1976, Gazetas 1984, Kagawa and Kraft 1982, Kaynia and Kausel 1982), boundary-element (Banerjee and Sen 1987, Fan et al. 1991, Kaynia 1980, Waas and Hartman 1984, Kaynia and Novak 1992), semi-analytical type methods (Tajimi 1977, Kobori et al. 1991, Nogami 1983), and a number of simplified solutions (Dobry and Gazetas 1988, Makris and Gazetas 1992, Makris and Gazetas 1993, Makris and Badoni 1995).

When the dynamic stiffness of a viscoelastic system is known, either in the form of approximate closed-from expressions or in numeric or graphical form, its time domain response can be obtained by a variety of approaches. The Fourier transform approach, in which the response is first computed in the frequency domain and then transformed in the time domain, is computationally convenient, but is limited to linear analyses. The convolution integral approach, in which the response is determined directly in the time domain, requires knowledge of the basic response functions (memory function or relaxation stiffness) of the system, which can theoretically be obtained from the dynamic stiffness or impedance of the system through integral transforms. When part of the structural system behaves nonlinearly, a common case in seismic response of bridges (*e.g.* yielding pier, nonlinear behavior of isolation bearings on pile-foundation), the convolution integral approach becomes very attractive, since an analysis with the Fourier transform approach requires cumbersome hybrid-frequency-domain-time-domain solutions. Another possibility is to get a rational approximation for the provided dynamic stiffness, and obtain the governing differential equations in state-space form.

In this chapter, two such time-domain techniques are developed. The first utilizes a convolution integral in which the kernel is the dynamic relaxation stiffness of the foundation. This is obtained by numerically transforming available frequency response data in an

appropriate manner. The second uses a state-space representation of the governing equations in conjunction with a ratio-of-polynomials approximation for the dynamic stiffness. In both cases, nonlinear behavior of the superstructure is represented by the Bouc-Wen model. The procedures are validated for a linear problem, and then at the linear limit by choosing the Bouc-Wen model parameters accordingly. Subsequently, a nonlinear analysis is carried out to demonstrate the capability of the method. The versatility of the proposed procedure is demonstrated by means of a qualitative analysis of two nonlinear models representing isolation systems for bridge decks.

3.1 The convolution integral method for time domain response of pile foundations

Once the dynamic stiffness of the pile foundation is known based on any realistic available method, the resulting force $P(t)$, for an arbitrary displacement $u(t)$ of the pile-cap, can be obtained through the inverse Fourier Transform

$$P(t) = \frac{1}{2\pi}\int_{-\infty}^{\infty} \mathcal{K}(\omega)u(\omega)e^{i\omega t}d\omega \tag{3.1}$$

where $u(\omega)$ is the Fourier Transform of $u(t)$ and $\mathcal{K}(\omega)$ is the dynamic stiffness of the pile foundation.

The restoring force from the pile-foundation, $P(t)$, can also be obtained through a time-domain integral, the convolution integral, which permits the computation of the response without going into the frequency domain as

$$P(t) = \int_{-\infty}^{t} M(t-\tau)u(\tau)d\tau \tag{3.2}$$

where $M(t-\tau)$ is the memory function of the pile foundation, and is defined as the resulting head-force at the present time t, for a unit-amplitude impulsive displacement input at

time τ, $(\tau \leq t)$. Equation (3.2) has been successfully used by Veletsos and Verbic (1974) to calculate the response of elastic foundations after developing approximate analytical expressions for $M(t-\tau)$.

From the convolution theorem of the Fourier integral given by (3.1), the memory function $M(t)$ can be directly obtained from the inverse Fourier Transform of the dynamic stiffness

$$M(t) = \frac{1}{2\pi}\int_{-\infty}^{\infty} \mathcal{K}(\omega)e^{i\omega t}d\omega \tag{3.3}$$

The Fourier transform given by (3.3) can be in general obtained with the Discrete Fourier Transform (DFT) method (Clough and Penzien 1993) via established Fast Fourier Transform (FFT) algorithms (Veletsos and Ventura 1985), and the resulting memory function could be used in the convolution integral given by (3.2). However, when this approach is directly followed, the numerical results for the response of pile foundations are poor, even when sophisticated time-domain integration algorithms are used.This is because the integral does not exist in the classical sense given the nature of $\mathcal{K}(\omega)$ for pile foundations, which is not absolutely integrable over the ω-axis. For instance, for the Kelvin model, for which $\mathcal{K}(\omega) = K + i\omega C$, the corresponding memory function is $M(t) = K\delta(t-0) - C\dot{\delta}(t-0)$. The strong singularity associated with the second term of this function makes it particularly susceptible to numerical error when applied directly.

To avoid this problem, one could develop approximate closed form expressions for the memory function of single piles, similar to the expressions developed by Veletsos and Verbic (1974) for elastic foundations, which could then be integrated analytically. Although this method could be a feasible approach for single piles, it becomes highly impractical when pile groups are considered. In general, pile groups yield a dynamic stiff-

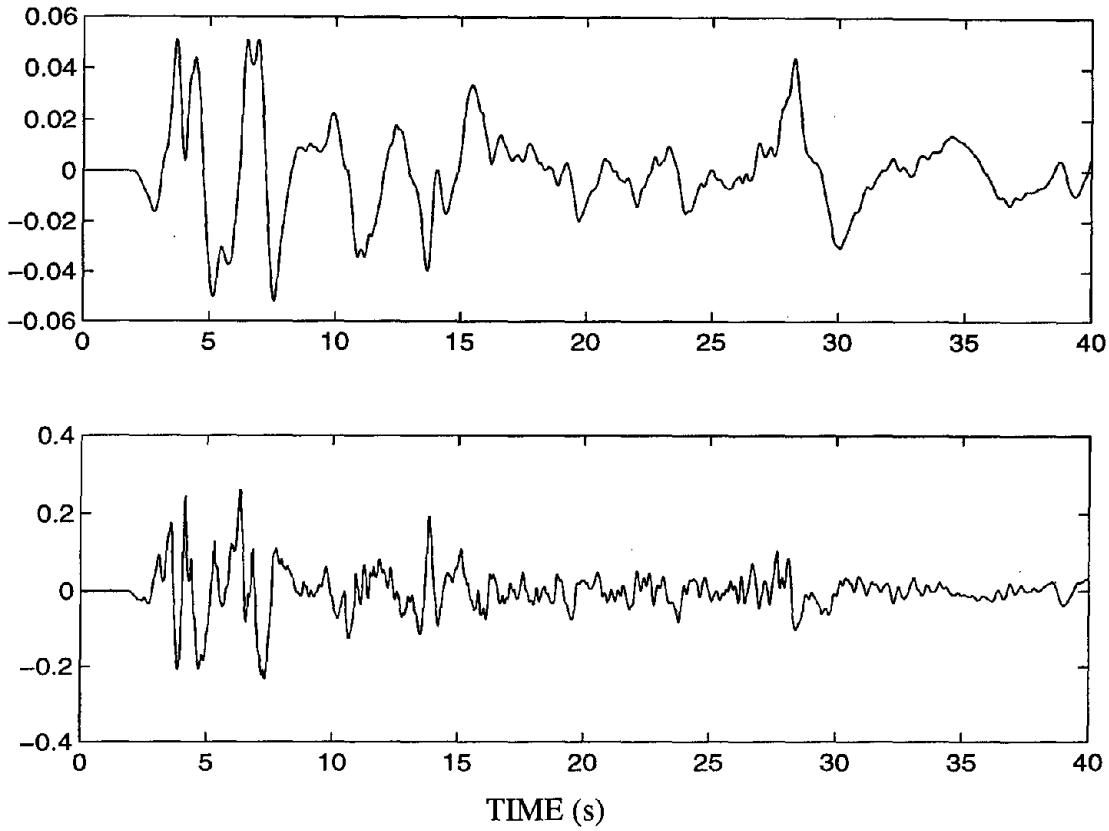

Figure 3.1: Displacement and velocity time history input (from 1940 El Centro earthquake).

ness that fluctuates much more with increasing frequency than for single piles. Moreover, the "peaks" and "valleys" of the dynamic stiffness of pile groups depend on the geometrical configuration of the pile group. Accordingly, even if an approximate analytical solution were possible, the parameters of the model would be different for every pile-group configuration, rendering such an approach rather difficult to implement.

Herein, the numerical evaluation of the basic response function of piles and pile groups is studied, and alternative techniques to bypass numerical singularities are presented. As an illustrative example, the time domain response of a 2x2 pile group is examined. The massless pile-cap is subjected to an induced transient motion. For simplicity, the selected motion is that of the 1940 El Centro earthquake, whose displacement u_g and velocity $\dot{u}_g$ time histories are shown in figure 3.1. It should be noted that, in reality, the

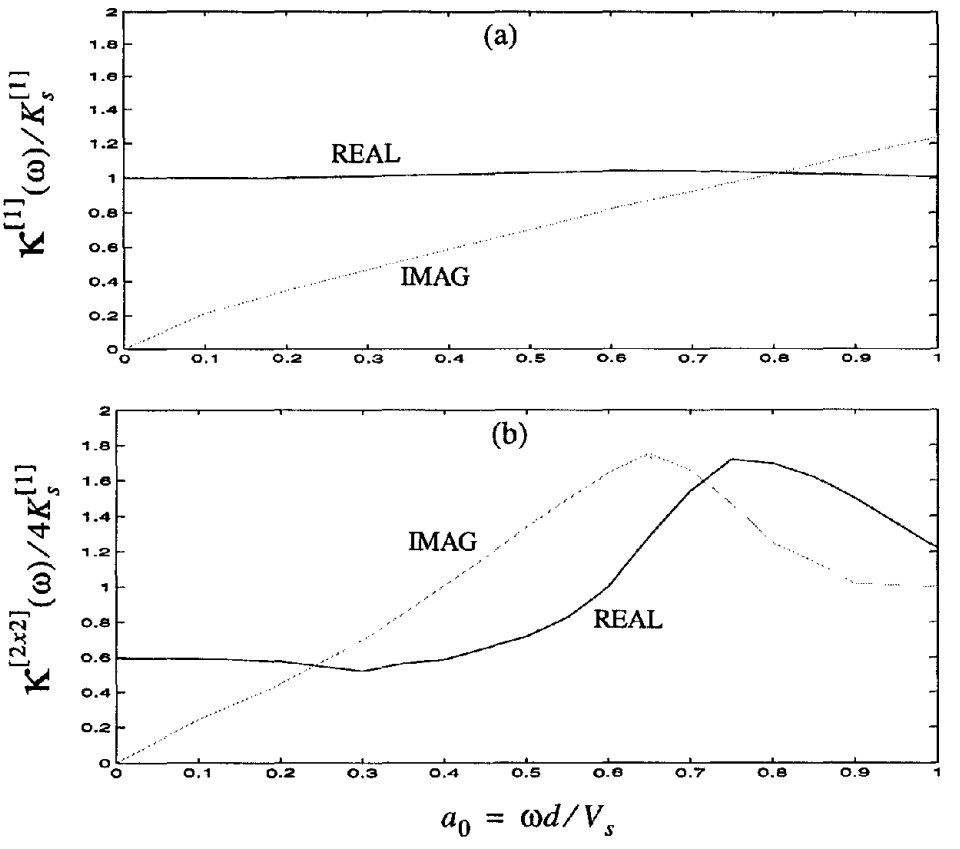

Figure 3.2: Dynamic horizontal stiffness factors as a function of dimensionless frequency for single pile (a) and 2x2 square group (b) with rigid pile-cap ($s/d = 5$; $E_p/E_s = 1000$; $\rho_p/\rho_s = 1.42$; $L/d = 15$; $\beta_s = 0.05$; $\nu = 0.4$).

pile-cap has a finite mass and its motion would be the result of an analysis including the pile-cap mass as well as the superstructure dynamics. The integrated dynamic analysis of such a system is presented in a subsequent section. Herein, the El Centro motion is selected only to examine the numerical performance of the proposed procedure under a realistic transient input. The memory function, $M(t)$, given by (3.3), is numerically computed using the dynamic stiffnesses from Kaynia and Kausel (1982) (Figure 3.2 (b)). This memory function is then used in the convolution integral equation (3.2) to compute the resulting force history which is plotted in Figure 3.3. It is compared against the "exact" solution obtained with the inverse Fourier transform given by (3.1). The prediction of the convolution integral is poor. The time-domain solution is inaccurate because of the singu-

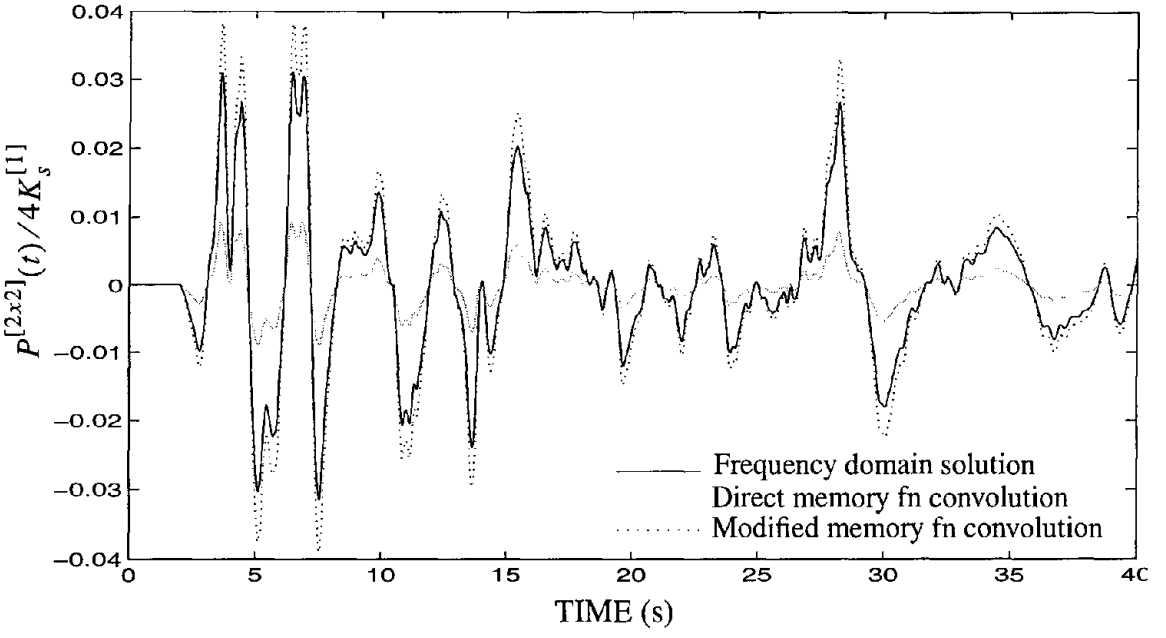

Figure 3.3: Accuracy of memory function convolution to solve the problem of a 2x2 pile group under an induced earthquake input.

larity in the memory function at the time origin mentioned previously. One way to bypass this difficulty is to express the dynamic stiffness $\mathcal{K}(\omega)$, of a pile-group as

$$\mathcal{K}(\omega) = K_s + i\omega C_o + \mathcal{K}_r(\omega) \tag{3.4}$$

where K_s is the (real-valued) static stiffness, C_o is the zero-frequency damping coefficient and $\mathcal{K}_r(\omega)$ represents the regular part of the dynamic stiffness which is absolutely integrable over the ω-axis.

Substituting (3.4) into (3.3) and breaking the integration one obtains

$$M(t) = K_s\delta(0-t) + C_o\dot{\delta}(0-t) + \frac{1}{2\pi}\int_{-\infty}^{\infty} \mathcal{K}_r(\omega)e^{i\omega t}d\omega \tag{3.5}$$

where the singularity of the memory function, $M(t)$, is lumped in the first two terms in which $\delta(0-t)$ is the Dirac delta function (Lighthill 1989). The third term, the inverse Fourier transform of $\mathcal{K}_r(\omega)$, can be more accurately computed with established FFT routines (IMSL 1987). Denoting this term by $M_r(t)$, we may write:

$$M_r(t) = \frac{1}{2\pi}\int_{-\infty}^{\infty} \mathcal{K}_r(\omega)e^{i\omega t}d\omega \tag{3.6}$$

and after using equations (3.5) and (3.2), the time-domain response of the pile-cap of a pile group is simply

$$P(t) = K_s u(t) + C_o \dot{u}(t) + \int_{-\infty}^{t} M_r(t-\tau)u(\tau)d\tau \tag{3.7}$$

This formulation gives better results than equation (3.2) as shown in Figure 3.3. Clearly, there is still a discrepancy in time and frequency domain results due to the nature of the regular part of the dynamic stiffness, which fluctuates considerably at the higher end of the frequency range of interest.

In the above numerical example, the maximum frequency present in the Fourier spectrum of the El Centro input motion is $\omega_{max} = \pi/\Delta t = 157.08$ rad/sec, where Δt=0.02 sec is the time step interval of the recorded input motion. Since the dynamic stiffness of the pile group from the Kaynia and Kausel plots is available only up to $a_{0,\max} = \omega d/V_s = 1.0$, the ratio V_s/d required to cover the entire frequency range present in the seismic input is V_s/d =157.08 rad/s (given by the Nyquist frequency = $\pi/\Delta t$ rad/s). This is indeed a realistic value (i.e., V_s = 80 m/sec, d=0.5 m). For values of $V_s/d < 157.08$ rad/sec, the high-frequency components of the seismic input will not be present in the response, unless the dynamic stiffness of the pile group is available at values of $a_{0,\max} > 1.0$. For example, if V_s/d =50 rad/sec and $a_{0,\max} = 1.0$, only the frequencies up to 8 Hz of the seismic input will participate in the response analysis of the system. For analysis of bridges which are flexible structures, 8Hz is a reasonable value. However, in cases where the superstructure is stiff (e.g., a nuclear power plant), the knowledge of the dynamic stiffness of piles at dimensionless frequencies $a_{0,\max} > 1.0$ might be needed.

Besides equation (3.2) or (3.7), the time domain response of a pile-foundation can be expressed through an alternative convolution integral. This alternative convolution integral relates the force, $P(t)$, at the present time t, with the entire velocity history $\dot{u}(\tau) = du(\tau)/d\tau$, $-\infty < \tau \leq t$.

$$P(t) = \int_{-\infty}^{t} K(t-\tau)\dot{u}(\tau)d\tau \tag{3.8}$$

where $K(t-\tau)$ is the relaxation stiffness of the pile group and is defined as the resulting force at the present time t, for a unit step displacement at time τ,.$(\tau \leq t)$

The relaxation stiffness $K(t)$ (symbolized with a times roman K) is a time-domain representation of the mechanical behavior of a system, and is directly related with the dynamic stiffness (symbolized with a calligraphic $\mathcal{K}$) by the relation

$$K(t) = \frac{1}{2}\mathcal{K}(0) + \frac{1}{2\pi}\int_{-\infty}^{\infty} \frac{\mathcal{K}(\omega)}{i\omega} e^{i\omega t} d\omega \tag{3.9}$$

where $\mathcal{K}(0) = K_s$ is the static stiffness of the system (Makris 1995).

Furthermore, the static stiffness term can be factored out of the dynamic stiffness to give

$$K(t) = \frac{1}{2}\mathcal{K}(0) + \frac{1}{2}sgn(t)\mathcal{K}(0) + \frac{1}{2\pi}\int_{-\infty}^{\infty} \frac{\mathcal{K}_d(\omega)}{i\omega} e^{i\omega t} d\omega \tag{3.10}$$

(Makris 1997a) where

$$\mathcal{K}_d(\omega) = \mathcal{K}(\omega) - \mathcal{K}(0). \tag{3.11}$$

Since we are only concerned with $t > 0$, this may be written as

$$K(t) = \mathcal{K}(0) + \frac{1}{2\pi}\int_{-\infty}^{\infty} \frac{\mathcal{K}_d(\omega)}{i\omega} e^{i\omega t} d\omega \tag{3.12}$$

If $K_d(t)$ denotes the second term in (3.12) for a pile group,

$$K_d(t) = \frac{1}{2\pi}\int_{-\infty}^{\infty} \frac{\mathcal{K}_d(\omega)}{i\omega} e^{i\omega t} d\omega \tag{3.13}$$

then, using (3.9) and (3.8), the resulting force from a pile-group is also

$$P(t) = K_s u(t) + \int_{-\infty}^{t} K_d(t-\tau)\dot{u}(\tau) d\tau \tag{3.14}$$

where $K_s = \mathcal{K}(0)$ is the real-valued static stiffness of the pile group. Note that for models with frequency independent hysteretic damping, this is not strictly true, since $\mathcal{K}(0)$ is not real. For the scope of this study, causality is assumed to be implied.

Equation (3.14) is an alternative time-domain expression for the pile foundation response, which gives much better results than (3.7). This is explained by the nature of the dynamic impedance $\mathcal{K}_d(\omega)/i\omega$, which decays with increasing frequency more strongly than $\mathcal{K}_r(\omega)$. The prediction of the time domain solution obtained with (3.14) is depicted in figure 3.4, where the response is compared against the "exact" solution obtained with the inverse Fourier Transform given by (3.1). A very good agreement is obtained between the two methods for this formulation.

It is interesting to note that the first term in equation (3.14) represents the purely elastic part of the reaction force from the pile group. The second term represents the "fading" memory of the pile group, which is the result of (a) the fluctuations of the group dynamic stiffness about the static stiffness and (b) damping.

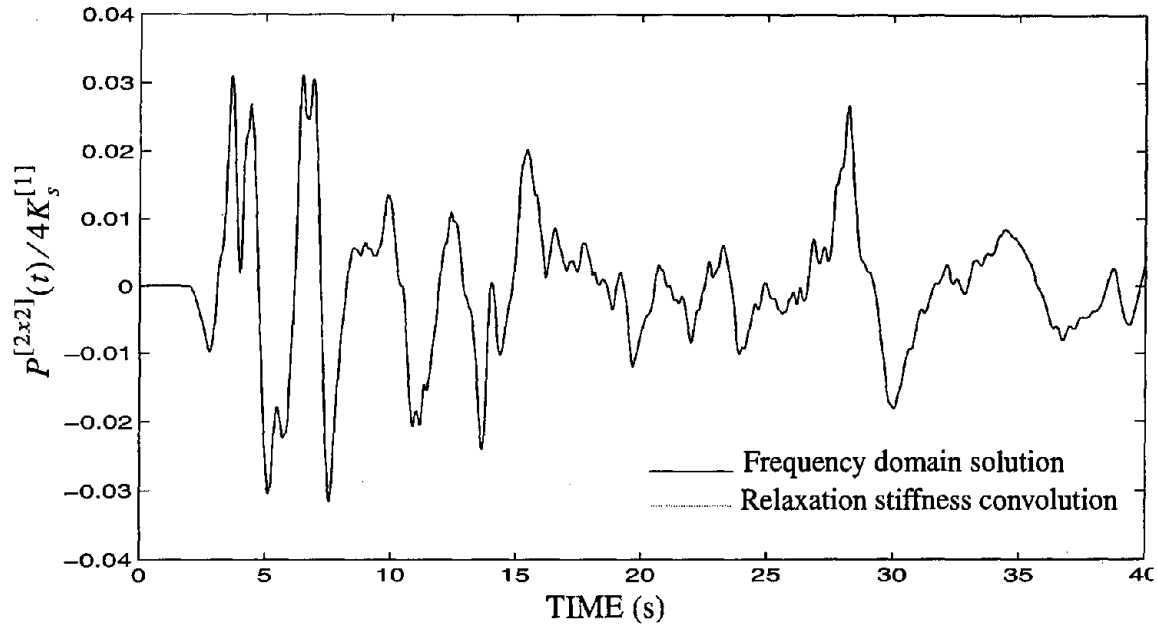

Figure 3.4: Accuracy of relaxation stiffness convolution in the problem of a 2x2 pile group under an induced earthquake excitation.

3.2 Dynamic relaxation stiffnesses of pile foundations

This section illustrates the nature of dynamic relaxation stiffnesses for pile groups as computed numerically using equation (3.12). The model chosen to compute foundation dynamic stiffnesses is one proposed by Makris & Gazetas (1992). The authors presented an approximate analytical model to estimate the lateral response to inertial loading of single piles and pile groups in a homogeneous half-space. The single pile model was a linear elastic beam on a Winkler foundation with frequency dependent coefficients. The procedure essentially involves solving the harmonic steady state equation for the system under an applied load P_0, given by

$$E_p I_p \frac{d^4}{dz^4} U(z) + (k_x + i\omega c_x - m\omega^2) U(z) = 0 \qquad (3.15)$$

with $k_x = 1.2E_s$ and $c_x = 6a_0^{-1/4}\rho_s V_s d + 2\beta_s k_x/\omega$, along with the appropriate boundary conditions, such as those below, for the case of a fixed-head floating pile

$$\frac{d}{dz}U(0) = 0;\ E_p I_p \frac{d^3}{dz^3}U(0) = P_0;\ \frac{d^2}{dz^2}U(L) = 0;\ \frac{d^3}{dz^3}U(L) = 0 \qquad (3.16)$$

The dynamic stiffness is simply given by

$$K(\omega) = \frac{P_0}{U(0)} \qquad (3.17)$$

Here, d, E_p, I_p, ρ_p and m are the diameter, Young's Modulus, second moment of inertia, mass density and mass per unit length of the pile, respectively. E_s, V_s, β_s and ρ_s are the Young's Modulus, shear wave velocity, damping ratio and mass density of the soil. These single pile stiffnesses can then be used to get pile group dynamic stiffnesses according to the method already discussed in section 2.2.2.

Figure 3.5 shows the dynamic stiffnesses (normalized with respect to static stiffness) of a single pile as a ratio of dimensionless frequency, a_0, for a single pile with $E_p/E_s = 1000$, $\rho_p/\rho_s = 1.42$, $L/d = 15$ $\beta_s = 0$ and $\nu = 0.49$ along with the corresponding dynamic relaxation stiffness (also normalized and shown as a function of dimensionless time ξ) obtained using a 1024 point FFT. The result closely resembles a delta-function, which is expected, since the single-pile model is in fact close to a Kelvin model within the frequency range taken. To illustrate the effect of frequency independent hysteretic damping, a case with $\beta_s = 0.05$ is also shown. This clearly leads to a non-causal response. In fact, the relaxation stiffness arising out of this term is symmetric about $\xi = 0$, and varies as the natural logarithm of ξ (Makris 1997a). A new causal hysteretic model has been recently proposed by Makris (1997b) to account for this behavior, but is beyond the scope of this study.

Figures 3.6, 3.7 and 3.8 depict the normalized (with respect to mxn times the single pile static stiffness) relaxation stiffnesses obtained for pile groups of different configurations with the parameters $E_p/E_s = 1000$, $\rho_p/\rho_s = 1.42$, $L/d = 15$ $\beta_s = 0$,

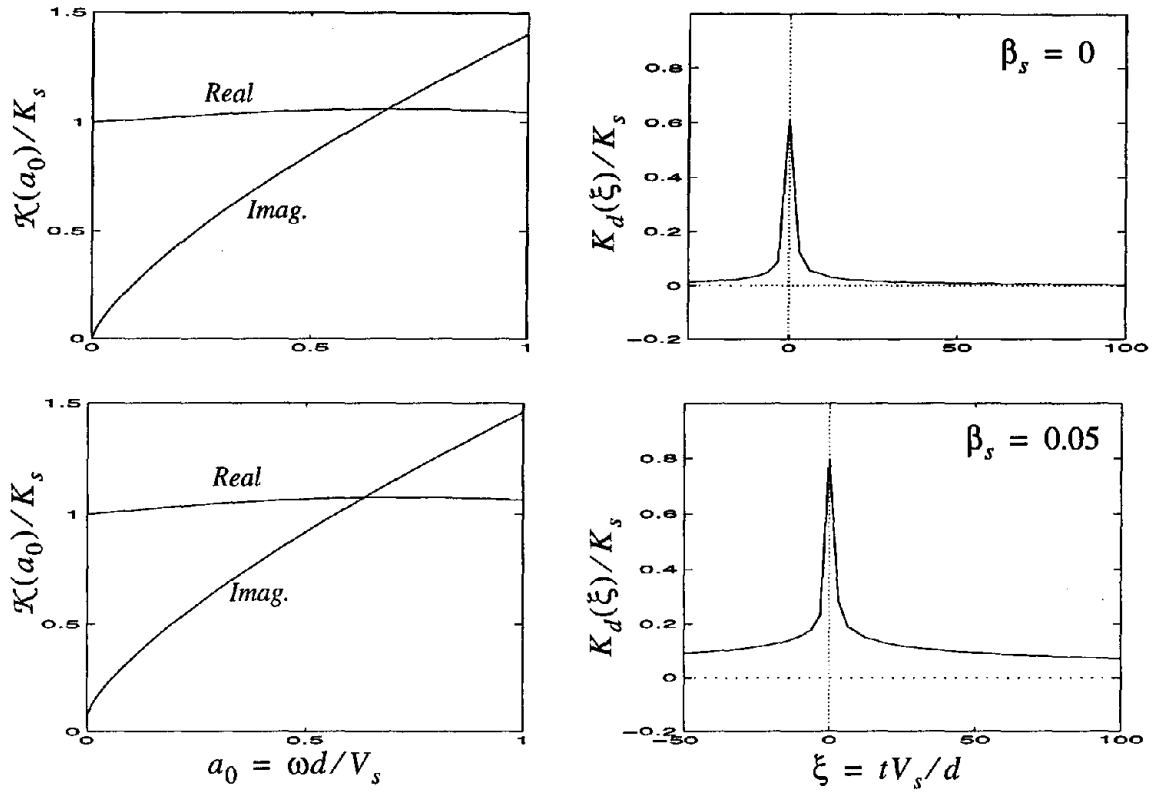

Figure 3.5: Dynamic relaxation stiffnesses for single pile model of Makris and Gazetas (1992).

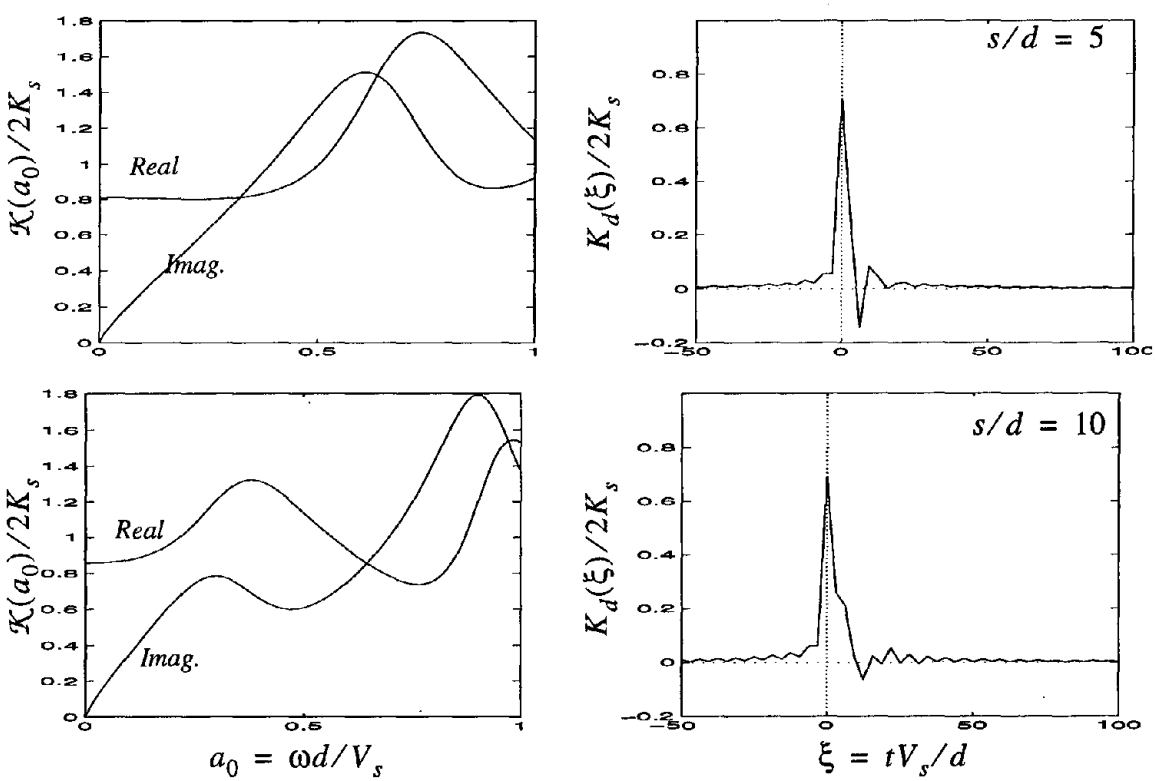

Figure 3.6: Dynamic relaxation stiffnesses for 1x2 pile group model of Makris and Gazetas (1992).

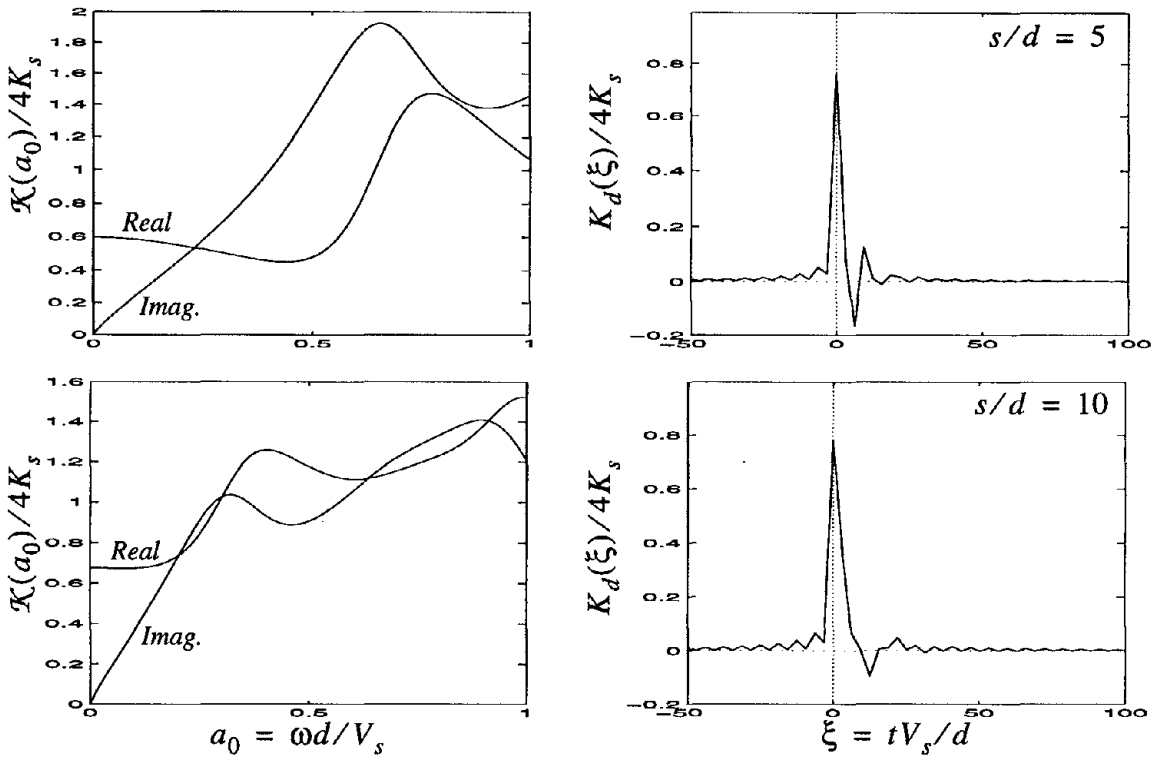

Figure 3.7: Dynamic relaxation stiffnesses for 2x2 pile group.

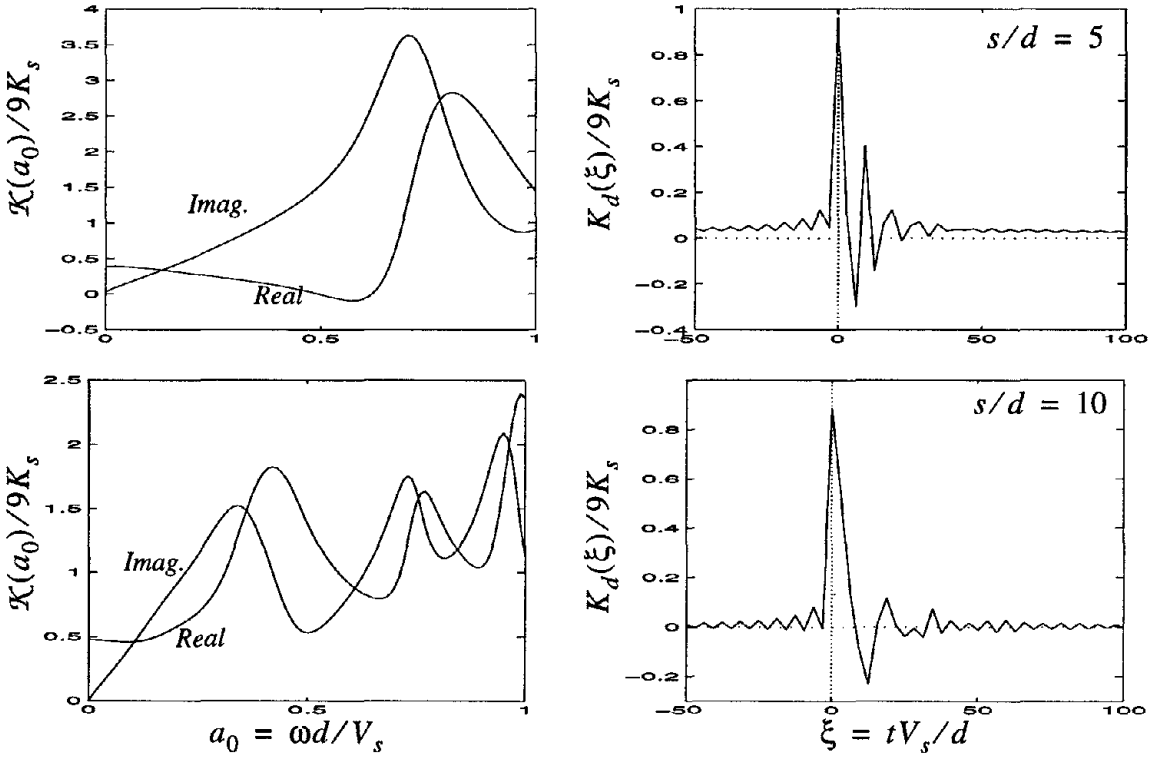

Figure 3.8: Dynamic relaxation stiffnesses for 3x3 pile group.

and spacing-to-diameter ratios as labelled in the respective figures. Clearly, there is significant "memory", especially for the higher spacings. This is in contrast to the single pile behavior which primarily behaves as a Kelvin model, at least for the case of no hysteretic damping.

3.3 Validation of proposed convolution integral approach for a linear system

In the previous section, the convolution integral method for time-domain analysis of pile foundations was presented for a massless pile-cap under an induced earthquake excitation. However, it is necessary to include the inertial effects of the superstructure in the total response of the system, since it can substantially modify the behavior of the pile foundation itself, making dynamic effects much more significant.

The problem studied herein is a simple two-degree-of-freedom system supported on a complex-valued foundation spring and excited by an earthquake ground motion, as illustrated in Figure 3.9. The complex valued foundation stiffness in the frequency domain is given by $\mathcal{K}_f(\omega)$, while the restoring force of the spring in the time domain is given by

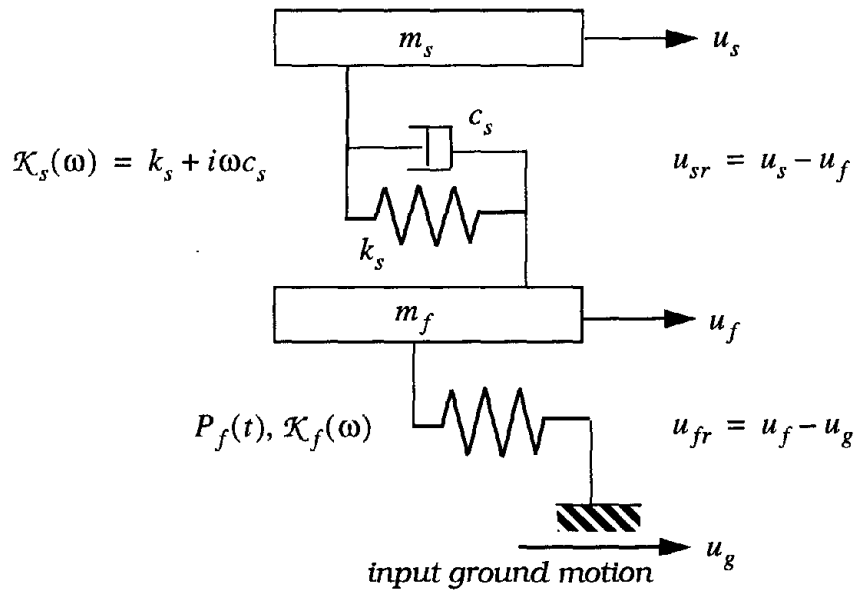

Figure 3.9: Simple linear two d.o.f. model to validate the convolution integral approach.

$P_f(t)$. The state variables selected for the analysis, the relative displacements u_{sR} and u_{fR}, are also shown in the figure.

3.3.1 Frequency domain governing equations

The transfer functions between ground acceleration $\ddot{u}_g$ and the aforementioned relative displacements in the frequency domain are obtained as:

$$\frac{u_{sr}(\omega)}{\ddot{u}_g(\omega)} = \frac{-\mathcal{K}_f(\omega)m_s}{[(\mathcal{K}_s(\omega)-m_s\omega^2)(\mathcal{K}_f(\omega)-m_f\omega^2)-\mathcal{K}_s(\omega)m_f\omega^2]} \tag{3.18}$$

$$\frac{u_{fr}(\omega)}{\ddot{u}_g(\omega)} = \frac{m_f m_s\omega^2-\mathcal{K}_s(\omega)(m_s+m_f)}{[(\mathcal{K}_s(\omega)-m_s\omega^2)(\mathcal{K}_f(\omega)-m_f\omega^2)-\mathcal{K}_s(\omega)m_f\omega^2]} \tag{3.19}$$

The accelerations may be obtained using the relations $\ddot{u}_{sr}(\omega) = -\omega^2 u_{sr}(\omega)$ and $\ddot{u}_{fr}(\omega) = -\omega^2 u_{fr}(\omega)$.

3.3.2 Time domain equations of motion

The equations of motion for the system may be written as:

$$\ddot{u}_{sr}(t) + c_s\left(\frac{1}{m_f}+\frac{1}{m_s}\right)\dot{u}_{sr}(t) + k_s\left(\frac{1}{m_f}+\frac{1}{m_s}\right)u_{sr}(t) = \frac{P_f(t)}{m_f} \tag{3.20}$$

$$\ddot{u}_{fr}(t) - \frac{c_s}{m_f}\dot{u}_{sr}(t) - \frac{k_s}{m_f}u_{sr}(t) = \frac{-P_f(t)}{m_f} - \ddot{u}_g(t) \tag{3.21}$$

where the restoring force from the foundation spring is given by:

$$P_f(t) = \mathcal{K}_f(0)u_{fr}(t) + \int_{-\infty}^{t} K_d(t-\tau)\dot{u}_{fr}(\tau)d\tau \tag{3.22}$$

K_d, the dynamic relaxation stiffness is obtained from:

$$K_d(t) = \frac{1}{2\pi}\int_{-\infty}^{\infty}\frac{\mathcal{K}_f(\omega)-\mathcal{K}_f(0)}{i\omega}e^{i\omega t}d\omega \tag{3.23}$$

Clearly, the above system of equations is coupled, and no explicit solution is possible. The scheme utilized herein is a fifth-order Runge-Kutta method with fourth-order step-size control. In this scheme, the convolution integral needs to be calculated at each of the intermediate time steps. The analysis is carried out using the Simulink utility in Matlab.

3.3.3 Results

The values of the foundation and superstructure parameters were taken from the Painter Street bridge analysis discussed in chapter 2. Accordingly, m_s = 1000 Mg, m_f = 225 Mg, $k_s = 5.69 \times 10^5$ kN/m, modal damping ratio ζ = 0.05. The dynamic foundation stiffnesses shown in figure 3.10 were obtained by multiplying the dynamic stiffness factors for the two 4x5 pile groups, shown in figure 2.6, with the appropriate single-pile static stiffness of $K_s^{[1]}$ = 65 MN/m. Other parameters needed were the pile

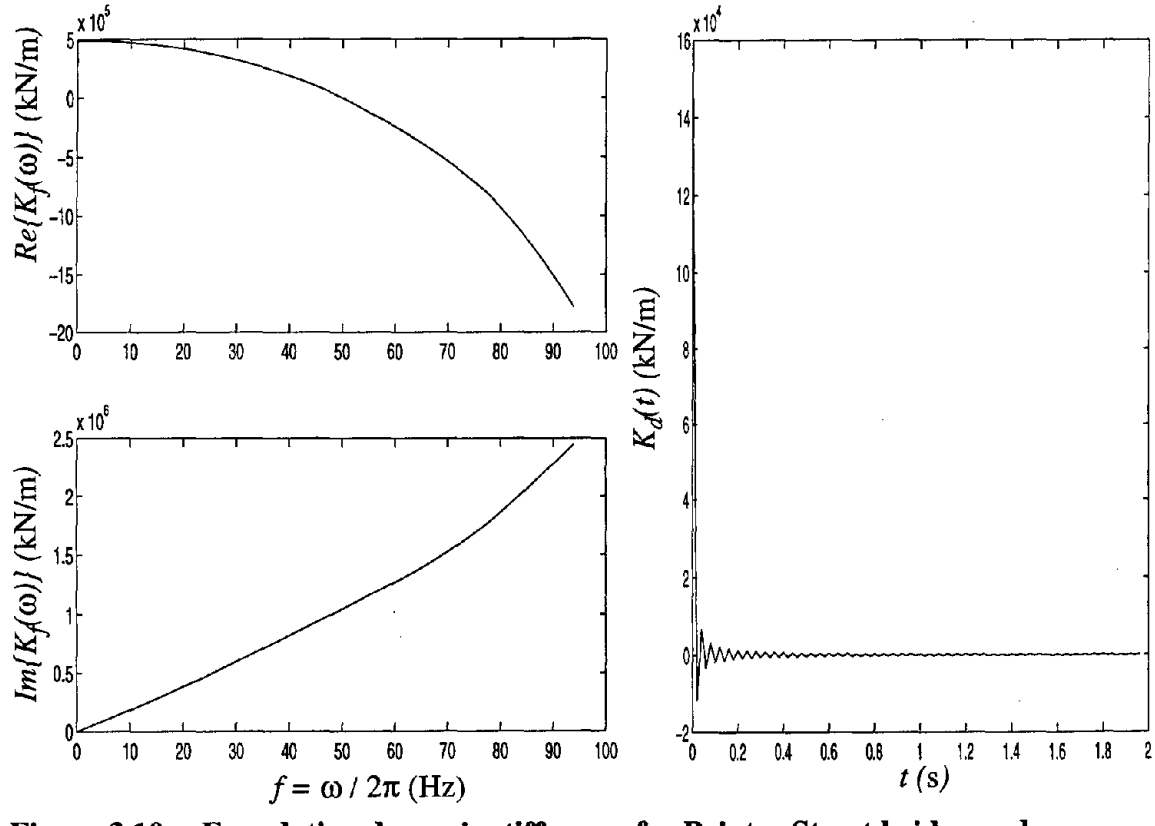

Figure 3.10: Foundation dynamic stiffnesses for Painter Street bridge and corresponding dynamic relaxation stiffness.

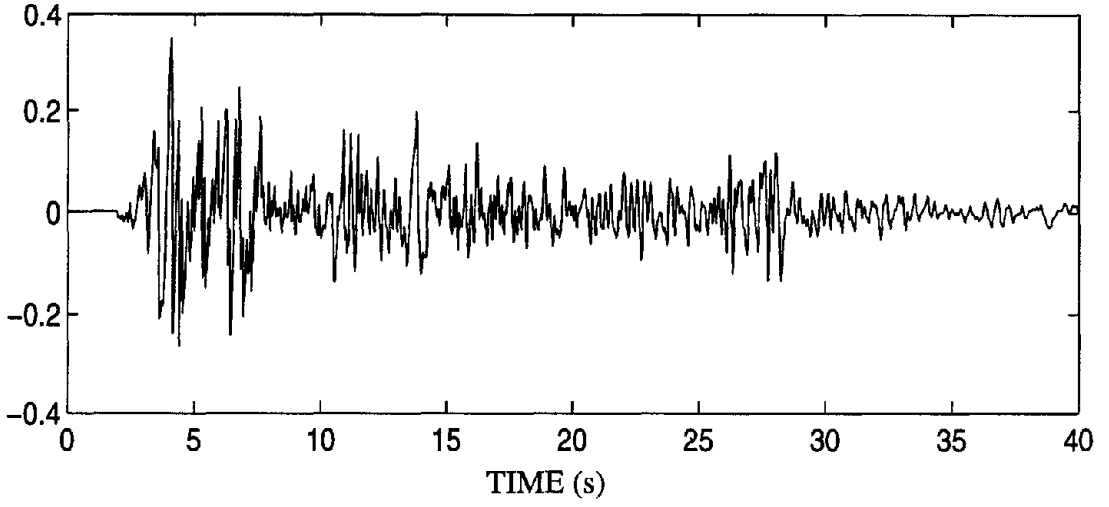

Figure 3.11: Ground acceleration input (from 1940 El Centro earthquake).

diameter, d = 0.36 m, and the shear-wave velocity, V_s = 250 m/s. The corresponding dynamic relaxation stiffness (obtained using a 1024 point fast Fourier transform) is also shown in the figure. Notice that the relaxation stiffness resembles a numerical delta function, which implies that the foundation damping coefficient is close to a constant. This can also be verified from the loss stiffness plot in figure 3.10. This actually represents a numerical worst case scenario for analysis, and is therefore a good example problem to validate the accuracy of the proposed procedure.

The input motion for the analysis was the 1940 El Centro earthquake, whose acceleration time history (*i.e.*, for the first 40s) is depicted in figure 3.11. The time step used for the analysis was 0.02s. Figure 3.12 shows the comparison between time and frequency domain solutions for both the deck drift u_{sr} and the foundation relative displacement u_{fr}, as well as the absolute accelerations at the two levels. The results are clearly in excellent agreement. The convolution integral approach can now be extended to a nonlinear analysis, which is discussed in the subsequent section.

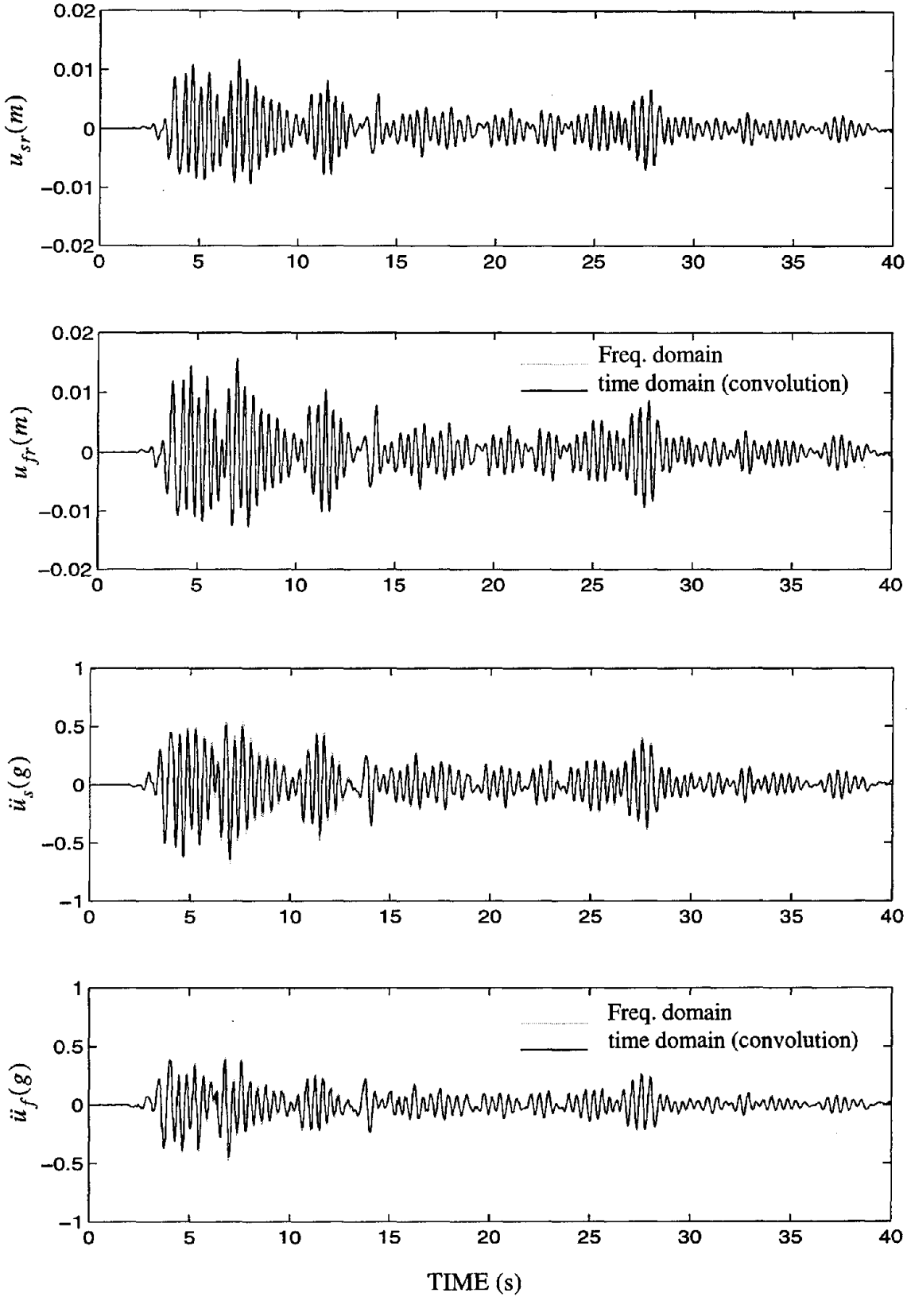

Figure 3.12: Comparison of frequency vs. time domain formulations for linear model.

3.4 The nonlinear superstructure linear- foundation interaction problem

As mentioned earlier, considerable advancements have been made in the nonlinear modeling of R/C structures such as are found in most bridge superstructures. An enhanced modeling scheme using a member-by-member modeling approach was proposed by Kunnath *et al.* (1990), which removed many of the drawbacks of older macro-models, thus substantially increasing the precision of analytical predictions. However, this scheme has so far been confined to the study of buildings, where foundations do not contribute to the system response. Hence it cannot be applied in the modeling of structures where foundation properties influence the structural dynamics without resorting to the kind of technique proposed in this section.

A recent paper by Ciampoli and Pinto (1995) investigated the relevance of soil-structure effects to the dynamic response of bridge piers on spread footing responding in the inelastic range. They modeled the problem as a vertical cantilever carrying a mass at the top. Inelasticity of the superstructure was modeled by prescribing a plastic hinge zone at the base of the cantilever, with a prescribed moment-curvature relationship. The foundation dynamic stiffnesses were obtained from analytical results (Gazetas 1983). However, the authors then derived equivalent viscous and hysteretic damping coefficients to model foundation response, justifying it by the nature of the dynamic stiffnesses over the frequency range of interest. Hence the proposed method has limited applicability. This type of problem can be better analyzed with the convolution integral method as illustrated in the next section.

3.4.1 Nonlinear analysis model

Figure 3.13 illustrates the model to be used for this analysis. In this case, the superstructure and foundation are connected with a nonlinear spring, which is governed by the

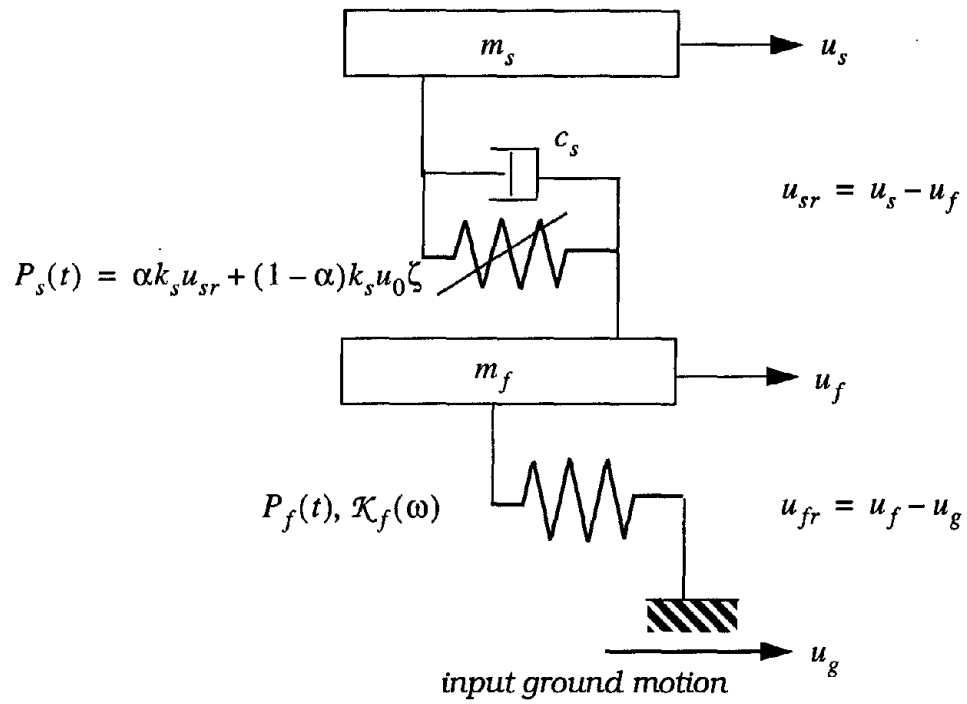

Figure 3.13: Simple model to study nonlinear-superstructure-linear-foundation interaction.

Bouc-Wen model constitutive equation. The restoring force in the spring, $P_s(t)$, is given as

$$P_s(t) = \alpha k_s u_{sr} + (1-\alpha) k_s u_0 \zeta \tag{3.24}$$

in which ζ (not to be confused with the modal damping ratio ζ_s for the superstructure) is governed by the nonlinear differential equation

$$u_0 \dot{\zeta} + \gamma |\dot{u}_{sr}| \zeta |\zeta|^{n-1} + \beta \dot{u}_{sr} |\zeta|^n - A \dot{u}_{sr} = 0 \tag{3.25}$$

in which β, γ, n and A are dimensionless quantities that control the shape of the hysteretic loop. The hysteretic model of (3.24) and (3.25) was originally proposed by Bouc (1967) for n = 1, and subsequently extended by Wen (1975, 1976), and used in random vibration studies of nonlinear systems. The formulation presented herein is different in that all the model parameters except k_s and u_0 are dimensionless.

One may eliminate the time variable in equation (3.25) to obtain

$$u_0 \frac{d\zeta}{du_{sr}} = A \pm (\beta \pm \gamma)\zeta^n \tag{3.26}$$

in which the $\pm$ sign depends on whether the values of $\dot{y}$ and ζ are positive or negative. The initial condition $\zeta(0) = 0$ implies that at $t = 0$,

$$u_0 \frac{d\zeta(t)}{du_{sr}(t)}\bigg|_{t=0} = A \tag{3.27}$$

Also, differentiating equation (3.24) with respect to u_{sr} gives

$$\frac{dP_s(t)}{du_{sr}(t)} = \alpha k_s + (1-\alpha)k_s u_0 \frac{d\zeta(t)}{du_{sr}(t)} \tag{3.28}$$

which implies that at $t = 0$,

$$\frac{dP_s(t)}{du_{sr}(t)}\bigg|_{t=0} = \alpha k_s + (1-\alpha)k_s A \tag{3.29}$$

From equation (3.29), it is easy to see that if $A = 1$ then k_s becomes the initial stiffness of the spring. Also note that, for a monotonic displacement input, the maximum value of ζ is obtained when $d\zeta/du_{sr} = 0$, and as such

$$\frac{dP_s(t)}{du_{sr}(t)}\bigg|_{\max} = \alpha k_s \tag{3.30}$$

Hence, α can be viewed as a post-yielding-to-pre-yielding stiffness ratio. Based on this observation, in the subsequent nonlinear analyses, the parameter $A = 1$. By virtue of (3.26), the maximum value of ζ is given by

$$\zeta_{\max} = \left(\frac{A}{\beta + \gamma}\right)^{1/n} \tag{3.31}$$

Thus, if $\beta + \gamma = 1$, then the hysteretic variable ζ lies in the range $-1 < \zeta < 1$, which is a convenient formulation extensively used in base isolation studies (Constantinou and Adnane 1987).

The ratio β/γ controls the shape of the unloading curves, while n controls the sharpness of transition from the linear-to-nonlinear range, with large values of n corresponding to bilinear behavior.

The equations of motion for this system can now be written as

$$\ddot{u}_{sr}(t) + c_s\left(\frac{1}{m_f} + \frac{1}{m_s}\right)\dot{u}_{sr}(t) + \alpha k_s\left(\frac{1}{m_f} + \frac{1}{m_s}\right)u_{sr}(t) + (1-\alpha)k_s u_0\left(\frac{1}{m_f} + \frac{1}{m_s}\right)\zeta(t) + (1-\alpha)k_s u_0\left(\frac{1}{m_f} + \frac{1}{m_s}\right)\zeta(t) = \frac{P_f(t)}{m_f} \tag{3.32}$$

$$\ddot{u}_{fr}(t) - \frac{c_s}{m_f}\dot{u}_{sr}(t) - \alpha\frac{k_s}{m_f}u_{sr}(t) - (1-\alpha)\frac{k_s}{m_f}u_0\zeta(t) = \frac{-P_f(t)}{m_f} - \ddot{u}_g(t) \tag{3.33}$$

where $P_f(t)$ is given by equation (3.22). The method of solution is the same as that for the linear problem, *i.e.*, a fifth order Runge-Kutta integration scheme.

3.4.2 Validation of nonlinear model

The parameters for the Bouc-Wen model that govern the behavior of the nonlinear spring were first chosen as: $\alpha = 0$, $u_0 = 0.02m$, $A = 1$, $\beta = 0.5$, $\gamma = 0.5$ and $n = 10$. The chosen large value for n ensures that the spring behaves elastically, and the chosen u_0 ensures that the yield limit is not reached, as can be seen from figure 3.14. In this limiting case, the behavior of the system is expected to be linear, and the comparison shown in figure 3.16 proves that this is indeed the case.

Having validated the nonlinear formulation at the linear limit, the value of n is changed to $n = 1$ to provide a smoother transition to the yield limit. This could possibly represent yielding of the column or formation of a plastic hinge at the pile cap. The corresponding spring force-displacement loops are shown in figure 3.15, and the resulting relative displacement and absolute acceleration time histories in figure 3.17. The time step used for both the analyses was 0.02s. The drifting behavior of the deck, characteristic of a

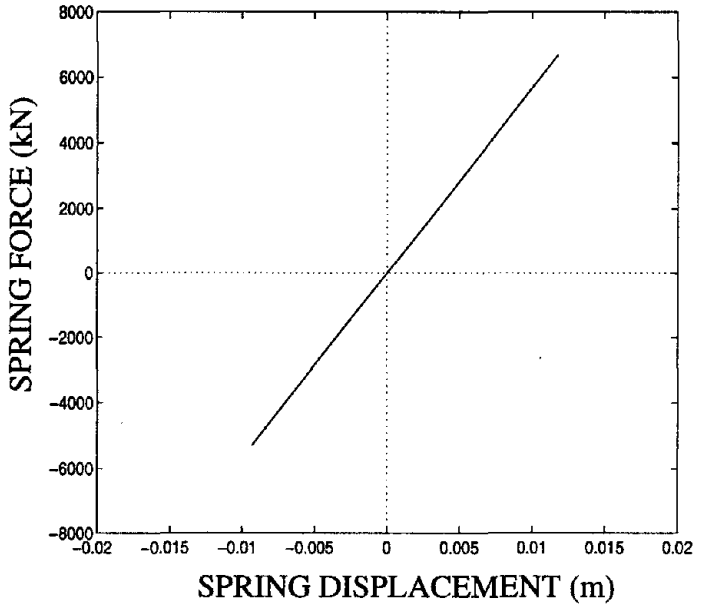

Figure 3.14: Force-displacement behavior of nonlinear spring with $\alpha = 0$, $u_0 = 0.02$ m, $A = 1$, $\beta = 0.5$, $\gamma = 0.5$ and $n = 10$.

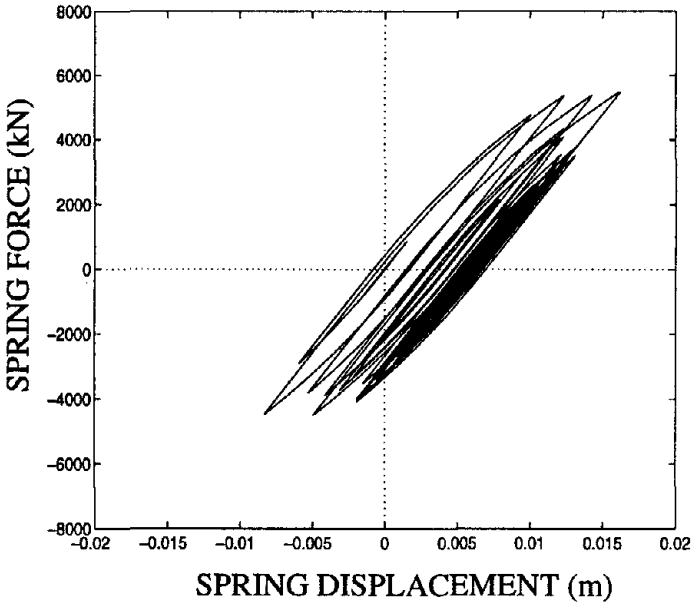

Figure 3.15: Force-displacement behavior of nonlinear spring with $\alpha = 0$, $u_0 = 0.02$ m, $A = 1$, $\beta = 0.5$, $\gamma = 0.5$ and $n = 1$.

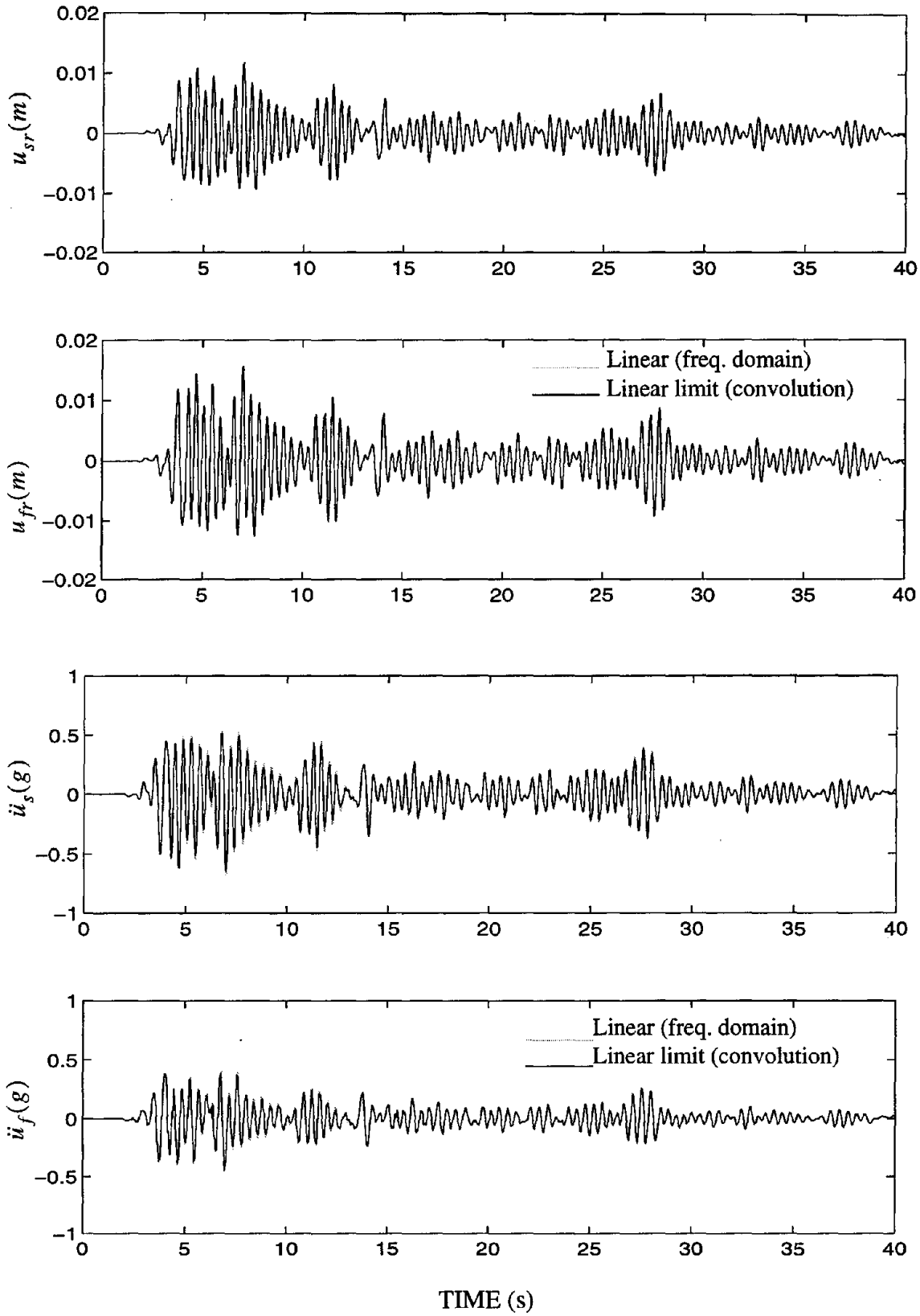

Figure 3.16: Comparison of nonlinear model response at the linear limit (u_0 = 0.02 m, n = 10) vs. frequency domain results.

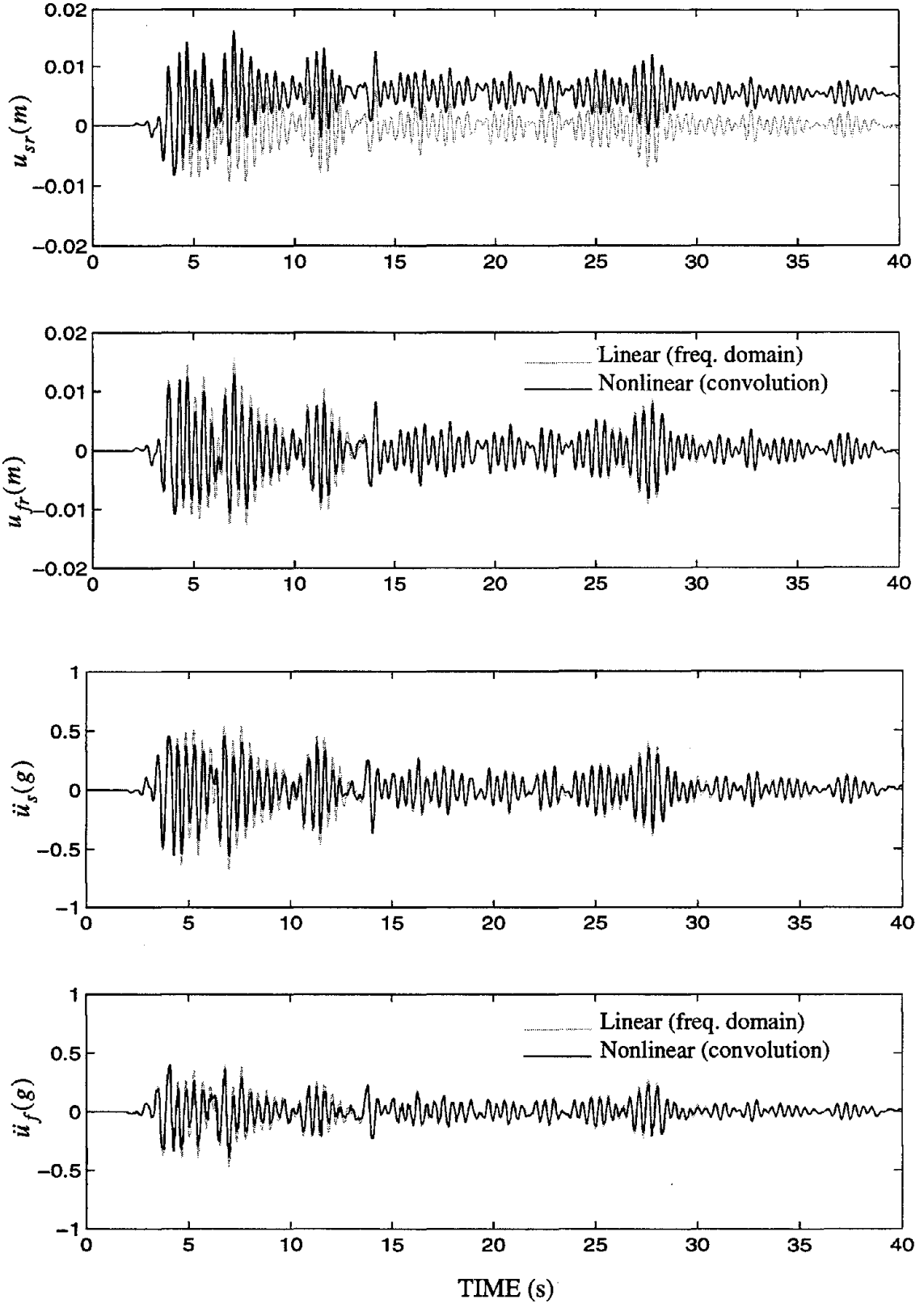

Figure 3.17: Nonlinear system response for n=1.

non-self-centering system, is clearly observed. It is clear that the reduced accelerations result in reduced inertial loading from the superstructure, which reduces foundation relative motion. This implies that yielding of the superstructure reduces the inertial forces on the foundation, and if these forces fall within or are close to the linear range of foundation response, the use of linear or equivalent linear foundation models can be justified.

3.5 The state-space realization approach

An alternative approach to the solution of the same problem is considered in this section. The theory of obtaining a state-space formulation is well established, and it is a widely used technique for vibration analysis and system identification. Herein, the method is formulated for a two-degree-of-freedom superstructure resting on a linearly behaving foundation with dynamic stiffnesses specified within a given frequency range. The proposed model also serves the useful purpose of assessing the accuracy of the convolution integral approach proposed in the previous section.

3.5.1 Development of state-space equations

The approach involves four basic steps:

1) Approximate the provided dynamic stiffnesses of the foundation subsystem as a ratio of two polynomials to a desired accuracy,
2) obtain a state-space realization for the approximated subsystem,
3) obtain state-space matrices for superstructure, and
4) link the state-space matrices of the foundation with that of the superstructure and solve the resulting system for the given input.

Step 1: Rational polynomial approximation for dynamic stiffness

The provided dynamic stiffness for the foundation, $\mathcal{K}_f(i\omega)$, may be approximated by $\overline{\mathcal{K}}_f(i\omega)$, a ratio of two polynomials in $i\omega$, written as

$$\mathcal{K}_f(\omega) \approx \overline{\mathcal{K}}_f(i\omega) = \frac{P(i\omega)}{Q(i\omega)}$$
$$= \frac{p_0 + p_1(i\omega) + p_2(i\omega)^2 + \ldots + p_{M-1}(i\omega)^{M-1} + p_M(i\omega)^M}{q_0 + q_1(i\omega) + q_2(i\omega)^2 + \ldots + q_{N-1}(i\omega)^{N-1} + (i\omega)^N} \quad (3.34)$$

where the coefficients p_i and q_i are real and may be determined using an appropriate least-squares curve fitting technique for complex functions. This approximation has also been discussed in Wolf (1988) in the context of a recursive equation formulation in the frequency domain. The order of the numerator and denominator may be chosen depending on the accuracy of the resulting function, within the constraint $M < N$. It is also shown in the next section that this requirement may be relaxed to $M \leq N$ if an appropriate formulation is obtained.

Step 2: State-space representation for foundation substructure

The governing equation for the foundation subsystem in the frequency domain is

$$P_f(i\omega) = \mathcal{K}_f(i\omega) u_{fr}(i\omega) \quad (3.35)$$

which may be written in the approximated form as

$$P_f(i\omega) = \overline{\mathcal{K}}_f(i\omega) u_{fr}(i\omega) \quad (3.36)$$

Substituting for $\overline{\mathcal{K}}_f(i\omega)$ from equation (3.34) and defining the states for this system as

$$x(t) = \begin{bmatrix} x_1(t) \\ x_2(t) \\ x_3(t) \\ \vdots \\ x_N(t) \end{bmatrix} \quad (3.37)$$

a state-space realization for this system is (Rohrs, Melsa and Schultz 1993)

$$\dot{x}(t) = \begin{bmatrix} 0 & 1 & 0 & \cdots & 0 & 0 \\ 0 & 0 & 1 & \cdots & 0 & 0 \\ \vdots & \vdots & \vdots & \ddots & \vdots & \vdots \\ 0 & 0 & 0 & \cdots & 0 & 1 \\ -q_0 & -q_1 & -q_2 & \cdots & -q_{N-2} & -q_{N-1} \end{bmatrix} x(t) + \begin{bmatrix} 0 \\ 0 \\ \vdots \\ 0 \\ 1 \end{bmatrix} u_{fr}(t) \qquad (3.38)$$

$$P_f(t) = \begin{bmatrix} p_0 & p_1 & p_2 & \cdots & p_{M-1} & p_M & 0 & \cdots & 0 \end{bmatrix} x(t) \qquad (3.39)$$

or denoting by an appropriate matrix notation

$$\dot{x}(t) = A_f x(t) + B_f u_{fr}(t) \qquad (3.40)$$

$$P_f(t) = C_f x(t) \qquad (3.41)$$

Note that equation (3.41) above is for the case of a strictly proper $\overline{\mathcal{K}}_f(i\omega)$, with $M < N$. In the case where $M = N$, $\overline{\mathcal{K}}_f(i\omega)$ may be rewritten as

$$\overline{\mathcal{K}}_f(ia_0) = D_f + \frac{P_1(i\omega)}{Q_1(i\omega)} \qquad (3.42)$$

where the second term is again a strictly proper function. This leads to an additional term in equation (3.41), which may be written in a more general form as

$$P_f(t) = C_f x(t) + D_f u_{fr} \qquad (3.43)$$

It can be inferred that D_f is the static stiffness of the system.

Step 3: State-space representation for superstructure

The governing equations for the superstructure, as given by equations (3.32) and (3.33), may be written in state-space form as

$$\begin{bmatrix} \dot{Y}_1(t) \\ \dot{Y}_2(t) \\ \dot{Y}_3(t) \\ \dot{Y}_4(t) \end{bmatrix} = \begin{bmatrix} 0 & 1 & 0 & 0 \\ 0 & 0 & \alpha\dfrac{k_s}{m_f} & \dfrac{c_s}{m_f} \\ 0 & 0 & 0 & 1 \\ 0 & 0 & -\alpha\left(\dfrac{1}{m_f}+\dfrac{1}{m_s}\right)k_s & -\left(\dfrac{1}{m_f}+\dfrac{1}{m_s}\right)c_s \end{bmatrix} \begin{bmatrix} Y_1(t) \\ Y_2(t) \\ Y_3(t) \\ Y_4(t) \end{bmatrix}$$
$$+ \begin{bmatrix} 0 & 0 & 0 \\ -1 & -\dfrac{1}{m_f} & (1-\alpha)\dfrac{k_s}{m_f}u_0 \\ 0 & 0 & 0 \\ 0 & \dfrac{1}{m_f} & -(1-\alpha)\left(\dfrac{1}{m_f}+\dfrac{1}{m_s}\right)k_s u_0 \end{bmatrix} \begin{bmatrix} \ddot{u}_g(t) \\ P_f(t) \\ \zeta(t) \end{bmatrix} \tag{3.44}$$

where $Y_1 = u_{fr}$; $Y_2 = \dot{u}_{fr}$; $Y_3 = u_{sr}$; $Y_4 = \dot{u}_{sr}$. This is of the form

$$\dot{\boldsymbol{Y}}(t) = \boldsymbol{A}_s\boldsymbol{Y}(t) + \boldsymbol{B}_s\boldsymbol{U}(t) \tag{3.45}$$

where the input vector $\boldsymbol{U}(t)$ incorporates the foundation restoring force P_f (given by equation (3.43)) as well as the superstructure nonlinearity, contained in the term ζ, which is governed by the equation (obtained from equation (3.25) by replacing $\dot{u}_{sr}$ with Y_4)

$$u_0\dot{\zeta} + \gamma|Y_4|\zeta|\zeta|^{n-1} + \beta Y_4|\zeta|^n - AY_4 = 0 \tag{3.46}$$

Step 4: Integrated state-space representation

Equation (3.44) may be rewritten as

$$\begin{bmatrix} \dot{Y}_1(t) \\ \dot{Y}_2(t) \\ \dot{Y}_3(t) \\ \dot{Y}_4(t) \end{bmatrix} = \begin{bmatrix} 0 & 1 & 0 & 0 \\ 0 & 0 & \alpha\frac{k_s}{m_f} & \frac{c_s}{m_f} \\ 0 & 0 & 0 & 1 \\ 0 & 0 & -\alpha\left(\frac{1}{m_f}+\frac{1}{m_s}\right)k_s & -\left(\frac{1}{m_f}+\frac{1}{m_s}\right)c_s \end{bmatrix} \begin{bmatrix} Y_1(t) \\ Y_2(t) \\ Y_3(t) \\ Y_4(t) \end{bmatrix}$$

$$+ \begin{bmatrix} 0 & 0 \\ -1 & (1-\alpha)\frac{k_s}{m_f}u_0 \\ 0 & 0 \\ 0 & -(1-\alpha)\left(\frac{1}{m_f}+\frac{1}{m_s}\right)k_s u_0 \end{bmatrix} \begin{bmatrix} \ddot{u}_g(t) \\ \zeta(t) \end{bmatrix} + \begin{bmatrix} 0 \\ -\frac{1}{m_f} \\ 0 \\ \frac{1}{m_f} \end{bmatrix} P_f(t) \tag{3.47}$$

or

$$\dot{\boldsymbol{Y}}(t) = \boldsymbol{A}_s \boldsymbol{Y}(t) + \boldsymbol{B}_{s_1} \boldsymbol{U}_s(t) + \boldsymbol{B}_p P_f(t) \tag{3.48}$$

in which $\boldsymbol{U}_s(t)$ is the input vector $\{\ddot{u}_g(t) \qquad \zeta(t)\}^T$.

From equation (3.43), $P_f(t)$ may be written in terms of $Y_1(t)$ as

$$P_f(t) = \boldsymbol{C}_f \boldsymbol{x}(t) + D_f Y_1(t) \tag{3.49}$$

Substituting in equation (3.48),

$$\dot{\boldsymbol{Y}}(t) = \boldsymbol{A}_s \boldsymbol{Y}(t) + \boldsymbol{B}_{s_1} \boldsymbol{U}_s(t) + \boldsymbol{B}_p \boldsymbol{C}_f \boldsymbol{x}(t) + \boldsymbol{B}_p D_f Y_1(t) \tag{3.50}$$

we note that the last term simply adds to the first column of $\boldsymbol{A}_s$. Defining

$$\boldsymbol{A}_{s_1} = \boldsymbol{A}_s + \left[\boldsymbol{B}_p D_f \ \boldsymbol{0}_{nxn-1}\right] \tag{3.51}$$

where $\boldsymbol{0}_{nxn-1}$ is a matrix of n x n-1 zeros, n being the number of states for the superstructure and hence the size of the $\boldsymbol{A}_s$ matrix, and rewriting equation (3.40) as

$$\dot{\boldsymbol{x}}(t) = \boldsymbol{A}_f \boldsymbol{x}(t) + \boldsymbol{B}_f Y_1(t) \tag{3.52}$$

the governing state-space representation of the entire system is obtained to be

$$\begin{bmatrix} \dot{Y}(t) \\ \dot{x}(t) \end{bmatrix} = \begin{bmatrix} A_{s_1} & B_p C_f \\ \begin{bmatrix} B_f & \mathbf{0}_{Nxn-1} \end{bmatrix} & A_f \end{bmatrix} \begin{bmatrix} Y(t) \\ x(t) \end{bmatrix} + \begin{bmatrix} B_{s_1} \\ \mathbf{0}_{Nxl} \end{bmatrix} U_s(t) \tag{3.53}$$

where l is the length of the input vector $U_s(t)$ (=2 in equation (3.47)). Note that the input vector contains the nonlinear hysteretic term ζ, governed by equation (3.46), which contains the state variable Y_4.

3.5.2 Validation of proposed procedure

The problem analyzed is the same as in section 3.4, with the foundation dynamic stiffnesses as illustrated in figure 3.10. To first verify the procedure, the completely linear case is taken in which $\alpha = 0$. This ensures that the nonlinear variable ζ does not contribute to the solution.

The foundation stiffness is first approximated as a ratio of a third order to a fourth order polynomial. An excellent fit is obtained in the frequency range of interest as shown in figure 3.18, using a uniformly weighted least-squares minimization algorithm. However, when the resulting state-space matrices are used in the analysis, it leads to numerical instability due to the presence of an unstable pole (at ω= 142 Hz). The same problem is encountered with other "strictly proper" approximations for $\overline{\mathcal{K}}_f(i\omega)$ using the same algorithm.

The chosen approximation for this analysis is shown in figure 3.19 for the case $M = N = 4$, along with the corresponding ratio-of-polynomials expression. This expression was obtained by constraining the poles to be stable for the foundation subsystem as well as the overall system matrix, and by judiciously choosing the poles and zeros to match magnitude and phase of the complex valued dynamic stiffness. The approximation is slightly inaccurate at frequencies above 80Hz, but this is not expected to produce significant error given the low frequency content of the induced seismic excita-

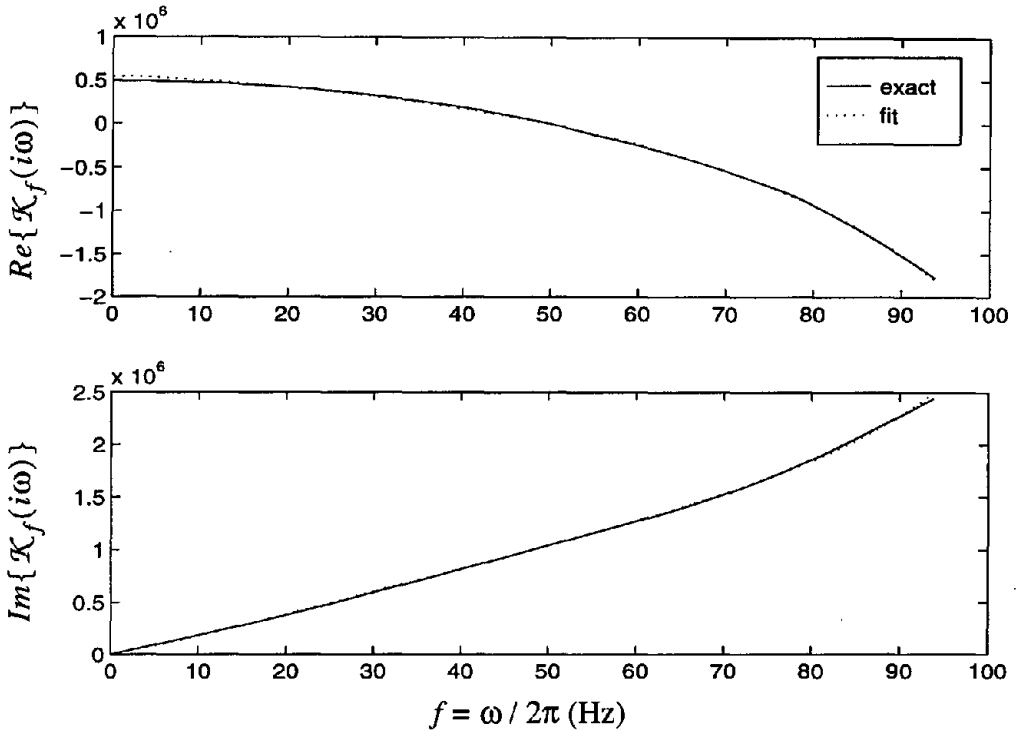

Figure 3.18: Ratio of polynomials approximation for foundation dynamic stiffness (M = 3; N = 4).

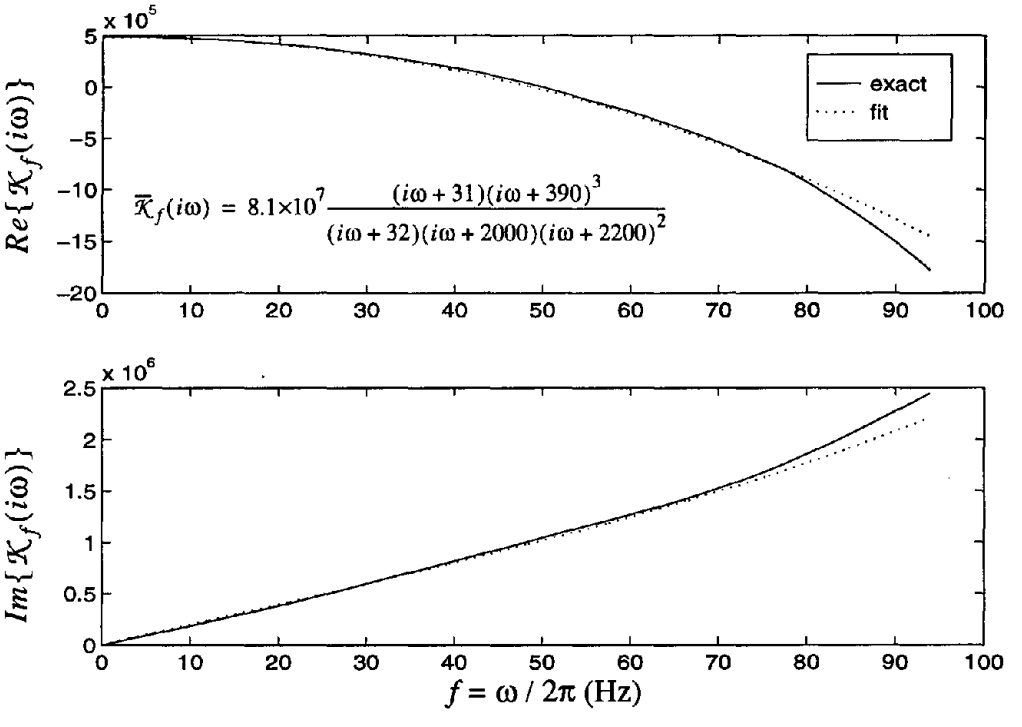

Figure 3.19: Ratio of polynomials approximation for foundation dynamic stiffness (M = N = 4).

tion. Keeping in mind that the largest pole in this system is at 350Hz, the time-step for simulation was chosen as 0.001s. The results for deck drift and foundation relative motion, obtained using the Simulink utility in Matlab, are shown in figure 3.20. The comparison with the frequency domain approach (equations (3.18) and (3.19)) demonstrates the accuracy of the proposed procedure for a linear analysis.

3.5.3 Nonlinear analysis

As in the case of the convolution integral method, a limiting case nonlinear analysis is first carried out. Accordingly, the parameters of the Bouc-Wen model were chosen as: $\alpha = 0$, $u_0 = 0.02m$, $A = 1$, $\beta = 0.5$, $\gamma = 0.5$ and $n = 10$. At this large value of n, the spring behaves in an elastic-perfectly-plastic manner, and since the yield limit is chosen to be fairly large compared with the actual spring displacement, the behavior is essentially elastic, as shown in figure 3.21. Figure 3.23 shows that the results of the nonlinear analysis indeed converge to the linear solution (obtained via frequency domain approach).

Subsequently, the parameters were selected for the nonlinear spring as: $\alpha = 0$, $u_0 = 0.02m$, $A = 1$, $\beta = 0.5$, $\gamma = 0.5$ and $n = 1$. Figure 3.22 shows the force-displacement behavior of the nonlinear spring, and figure 3.24 shows the resulting time histories for the deck drift and foundation relative motion, and the absolute accelerations. The drifting effect of the deck is again captured, and the results seem to be in agreement with those obtained via the convolution integral approach. This is confirmed by a direct comparison of the two methods shown in figure 3.25. The time step used for this analysis was also 0.001s.

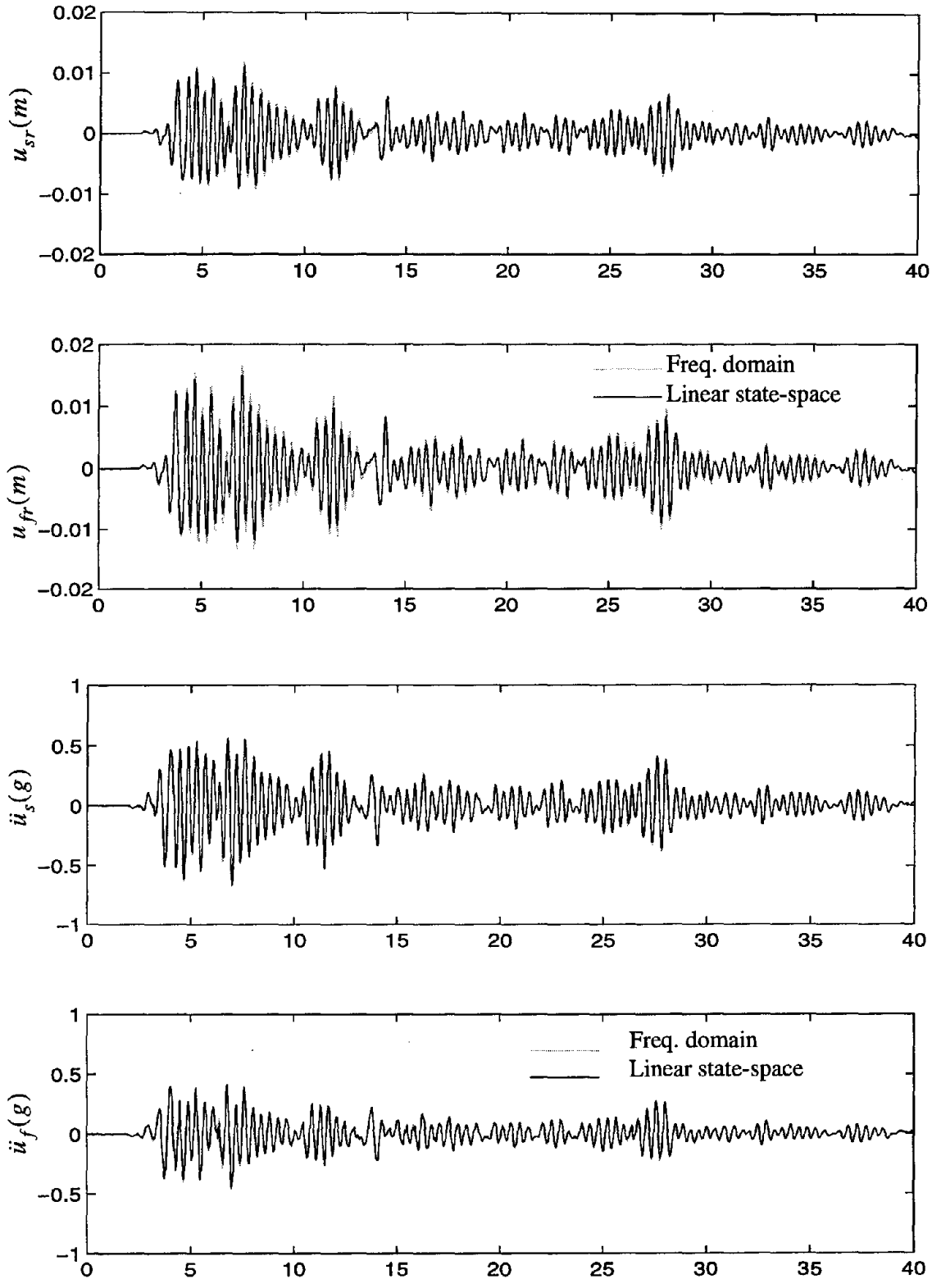

Figure 3.20: Comparison of results from state-space formulation with frequency domain approach for linear system.

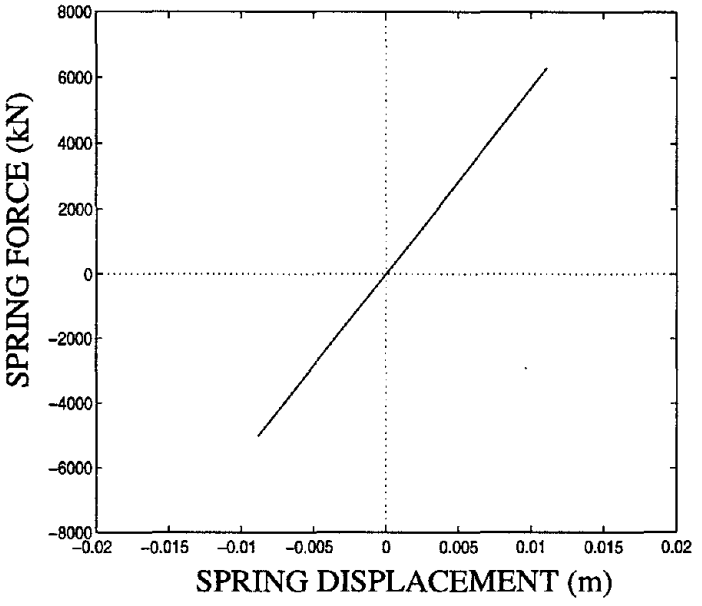

Figure 3.21: Force-displacement behavior of nonlinear spring (n=10).

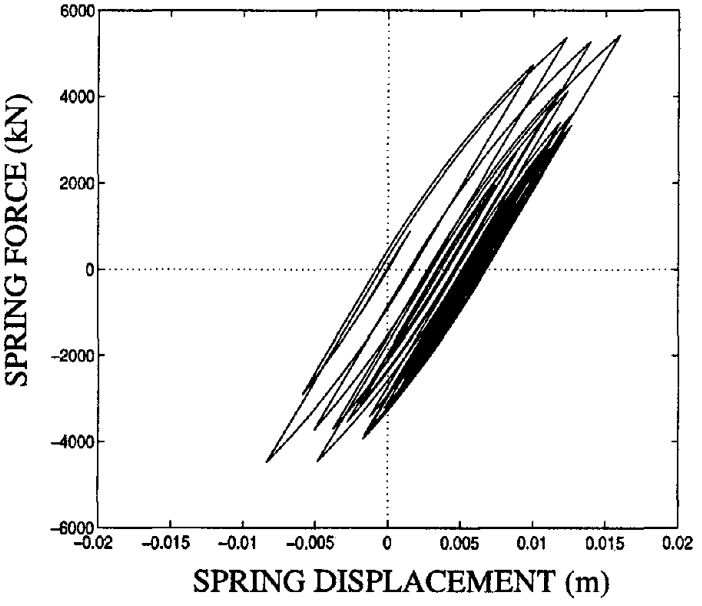

Figure 3.22: Force-displacement behavior of nonlinear spring (n=1).

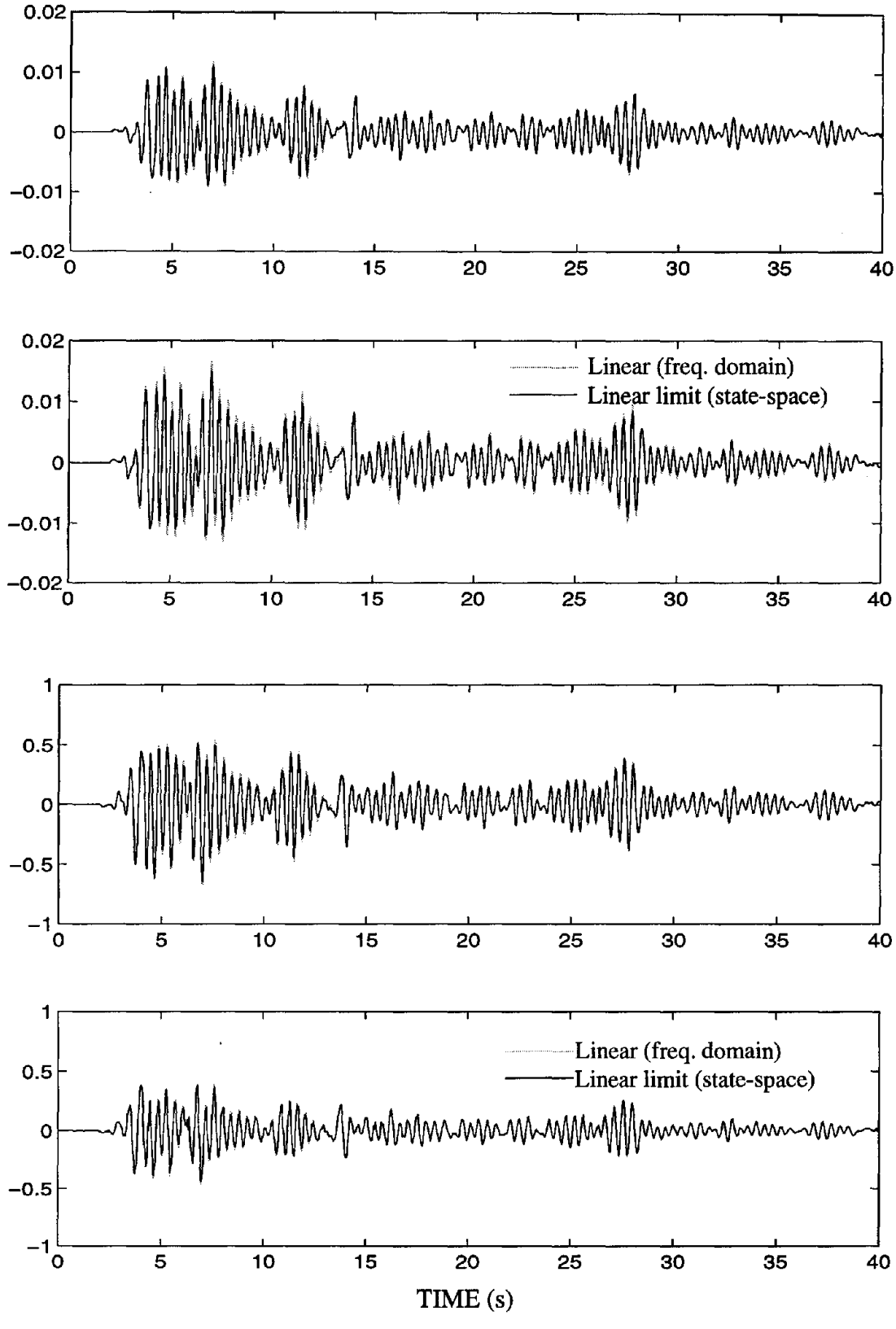

Figure 3.23: Validation of state-space formulation at linear limit (n=10).

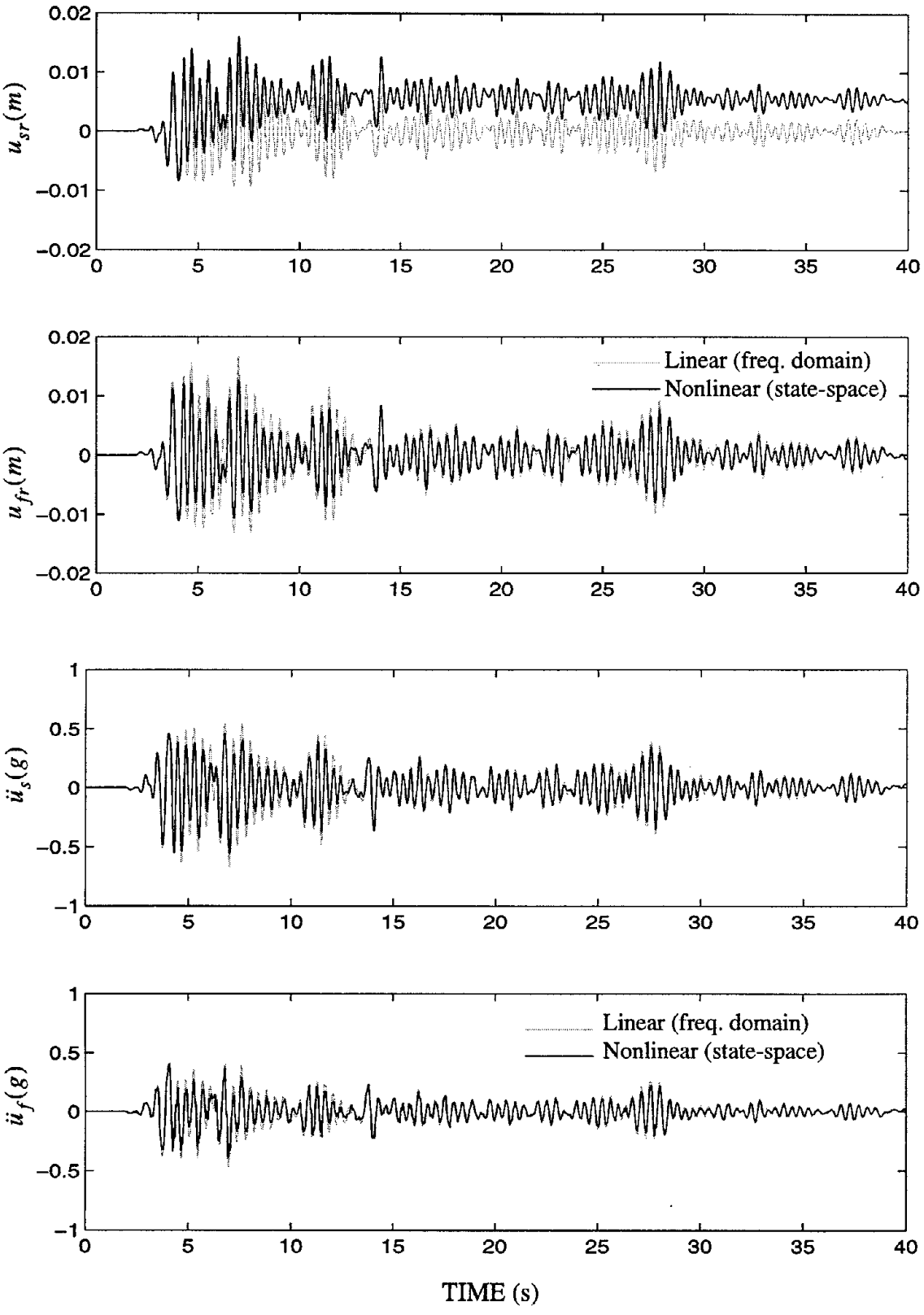

Figure 3.24: Displacement time histories using state-space formulation (n=1).

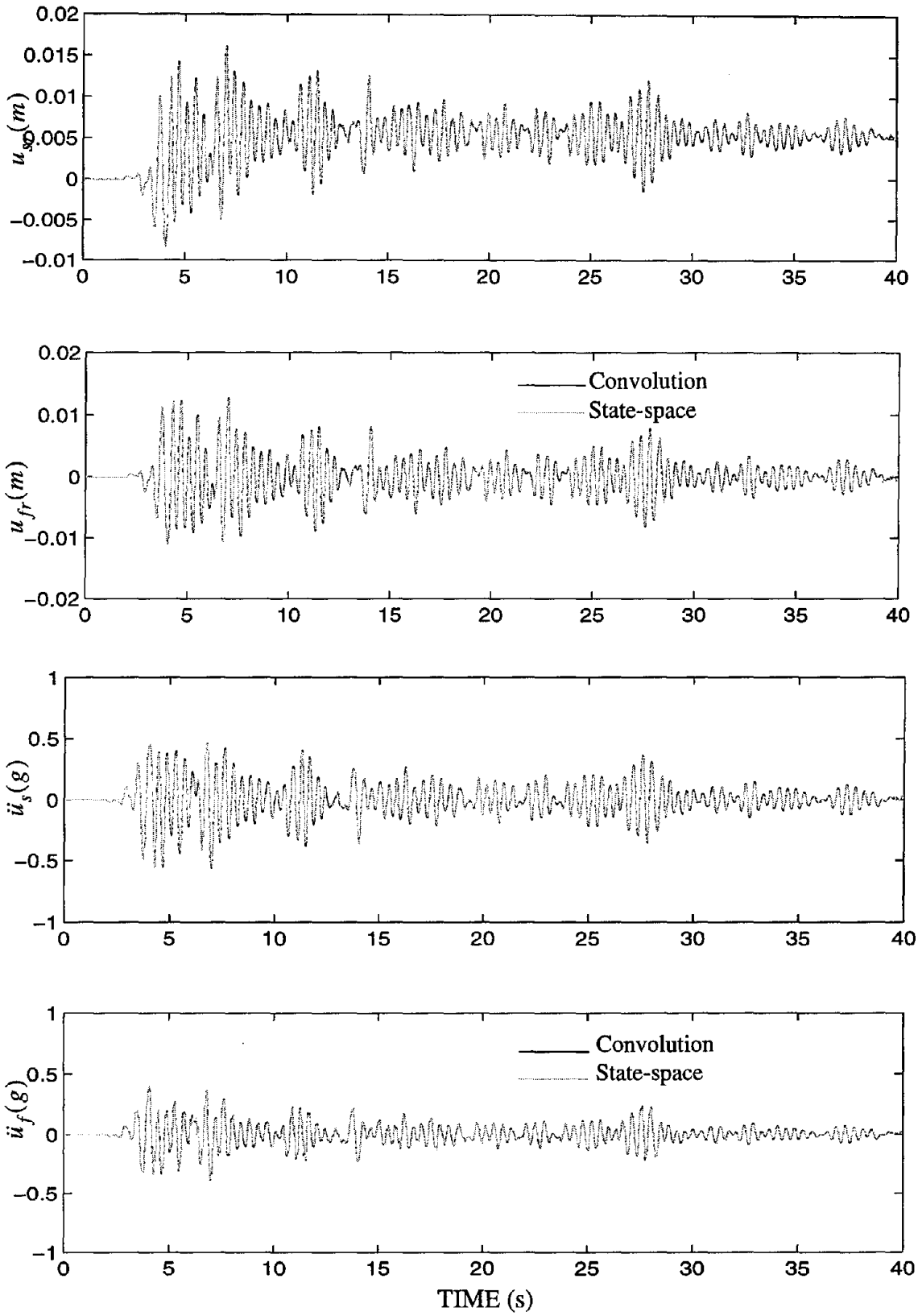

Figure 3.25: Comparison of state space vs. convolution integral method results for n=1.

3.6 Application to analysis of bridge-response employing isolation and energy dissipation devices

Either of the two methods discussed previously can be very useful in the nonlinear seismic response analysis of bridge superstructures that use isolators or energy dissipation devices, schematically illustrated in figure 3.26. This is qualitatively illustrated with the two example systems that follow.

3.6.1 Lead-rubber bearings

These are popular isolation devices for bridge superstructures and exhibit typically bilinear hysteretic force-deflection behavior. Such a relationship can be reproduced by choosing the Bouc-Wen model parameters as: $\alpha = 0.1$, $u_0 = 0.005m$, $A = 1$, $\beta = 0.05$, $\gamma = 0.95$ and $n = 5$. In a practical example, the value of α would depend on the rubber height (or plan size), and u_0 would depend on the lead plug size. With these

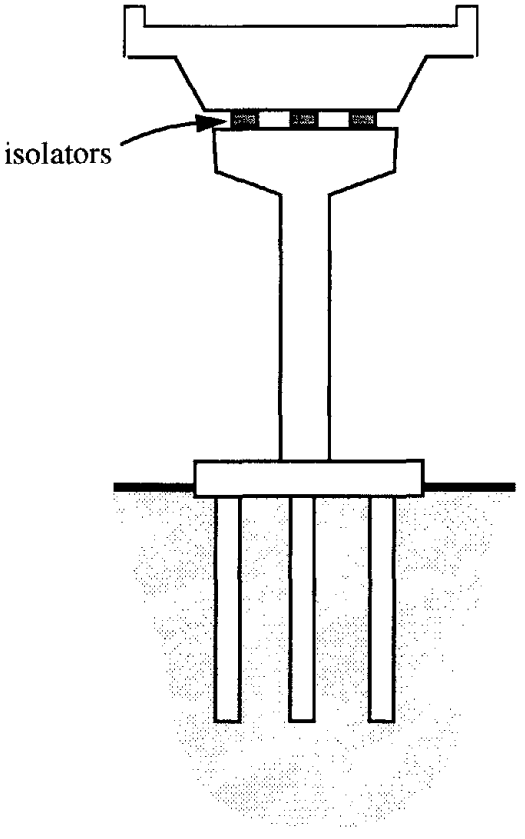

Figure 3.26: Model for an isolated bridge on pile foundation.

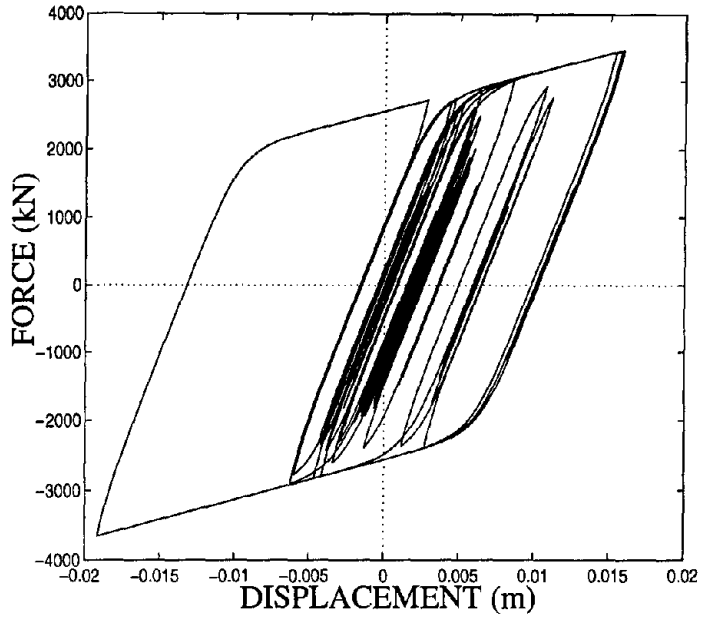

Figure 3.27: Idealized force displacement loops for lead-rubber bearing.

parameters, and an analysis identical to the one in section 3.5.3, the force displacement loop is obtained as shown in figure 3.27. The corresponding displacement and acceleration time-histories are depicted in figure 3.29.

3.6.2 Sliding bearings with restrainers

For this example, a slip-lock element (zero stiffness within sliding zone and infinite stiffness otherwise) is connected in series with the nonlinear spring illustrated in figure 3.13. The parameters were chosen as $\alpha = 0.01$, $u_0 = 0.02m$, $A = 1$, $\beta = 0.05$, $\gamma = 0.95$ and $n = 5$. The length of sliding zone was taken as 0.04m. The resulting force-displacement loops are shown in figure 3.28, and the time-histories of deck and foundation motion in figure 3.30. The model is able to reproduce the nature of desired force-displacement history very well. The substantial increase in the accelerations of the foundation illustrate the importance of modeling foundation dynamics in this problem.

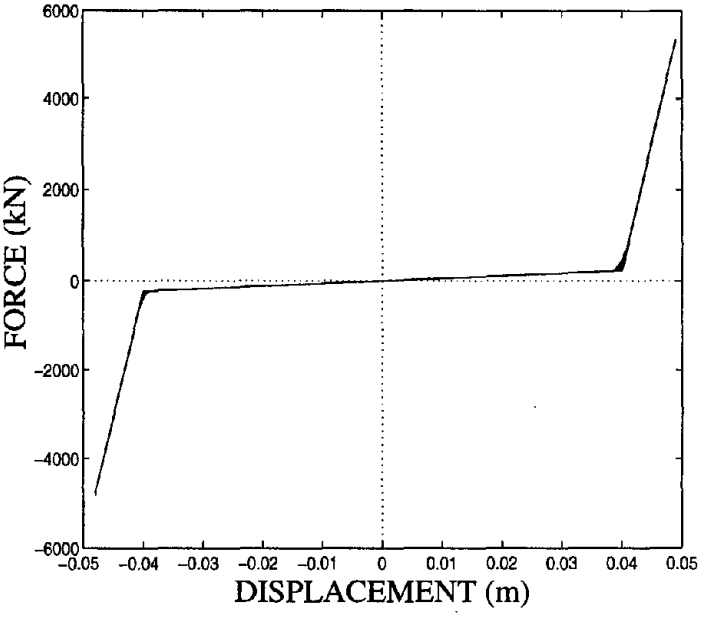

Figure 3.28: Idealized force-displacement relation for sliding bearing with restrainers.

3.7 Concluding remarks

Two time-domain techniques to analyze the nonlinear foundation-superstructure problem were developed in this chapter. The first approach, employing a convolution integral formulation, was shown to be capable of predicting accurately and economically the response of a simple two degree-of-freedom system with nonlinear behavior incorporated in the superstructure model. The method employs direct numerical transformation of available dynamic impedances to obtain foundation relaxation stiffness, which was shown to be more accurate than memory function convolution.

The second approach utilized a state-space formulation for the governing equations by using a rational polynomial approximation for the foundation dynamic stiffness. However, it is not trivial to obtain a stable realization for the foundation states. Even when the foundation subsystem has stable poles, when combined with the superstructure matri-

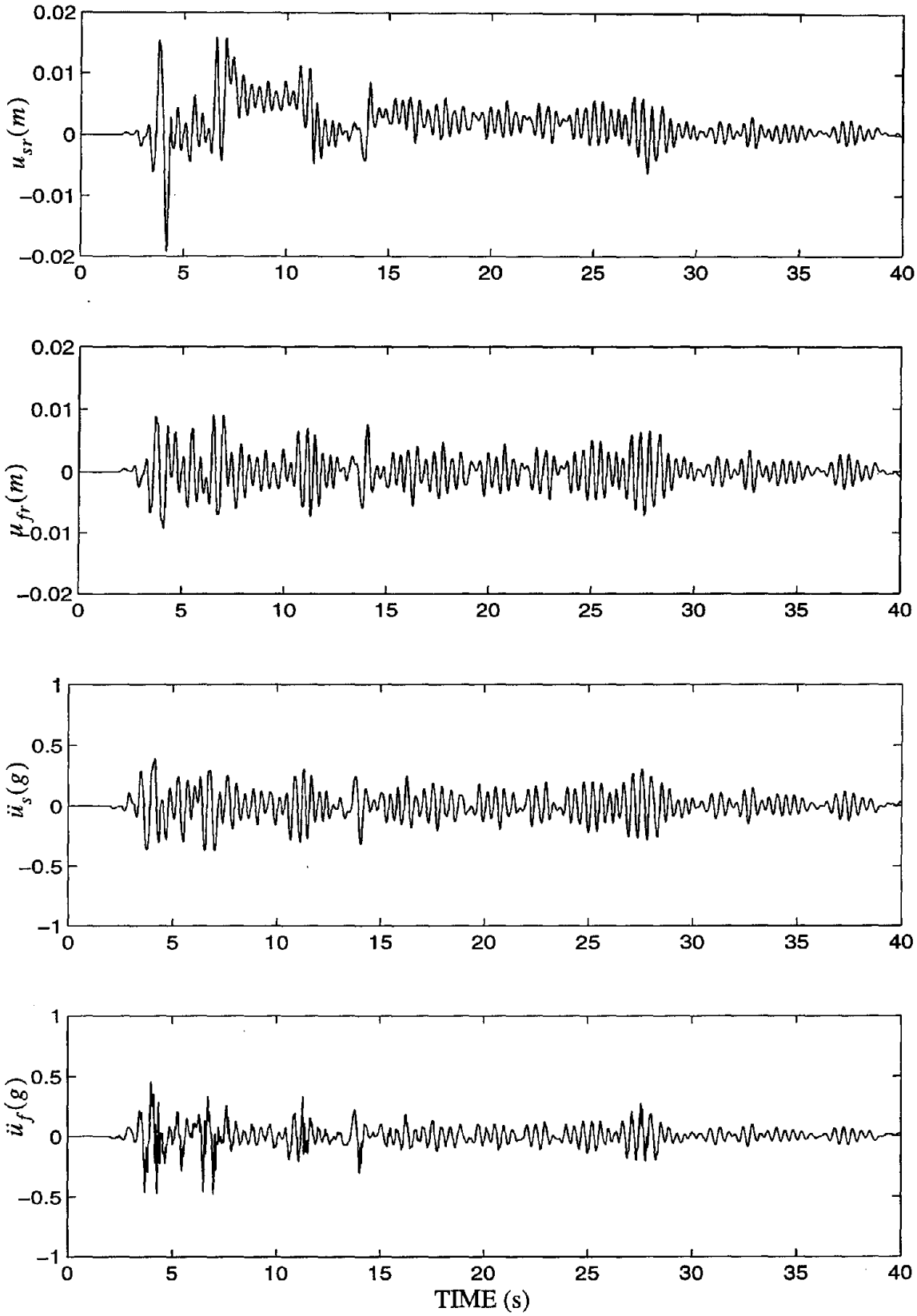

Figure 3.29: Response of idealized bridge using lead-rubber isolation system.

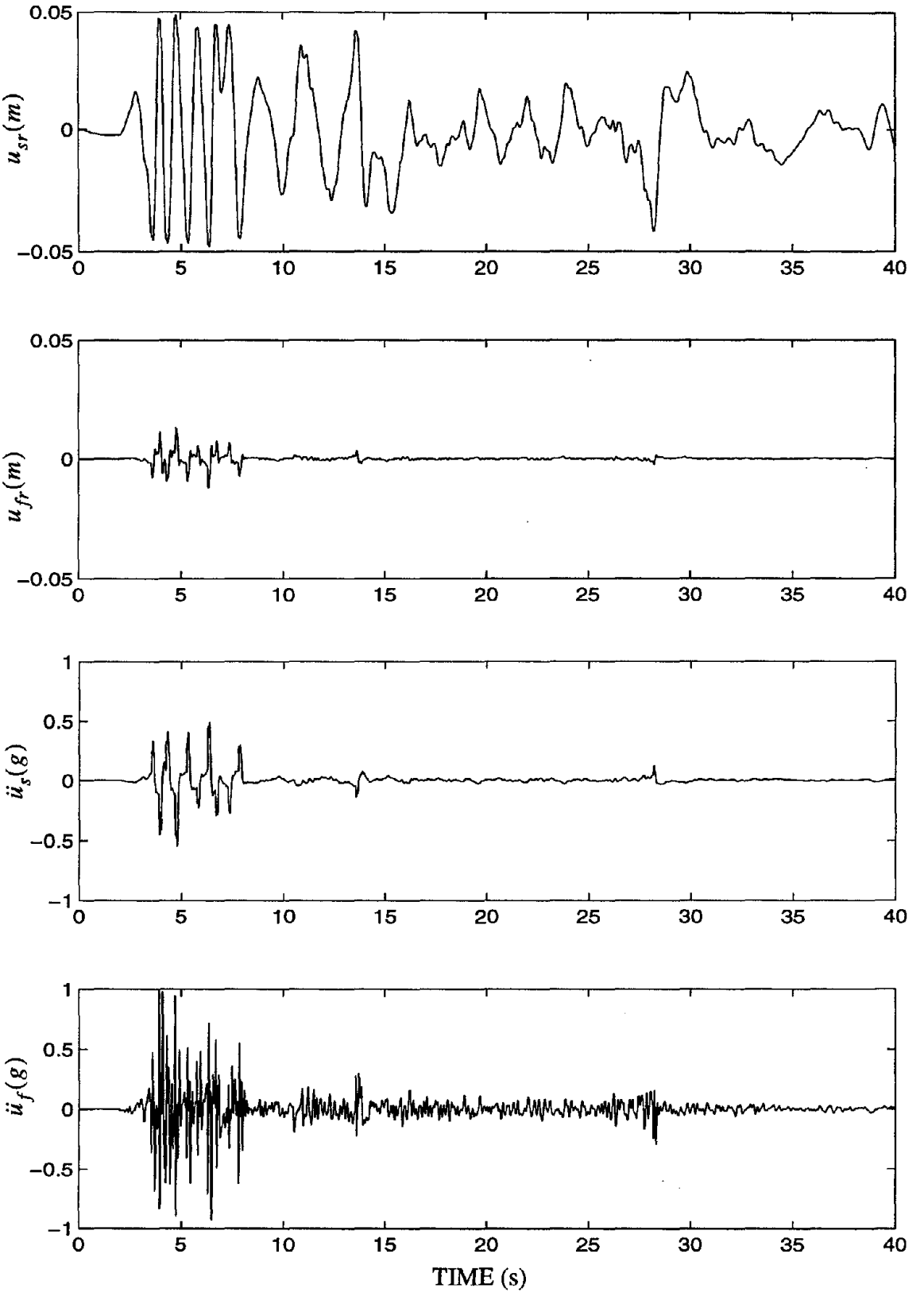

Figure 3.30: Response of idealized bridge using sliding bearing-restrainer mechanism for isolation.

ces, it can lead to numerical instability. Also, in the case that a stable realization has been found for the system, the required time-step for simulation may be prohibitively small. However, these problems can be countered by using model reduction and balancing techniques, which are outside the scope of this study.

Both methods can incorporate foundation dynamics over a provided frequency range, implying greater dependability under different loading conditions. Note that, even though these methods were discussed in this chapter in the context of pile-foundations, they can be applied to virtually any type of foundation, as long as the dynamic stiffnesses are available. Also, the methods, formulated herein for simple two degree-of-freedom systems, can be easily extended to more complicated systems as long as the governing equations can be derived in a suitable form.

It was shown in this chapter that superstructure nonlinear behavior can be modeled efficiently using the Bouc-Wen model. Results from the nonlinear analyses indicated that the presence of a nonlinearly behaving superstructure reduces foundation response and, under moderate loading conditions, this could be justification for the use of linear or equivalent linear models for foundation response. In the next chapter, the problem of obtaining these equivalent linear stiffnesses for pile foundations is addressed.

CHAPTER 4

PILE-TO-PILE INTERACTION IN THE TIME DOMAIN- NONLINEAR RESPONSE OF PILE GROUPS

Most available numerical and analytical techniques to compute foundation response accounting for pile-soil-pile interaction are restricted to small-amplitude vibrations where linear viscoelasticity approximates satisfactorily the physical problem. The mechanical properties of pile foundations are strongly frequency dependent, and the assumption of linear viscoelasticity makes possible the analysis of the problem in the frequency domain. Accordingly, most of the results available on the mechanical properties of piles and pile groups are presented in terms of complex dynamic stiffnesses and frequency dependent kinematic response factors. Several researchers have developed a variety of numerical (Blaney *et al.* 1976, Tajimi 1977, Novak 1974, Wolf and von Arx 1978, Kaynia and Kausel 1982, Sheta and Novak 1982, Mamoon and Banerjee 1990) and approximate analytical (Dobry and Gazetas 1988, Makris and Gazetas 1992, Makris and Badoni 1995) methods for assessing pile-soil-pile interaction and calculating the dynamic stiffness and kinematic response factors of pile groups. More recently, Mamoon and Banerjee (1992) developed a hybrid boundary element formulation to compute the transient vertical response of a linear pile-soil system.

The success of the aforementioned approximate analytical solutions relies on an

approximate expression for the dynamic interaction factors, which was proposed by Dobry and Gazetas (1988). This is based on the asymptotic cylindrical wave expression for the displacement field, $v(z, r, \omega)$, generated in a homogeneous continuum due to the vertical oscillations of an infinite long rod with diameter d, (Morse and Ingard 1968):

$$v(z, r, \omega) = w(z, \omega)\sqrt{\frac{d}{2r}}exp\left(-\beta\omega\frac{r-\frac{d}{2}}{V_s}\right)exp\left(-i\omega\frac{r-\frac{d}{2}}{V_s}\right) \tag{4.1}$$

where $w(z, \omega)$ represents the elongation-contraction of the rod at depth z, ω is the frequency of oscillation, β is the hysteretic damping of the soil and V_s is the shear wave velocity of the deposit. The term $\sqrt{d/2r}$ in equation (4.1) accounts for radiation damping. The first exponential term accounts for the energy loss in the deposit due to hysteretic behavior of the soil, and the second exponential term is the phase difference between the motion of a point at distance r, and the motion of a point on the pile at the same depth. The efficiency of equation (4.1) was demonstrated in the papers by Dobry and Gazetas (1988) and Makris and Gazetas (1992).

An expression similar to equation (4.1) has been proposed by Nogami (1983). However, Nogami's expression, which involves modified Bessel functions with complex arguments, cannot be transformed in a closed-form manner into the time domain, and one has to construct approximate expressions in the time domain in order to analyze the nonlinear response of pile groups (Nogami and Konagai 1987). The advantage of equation (4.1) is that its time domain representation can be computed in closed form which is presented in section 4.1 of this chapter.

Equation (4.1) can be written in the form

$$v(z, r, \omega) = \Psi(r, \omega)w(z, \omega) \tag{4.2}$$

where $\Psi(r, \omega)$ is the attenuation function

$$\Psi(r,\omega) = \sqrt{\frac{d}{2r}} exp\left(-\beta\omega\frac{r-\frac{d}{2}}{V_s}\right) exp\left(-i\omega\frac{r-\frac{d}{2}}{V_s}\right) \tag{4.3}$$

Dobry and Gazetas (1988) assumed that the vertical elongation-contraction of a neighboring passive pile at distance S can be approximated by the displacement of the free-field at its location $v(S,\omega)$. Using this simplifying assumption, they proposed that the vertical dynamic interaction factor, $\alpha_v(S,\omega) \approx \Psi(S,\omega)$. As an example, the dynamic stiffness of a two by two pile group is provided by the simple expression (Dobry and Gazetas 1988):

$$\mathcal{K}_z^{[2X2]}(\omega) = \mathcal{K}_z^{[1]}(\omega)\frac{4}{1+2\Psi(S,\omega)+\Psi(S\sqrt{2},\omega)} \tag{4.4}$$

where $\mathcal{K}_z^{[1]}(\omega)$ is the vertical dynamic stiffness of a single pile.

In this chapter, an approximate, physically-motivated procedure is presented to compute nonlinear, axial group-response in the time domain. First, a closed-form expression for the attenuation function, Ψ, in the time domain is derived from an existing frequency domain formulation. Subsequently, a phenomenological model that is based on the theory of viscoplasticity is proposed to approximate the nonlinear dynamic response of single piles under harmonic axial loading. The parameters of the distributed viscoplastic model are calibrated from data obtained from full-scale experiments. Herein, two different experiments conducted by Muster and O'Neill (1986) and Bond and Jardine (1995) are used. The time-domain formulation for pile-to-pile interaction is used in conjunction with the nonlinear shaft model to compute the nonlinear axial response of 2x1 and 2x2 pile groups embedded in actual soil profiles. The effect of nonlinear behavior on the group response is then discussed in terms of equivalent linear stiffness and damping.

The model presented herein forms a complement to a model for lateral response of pile groups developed earlier (Badoni 1995, Badoni and Makris 1996). An outline of this companion model is provided at the end of this chapter for the sake of completeness. It is

worth mentioning that the response of piles to vertical loads is influenced by the soil properties along the entire pile length, as opposed to a few pile diameters for the case of lateral loading. The analysis of axial response also includes tip soil reaction and the influence of slippage as additional modeling considerations. At the same time, the symmetry of wave propagation outward from the pile makes the attenuation function simpler in form than the corresponding function for lateral response.

4.1 Attenuation function for vertical response in the time domain

Under harmonic steady-state vibrations, the diffracted wave field, $v(z, r, \omega)$, is provided by equation (4.2), which is the product of two functions in the frequency domain. Accordingly, the time domain expression of the diffracted wave field can be expressed in terms of a convolution integral:

$$v(z, r, t) = \int_{-\infty}^{\infty} \Psi(r, t-\tau) w(z, \tau) d\tau \tag{4.5}$$

where $\Psi(r, t-\tau)$ is the time domain kernel given by

$$\Psi(r, t) = \frac{1}{2\pi} \int_{-\infty}^{\infty} \Psi(r, \omega) e^{i\omega t} d\omega \tag{4.6}$$

Substituting (4.3) into (4.6) and denoting by $t_s = (r - d/2)/V_s$, the travel time needed for the shear waves emanating from the active pile to reach the passive pile, equation (4.6), takes the form:

$$\Psi(r, t) = \sqrt{\frac{d}{2r}} \frac{1}{2\pi} \int_{-\infty}^{\infty} e^{-\beta\omega t_s} e^{-i\omega t_s} e^{i\omega t} d\omega \tag{4.7}$$

The integral in equation (4.7) is computed by using again the convolution integral theorem. First, the Fourier transform of the term $F_1(\omega) = e^{-\beta\omega t_s}$ is examined. Clearly, since

this is a real function, it must be an even function of frequency in order to yield a real-valued solution in the time domain (Papoulis 1988). Accordingly, $e^{-\beta\omega t_s}$ is replaced with $e^{-\beta|\omega|t_s}$, and therefore:

$$f_1(t) = \mathcal{F}^{-1}\{F_1(\omega)\} = \frac{1}{2\pi}\int_{-\infty}^{\infty} e^{-\beta|\omega|t_s}e^{i\omega t}d\omega = \frac{1}{\pi}\frac{\beta t_s}{\beta^2 t_s^2 + t^2} \tag{4.8}$$

where $\mathcal{F}^{-1}\{\ \}$ denotes the inverse Fourier transform operator. Furthermore, recognizing that

$$F_2(\omega) = e^{-i\omega t_s} = \int_{-\infty}^{\infty} \delta(t - t_s)e^{-i\omega t}dt \tag{4.9}$$

one may write

$$\frac{1}{2\pi}\int_{-\infty}^{\infty} e^{-\beta|\omega|t_s}e^{-i\omega t_s}e^{i\omega t}d\omega = \mathcal{F}^{-1}\left\{\mathcal{F}\left\{\frac{1}{\pi}\frac{\beta t_s}{\beta^2 t_s^2 + t^2}\right\}\mathcal{F}\{\delta(t - t_s)\}\right\} \tag{4.10}$$

and from the convolution integral theorem and equation (4.7), one obtains

$$\Psi(r, t) = \frac{1}{\pi}\sqrt{\frac{d}{2r}}\frac{\beta t_s}{\beta^2 t_s^2 + (t - t_s)^2}, \qquad \beta \neq 0 \tag{4.11}$$

Equation (4.11) is the closed form time domain expression for the attenuation function, and is valid for $\beta \neq 0$. Equation (4.11) is a dispersive kernel with finite amplitude at the time origin due to the hysteretic behavior of the soil. Figure 4.1 plots the attenuation function for different values of β. For the hypothetical case of a purely elastic medium with zero hysteretic damping ($\beta = 0$), the kernel becomes singular and reduces to

$$\Psi(r, t) = \frac{1}{\pi}\sqrt{\frac{d}{2r}}\delta(t - t_s), \qquad \beta = 0 \tag{4.12}$$

where $\delta(t - t_s)$ is the Dirac delta function (Lighthill 1989).

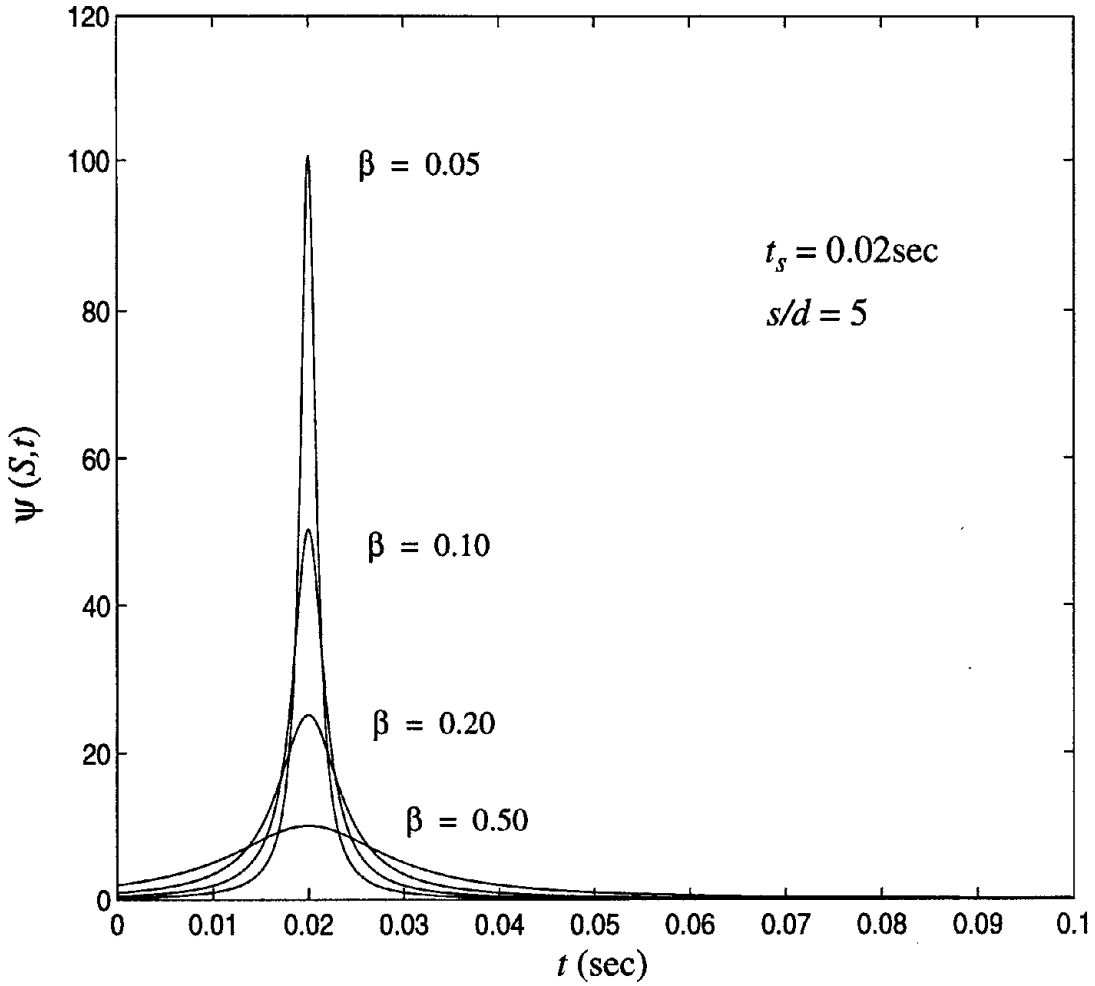

Figure 4.1: The attenuation function in the time domain.

With the help of (4.11), equation (4.5) takes the form

$$v(z, S, t) = \frac{1}{\pi}\sqrt{\frac{d}{2S}}\int_{-\infty}^{\infty} \frac{\beta t_s}{\beta^2 t_s^2 + (t - t_s - \tau)^2} w(z, \tau) d\tau, \tag{4.13}$$

Equation (4.13) is the general expression that describes, in the time domain, the displacement field generated by a vertically vibrating pile under any transient load. As an example, consider a vertical pile subjected to a transient load, and assume that the motion of the pile at depth z is the time history shown in figure 4.2 (center). Figure 4.2 (bottom) shows the computed motion (using equation (4.13)) of a soil point at distance $r = 3d$ and the

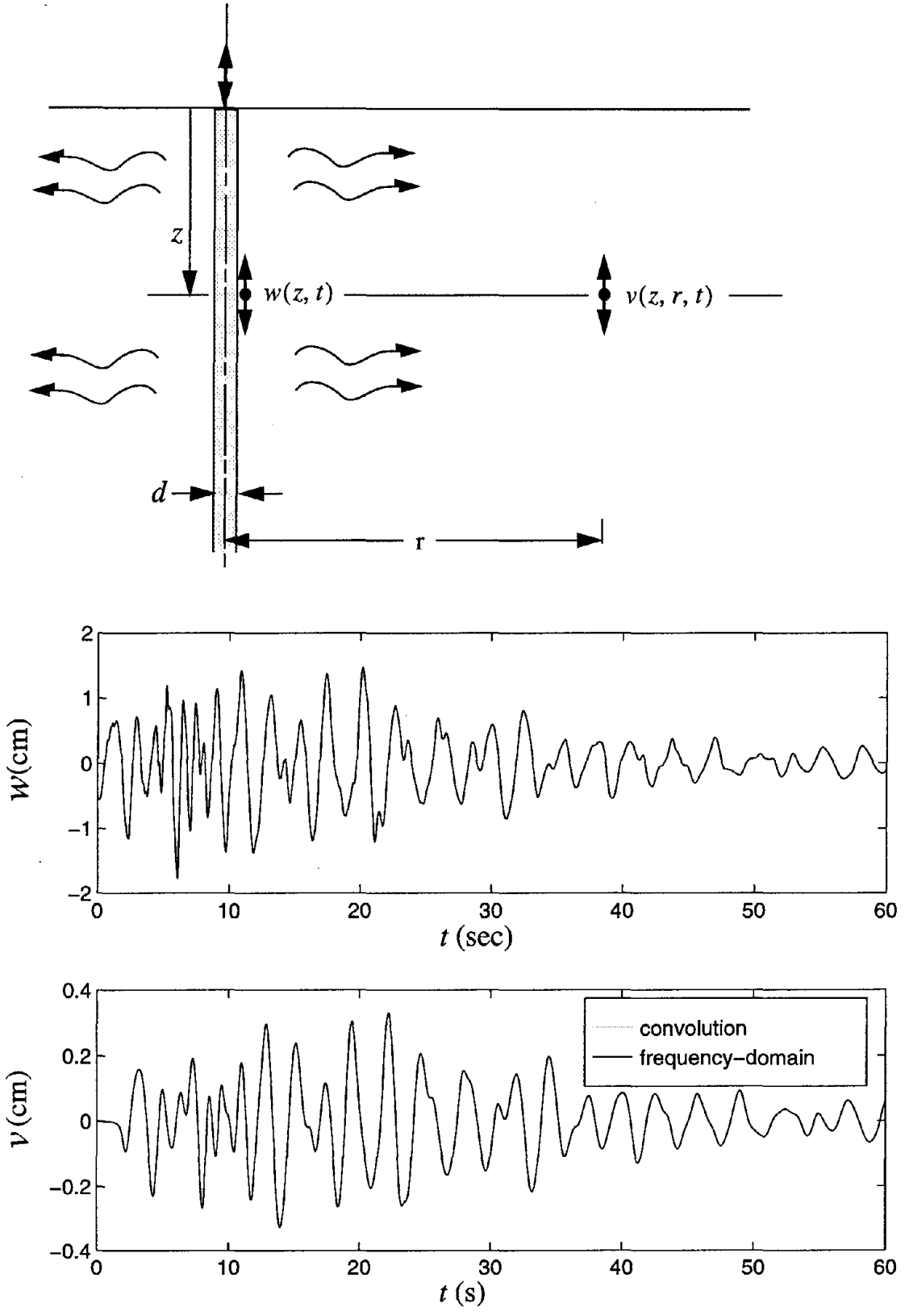

Figure 4.2: **Numerical verification of the time-domain formulation for the attenuation function ($r/d = 3$; $t_s = 2$ s; $\beta_s = 0.10$).**

same depth z. The result obtained with equation (4.13) is identical with the frequency domain solution.

In the special case of steady-state vibrations, standing waves are developing along the active pile, and the spatial and temporal dependence of the pile displacements can be decoupled as

$$w(z, t) = W(z)f(t) \tag{4.14}$$

where $W(z)$ is the amplitude of elongation-contraction of the active pile along its length. As an example, in the case of harmonic vibrations with frequency Ω, (*i.e.*, $f(\tau) = sin\Omega\tau$), the integral in (4.13) can be integrated analytically by using the result (Gradshteyn and Ryzhik 1980):

$$\int_{-\infty}^{\infty} \frac{sin\Omega(t-\xi)}{c^2+\xi^2} d\xi = \frac{\pi}{c} e^{-\Omega c} sin\Omega t \tag{4.15}$$

and the closed form expression

$$v(z, r, t) = \sqrt{\frac{d}{2r}} W(z) e^{-\beta\Omega t_s} sin\Omega(t-t_s) \tag{4.16}$$

is obtained. This result can also be verified directly from the frequency domain expression given by equation (4.1).

4.2 Nonlinear model for axial response of single pile

A limited number of studies have been presented in the literature on the nonlinear axial response of single piles. Angelides and Roesset (1980) have extended the finite element formulation originally developed by Blaney *et al.* (1976) to consider nonlinear soil behavior in the frequency domain. Nogami and Konagai (1986) proposed a polynomial expression to approximate the pile displacement at discrete depths and a six-parameter generalized Kelvin model to approximate the soil reaction along the pile. Recently, El

Naggar and Novak (1994) presented a similar shaft model that combines springs, dashpots and sliders to approximate the behavior of the pile-soil interface ("inner field") and the "outer field". In order to analyze pile-to-pile interaction, El Naggar and Novak utilized a special case of equation (4.1) (equation (18) in their paper), where the hysteretic damping term was neglected ($\beta = 0$). Furthermore, the nonlinear hysteretic model they adopt to describe the behavior of the pile-soil interface consists of two separate equations to model the ascending and descending branches of the force-deflection curve, thus necessitating the detection of any reversal of loading, and leading to a computationally complex procedure.

The most comprehensive study on the nonlinear response of piles using a nonlinear Winkler-type foundation model is probably that of Trochanis *et al.* (1991), who utilized the Bouc-Wen model to describe the force-displacement relation of distributed nonlinear springs that approximate the soil reaction along the pile. Their study concentrated on the static and quasi-static (zero-frequency limit) loading of piles, and for this type of loading, it was shown that the Bouc-Wen model predicts satisfactorily the response of a variety of soil-pile systems.

In this study, the distributed (along the pile length) nonlinear spring described by the Bouc-Wen model is combined with a distributed viscous dashpot placed in parallel, together with a slider connected in series as shown in figure 4.3. The presence of the damper makes the model realistic for the prediction of the pile response under dynamic loading, since it accounts for the energy that radiates away from the pile-soil interface. The slider accounts for slippage along the pile-soil interface, which is a phenomenon that often governs the nonlinear response, since the adhesive capacity at the pile-soil interface can be exceeded before the surrounding soil reaches its ultimate strength.

A primary aim during the formulation of this model was to readily associate most

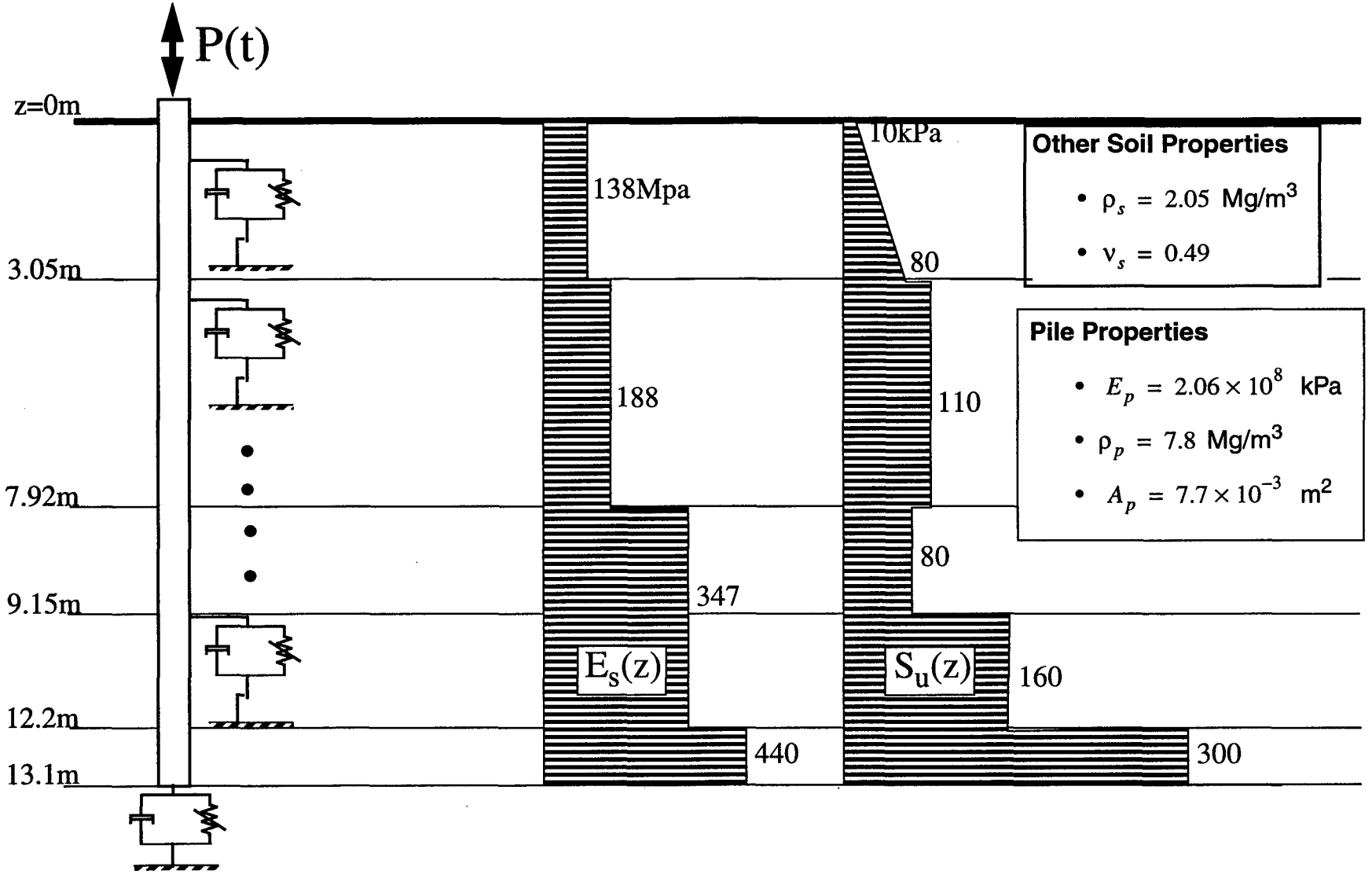

Figure 4.3: Schematic illustration of dynamic nonlinear axial pile-soil interaction in a layered soil deposit.

mathematical parameters with physical soil properties. For instance, the Young's modulus, E_s, and the undrained shear strength of cohesive soils, S_u, are explicit parameters of the proposed model. Furthermore, while the hysteretic springs described with the Bouc-Wen model account for the energy loss due to friction (hysteretic damping), the distributed dashpots governed by a realistic frequency dependent expression (Gazetas and Makris 1991; Makris and Gazetas 1993) account for radiation damping. Consequently, the proposed model, at the limit of small amplitudes, reduces to the linear frequency-dependent Kelvin model, which has been used with success for the prediction of the linear inertial and seismic response of piles and pile-groups (Gazetas and Makris 1991, Makris 1994, Makris and Badoni 1995). The parameters of the proposed model are calibrated from well- instrumented, full-scale, field experiments conducted by Muster and O'Neill (1986) and by Bond and Jardine (1995).

The pile is modeled as a linear-elastic rod with circular-cross-section area A_p, diameter d, Young's modulus E_p and mass density ρ_p. The surrounding soil is considered to be an inhomogeneous deposit with Young's modulus, $E_s(z)$, shear wave velocity, $V_s(z)$, and shear strength, $S(z)$, that vary with depth z.

The general form of the constitutive law that describes the nonlinear spring alone is

$$F_s = \alpha k w + (1-\alpha) k w_0 \zeta \tag{4.17}$$

where w is the elongation-contraction of the spring, k is the small amplitude distributed elastic stiffness, α is the ratio of post yielding stiffness to initial stiffness k, w_0 is the value of pile deflection that initiates yielding in the spring, and ζ is a hysteretic dimensionless quantity that is governed by the following equation

$$w_0 \dot{\zeta} + \gamma |\dot{w}| \zeta |\zeta|^{n-1} + \beta \dot{w} |\zeta|^n - \dot{w} = 0 \tag{4.18}$$

In the above equation β, γ, n are dimensionless quantities that control the shape of the hysteresis loop. The expressions given by (4.17) and (4.18) are preferred to similar expressions used by Trochanis *et al.* (1991), since in the present formulation the hysteretic parameter ζ is dimensionless, whereas in Trochanis' formulation, ζ has dimensions of length.

4.2.1 Pile shaft parameters

According to API (1986), the vertical shear strength for piles in clays or sands is represented by the unit skin friction capacity, f_s, (skin friction per shaft surface). For clays other that the ones found in the Gulf of Mexico, f_s should be taken equal to the undrained shear strength of clay (*i.e.*, $S = S_u$) in the case where $S_u < 24kPa$, and equal to one half of S_u in the case where $S_u > 72kPa$. Linear interpolation is employed for intermediate values. Herein the maximum shear capacity is simply expressed as

$$f_s(z) = \lambda(z)S(z) \tag{4.19}$$

where $\lambda(z)$ is a scalar parameter, which is a function of depth and is calibrated from experimental data. Combining (4.17) with (4.19) and using the fact that the post yielding stiffness of the pile-soil interface is assumed zero (*i.e.*, $\alpha = 0$), the restoring force from the nonlinear spring alone, which is given by (4.17), simplifies to

$$F_s(z) = \pi d\lambda(z)S(z)\zeta \tag{4.20}$$

where ζ is provided from the solution of (4.18), and the value of w_o in (4.17) is given by

$$w_0(z) = \lambda(z)\frac{S(z)}{k}\pi d \tag{4.21}$$

where k is the small-amplitude elastic stiffness of the distributed springs. Scott (1981) suggests that the zero-frequency limit of k for rigid piles is

$$k = \frac{\pi}{4}\frac{1}{1-\nu^2}E_s \tag{4.22}$$

and for flexible piles is

$$k = \frac{\pi}{4}\frac{1}{1+\nu}E_s \tag{4.23}$$

As an example, for an average value of Poisson's ratio, $\nu = 0.45$ the static stiffness value for the distributed springs is: $0.54E_s < k < 0.98E_s$. This range of values is in agreement, at the zero-frequency limit, with the expression proposed by Makris and Gazetas (1993) to analyze vertical vibrations of single piles and used in this model:

$$k(a_0) = 0.6E_s\left(1 + \frac{1}{2}\sqrt{a_0}\right) \tag{4.24}$$

in which a_o is the dimensionless frequency parameter $a_0 = \frac{\omega d}{V_s}$.

The parameters n and λ, in equations (4.18) and (4.20) respectively, can be readily calibrated from experimental data (*t-z* curves) or from empirical *t-z* curves (Coyle and Reese (1966) for steel-pipe friction piles in clay). A systematic procedure to estimate model parameters using established nonlinear regression algorithms (Marquardt 1963) is highly impractical because of the limited availability and scatter of data. In the analyses presented herein, a systematic trial and error approach employing engineering judgment was used. For instance, the parameters for the tip spring are calibrated first, and then the parameters of the shaft springs are calibrated using available t-z curves at given depths. The parameters at intermediate depths can then be estimated based on the soil layering configuration. Parameters λ and n control the yielding behavior of the soil immediately surrounding the pile. This behavior is nearly rate independent under monotonic loading (Kramer 1996) and of a hysteretic nature (frequency independent) under cyclic loading; therefore the associated parameters are also frequency independent.

Under dynamic loading (*i.e.,* finite frequencies), part of the input energy is dissipated through hysteresis in the vicinity of the pile-soil interface, and the remaining

energy radiates outwards. In this case, the nonlinear spring alone is not sufficient to model realistically the response, since the radiation damping is of a viscous type. This insufficiency motivated the addition of the viscous dashpot in parallel with the nonlinear spring as shown in figure 4.3. Of course, one could adjust the parameters of the Bouc-Wen model to incorporate the energy loss due to radiation into the hysteretic loops generated by the nonlinear spring. However, this will result in poor modeling since radiation damping is frequency dependent, and, therefore, the parameters of the nonlinear spring would have to be re-adjusted for different frequencies. Moreover, the incorporation of all the energy loss into one hysteretic loop implies that all the energy is dissipated along the pile-soil interface with no waves propagating outwards. Accordingly, for the case of dynamic loading, the presence of a frequency dependent dashpot accounts for the energy dissipated due to radiation.

A reasonable expression that describes the force resulting from the dashpot also has to be valid for small-amplitude motions. In this linear range, theoretical studies (Blaney *et al.* 1976) show that the frequency dependence of the distributed damping coefficient can be approximated with the expression

$$c_z = \pi d a_0^{-1/4} V_s \tag{4.25}$$

which has been used extensively in computing pile-group response at the linear limit (Gazetas and Makris 1991, Makris and Gazetas 1993).

Slippage effects are taken into account by introducing a slip element in series (see figure 4.3) with the nonlinear spring and dashpot model described previously. The friction capacity provided by the slider, τ_s, is a measure of the adhesion at the pile-soil interface, which may have a smaller value than the yield strength of soil f_s (given by equation (4.19)). It can be approximated with the Mohr-Coulomb friction law:

$$\tau_s = \sigma'_{rr} tan\delta \tag{4.26}$$

where σ'_{rr} is the radial effective stress and δ is the angle of interface friction between soil and pile.

In the case of perfect bonding between the pile and soil ($\tau_s > f_s$), the soil restoring force would transition in a smooth manner to the value of ultimate soil strength. However, if the friction capacity, τ_s, is less than the soil strength f_s at some depth, slippage will occur, and the soil reaction at that depth will abruptly reach a constant value, independent of settlement.

4.2.2 Pile tip parameters

The soil reaction at the pile tip is modeled by a single nonlinear spring and dashpot in parallel. At the pile tip, $z = L$, the restoring force from the spring is given as

$$F_{tip} = 9\pi\frac{d^2}{4}S(L)\zeta \tag{4.27}$$

where ζ is again governed by equation (4.18), the yield displacement w_0 in this case is given by

$$w_0 = 9\pi\frac{d^2}{4}\frac{S(L)}{k_{\text{tip}}} \tag{4.28}$$

The elastic stiffness k_{tip} for the reaction of a homogeneous elastic half-space to a rigid massless disk undergoing harmonic vibration is given as (Lysmer and Richart 1966)

$$k_{\text{tip}} = \frac{E_s(L)d}{1-\nu_s^2(L)} \tag{4.29}$$

and the dashpot constant is given as

$$c_{\text{tip}} = 3.4\frac{d^2 V_s(L)\rho_s(L)}{4(1-\nu_s(L))} \tag{4.30}$$

With the proposed macroscopic model, the nonlinear dynamic analysis of a single pile reduces to a one-dimensional problem, which is solved with the finite element method. The governing equation for the pile motion and the finite element formulation are provided in Appendix A.

4.3 Calibration of nonlinear model parameters

As indicated in the previous section, the parameters λ and n for the nonlinear springs along the pile shaft, as well as n for the base spring, need to be calibrated from static test data. This is done in the subsections that follow for two different geotechnical profiles.

4.3.1 Pile in medium stiff clay

O'Neill, Hawkins and Mahar (1982) carried out static load testing of two single piles and a 3x3 pile-group in a nonhomogeneous soil deposit consisting of four recognizable layers of very stiff to medium stiff clay. The same site was later used in dynamic testing of a single pile by Muster and O'Neill (1986), who also presented geotechnical data obtained from the site.

The test pile was a 273 mm outside diameter closed-ended steel pipe with a 9.3 mm thick wall. For the static tests, it was driven to a depth of 13.1 m (43 ft.). The pile and soil properties used in this analysis are those presented in figure 4.3. The chosen undrained shear strength profile follows closely the Cone Penetration Test (CPT) trend obtained in the field. Results from Unconsolidated-Undrained (UU) triaxial tests show large variation and are not used.

Figure 4.4 shows the results of the calibration procedure. Figure 4.4(a) shows observed *t-z* curves at four different depths along the pile and the corresponding model-predictions after calibration. The calibrated values of λ and n are also shown. The influ-

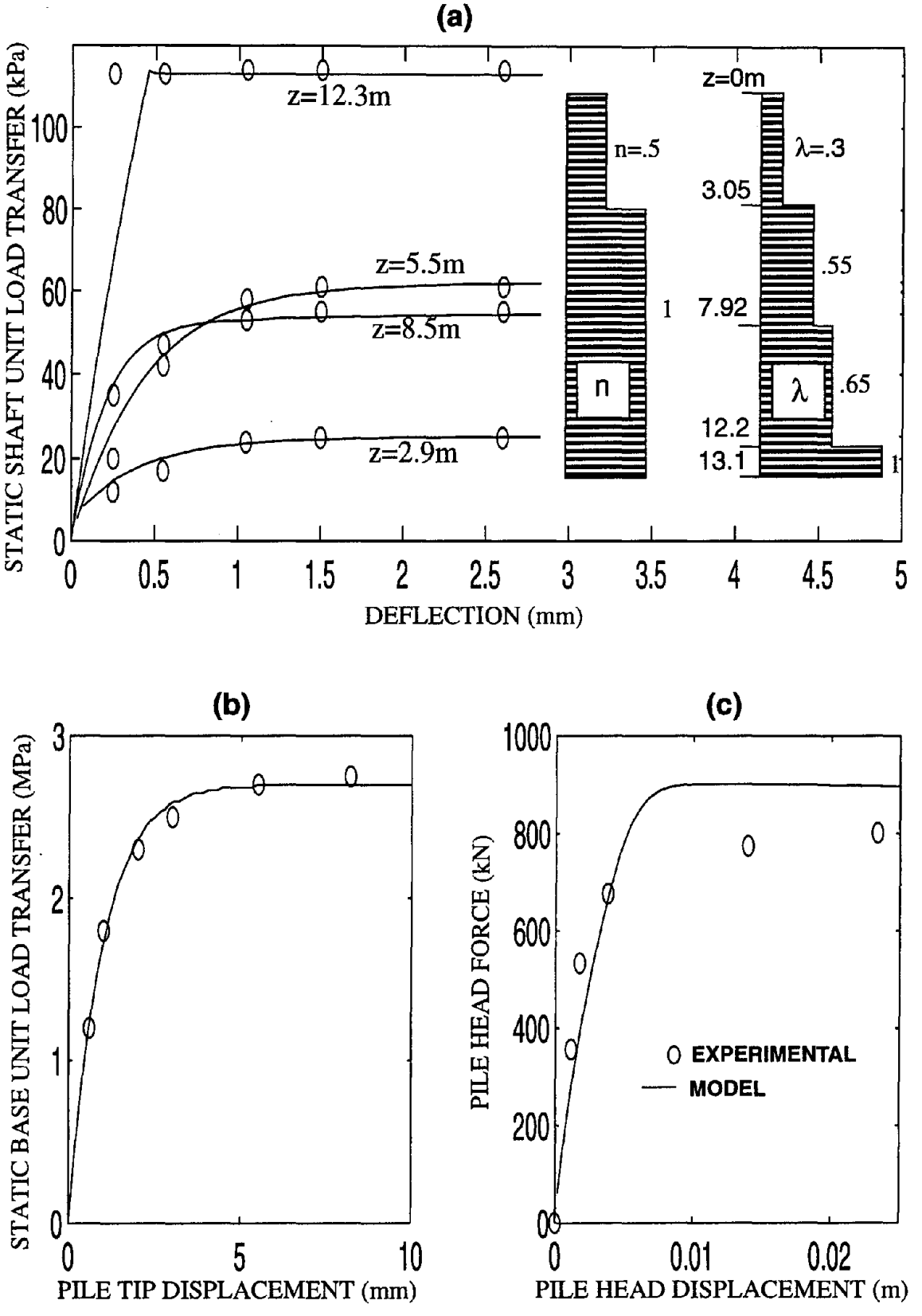

Figure 4.4: Model calibration from static test data of O'Neill *et al.* (1982).

ence of pile-soil slip is clearly visible from the abrupt levelling of the *t-z* curve at 12.3 m depth, implying that at this depth the adhesive strength along the interface governs the ultimate soil resistance. The value of this adhesive strength is taken equal to 113 kPa and used directly in the analysis for lack of effective radial stress measurements or angle of interface friction values. The smooth transitions to failure observed in *t-z* curves at the other levels indicate that yielding, as opposed to slippage, governs the behavior of the soil.

Figure 4.4(b) shows the static base unit load transfer curve from which the parameter n of the tip spring is calibrated. The soil strength obtained from this curve is consistent with measured values of S_u at the pile tip.

Figure 4.4(c) compares the measure pile head load-settlement curve and the model prediction. The agreement is fairly good, especially considering the uncertainty in soil parameters at different depths, all of which contribute to the head response comparably, unlike in the case of lateral loading, in which the major contribution is confined to a few pile diameters below the surface (Badoni 1995, Badoni and Makris 1996).

4.3.2 Pile in high OCR clay

Bond and Jardine (1995) described a series of field experiments carried out on instrumented closed-ended steel piles (102 mm diameter) in heavily over-consolidated London clay. A variety of measurements were made to investigate the influence of different factors on shaft capacity. From their observations, they concluded that the shaft capacity for this particular case was governed by an effective stress interface sliding criterion and not by failure of the surrounding continuum. This observation also provides justification for the presence of the slider in this model.

In order to show the significance of the presence of the slider, two predictions are offered. In the first more traditional approach, the undrained shear strength S_u of the clay

was multiplied with an empirical factor λ as recommended in API (1986) (described earlier in the section on pile shaft modeling) to account for slippage. Accordingly, the slider was constrained to behave as a rigid support. In the second approach, the slider was assumed to be governed by the Mohr-Coulomb friction criterion given by (4.26). The measured effective radial stresses from the field were used as input to the model, and the value of the angle of interface friction δ was calibrated from the force-displacement curve.

Figure 4.5 shows the predictions with the two methods. The soil and pile properties used in the analysis are also illustrated. The API method underpredicts the pile capacity. On the other hand, the calibrated value of $\delta = 10^0$ obtained with the second approach is in good agreement with the values obtained from interface ring shear tests reported by Tika (1989). Of course more tests on a wider variety of soil types are needed to fully validate the proposed procedure.

4.4 Prediction of nonlinear dynamic response of single piles

The calibrated model can be used to predict dynamic force-displacement loops at different levels of loading and induced frequency. Figure 4.6 shows dynamic force-displacement loops at the pile head for four selected frequencies (f= 0.1, 1.0, 10 and 20 Hz), where the pile properties and soil profile are those reported by Muster and O'Neill (1986). It is interesting to note that, as frequency increases, the shape of the loops tends to that of an ellipse, since viscous forces due to radiation damping prevail over the hysteretic forces. For the sake of comparison, the loops corresponding to linearly elastic soil behavior are also shown in the figure. There is a substantial difference in the predicted stiffness and damping of the pile-soil system.

In the context of an equivalent linear analysis, the "loss" stiffness, $K_2(\omega)$, of the

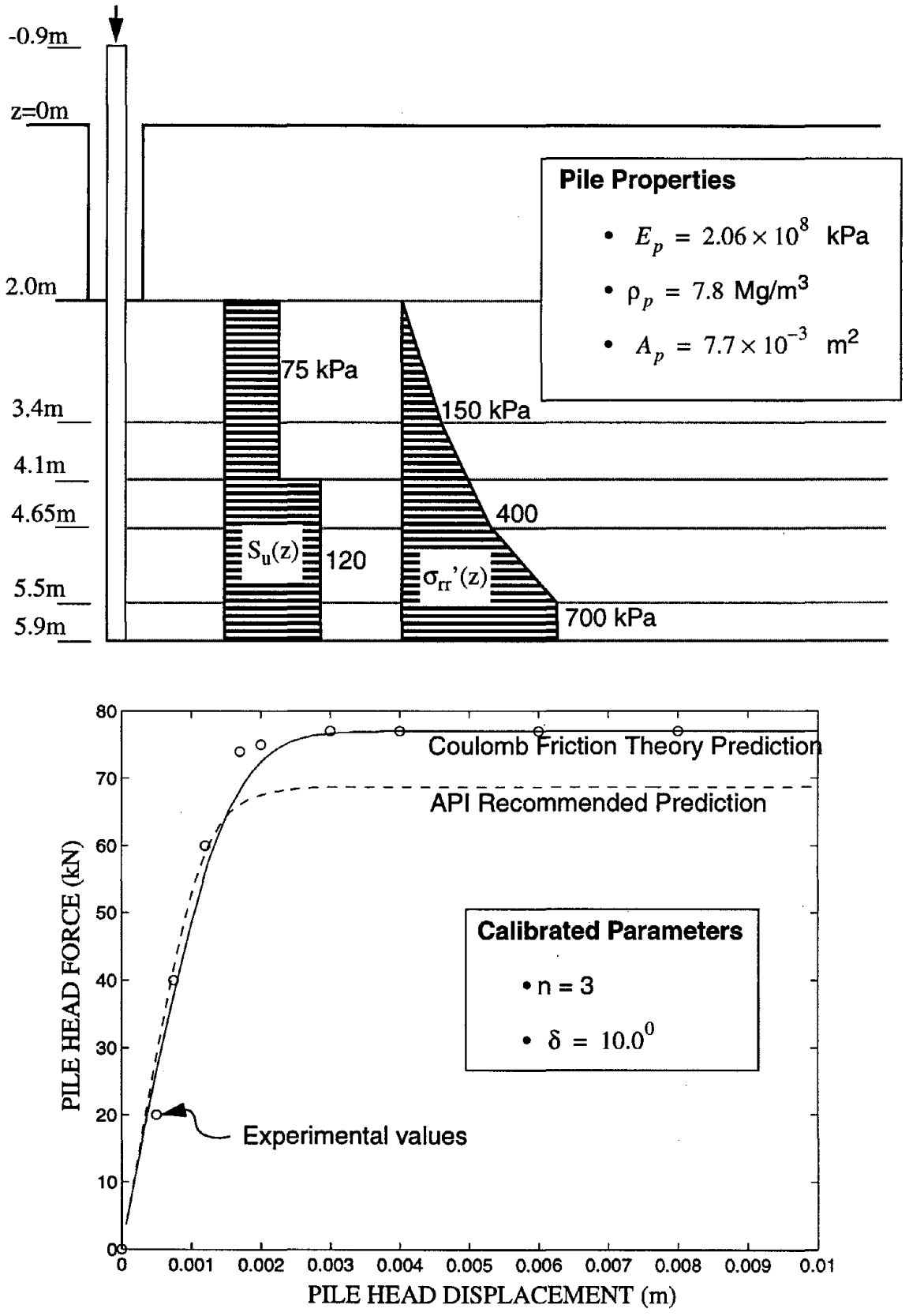

Figure 4.5: Model calibration from static test data of Bond & Jardine (1995).

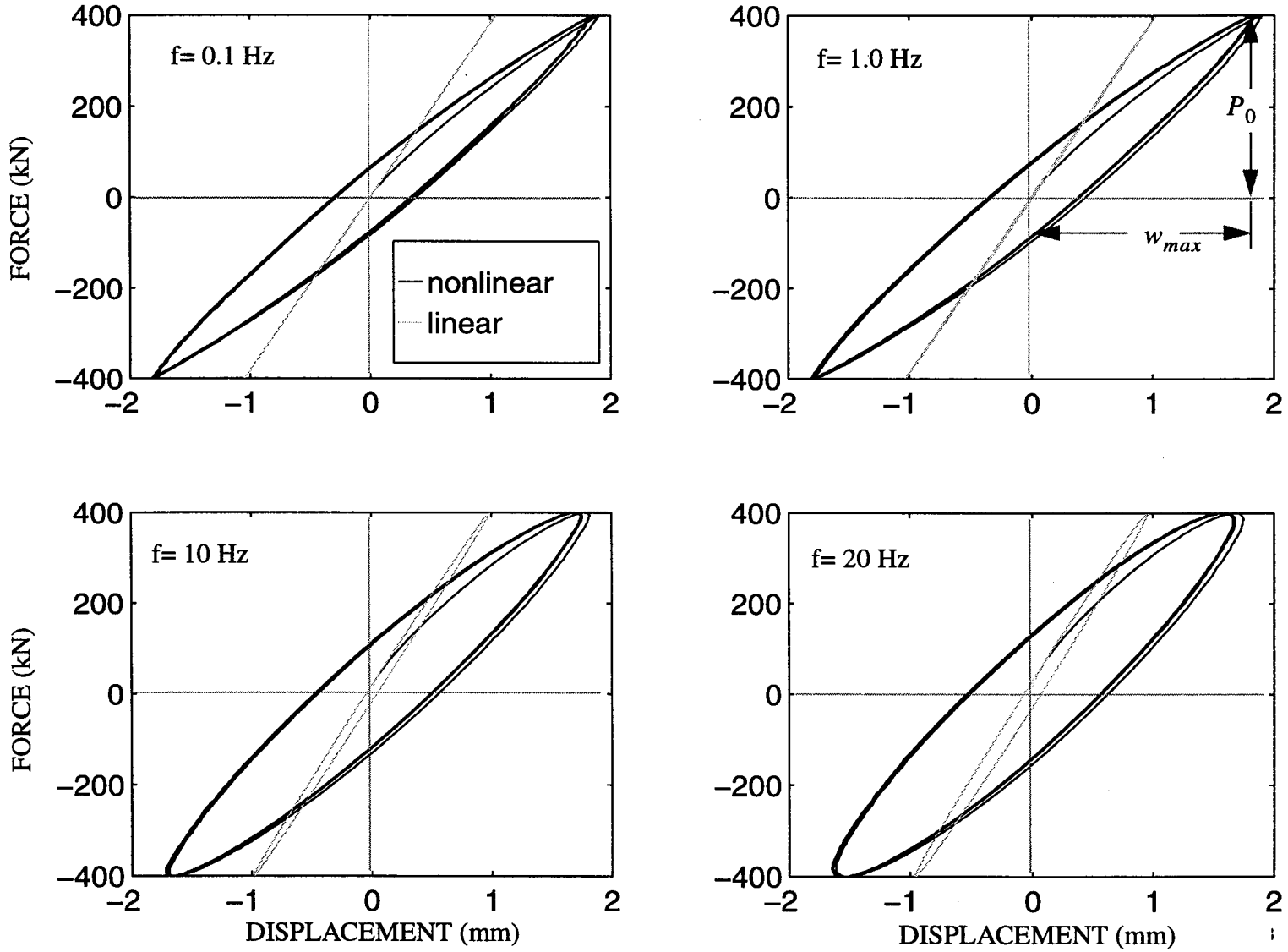

Figure 4.6: **Dynamic head force-displacement loops (P_0= 400kN) under harmonic force input at different frequencies: Pile and soil properties from O'Neill *et al.* (1982).**

nonlinearly behaving pile is:

$$K_2(\omega) = \omega C(\omega) = \frac{W_D}{\pi w_{max}^2} \tag{4.31}$$

where W_D is the area of the force-displacement loop at the pile-head and w_{max} is the maximum pile-head settlement. This area corresponds to the total energy loss by hysteretic and radiation damping. The "storage" stiffness of the nonlinearly behaving pile, $K_1(\omega)$, is obtained from:

$$K_1(\omega) = \left[\left\{\frac{P_0}{w_{max}}\right\}^2 - \{K_2(\omega)\}^2\right]^{1/2} \tag{4.32}$$

The equivalent linear dynamic stiffness of the pile is

$$K(\omega) = K_1(\omega) + iK_2(\omega) \tag{4.33}$$

In most dynamic testing, a mass, m, is placed on the pile cap, and in this case the complex frequency response function of the pile-mass system is

$$H(\omega) = \frac{w(\omega)}{P_0} = \frac{1}{K_1(\omega) + iK_2(\omega) - m\omega^2} \tag{4.34}$$

Figures 4.7 and 4.8 show the model predictions for the equivalent linear dynamic storage and loss stiffnesses, normalized with respect to the small-amplitude static stiffness, for the two case histories studied in section 4.3. The applied load amplitudes are indicated as ratios of the ultimate load capacity P_{ult} ($P_{ult} \approx 900$ kN on figure 7, and $P_{ult} \approx 80$ kN on figure 8).

Limited experimental data is available in the geotechnical literature on vertical dynamic nonlinear response of piles. Muster and O'Neill (1986) used, for dynamic testing, a pile of the same dimensions and properties as in the static case, which was driven to a depth of 12.61 m with a protruding portion of 0.81 m. It was capped with a rigid mass

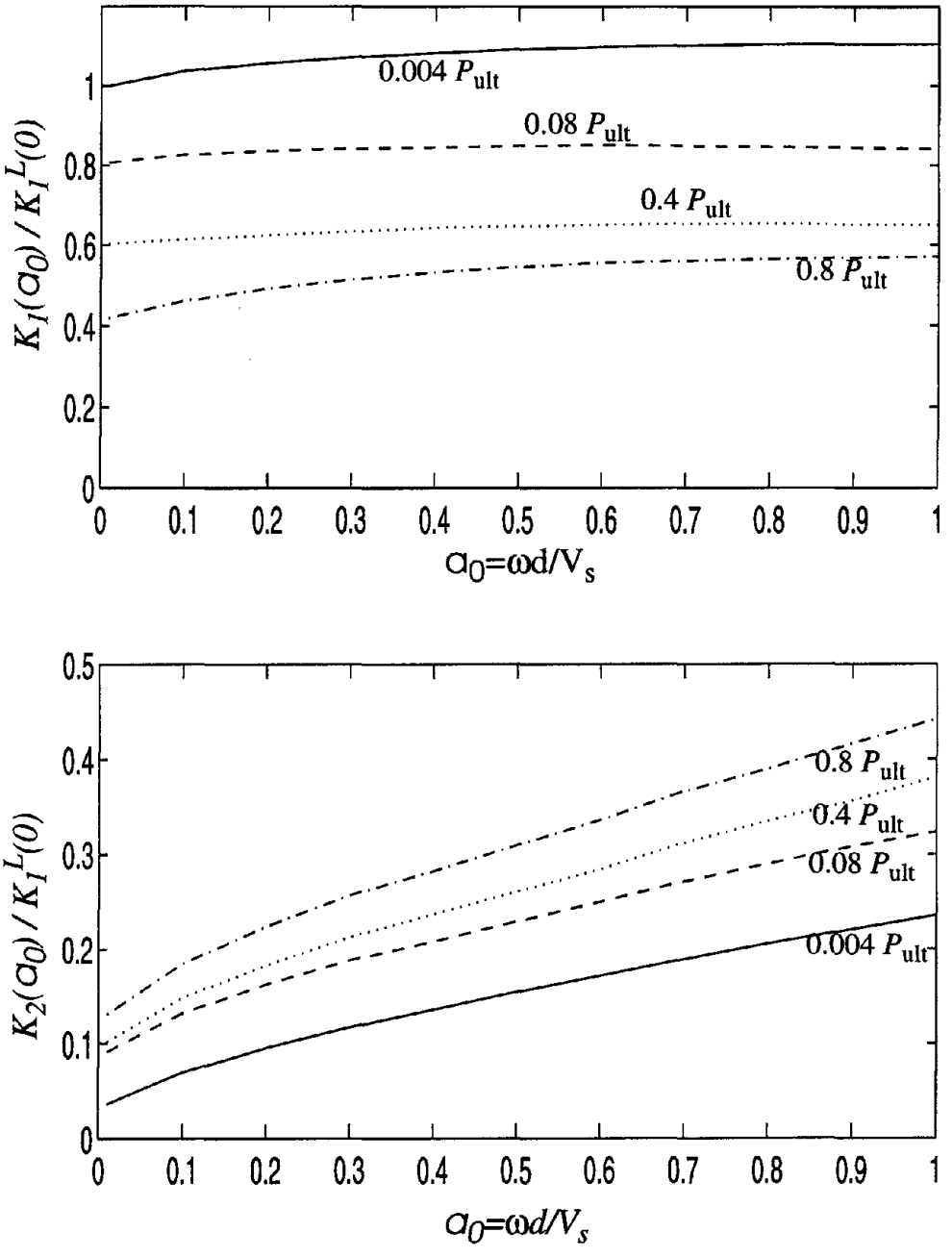

Figure 4.7: Dynamic storage and loss stiffnesses for single pile from Muster and O'Neill (1986).

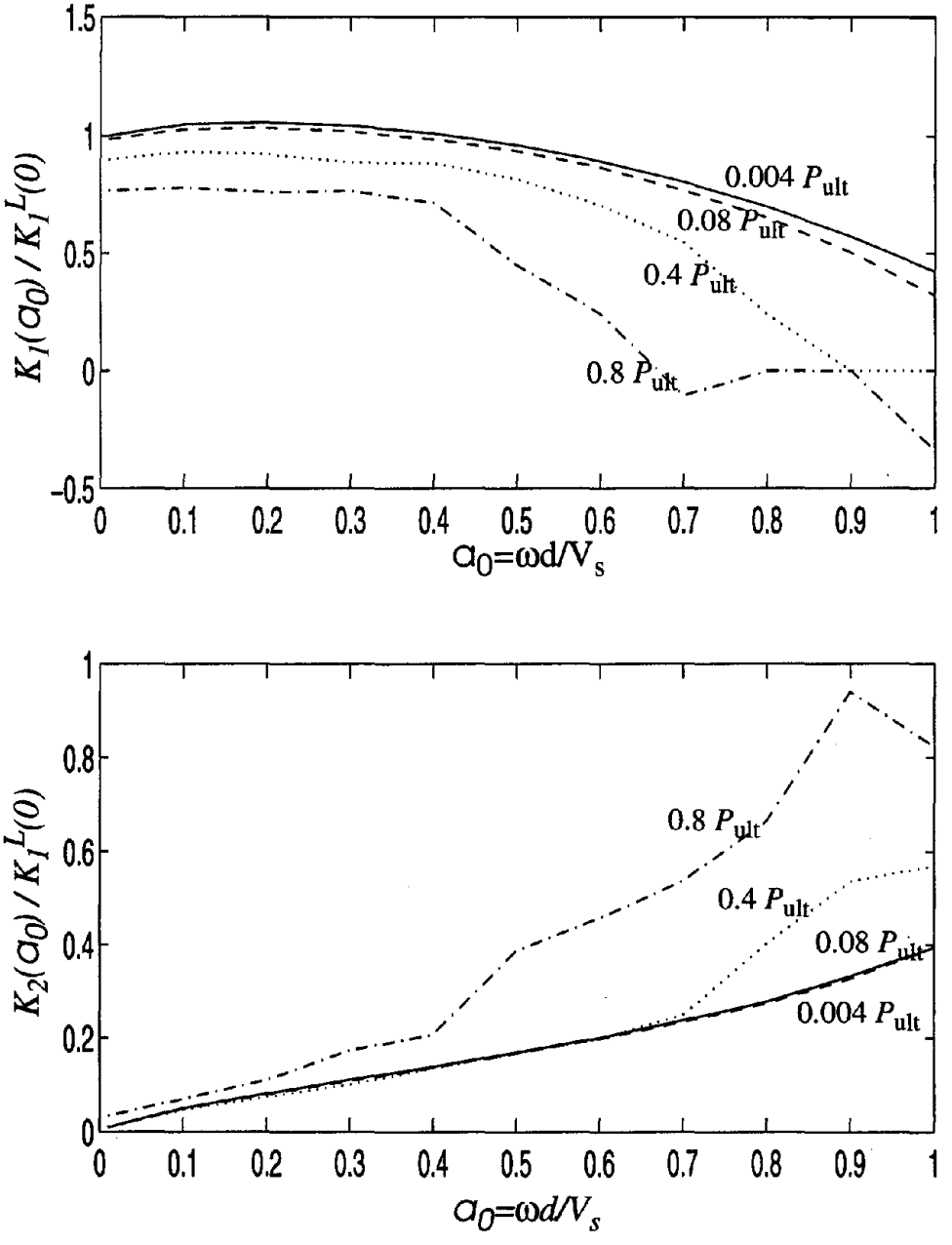

Figure 4.8: Dynamic storage and loss stiffnesses for single pile from Bond and Jardine (1995).

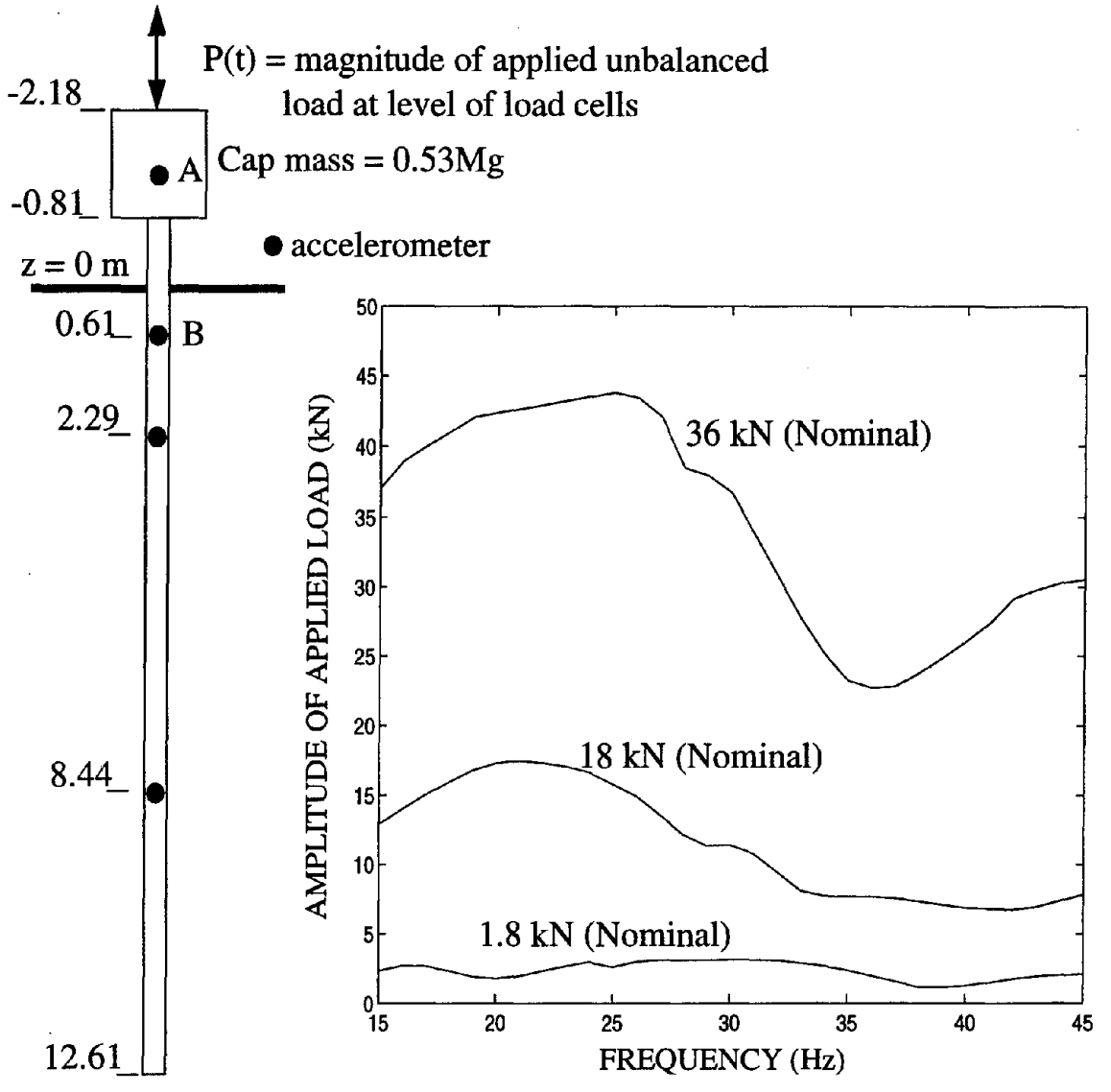

Figure 4.9: Dynamic test model setup and frequency dependence of applied loading for experiment conducted by Muster and O'Neill (1986).

weighing 55.3 kN, and subsequently excited using a linear inertial mass vibrator. The arrangement is depicted in figure 4.9. The applied load to the pile cap was measured by load cells placed in between the cap-mass and vibrating assembly, and as such the weight of the vibrator need not be included in the analysis. Accelerometers were located in the cap and at various depths along the pile. Details of test arrangements and procedures can be found in the original paper by Muster and O'Neill.

Three levels of dynamic loading (amplitudes 1.8kN, 18kN and 36kN) were succes-

sively applied in frequency sweep tests. Because of the dynamics of the pile-cap-vibrator system however, the applied load amplitudes vary with frequency, as illustrated in figure 4.9. This is an important factor taken into consideration in this analysis.

Figure 4.10 shows the computed complex-frequency-response-function magnitudes (equation (4.34)) obtained with the calibrated model and experimentally obtained transfer functions (referred to as "vertical flexibility" in the figure according to Muster and O'Neill's nomenclature) between displacements and applied load amplitudes for two different accelerometer locations. The resonance frequencies are predicted fairly well for all three levels of loading, whereas the magnitudes at resonance are, in general, overpredicted by approximately 20%. It should be noted that the observed peak for the 36kN load shows a sudden increase in flexibility which may be attributed to the formation of a "gap" through soil erosion at the surface during the earlier tests.

4.5 Nonlinear dynamic group response

The procedure utilized herein to compute pile-soil-pile interaction is an extension of the approximate procedure developed by Gazetas and Makris (1991). It is assumed that the nonlinear behavior is concentrated in the vicinity of the pile-soil interface (*i.e.,* in the near field; Nogami *et al.* 1992, El Naggar and Novak 1994), and that the remaining soil between piles (the far field) behaves elastically. This assumption allows for the use of wave propagation expressions in the far field. The original procedure, initially developed for linear response analysis of pile groups, is also used herein. The procedure consists of three steps.

Step 1: The axial elongation-contraction, $w(z, t)$, of a single pile, subject to inertial loading at its head, is determined using the proposed nonlinear model.

Step 2: The induced soil-deformations due to the oscillations of the pile generate P

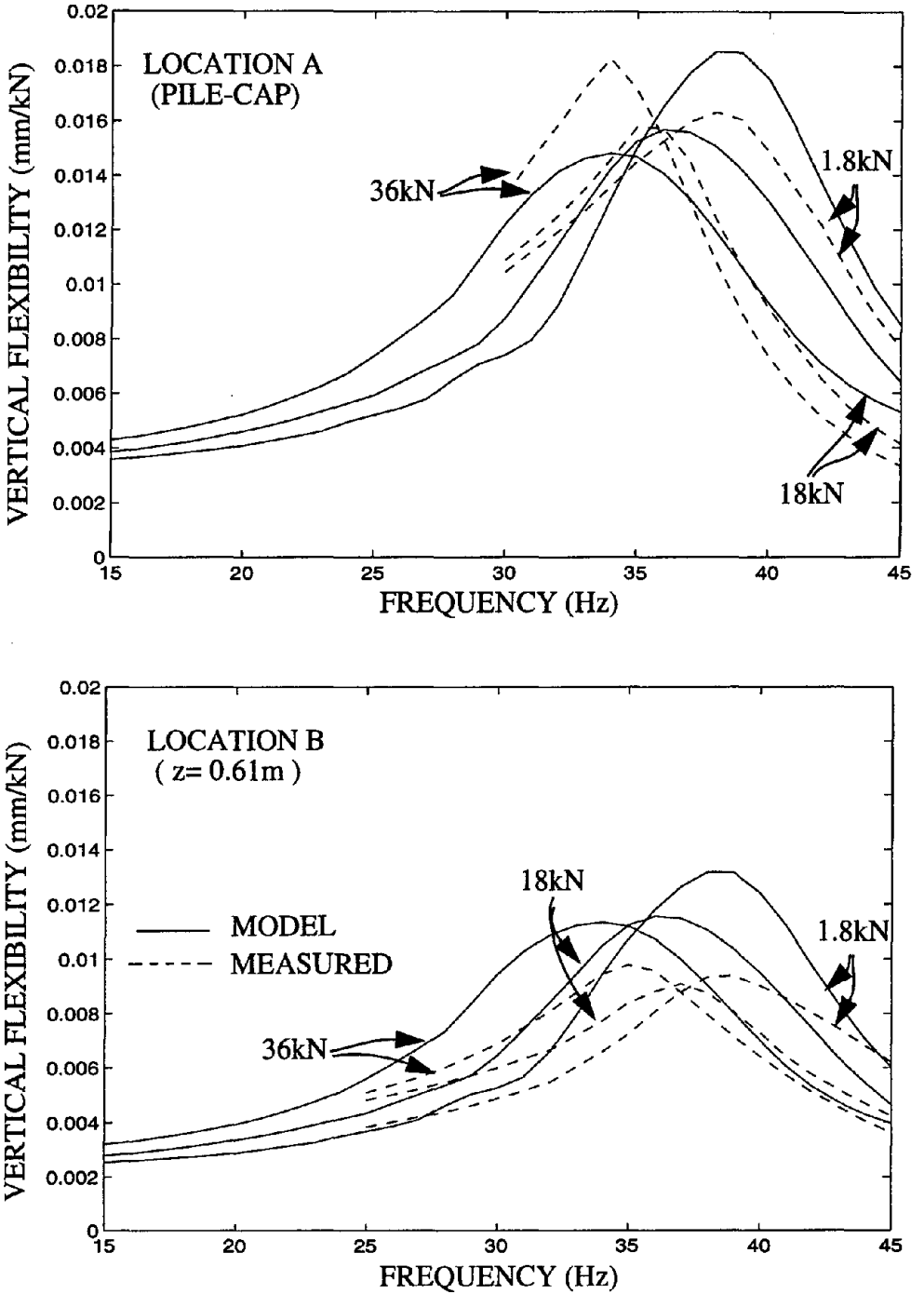

Figure 4.10: Comparison of experimental and predicted transfer functions: Test data from Muster and O'Neill (1986).

and S-waves travelling radially outward from the pile and also being reflected from the soil free surface. To simplify the problem, it is assumed that these waves spread out only along the horizontal direction in the outer field, attenuating in the process. These attenuated waves will eventually reach the near field of the neighboring ("receiver" or "passive") pile. Here, the soil displacements produced by the waves emanating from the "active" pile are used as support motion on the nonlinear springs and dashpots associated with the receiver pile. A schematic illustration of this approach is shown in figure 4.11.

Step 3: The response of a pile belonging to a group is the result of its own load plus the additional influences originating from its neighboring piles in the form of support motion at the pile-soil interface. The time domain expression for the additional wave field, given by equation 4.13, is employed to obtain this support motion at each time step of the time-marching scheme.

With this method, the simplest pile-group configurations that can be analyzed are the 2x1 and 2x2, since each pile in the group is subjected to identical loading conditions. In such cases, the problem reduces to the analysis of a single pile subjected to the head loading as well as the displacement field emitted from the neighboring piles. The governing equations and finite-element formulation for combined head loading and wave loading induced from the diffracted wave field are described in Appendix A.

The model was used to determine the effect of nonlinearity on the vertical response of pile groups. The results for a 2x1 and 2x2 pile group, embedded in the soil profile reported by Muster and O'Neill, for different pile-to-pile spacings are shown in figures 12 and 13, respectively. The reference shear wave velocity used to determine a_0 is V_s = 116 m/s. The storage and loss stiffness coefficients are normalized with respect to n-times (n = number of piles in the group) the linear static stiffness of a single pile, while the applied load levels are indicated in terms of the ultimate load capacity of a single pile

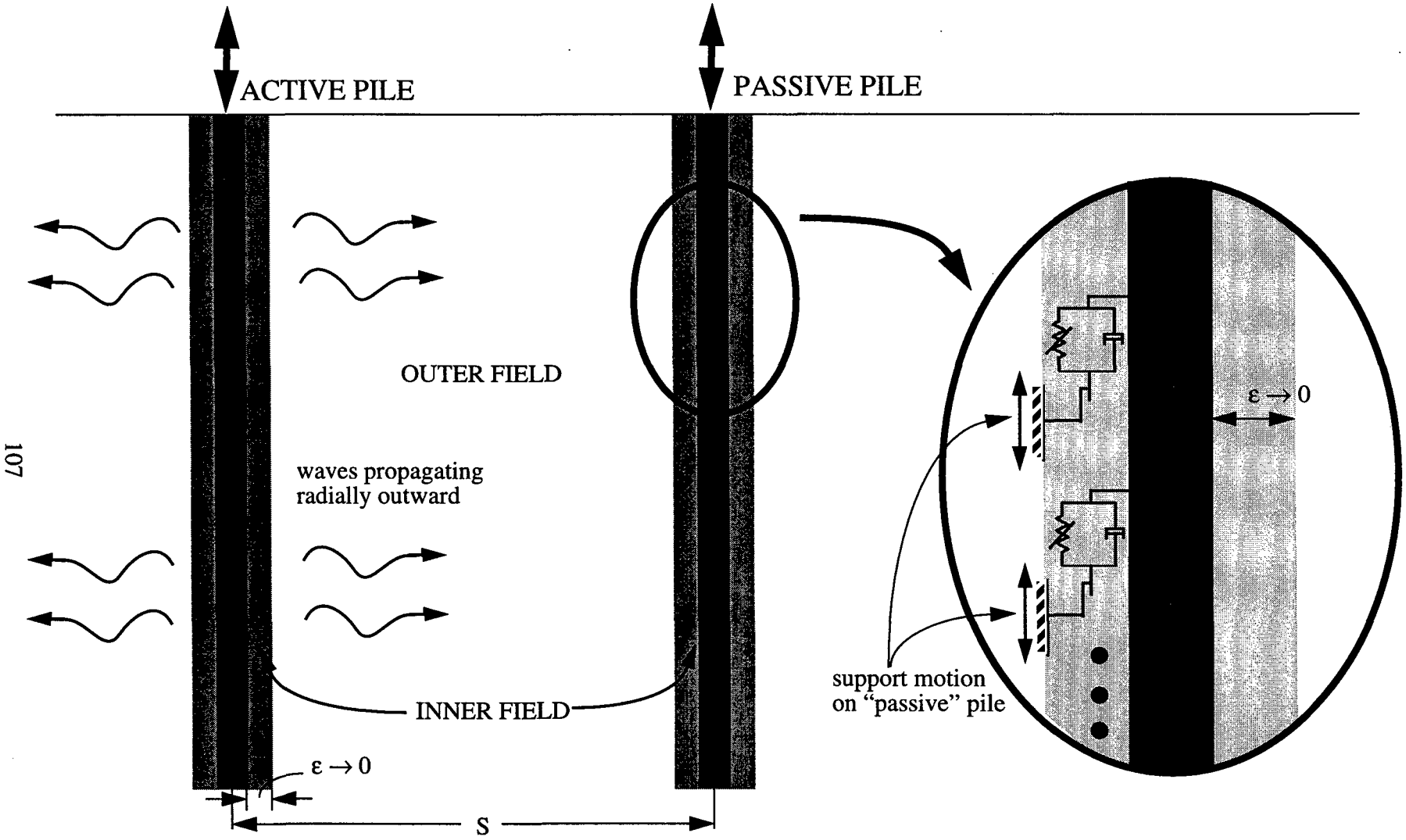

Figure 4.11: Schematic illustration of pile-soil-pile interaction model.

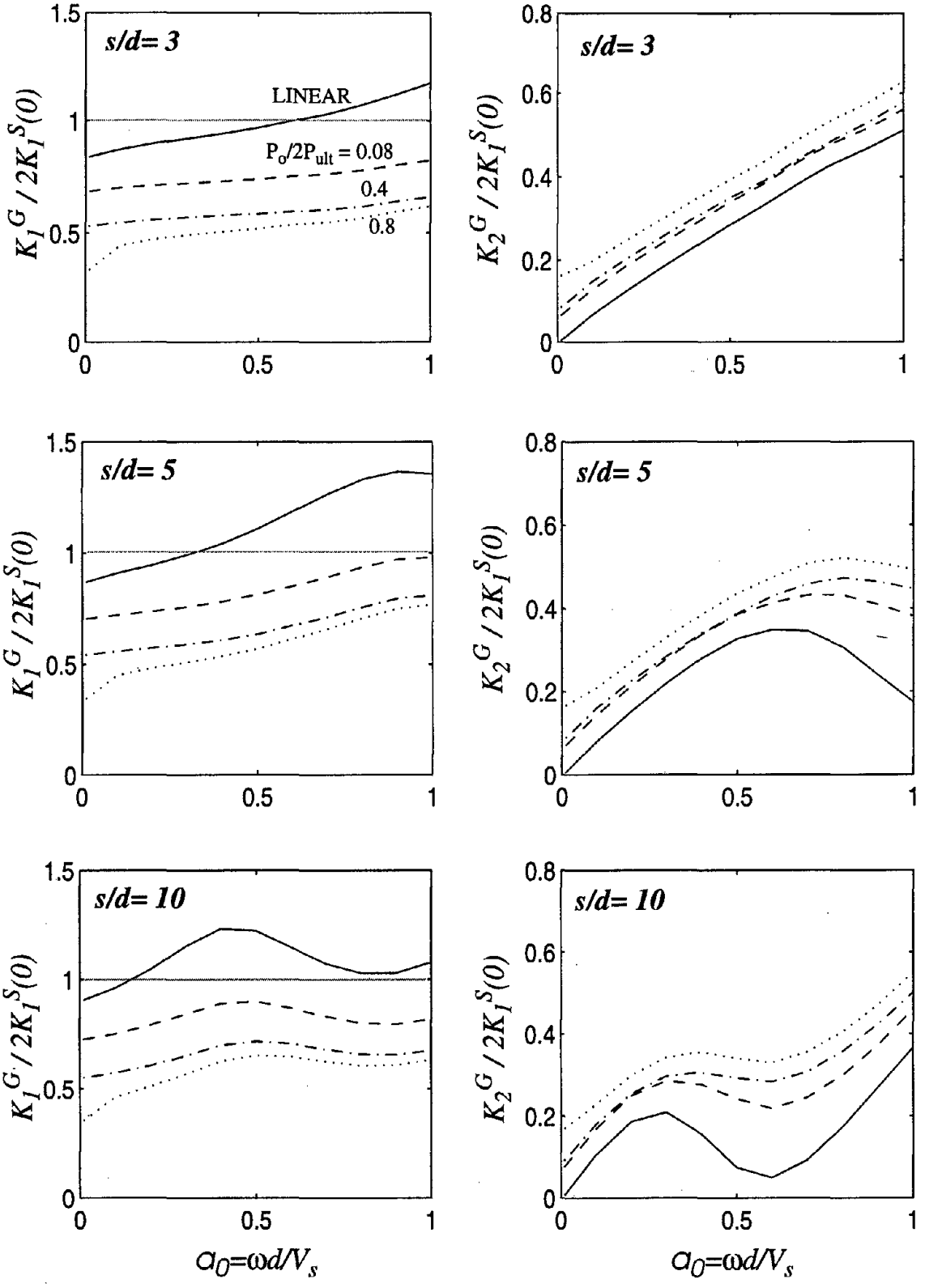

Figure 4.12: Normalized storage and loss stiffness coefficients for a 2x1 pile group embedded in the soil profile from Muster and O'Neill (1986).

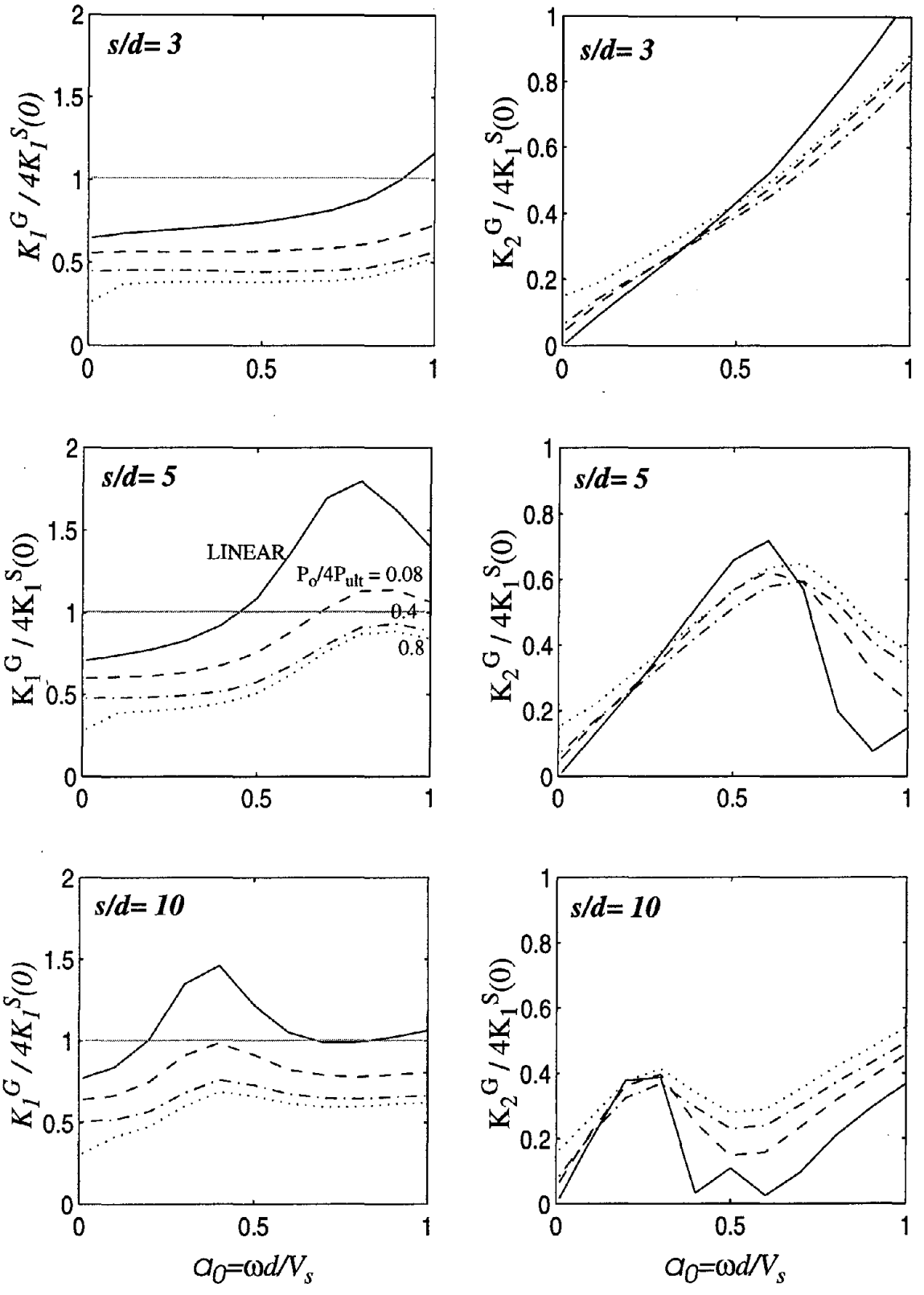

Figure 4.13: Normalized storage and loss stiffness coefficients for a 2x2 pile group embedded in the soil profile from Muster and O'Neill (1986).

P_{ult} and n. It is clear that increasing load levels, and thereby increasing nonlinearity in the response, leads to substantial decrease in the equivalent linear stiffness (storage stiffness) while increasing equivalent linear damping (loss stiffness). Also noticeable is the flattening of peak response for increasing load levels indicating that pile-soil-pile interaction effects are suppressed due to increasing nonlinearity.

4.6 Lateral response of pile groups: summary of the companion model

This section presents a description of the companion model for lateral response of pile groups developed earlier (Badoni 1995, Badoni and Makris 1996). The salient features of the model are described first, along with the method of determination of model parameters. The results from a calibration procedure undertaken for five full-scale experiments are then outlined. Subsequently, a few results for the dynamic lateral response of single piles are presented.

4.6.1 Attenuation function in the time domain

In the case of lateral response, the expression for the displacement field $u(z, r, \phi, \omega)$ at depth z at a distance r away from the pile and at an angle ϕ with respect to the direction of pile motion may be written as

$$u(z, r, \phi, \omega) = \psi(r, \phi, \omega) y(z, \omega) \tag{4.35}$$

where $y(z, \omega)$ represents the lateral displacement of the pile at depth z and ω is the frequency of oscillation. $\psi(r, \phi, \omega)$ is an approximate attenuation function proposed by Makris and Gazetas (1992) given by

$$\psi(r, \phi, \omega) = \psi(r, 0, \omega)(cos\phi)^2 + \psi\left(r, \frac{\pi}{2}, \omega\right)(sin\phi)^2 \tag{4.36}$$

$$\psi(r, 0, \omega) = \left(\frac{d}{2r}\right)^{1/2} exp\left[-\beta_s \frac{\omega\left(r-\frac{d}{2}\right)}{V_{La}}\right] exp\left[i\frac{\omega\left(r-\frac{d}{2}\right)}{V_{La}}\right] \tag{4.37}$$

$$\psi\left(r, \frac{\pi}{2}, \omega\right) = \left(\frac{d}{2r}\right)^{1/2} exp\left[-\beta_s \frac{\omega\left(r-\frac{d}{2}\right)}{V_s}\right] exp\left[i\frac{\omega\left(r-\frac{d}{2}\right)}{V_s}\right] \tag{4.38}$$

in which d is the pile diameter, V_s is the shear wave velocity and $V_{La} = [3.4/\pi(1-\nu)]$ is the Lysmer's analogue wave velocity (ν being the soil Poisson's ratio). Equation (4.35) can be transformed in the time domain with the help of the convolution integral.

$$u(z, t) = \int_{-\infty}^{\infty} \psi(r, \phi, t-\tau) y(z, \tau) d\tau \tag{4.39}$$

where

$$\psi(r, \phi, t) = \frac{1}{2\pi} \int_{-\infty}^{\infty} \psi(r, \phi, \omega) e^{i\omega t} d\omega \tag{4.40}$$

Denoting the travel times for the compression-extension and shear waves by $t_L = \frac{r-d/2}{V_{La}}$ and $t_s = \frac{r-d/2}{V_s}$ respectively, and using equations (4.36) to (4.38), equation (4.40) takes the form:

$$\begin{aligned} \psi(r, \phi, t) = {} & cos^2\phi \sqrt{\frac{d}{2r}} \frac{1}{2\pi} \int_{-\infty}^{\infty} e^{-\beta\omega t_L} e^{i\omega t_L} e^{i\omega t} d\omega \\ & + sin^2\phi \sqrt{\frac{d}{2r}} \frac{1}{2\pi} \int_{-\infty}^{\infty} e^{-\beta\omega t_s} e^{i\omega t_s} e^{i\omega t} d\omega \end{aligned} \tag{4.41}$$

which can be obtained, by a process similar to that in section 4.1, as

$$t\,\psi(S,\phi,t) = \frac{1}{\pi}\sqrt{\frac{d}{2r}}\left[\cos^2\phi\frac{\beta t_L}{\beta^2 t_L^2 + (t-t_L)^2} + \sin^2\phi\frac{\beta t_s}{\beta^2 t_s^2 + (t-t_s)^2}\right],\ \beta \neq 0 \qquad (4.42)$$

$$\psi(S,\phi,t) = \frac{1}{\pi}\sqrt{\frac{d}{2r}}[\cos^2\phi\,\delta(t-t_L) + \sin^2\phi\,\delta(t-t_s)],\ \beta = 0 \qquad (4.43)$$

The displacement field given by (4.39) may now be written as

$$u(z,t) = \frac{1}{\pi}\sqrt{\frac{d}{2r}}\left[\cos^2\phi\int_{-\infty}^{\infty}\frac{\beta t_L}{\beta^2 t_L^2 + (t-t_L-\tau)^2}y(z,\tau)d\tau + \sin^2\phi\int_{-\infty}^{\infty}\frac{\beta t_s}{\beta^2 t_s^2 + (t-t_s-\tau)^2}y(z,\tau)d\tau\right],\ \beta \neq 0 \qquad (4.44)$$

$$u(z,t) = \sqrt{\frac{d}{2r}}Y(z)[\cos^2\phi\,y(t-t_L) + \sin^2\phi\,y(t-t_s)],\ \beta = 0 \qquad (4.45)$$

4.6.2 Nonlinear model for lateral response of single piles

The problem herein is that of a single pile embedded in a layered soil and subjected to lateral motion. The pile is modeled as a linear elastic beam with circular cross-section area A_p, diameter d, moment of inertia I_p, Youngs modulus E_p and mass density ρ_p. The surrounding soil is considered to be an inhomogeneous deposit with shear wave velocity V_s, density ρ_s, shear strength S, or angle of internal friction ϕ, that vary with depth. The soil-pile interface is modeled as a Winkler foundation interacting with the pile through continuously distributed nonlinear springs and linear dashpots as sketched in figure 4.14.

The restoring force from the nonlinear spring at depth z is given by

$$F_s(z) = \lambda(z)S(z)d\zeta, \quad \text{for cohesive soils} \qquad (4.46)$$

$$F_s(z) = \mu\gamma_s d\frac{1+\sin\phi}{1-\sin\phi}z\zeta, \quad \text{for cohesionless soils} \qquad (4.47)$$

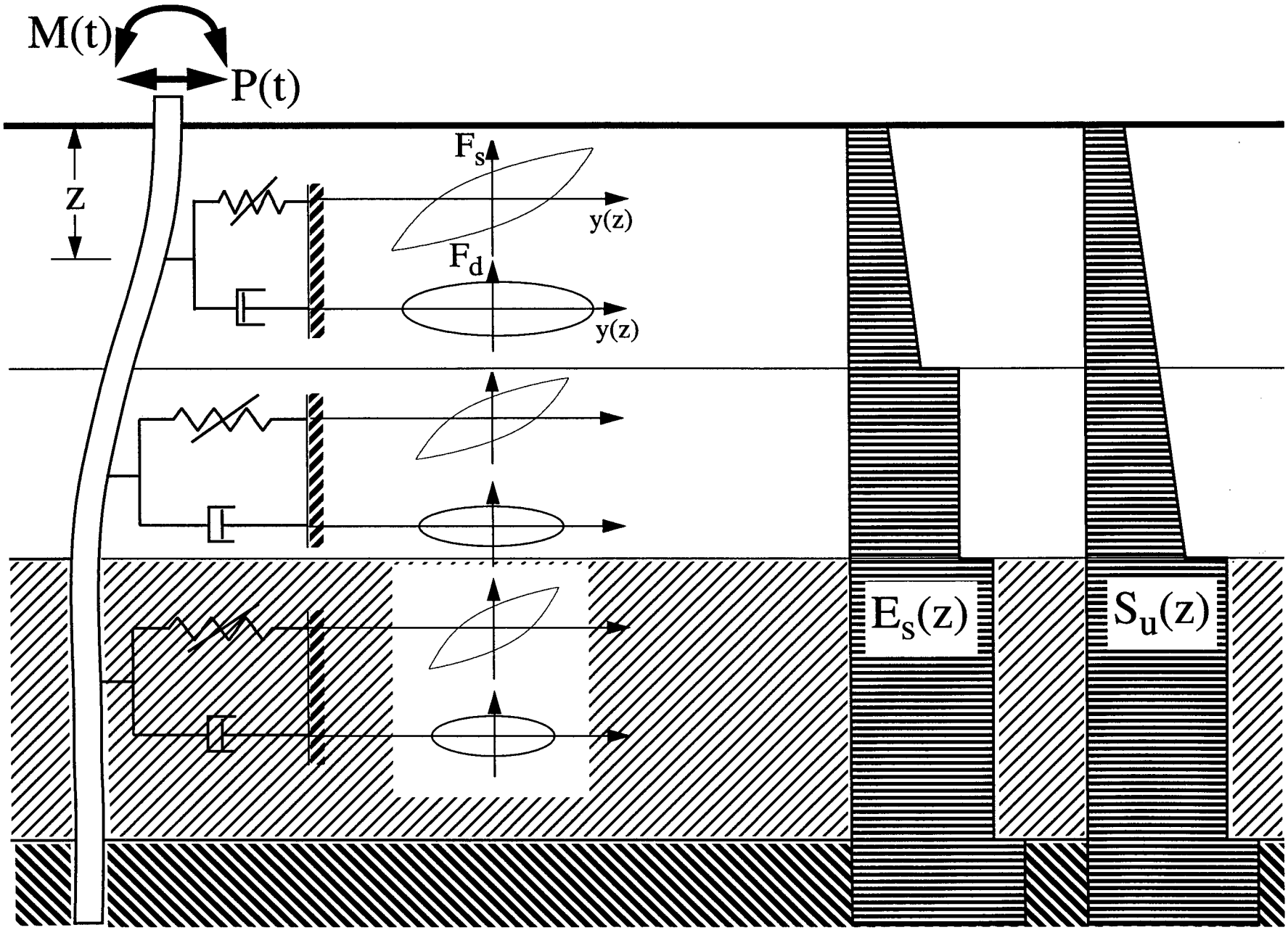

Figure 4.14: Schematic illustration of dynamic nonlinear lateral pile-soil interaction.

where λ varies linearly from 3 to 9 according to the equation

$$\lambda(z) = 3 + \frac{\sigma_z}{S(z)} + J\frac{z}{d} \tag{4.48}$$

as recommended by Matlock (1970).

Here, d is the pile diameter, γ_s the soil specific weight, σ_z the overburden pressure, and ζ is a hysteretic dimensionless quantity that is governed by the following nonlinear equation

$$y_0\dot{\zeta} + \gamma|\dot{y}|\zeta|\zeta|^{n-1} + \beta\dot{y}|\zeta|^n - A\dot{y} = 0 \tag{4.49}$$

in which y is the pile deflection at the location of the spring, and y_0 is the yield limit defined by $y_0 = S/k$ where k is the small-amplitude distributed elastic stiffness usually approximated by (Gazetas and Dobry 1984, Makris and Gazetas 1992, Makris 1994)

$$k \approx 1.2E_s \tag{4.50}$$

β, γ, n and A (=1 in this formulation) are dimensionless quantities that control the shape of the hysteretic loop. The parameters that need to be identified from static test data are n, and J or μ for cohesive and cohesions soils respectively.

At the small-amplitude linear limit, the restoring force from the dashpot is of the form

$$F_d = [Qa_0^{-0.25}\rho_s V_s d]\dot{y} \tag{4.51}$$

where the term within the brackets is the distributed frequency dependent damping coefficient $c(a_0) = Qa_0^{-0.25}\rho_s V_s d$. $a_0 = \omega d/V_s$ is the dimensionless frequency, and the coefficient Q is given by the expression

$$Q = 2\left[1 + \frac{3.4}{\pi(1-\nu_s)}\right]^{1.25}\left(\frac{\pi}{4}\right)^{0.75} \tag{4.52}$$

At shallow depths (i.e., less than three diameters) the expression given by (4.52) can be simply replaced by $Q = 3$ (Gazetas and Dobry 1984).

Under harmonic vibrations with frequency ω, equation (4.51) yields a force proportional to ωy. However, when the response becomes nonlinear ($y > y_0$), the force generated from radiation damping does not increase considerably compared to the maximum damping force that develops under linear conditions. Accordingly, in order to account for large pile deflections under harmonic excitation, equation (4.51) is refined to

$$F_d = Qa_0^{-0.25}\rho_s V_s d\omega\langle y\rangle \tag{4.53}$$

where

$$\langle y\rangle = y_0 \quad \text{for} \quad y > y_0 \tag{4.54}$$

and

$$\langle y\rangle = y \quad \text{for} \quad y < y_0 \tag{4.55}$$

With this formulation, the nonlinear spring equation, (4.46) or (4.47), and the dashpot equation, (4.53), of the constitutive model are consistent with the viscoplastic analysis at the limit of small-deflections and the plasticity analysis at the zero-frequency limit. A more detailed description of the model can be obtained in Badoni (1995).

4.6.3 Calibration of model parameters

Five well instrumented full-scale experiments were selected where the pile response was recorded beyond the elastic limit. In all cases, the model was first calibrated using static test data and subsequently used to predict dynamic response. Table 1 summarizes the soil properties, pile characteristics and the values of the calibrated model parameters. The primary purpose of Table 1 is also to provide a realistic range for the values of n, J and μ. Recall that parameter n controls the transition from the linear to the nonlinear range, and parameters J and μ are associated with the strength of a cohesive or cohesionless soil respectively. It is observed that, for cohesive soils, $n \le 1$ and $5 \le \lambda \le 9$, whereas for cohesionless soils $2 \le n \le 3$ and $3 \le \mu \le 5$.

TABLE 1

Constitutive model parameters for different experiments

Test / Year	Soil Properties	Pile Characteristics	Model Parameters	
Cohesive Soils			J	n
Kramer *et. al.* 1990 Crouse *et. al.* 1993	ν_s= 0.49 V_s (tip) = 30 m/s ρ_s= 1.12 Mg/m^3	L= 14.9 m d= 0.20 m t= 0.0064 m E_pI_p= 3.81x10^3 kN-m^2	0.5	1.0
Brown *et. al.* 1987 Blaney & O'Neill 1986	ν_s= 0.49 V_s (tip) = 115 m/s ρ_s= 2.1 Mg/m^3	L= 13.4 m d= 0.273 m t= 0.0093 m E_pI_p= 7.3x10^3 kN-m^2	0.15	0.25
Cohesionless Soils			μ	n
Brown *et. al.* 1988 (Sand)	ν_s= 0.48 V_s(tip) = 160 m/s ρ_s= 1.6 Mg/m^3	L= 13.1 m d= 0.273 m t= 0.0093 m E_pI_p= 7.3x10^3 kN-m^2	5.0	3.0
Jennings *et. al.* 1984	ν_s= 0.49 V_s(tip) = 125 m/s ρ_s= 1.6 Mg/m^3	L= 6.75 m d= 0.45 m t= 0.010 m E_pI_p= 0.8x10^5 kN-m^2	5.0	3.0
Ting *et. al.* 1987	ν_s= 0.48 V_s(tip) =70 m/s ρ_s= 2.0 Mg/m^3	L=9.75 m d= 0.61 m t= 0.013 m E_pI_p= 2.2x10^5 kN-m^2	3.0	2.0

4.6.4 Nonlinear dynamic response of single piles to lateral loading

Figures 4.15 and 4.16 show equivalent storage and loss stiffnesses normalized with respect to the static small-amplitude linear stiffness, as a function of dimensionless frequency, for two of the aforementioned pile-soil data sets. The "rigorous" solutions of Kaynia and Kausel (1982) for linear response are also illustrated for the sake of compari-

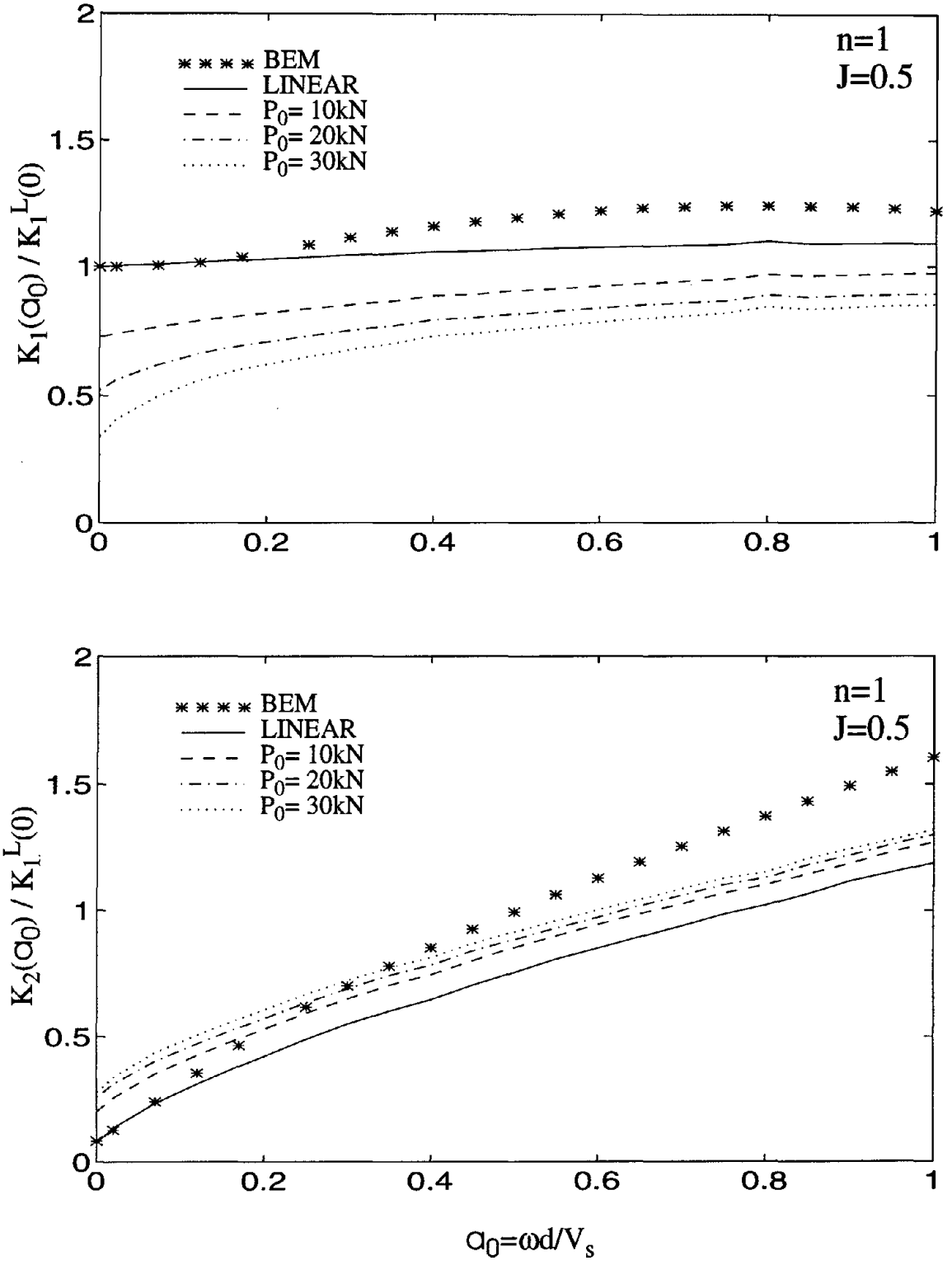

Figure 4.15: Dynamic stiffness coefficients for single fixed-head pile embedded in soft peat (Kramer et al, 1990).

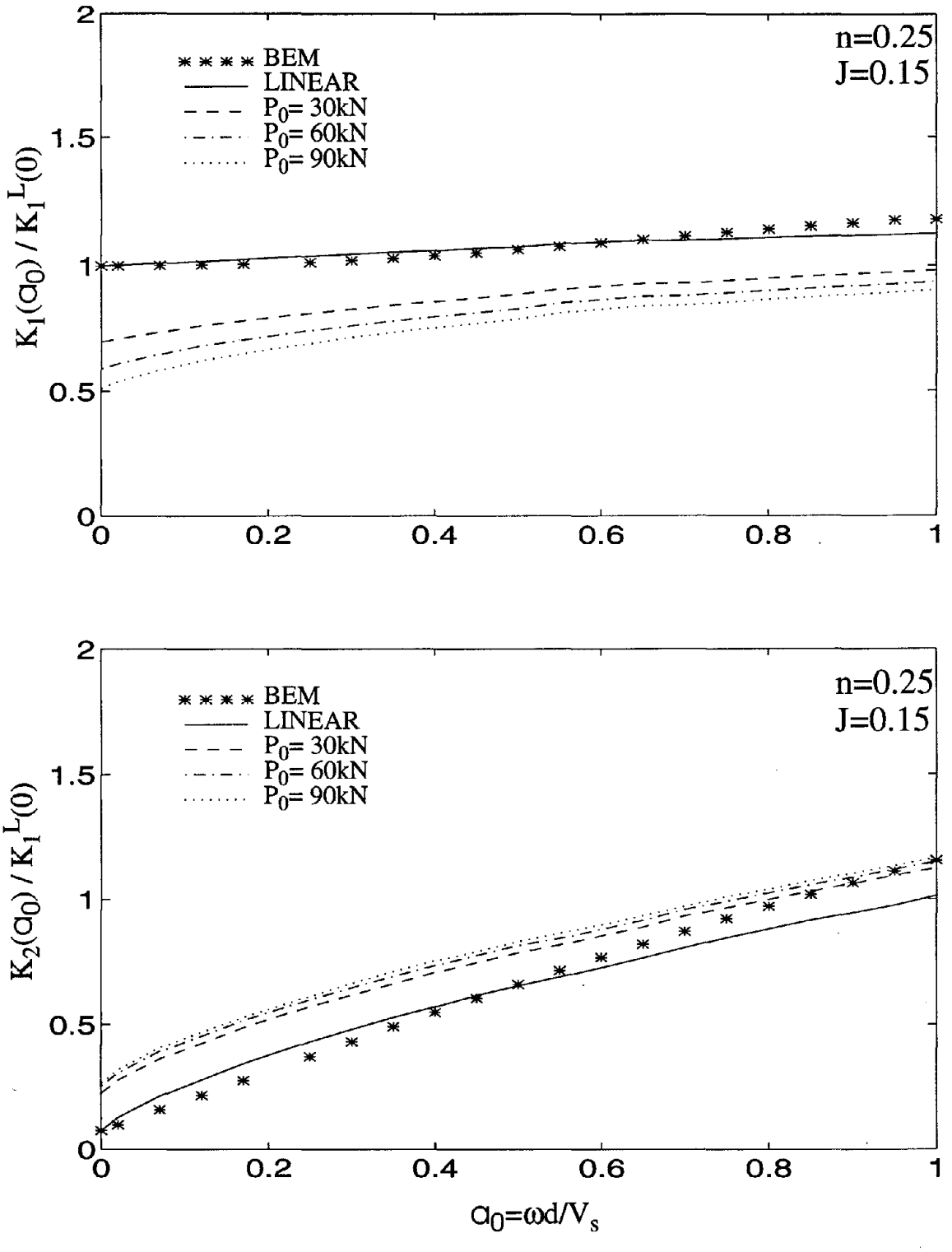

Figure 4.16: Dynamic storage and loss stiffness coefficients for single fixed-head pile embedded in medium-stiff clay (Blaney and O'Neill,1986).

son. This boundary-element formulation uses Green's functions defining displacement fields due to uniform barrel and disc loads associated with pile-soil interface tractions, which are computed by solving the wave equation through Fourier and Hankel transforms.

4.7 Concluding remarks

In this chapter, a simple, physically motivated procedure has been presented to compute the nonlinear axial dynamic response of pile foundations. This complements the earlier model for lateral response developed in Badoni (1995) and Badoni and Makris (1996). The single pile response was computed using a nonlinear viscoelastoplastic model. Yielding of the soil surrounding the pile and slippage along the pile-soil interface were identified as two different failure mechanisms and modeled separately in accordance with experimental observations. Distributed nonlinear hysteretic springs described by the Bouc-Wen model were found capable of modeling soil reaction and hysteretic damping, whereas radiation damping was modeled with distributed frequency dependent dashpots. The proposed model was calibrated with data recorded during full-scale experiments. A plane-strain theory of wave propagation was subsequently utilized to compute pile-to-pile interaction in the time domain. The nonlinear response of single piles and pile groups shows a significant deviation from linear behavior at high load amplitudes, with reduced equivalent stiffness and augmented equivalent damping. Nonlinear effects were also found to suppress pile-to-pile interaction to some extent.

CHAPTER 5

YIELDING BEHAVIOR OF REINFORCED CONCRETE PILES UNDER LATERAL LOADS

Under moderate and strong seismic loading, pile foundations are subject to large deformations, and the behavior of the soil-pile system departs significantly from the linear limit. This was observed after the Northridge and Kobe earthquakes, where the motion of the ground near pile groups supporting highway bridges, overcrossings and ramps was of the order of a pile diameter (Porcella *et al.* 1994, Comartin *et al.* 1995). An example of strong ground motion is the Sylmar Converter Station record from the Northridge earthquake (figure 5.1), where the maximum peak-to-peak ground displacement reached one meter (two to four times the typical pile diameters used by Caltrans). In Japan, the effects of near-source long period pulses is becoming a subject of concern, in light of the collapse of elevated highways and severe damage of newly constructed high-rise apartments during the Kobe earthquake. Due to the high displacements involved, nonlinearity is expected to play a substantial part in the system response to such input.

To address this problem, a rigorous analysis of the pile foundation itself is required, accounting for nonlinear pile-soil interaction as well as yielding of the pile itself. However, while great advancements have been made in recent years in the modeling of

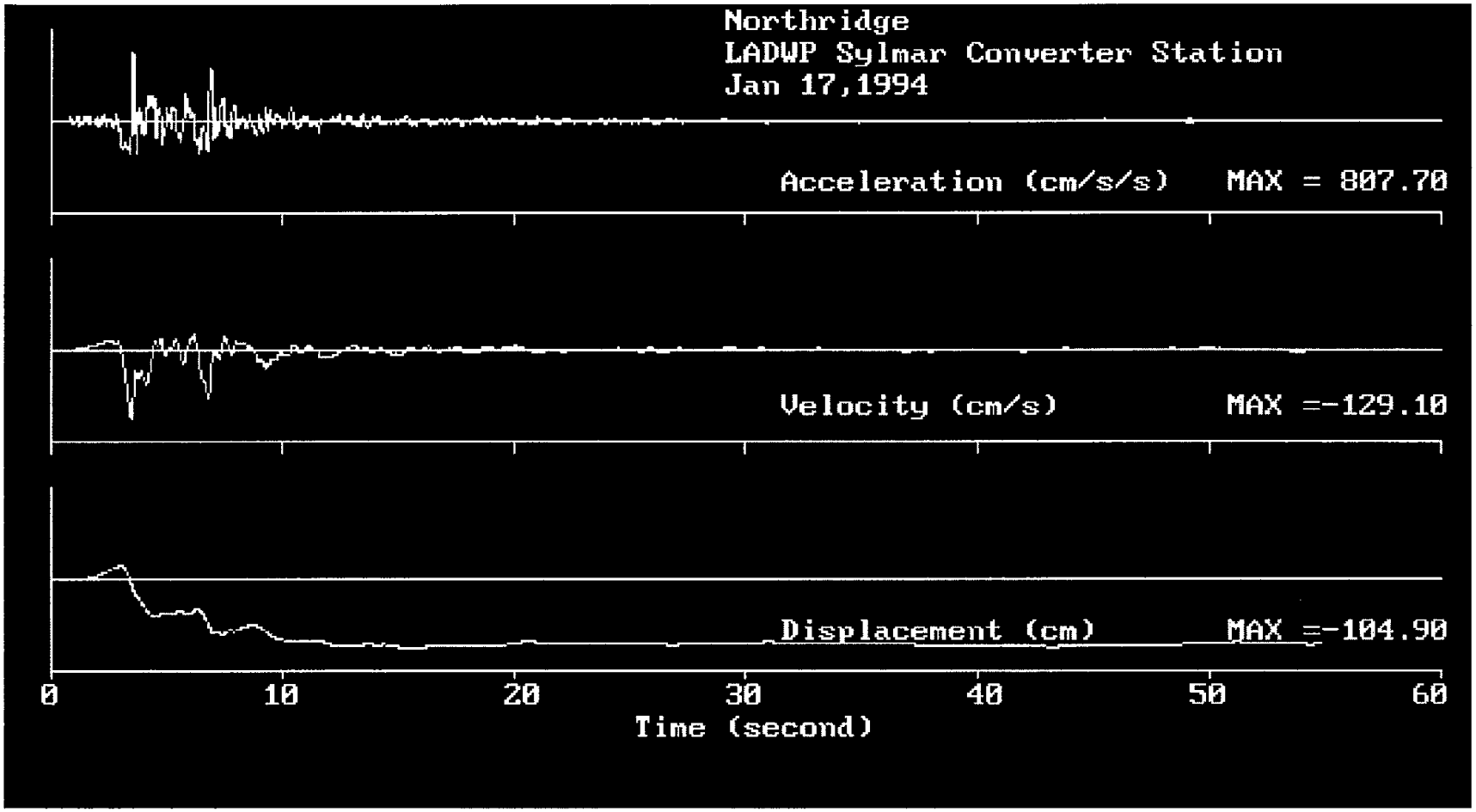

Figure 5.1: The Sylmar Converter station record from the 1994 Northridge earthquake

soil-pile interaction, the assumption of a linearly elastic pile is still used in most of these analyses. A nonlinear pile-soil interaction model developed earlier (Badoni 1995, Badoni and Makris 1996) is extended herein to include yielding of the pile in the analysis. This is accomplished by incorporating a special element formulation, that accounts for the formation of a plastic hinge of finite length, into the existing model. The moment-curvature relationship for the plastic zone is governed by a bilinear hysteretic model of the type used by Roufaiel and Meyer (1983, 1987). The advantage of this formulation is the ability to get accurate results using a small number of elements.

Note that pile yielding is most relevant for reinforced concrete piles under lateral loads in the low frequency-high amplitude range. Hence, this chapter specifically targets this case. The problem is first defined, followed by a description of the model and the procedure employed for incorporation of this model into a one-dimensional finite-element analysis scheme. The model is validated using an example presented by Priestley *et al.* (1996). A qualitative analysis of pile yielding is then presented.

5.1 Problem definition

The problem studied herein is that of a single pile embedded in a layered soil and subjected to lateral loading. The pile is modeled as a beam with circular cross-section area A_p, diameter d, moment of inertia I_p, Youngs modulus E_p and mass density ρ_p. Additional parameters required to model pile yielding and hysteresis are the yield moment M_y, the yield curvature ϕ_y, a post-to-pre-yielding-stiffness ratio p, and an empirical pinching factor α_p. These are explained in a subsequent section. The surrounding soil is considered to be an inhomogeneous deposit with shear wave velocity V_s, density ρ_s, shear strength S, or angle of internal friction ϕ, that vary with depth. The soil-pile interface is modeled as a Winkler foundation interacting with the pile through continuously distributed nonlin-

ear springs and linear dashpots, as shown in figure 5.2. The governing expressions for these have been described in section 4.6.2.

5.2 Model for reinforced concrete

The choice of selecting a proper model for reinforced concrete behavior in this analysis is not a simple one because of the large number of sophisticated models available in the literature. Miramontes *et al* (1996) classify the various available numerical models according to scale as:

1) Local models, which start at the level of material constitutive laws (stress-strain relationships), and involve integration of stress across spatial coordinates to arrive at the macroscopic behavioral law. They offer the advantage that all parameters involved have physical meaning and can be utilized independent of geometry. Of course, the computational effort required is immense.

2) Global models, which use generalized variables that incorporate both concrete and steel properties into uniaxial behavioral laws and utilize simplified kinematic hypotheses. These models are cross-section and load history specific. Also, they do not provide any information at the local level (*e.g.* stress distribution across the cross-section). However, they are very suitable for nonlinear dynamic analysis, where global behavior needs to be modeled and where computational time is at a premium.

3) Semi-local models, in which the equilibrium and kinematic conditions are managed at a global scale, while stress and internal variables are calculated at the local level. Thus, these models can exploit simplified kinematic hypotheses as well as uniaxial behavioral laws, resulting in reduced computational effort required in the integration of stresses.

4) Adaptive models, which involve progressive mesh refinement to account for the spread of inelasticity across members. Inelastically behaving members use local (or semi-

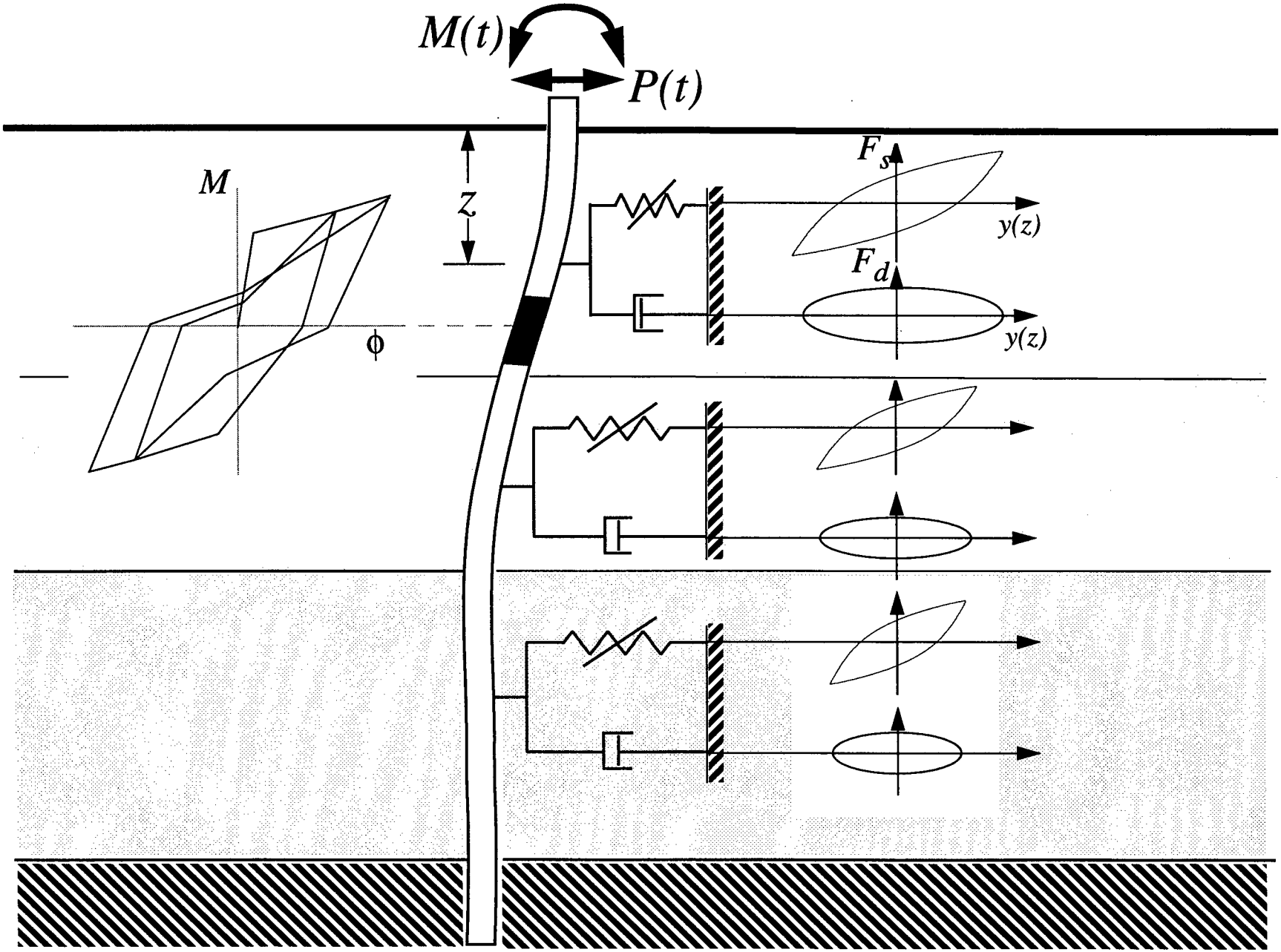

Figure 5.2: Schematic illustration of dynamic nonlinear pile-soil interaction with pile yielding

local) models, while elastic members are modeled with global models. This approach is both economical and accurate even though it is somewhat complicated to implement.

In this study, the primary aim was to use a model that would be easy to incorporate into the existing one-dimensional finite-element formulation for the pile-soil system, without compromising accuracy. Local and semi-local models would clearly be difficult to implement and also unnecessary, since we are primarily interested in simulating global behavior. A type of simplified adaptive model was also considered in which plastically behaving elements would be constrained to follow a hysteretic moment-curvature relationship. However, this could not account for the spread of plasticity suitably without resorting to very fine discretization.

The model chosen for this study is based on the global frame member model proposed by Roufaiel and Meyer (1987). It accounts for the finite size of plastic regions and requires the specification of only a few parameters for analysis, which can be readily obtained. It uses modified Takeda-type hysteresis rules (Takeda *et al.* 1970) to simulate the hysteretic moment-curvature relationships. The effects of shear and strength degradation can be modeled but are not included in this analysis to keep the model simple. The model has been tested extensively and verified for reinforced-concrete frame members under strong cyclic loads and under high shear and axial forces. It is therefore ideally suited to the analysis of pile yielding. In this study, the model has been adapted to the finite-element scheme employed in Badoni (1995).

The Bouc-Wen model was also considered to model the moment-curvature relationship for concrete, but that would increase the number of parameters to be identified and multiply the uncertainties involved in identification from scattered data that is usually available for most pile analysis experiments. The present model, on the other hand, has already been employed extensively for the study of plastic deformation of columns, and

all its parameters are already defined or well established.

5.2.1 Primary moment-curvature relationship

The primary moment-curvature relationship for this model is obtained using the assumption that plane sections remain plane even after cracking of concrete. Roufaeil and Meyer (1983) describe a procedure to analytically obtain this $M - \phi$ relationship starting from assumed bilinear stress-strain curves for steel and trilinear $\sigma - \varepsilon$ curves for concrete, and using conventional reinforced concrete theory. This leads to a close-to-bilinear curve, the deviation being small enough to be ignored. The idealized primary moment-curvature relationship is shown in figure 5.3. The two points of interest are the yield point (ϕ_y, M_y) and a point (ϕ_m, M_m) which corresponds to the failure of the concrete cover, assumed to occur when the concrete at the extreme fiber is strained to its failure value ε_m. EI is the elastic stiffness for the section, and p is the ratio of post-yielding stiffness to elastic stiffness.

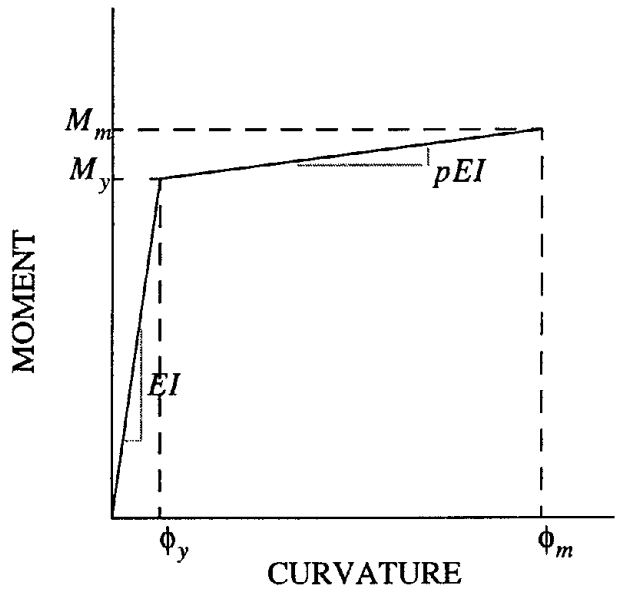

Figure 5.3: Idealized primary moment-curvature relationship for reinforced concrete pile section.

This primary moment curvature relationship can also be determined by any alternate approach (*e.g.* finite-element analysis or by experiment), and an appropriate bilinear idealization may be obtained. In effect, this approach decouples the analysis of the cross-section properties from the analysis of the pile, making it a one-dimensional problem which can be easily incorporated into the existing formulation.

5.2.2 Model for hysteretic behavior of reinforced concrete

The model for hysteretic behavior used herein, as given in Roufaiel and Meyer (1983), is a modified Takeda-type model with five branches as illustrated in figure 5.4. These are enumerated below:

1) *Elastic loading and unloading*: Until the maximum moment has reached the yield moment, M_y, the incremental moment curvature relationship is given by:

$$\Delta M = (EI)_1 \Delta\phi \tag{5.1}$$

where $(EI)_1 = EI$ is the elastic flexural stiffness obtained from the primary $M-\phi$ curve in figure 5.3.

2) *Inelastic loading*: If (i) the moment is greater than the yield moment, (ii) the moment is also greater than the maximum inelastic moment reached in any previous cycle, and (iii) the moment is still increasing, then we have the relation

$$\Delta M = (EI)_2 \Delta\phi \tag{5.2}$$

where $(EI)_2 = pEI$ is the plastic loading stiffness also given in the primary $M-\phi$ curve.

3) *Inelastic unloading*: If (i) the yield limit has been previously exceeded, (ii) the absolute value of the moment is decreasing, and (iii) the sign of the moment is unchanged, then

$$\Delta M = (EI)_3 \Delta\phi \tag{5.3}$$

The calculation of $(EI)_3$ is described in section 5.2.3, along with $(EI)_4$ and $(EI)_5$.

4) *Inelastic reloading during closing of cracks*: If (i) the yield limit has been previously exceeded in the opposite direction of loading, (ii) the absolute value of moment is increasing, and (iii) its value is less than the "pinching moment" M_p for the current cycle, derived in section 5.2.3, then

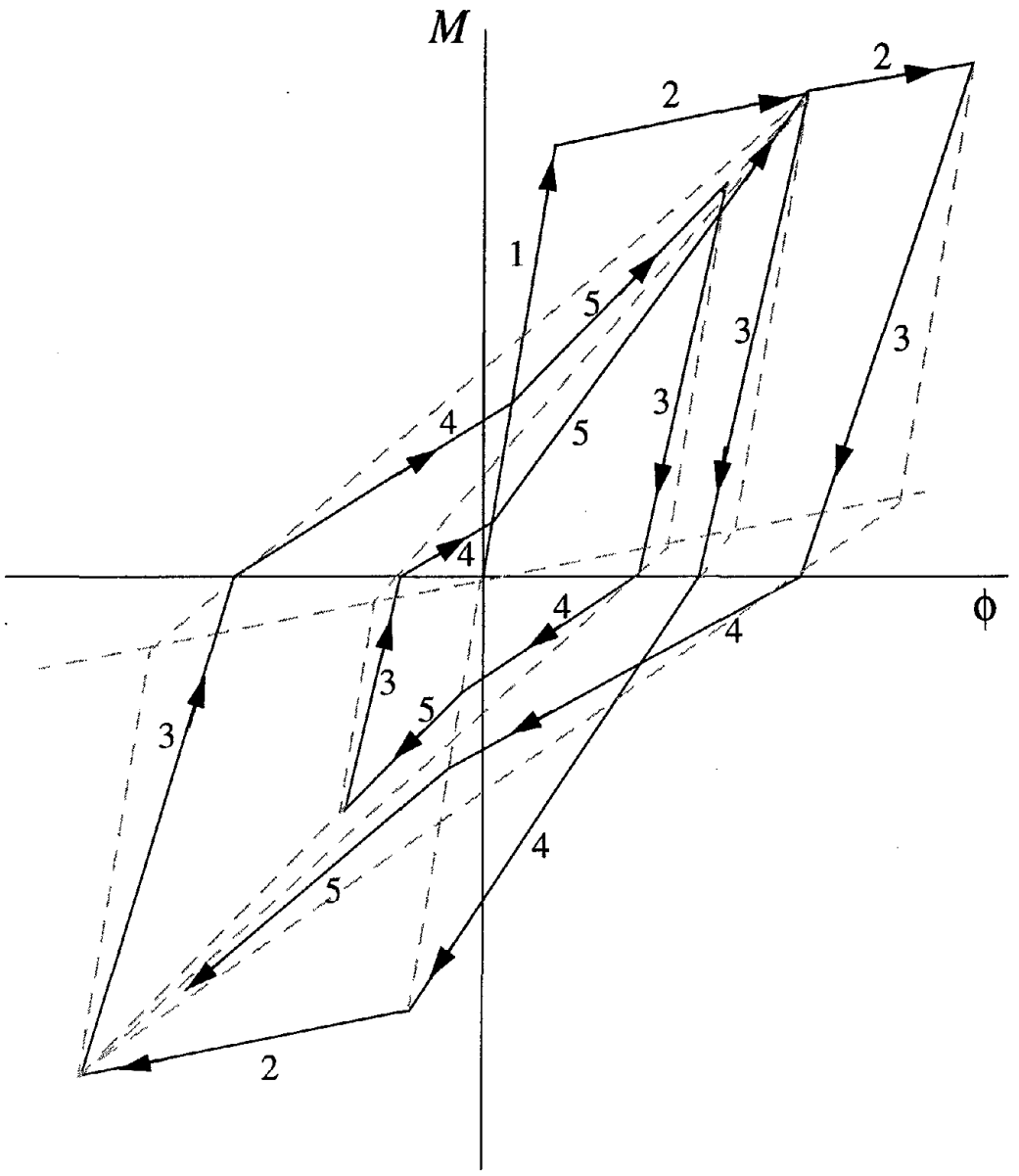

Figure 5.4: Hysteretic moment-curvature relationship for R/C pile section showing five branches of hysteresis loop.

$$\Delta M = (EI)_4 \Delta\phi \tag{5.4}$$

5) *Inelastic reloading during closing of cracks*: If (i) the yield limit has been previously exceeded in the opposite direction of loading, (ii) the absolute value of moment is increasing, and (iii) its value is greater than the "pinching moment" M_p for the current cycle, then

$$\Delta M = (EI)_5 \Delta\phi \tag{5.5}$$

5.2.3 Determination of pinching point and unloading/reloading flexural stiffnesses

Inelastic reloading involves closing of previously opened cracks leading to "pinching" behavior, especially under the action of high shear forces. In this model, this is incorporated by having two reloading branches (4 and 5). The coordinates of the pinching point and the stiffnesses for branches 3, 4 and 5 are calculated in the following steps for the half-cycle illustrated in figure 5.5.

The coordinates of an auxiliary point (M_0, ϕ_0) are first established as:

$$M_0 = \frac{p}{1-p}(\bar{\phi_1} EI - \bar{M_1}) \tag{5.6}$$

$$\phi_0 = \frac{1}{1-p}\left(\bar{\phi_1} - \frac{\bar{M_1}}{EI}\right) \tag{5.7}$$

where $\bar{M_1}$ and $\bar{\phi_1}$ are the maximum moment and curvature reached in the negative direction during the *current load cycle.*

A hypothetical "no-pinching" reloading stiffness, depicted by $\overline{EI}$, is then:

$$\overline{EI} = \frac{M_x^{+} - M_0}{\phi_x^{+} - \phi_0} \tag{5.8}$$

where M_x^{+} and ϕ_x^{+} are the maximum moment and curvature reached in the positive direction during *any previous loading cycle.*

The residual curvature, ϕ_r^-, can now be obtained from

$$\phi_r^- = \phi_0 - \frac{M_0}{\overline{EI}} \tag{5.9}$$

A "point of no pinching," (M_n, ϕ_n), is then defined as

$$\phi_n = \phi_r^- \frac{\overline{EI}}{\overline{EI} - EI} \tag{5.10}$$

$$M_n = EI\phi_n \tag{5.11}$$

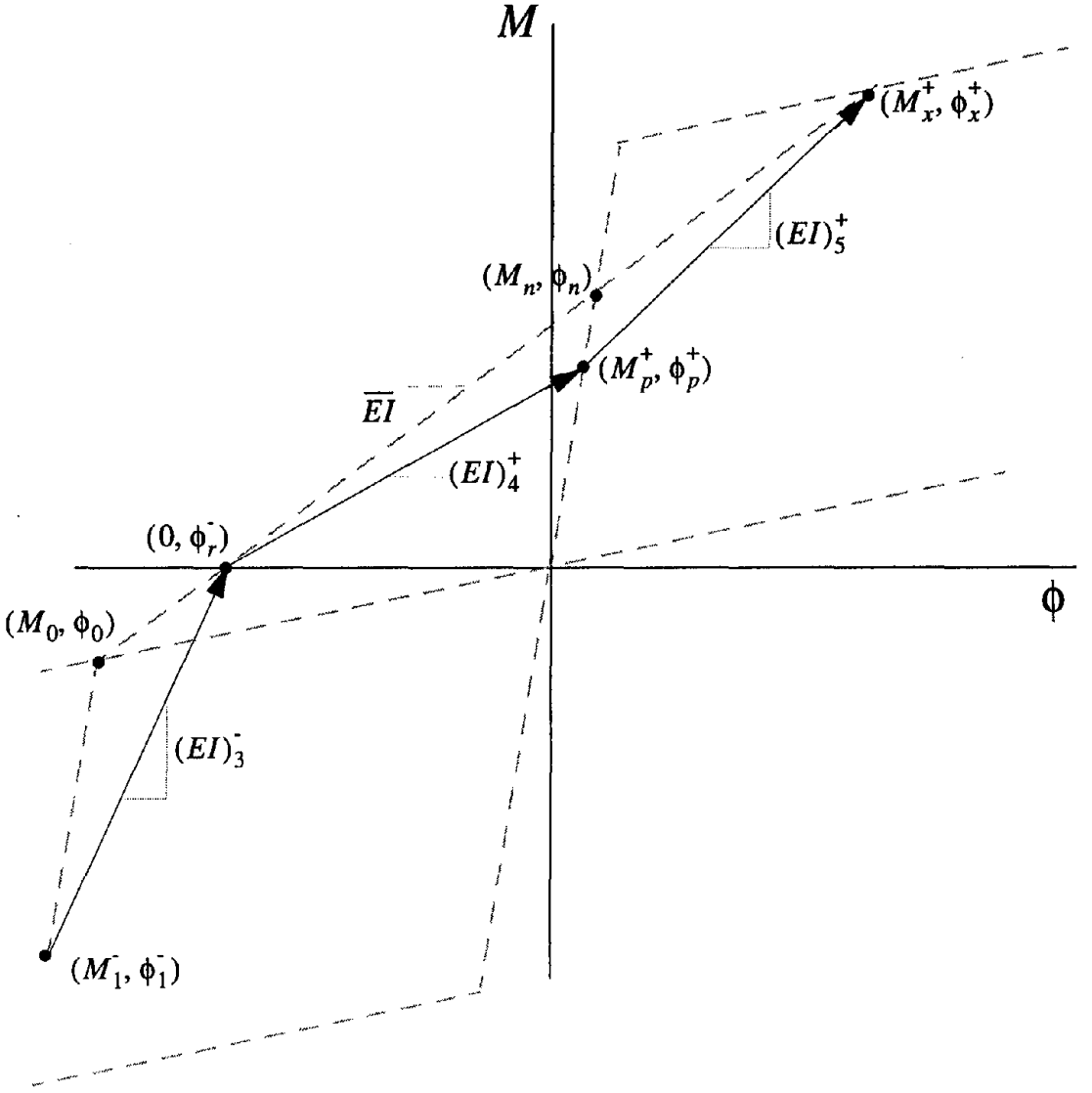

Figure 5.5: Unloading and reloading stiffnesses incorporating pinching behavior of reinforced concrete.

From this the pinching point, (M_p^+, ϕ_p^+), can be calculated as

$$M_p^+ = \alpha_p M_n \tag{5.12}$$

$$\phi_p^+ = \alpha_p \phi_n \tag{5.13}$$

where α_p is an empirical "pinching factor" that represents the effect of shear stress on pinching behavior. Thus, if the shear effect is negligible, $\alpha_p = 1$, and branches 4 and 5 will be in a straight line with slope $\overline{EI}$ (no pinching). For $\alpha_p = 0$, that is when shear effect completely controls the load-deformation behavior, branch 4 will be along the ϕ-axis. Roufaiel and Meyer (1983) provide an empirical correlation of α_p with a shear-span to effective depth ratio, a/d, as

$$\alpha_p = 0.4\frac{a}{d} - 0.6 \tag{5.14}$$

where $\alpha_p = 0$ if a/d < 1.5, and $\alpha_p = 1$ if a/d > 4. In our analysis, α_p has been kept as a model parameter which can possibly be identified from experimental testing or otherwise.

The stiffnesses for branches 3, 4 and 5 are now given as

$$(EI)_3^- = \frac{M_1^-}{\phi_1^- - \phi_r^-} \tag{5.15}$$

$$(EI)_4^+ = \frac{M_p^+}{\phi_p^+ - \phi_r^-} \tag{5.16}$$

$$(EI)_5^+ = \frac{M_x^+ - M_p^+}{\phi_x^+ - \phi_p^+} \tag{5.17}$$

5.2.4 Finite-element formulation

Consider the finite element formulation for the linear-elastic pile, nonlinear soil

system studied earlier (Badoni 1995). The equation of motion for this system was given by:

$$\rho_p A_p \ddot{y}(z,t) + E_p I_p y''(z,t) + \alpha k y(z,t) + (1-\alpha) k y_0 \zeta(z,t) + c\dot{y}(z,t) = 0 \qquad (5.18)$$

The discretized form of this equation using standard cubic-hermitian shape functions, $N(z)$, are

$$[M]\{\ddot{y}(t)\} + [C]\{\dot{y}(t)\} + \{F^{\text{int}}(t)\} = \{F^{\text{ext}}(t)\} \qquad (5.19)$$

where

$$[M] = \sum_{n=1}^{\text{nel}} \int_0^{L_n} \rho_p A_p \{N(z_n)\}\{N(z_n)\}^T dz_n \qquad (5.20)$$

$$[C] = \sum_{n=1}^{\text{nel}} \int_0^{L_n} c\{N(z_n)\}\{N(z_n)\}^T dz_n \qquad (5.21)$$

$$\begin{aligned} \{F^{\text{int}}(t)\} &= ([K_b] + \alpha[K_s])\{y(t)\} \\ &+ \sum_{n=1}^{\text{nel}} \int_0^{L_n} (1-\alpha) k y_0 \{N(z_n)\}\zeta(z_n, t) dz_n \end{aligned} \qquad (5.22)$$

and $\{F^{\text{ext}}(t)\}$ is the vector of nodal point loads and

$$[K_b] = \sum_{n=1}^{\text{nel}} \int_0^{L_n} E_p I_p \{N''(z_n)\}\{N''(z_n)\}^T dz_n \qquad (5.23)$$

$$[K_s] = \sum_{n=1}^{\text{nel}} \int_0^{L_n} k\{N(z_n)\}\{N(z_n)\}^T dz_n \qquad (5.24)$$

In all the above equations, z_n is the local length coordinate within each element of length L_n.

In the present model, the moment-curvature relationship for reinforced concrete is assumed to be piecewise linear, so equation (5.19) is still valid within each branch. However, from one branch to the next, the value of E_pI_p changes depending on the prescribed $M-\phi$ relationship. This affects the matrix $[K_b]$ directly, and since the moment and curvature vary across the length of the element, a special formulation is required that can accommodate discontinuous E_pI_p along the element length.

The element used herein is schematically illustrated in figure 5.6. Note that the soil springs and dashpots are not shown but are modeled as part of the element. As shown in the figure, there are eight degrees of freedom. The intermediate d.o.f.s can, however, be factored out by a process of static condensation. Within each section, the cubic hermitian shape functions are still valid. The symmetric element stiffness matrix can therefore be written as:

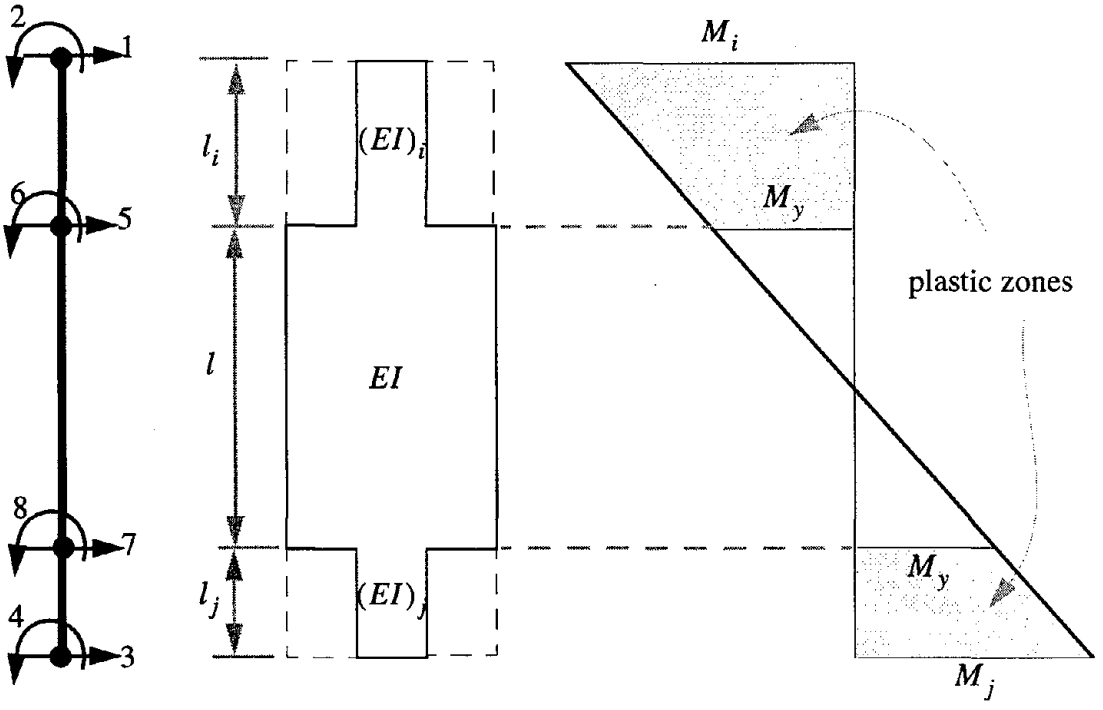

Figure 5.6: Special element used to model variable elasticity showing uncondensed dof numbering, and plastic zones.

$$[\hat{K}_b] =$$

$$\left[\begin{array}{cccc|cccc}
12\frac{(EI)_i}{l_i^3} & 6\frac{(EI)_i}{l_i^2} & 0 & 0 & -12\frac{(EI)_i}{l_i^3} & 6\frac{(EI)_i}{l_i^2} & 0 & 0 \\
6\frac{(EI)_i}{l_i^2} & 4\frac{(EI)_i}{l_i} & 0 & 0 & -6\frac{(EI)_i}{l_i^2} & 2\frac{(EI)_i}{l_i} & 0 & 0 \\
0 & 0 & 12\frac{(EI)_j}{l_j^3} & -6\frac{(EI)_j}{l_j^2} & 0 & 0 & -12\frac{(EI)_j}{l_j^3} & 6\frac{(EI)_j}{l_j^2} \\
0 & 0 & -6\frac{(EI)_j}{l_j^2} & 4\frac{(EI)_j}{l_j} & 0 & 0 & -6\frac{(EI)_j}{l_j^2} & 2\frac{(EI)_j}{l_j} \\
\hline
-12\frac{(EI)_i}{l_i^3} & -6\frac{(EI)_i}{l_i^2} & 0 & 0 & 12\frac{(EI)_i}{l_i^3}+12\frac{EI}{l^3} & -6\frac{(EI)_i}{l_i^2}+6\frac{EI}{l^2} & -12\frac{EI}{l^3} & 6\frac{EI}{l^2} \\
6\frac{(EI)_i}{l_i^2} & 2\frac{(EI)_i}{l_i} & 0 & 0 & -6\frac{(EI)_i}{l_i^2}+6\frac{EI}{l^2} & 4\frac{(EI)_i}{l_i}+4\frac{EI}{l} & -6\frac{EI}{l^2} & 2\frac{EI}{l} \\
0 & 0 & -12\frac{(EI)_j}{l_j^3} & -6\frac{(EI)_j}{l_j^2} & -12\frac{EI}{l^3} & -6\frac{EI}{l^2} & 12\frac{(EI)_j}{l_j^3}+12\frac{EI}{l^3} & 6\frac{(EI)_j}{l_j^2}-6\frac{EI}{l^2} \\
0 & 0 & 6\frac{(EI)_j}{l_j^2} & 2\frac{(EI)_j}{l_j} & 6\frac{EI}{l^2} & 2\frac{EI}{l} & 6\frac{(EI)_j}{l_j^2}-6\frac{EI}{l^2} & 4\frac{(EI)_j}{l_j}+4\frac{EI}{l}
\end{array}\right] \tag{5.25}$$

which is defined by

$$[\hat{K}_b]\{y\} = \{F\} \tag{5.26}$$

where $\{y\}$ is the 8x1 vector of nodal displacements and rotations, and $\{F\}$ is the nodal load vector for the element. If we set the nodal load values for the internal nodes to be zero, we can rewrite this equation as

$$\begin{bmatrix} K_{bb} & K_{br} \\ K_{rb} & K_{rr} \end{bmatrix} \begin{bmatrix} y_b \\ y_r \end{bmatrix} = \begin{bmatrix} F_b \\ 0 \end{bmatrix} \tag{5.27}$$

where the subscript r denotes the degrees of freedom to be condensed out. The condensed equation is then obtained as

$$[K_{bb} - K_{br}K_{rr}^{-1}K_{rb}]\{y_b\} = \{F_b\} \tag{5.28}$$

which gives the modified beam stiffness matrix as

$$[K_b] = [K_{bb} - K_{br}K_{rr}^{-1}K_{rb}] \tag{5.29}$$

where

$$[K_{bb}] = \begin{bmatrix} 12\dfrac{(EI)_i}{l_i^3} & 6\dfrac{(EI)_i}{l_i^2} & 0 & 0 \\ 6\dfrac{(EI)_i}{l_i^2} & 4\dfrac{(EI)_i}{l_i} & 0 & 0 \\ 0 & 0 & 12\dfrac{(EI)_j}{l_j^3} & -6\dfrac{(EI)_j}{l_j^2} \\ 0 & 0 & -6\dfrac{(EI)_j}{l_j^2} & 4\dfrac{(EI)_j}{l_j} \end{bmatrix} \tag{5.30}$$

$$[K_{rr}] = \begin{bmatrix} 12\dfrac{(EI)_i}{l_i^3} + 12\dfrac{EI}{l^3} & -6\dfrac{(EI)_i}{l_i^2} + 6\dfrac{EI}{l^2} & -12\dfrac{EI}{l^3} & 6\dfrac{EI}{l^2} \\ -6\dfrac{(EI)_i}{l_i^2} + 6\dfrac{EI}{l^2} & 4\dfrac{(EI)_i}{l_i} + 4\dfrac{EI}{l} & -6\dfrac{EI}{l^2} & 2\dfrac{EI}{l} \\ -12\dfrac{EI}{l^3} & -6\dfrac{EI}{l^2} & 12\dfrac{(EI)_j}{l_j^3} + 12\dfrac{EI}{l^3} & 6\dfrac{(EI)_j}{l_j^2} - 6\dfrac{EI}{l^2} \\ 6\dfrac{EI}{l^2} & 2\dfrac{EI}{l} & 6\dfrac{(EI)_j}{l_j^2} - 6\dfrac{EI}{l^2} & 4\dfrac{(EI)_j}{l_j} + 4\dfrac{EI}{l} \end{bmatrix} \tag{5.31}$$

$$[K_{br}] = [K_{rb}]^T = \begin{bmatrix} -12\dfrac{(EI)_i}{l_i^3} & 6\dfrac{(EI)_i}{l_i^2} & 0 & 0 \\ -6\dfrac{(EI)_i}{l_i^2} & 2\dfrac{(EI)_i}{l_i} & 0 & 0 \\ 0 & 0 & -12\dfrac{(EI)_j}{l_j^3} & 6\dfrac{(EI)_j}{l_j^2} \\ 0 & 0 & -6\dfrac{(EI)_j}{l_j^2} & 2\dfrac{(EI)_j}{l_j} \end{bmatrix} \tag{5.32}$$

in which $(EI)_i$ and $(EI)_j$ are obtained from the $M - \phi$ relationships at the corresponding

element ends, according to the conditions described in section 5.2.2. For the special case where the middle of the element is uncracked, and end i is in branch 3, 4 or 5, the average of $(EI)_i$ and EI is taken to account for the variation along the cracked length.

The plastic region length l_i for end i is obtained as:

$$l_i = \frac{M_i - sgn(M_i)M_y}{M_i + M_j} L \tag{5.33}$$

for branch 2. For all other branches, the plastic region length is unchanged, since they do not involve additional cracking. Since the plastic zone length depends on the end moments at the current time step, a simple iterative technique is employed in which l_i is progressively refined until convergence is achieved according to the steps listed below:

For each time step

- Calculate l_i, l_j, $(EI)_i$ and $(EI)_j$ for all yielding elements based on the end moments at the previous time step.
- Calculate the modified beam stiffness matrix $\{K_b\}$ for these elements and assemble the global effective stiffness matrix and load vectors.
- Calculate nodal displacements and rotations.
- Update element end moments based on new nodal vector.
- Recalculate l_i, l_j, $(EI)_i$ and $(EI)_j$, and check for convergence. Repeat until convergence is achieved.

Note that this can also be accomplished by using an adaptive finite-element scheme with moving nodes, which would require considerable computational effort and be particularly susceptible to problems of numerical instability. It is also of note that Roufaeil and Meyer (1983) obtained their stiffness matrix from an inverse-flexibility formulation. It can be easily shown that these two formulations are identical.

There are a few assumptions involved in the static condensation technique

employed here. It is not strictly valid for a dynamic problem where the mass and damping matrices are included in the incremental stiffness matrix and load vector. However, if the number of elements chosen is not too small, the few elements with discontinuous curvatures will have little effect the accuracy of the finite-element scheme. This is the inherent advantage of using a finite-element scheme instead of a global beam member model.

5.3 Model validation: The viaduct example

Priestley *et al.* (1996) describe a detailed analysis example of a long regular viaduct. The problem is modeled as depicted in figure 5.7. Model A is the one used in the book, whereas Model B, which needs to be validated, is the one proposed here. Model A uses a lumped mass approach along with discrete linear soil springs and does not incorporate soil radiation damping. Model B has the capacity to model nonlinear soil behavior as well as radiation damping. It uses consistent mass matrices, except at the top where the mass of the superstructure is lumped, as in Model A. However, in this analysis, only the nonlinear model for reinforced concrete needs to be verified, and so the dashpot coefficients are set to zero, while the spring modeling equations are constrained to be linear.

5.3.1 Column, pile-shaft and soil properties

The column is circular with a diameter of 1.83 m. It is continued into the ground as a cast-in-drilled-hole (CIDH) pile shaft with the same dimensions and reinforcement details, as depicted in figure 5.8. The column reinforcement consists of 30 D36 mm (No.11) longitudinal bars and D19 mm spirals with a pitch of 115 mm. The assumed yield strength for reinforcement is f_y = 414 MPa, while the nominal concrete strength f_c' = 24.1 MPa. The moment-curvature relationship depicted in figure 5.8 is for an expected below-ground plastic hinge with an axial load of 8.85 MN, which includes the superstructure weight of 8 MN and the weight of the column. The equivalent mass density

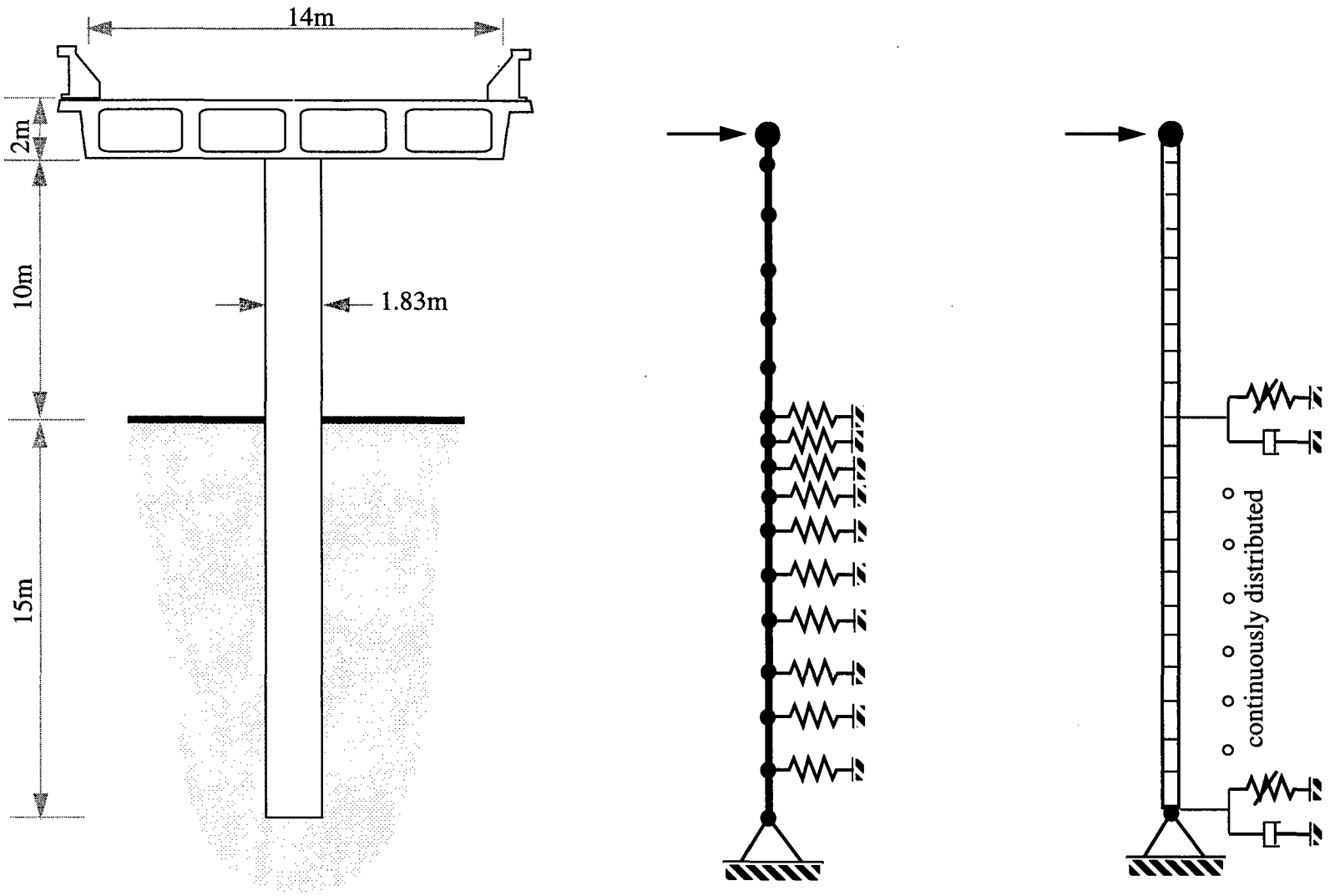

Viaduct cross-section | Model A (Priestley *et al.* (1996)) | Model B (proposed)

Figure 5.7: Models for analysis of viaduct.

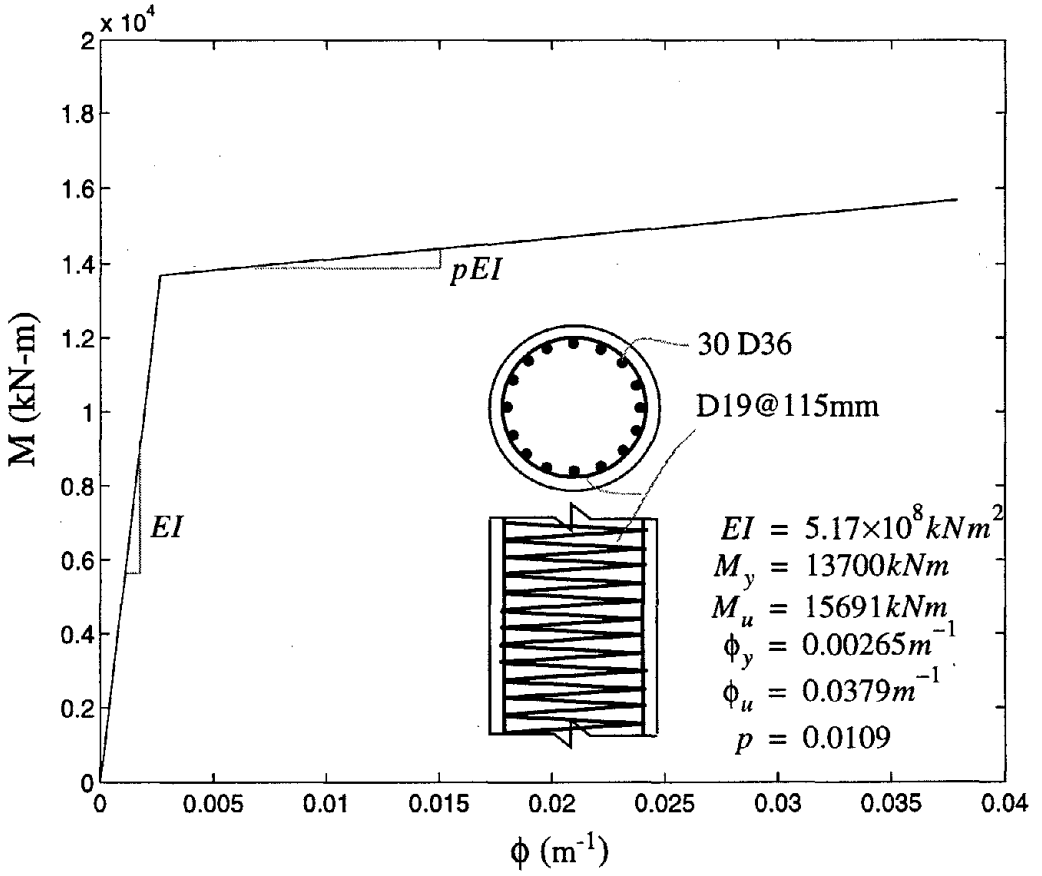

Figure 5.8: Primary moment-curvature relationship for expected below-ground plastic hinge (axial load = 8.85MN).

for the cross section with area A_p = 2.63 m^2, is ρ_p = 2.4 Mg/m^3.

The soil is characterized as a very dense sand with a linearly varying distributed elastic stiffness of $k_s(z) = 18.3z(MPa)$, where z is the depth below ground level.

5.3.2 Quasistatic analysis

To assess the quasistatic seismic response of the system, an equivalent lateral load applied at the center of mass of the superstructure is used. An approximate method is first employed to locate the position of the plastic hinge at a depth of 1 m below ground level. The lateral load corresponding to yielding at the base of an "equivalent" 12m cantilever is then calculated to be 1150kN.

The results from Model B for a lateral load of 1150kN are compared in figure 5.9

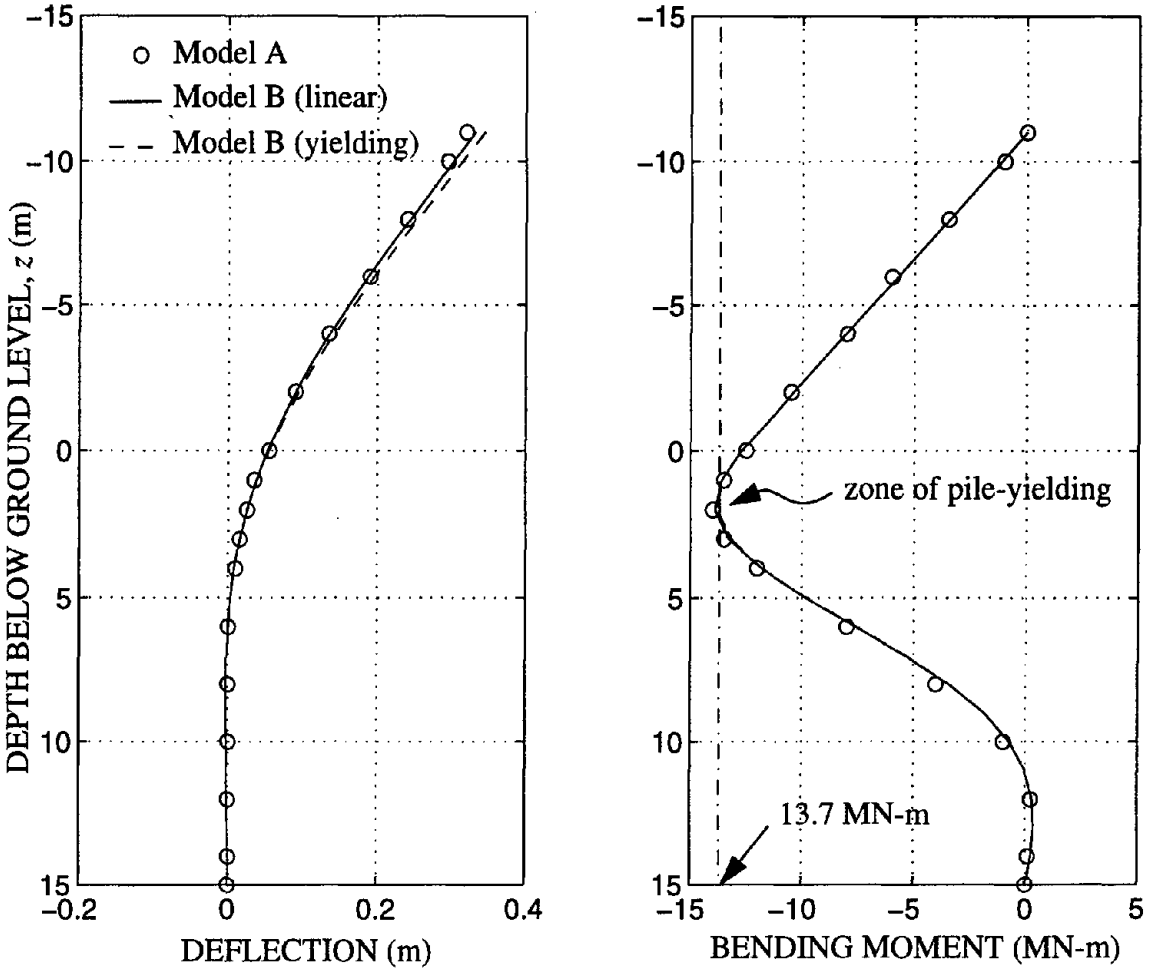

Figure 5.9: Static deflection and bending moment profiles for the viaduct models.

with the Model A predictions. Note that Model A is essentially a linear model, based on the assumption that the applied lateral load corresponds to the linear limit. However, it can be seen from the bending moment profile that there already is a significant plastic zone, even for this load level. To illustrate the error involved in this assumption, two cases were examined for Model B. In the first, the $M-\phi$ relationship for the pile section was constrained to be linear, and, as expected, the agreement obtained with Model A is excellent. The second case utilizes the bilinear $M-\phi$ curve of figure 5.8, and represents the actual inelastic action of the plastic region. There is a noticeable increase in the above-ground deflections, while the bending moment reduction in the plastic zone is barely visible

owing to the small magnitude of inelastic overloading.

To illustrate the effect of pile yielding in this example more clearly, the applied load amplitude was increased to 1250kN, and three quasistatic load cycles were applied. Figure 5.10 depicts the resulting force-displacement relationship at the top of the column, which shows the characteristic bilinear curve in the loading zone. The cyclic loading induces global $P-\Delta$ behavior similar to the local $M-\phi$ curves, which are illustrated in figure 5.11 for different depths along the pile shaft. The pinching factor was taken as $\alpha_p = 0.8$ in this analysis. The desired moment curvature relationships are reproduced along the depth of the pile.

The associated displacement and bending moment profiles corresponding to maximum loading at the column top are illustrated in figure 5.12. For the sake of comparison,

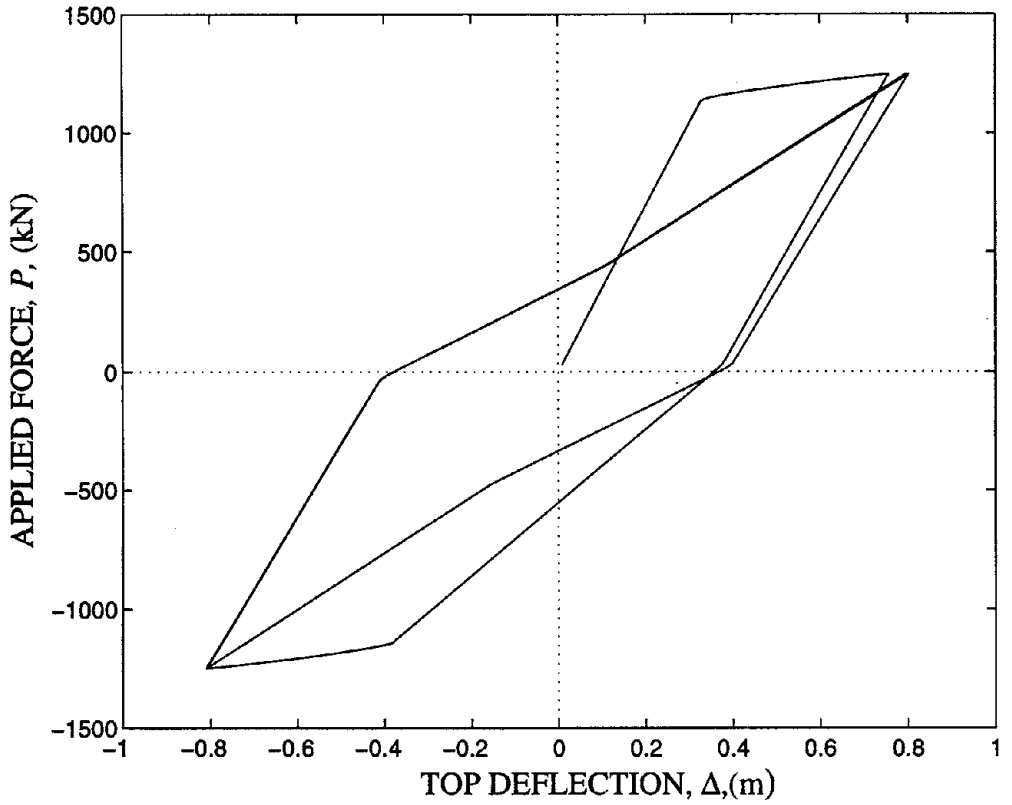

Figure 5.10: Cyclic force-deflection relationship at top of column (z = −11 m).

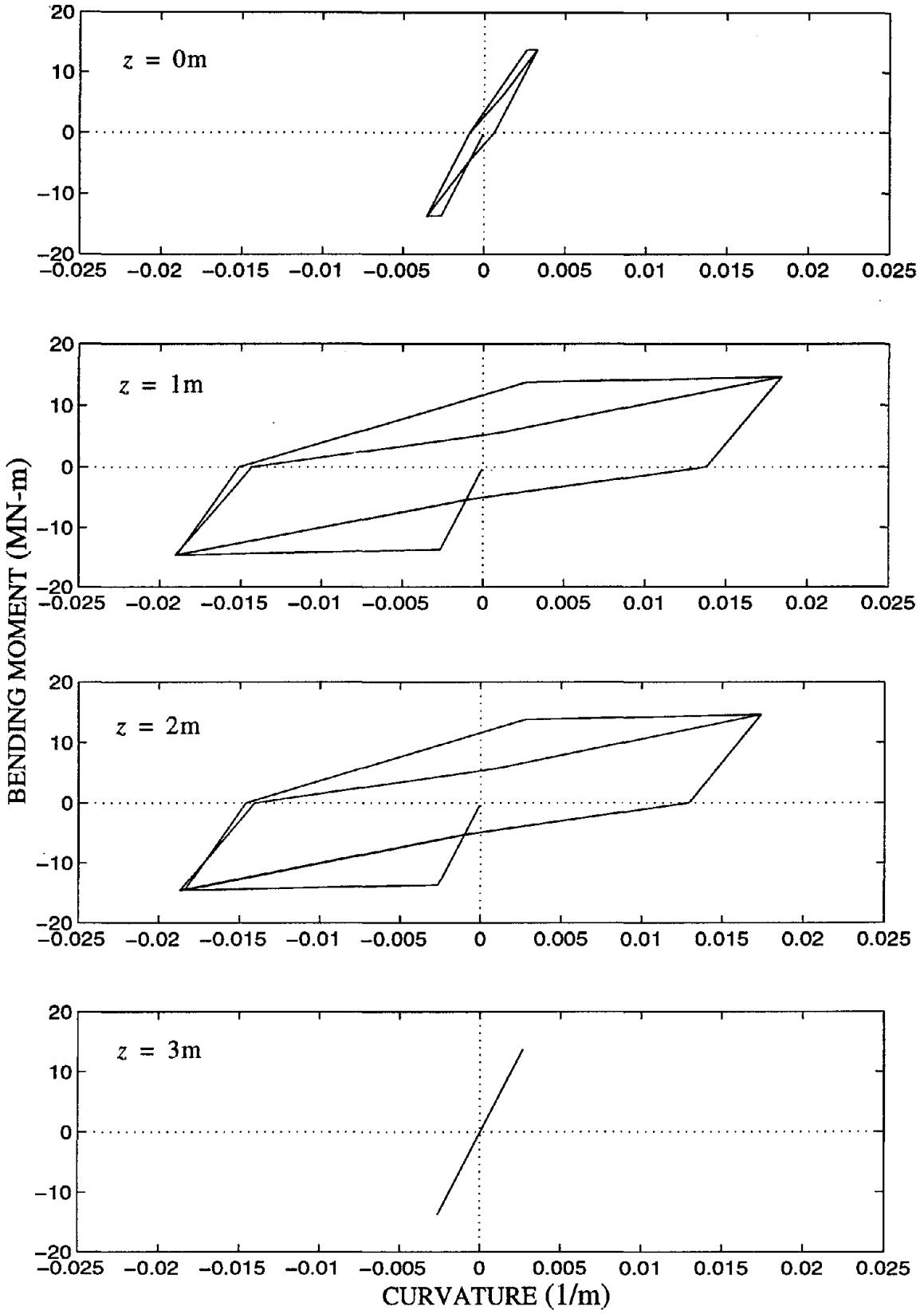

Figure 5.11: Observed moment-curvature relationships at different depths along the pile.

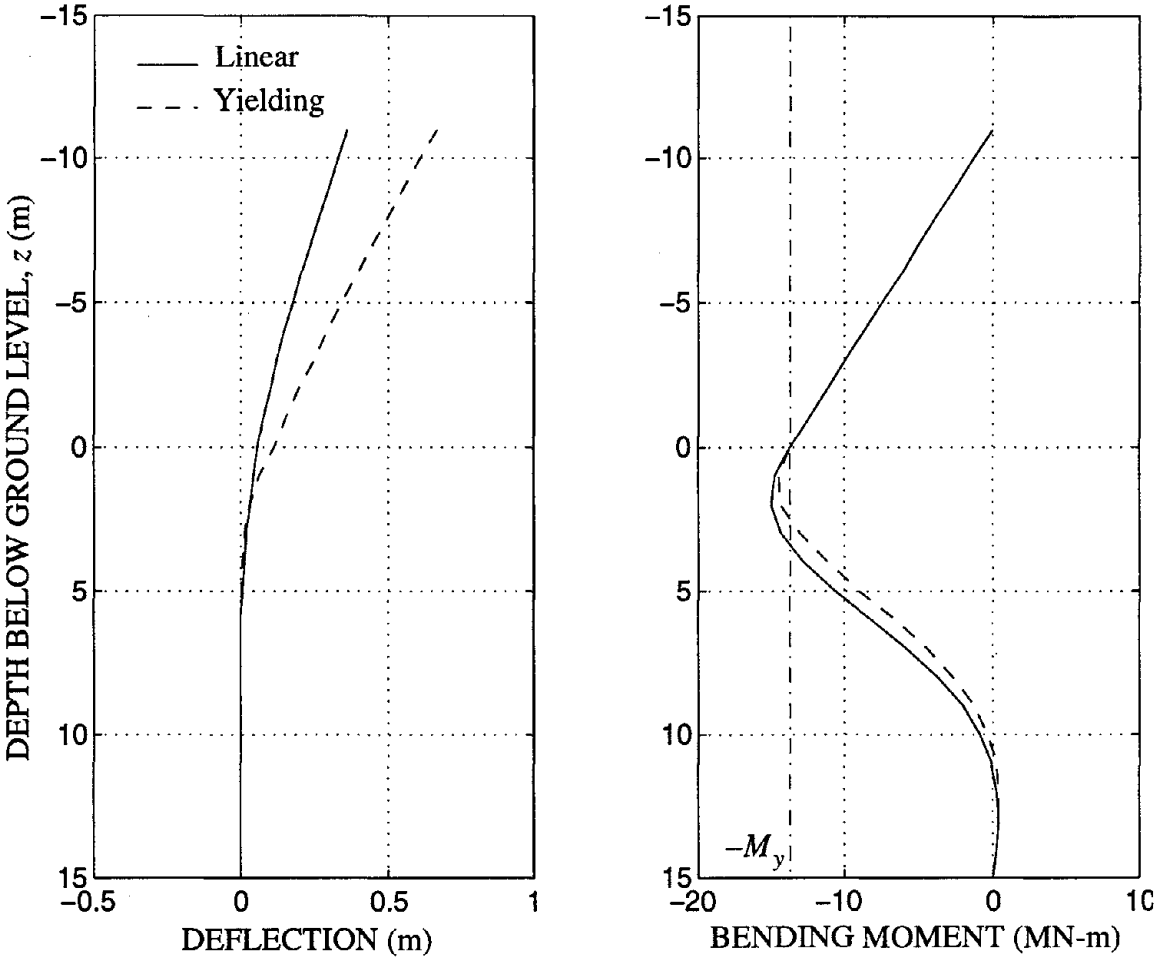

Figure 5.12: Linear vs. nonlinear (pile yielding) deflection and bending moment profiles for quasistatic cyclic loading with amplitude 1250kN.

the corresponding linear profiles are also shown, *i.e.*, the profiles corresponding to no yielding. The increase in displacement levels due to yielding is evident while bending moments are reduced around and below the yielding zone. Consequently, the length of the plastic hinge predicted from the bending moments from a linear analysis is greater than that actually obtained from the nonlinear analysis.

5.4 Influence of nonlinear soil behavior on yielding pile response

In the previous section, the soil springs were constrained to be linear, which is an unrealistic assumption given the significant magnitude of soil deflection close to the sur-

face. This fact was also pointed out by Priestley *et al.* (1996) in their example. In this section, the influence of soil nonlinearity to the overall viaduct response is investigated. In the absence of available geotechnical data, the angle of internal friction for the dense sand is taken as $\phi_s = 30^0$. According to the recommendations in Badoni (1995), the empirical parameters that control the shape of the soil spring force-displacement loops (see section 4.6.2) are chosen as $\alpha = 0$, $A = 1$, $\beta = 0.5$, $\gamma = 0.5$, $n = 2$ and $\mu = 3$. The yield displacement at a given depth $y_0(z)$ is given by the relation

$$y_0(z) = \mu \frac{\gamma_s d}{k_s(z)} \frac{1 + sin\phi_s}{1 - sin\phi_s} z \tag{5.34}$$

The resulting head-force displacement loops for an applied load of 1250 kN are shown in figure 5.13, and the corresponding displacement and bending moment profiles in figure

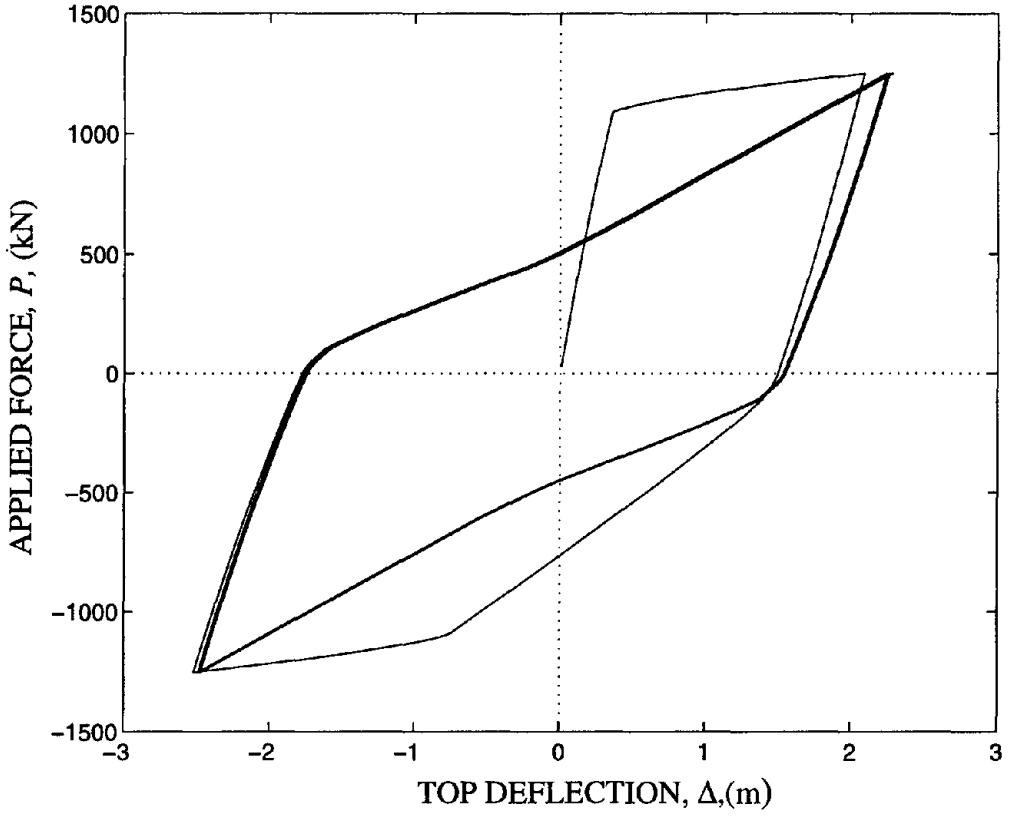

Figure 5.13: Force-deflection relationship at top of column with nonlinear soil behavior.

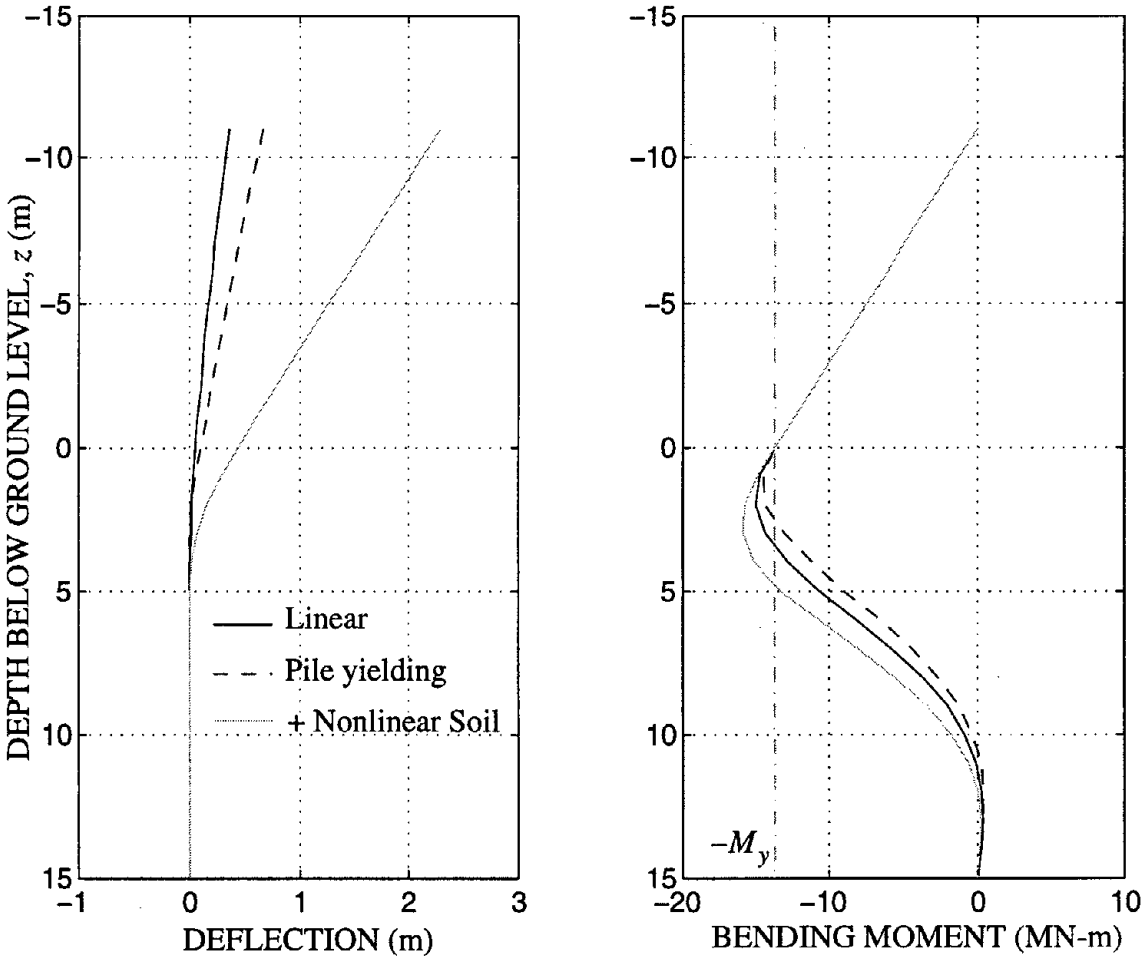

Figure 5.14: Maximum deflection and bending moment profiles under different modeling assumptions.

5.14 (gray line) along with the previously shown profiles which excluded soil nonlinearity (the solid line corresponds to no pile yielding) in the analysis. The substantial increase in deflections and bending moments is evident. This result is easily explained by considering the soil *p-y* curves at four depths as illustrated in figure 5.15. It is clear that the yield limit for this sand has been exceeded up to a significant depth. Notice that the maximum restoring force of the soil increases linearly with depth, being close to zero at the top. For cohesive soils, where this is constant with depth for the most part, the influence will not be as dramatic.

Perhaps the most significant result of this analysis is that the length of the plastic

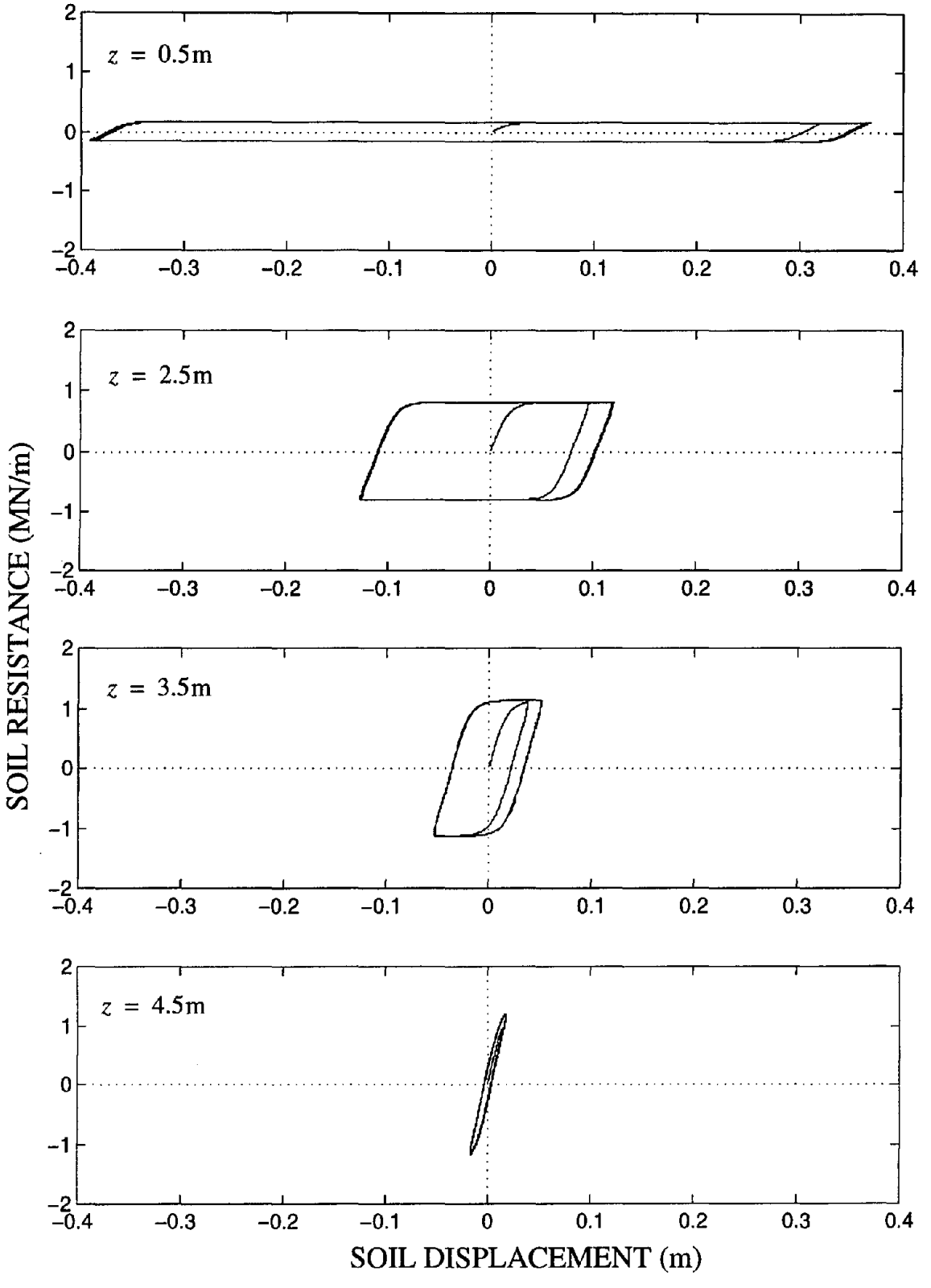

Figure 5.15: Soil *p-y* curves at different depths for quasistatically loaded pile with load amplitude 1250 kN.

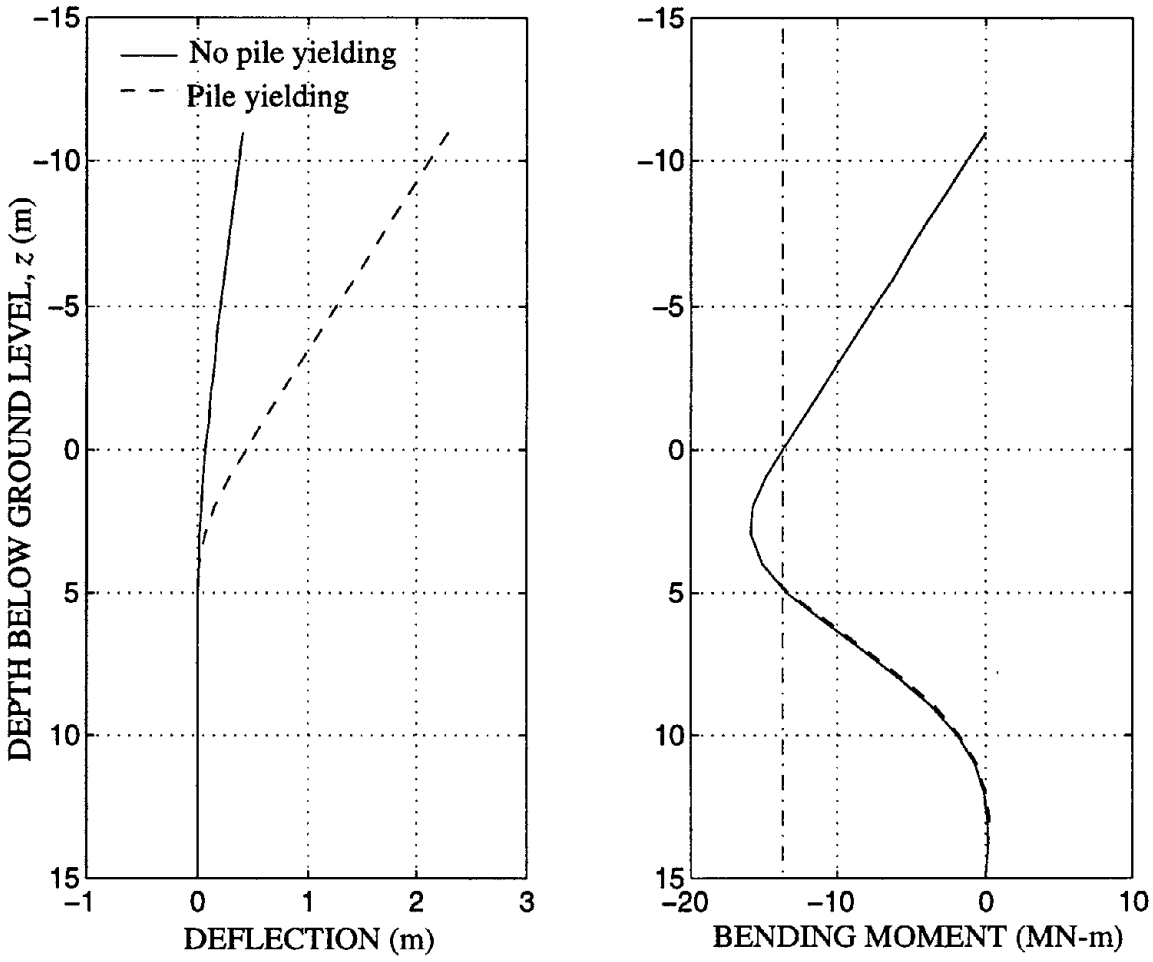

Figure 5.16: Deflections and bending moment profiles including soil nonlinear behavior but different pile modeling.

zone has been increased. Thus, the inclusion of pile-yielding alone, without incorporating nonlinear soil behavior, can actually give a non-conservative estimate of the plastic zone length and underestimate deflections. This is further investigated in figure 5.16, in which soil nonlinearity is included in both analyses, but the pile is modeled as linearly elastic in one of the cases (corresponding to the solid line). Clearly, the pile deflections after yielding are influenced greatly by soil nonlinearity. The bending moments, however, are barely affected in this case (compare with figure 5.12). As such, an analysis including soil nonlinearity can give a fairly good estimate of the plastic zone length, which can then be used in an equivalent fixity analysis of the type used by Priestley (1996) for subsequent time

history analyses.

5.5 Concluding remarks

In this chapter, a nonlinear model for soil-pile iteration has been presented that accounts for yielding of the pile itself according to a bilinear hysteretic moment-curvature relationship. This model for reinforced concrete has already been used extensively in other types of analysis, and so can be used with confidence here. A new finite-element procedure has been developed which accounts for spread of plasticity within an element, thus reducing computation time considerably compared to the alternative of adaptive or mesh refinement techniques. The model has been verified at the linear limit for a one-dimensional viaduct model resting in a CIDH pile shaft, and the significance of considering both soil nonlinearity and pile yielding to overall structural response has been established.

CHAPTER 6

CONCLUSIONS

In this research, the problem of nonlinear pile-foundation-superstructure interaction was addressed by utilizing a substructure approach and developing appropriate time-domain methodologies for the analysis of each subsystem in conjunction with two alternative techniques for integrated analysis of the system. The importance of foundation dynamics to overall system response was established first by studying the response of the Painter Street bridge to the Petrolia Earthquake of 1994. It was found that a simple six degrees-of-freedom model for the superstructure incorporating dynamic foundation stiffnesses gives much better results than using single-valued stiffness and damping relations for the foundation. The considerable error involved in assuming a rigid foundation base (*i.e.,* no soil-structure interaction) was also demonstrated.

Subsequently, the problem of a yielding superstructure on a linear foundation was studied. The superstructure considered was modeled by a simple two degrees-of-freedom system, while the Bouc-Wen model was used to model nonlinear behavior. Two different formulations were proposed for the system governing equations. The first method models the restoring force from the foundation in terms of a convolution integral that uses the relative velocity history of the foundation motion and the dynamic relaxation stiffness of the foundation, while the second utilizes a state-space formulation. Both methods were validated at the linear limit by comparing time with frequency domain analyses. The versatil-

ity of the Bouc-Wen model in modeling a variety of nonlinear behavior was demonstrated.

A time-domain procedure was presented to compute nonlinear axial dynamic response of pile groups under inertial loading. The phenomenon of soil yielding and slippage were modeled in a physically motivated manner, and linear wave propagation theory was used to compute pile-to-pile interaction using a novel time-domain formulation. It was found that there is a significant deviation from linear behavior for single piles and pile groups at high load amplitudes. Increased nonlinearity resulted in reduced equivalent stiffness and augmented equivalent damping, although pile-to-pile interaction was suppressed.

The significance of pile yielding to overall system behavior was studied with the help of a new model which incorporates a bilinear hysteretic moment curvature relationship for the pile cross-section into a nonlinear soil-pile interaction model for lateral motion. This one-dimensional finite element model was shown to be a promising tool in analyzing foundation-structure interaction under strong earthquake motion, especially for CIDH pile shaft foundations. It was observed that neglecting soil nonlinearity while considering pile yielding can provide unconservative estimates of plastic zone length and position.

One of the most important contributions of this research is the demonstration of the Bouc Wen model as an efficient tool to model nonlinear behavior in seismic analysis of pile foundation-superstructure systems. This model was used for soil as well as superstructure nonlinearity by developing appropriate formulations and associating the model parameters with physical properties of the system being modeled. It was found to be very versatile with respect to different types of nonlinearities that can be handled without requiring inordinately large computation times.

Another important concept used extensively was the convolution integral, which was used both in modeling foundation-structure interaction and in describing wave-propa-

gation functions for pile-to-pile interaction. It was shown that, when properly used, it can give very accurate results and make time domain analysis much easier without having to resort to complicated methods of analysis.

There is considerable scope for future work utilizing the techniques presented in this dissertation. Since the focus of this study was to develop and validate these methodologies, the implementation aspect was not addressed in much detail, even though real systems have been used as examples where possible and qualitative analyses have been carried out. It would be naive to assume, however, that these methods can be used indiscriminately for any type of problem. For example, the convolution integral approach is particularly susceptible to numerical error if the causality of the complex foundation stiffnesses is not ascertained. This clearly needs to be studied so that proper guidelines can be established to the applicability of this method. Along the same lines, the method for choosing an appropriate state-space model for foundation response needs to be formalized. The effect of pile yielding on the dynamic response of piles can be studied using the model proposed after suitable refinement of the nonlinear model for concrete to be stable under high frequencies. Also, the seismic response of piles with pile yielding has yet to be investigated and could give very meaningful results. A more direct application of the method proposed in this dissertation would be to carry out a complete nonlinear analysis of the Painter Street bridge example. This is obviously contingent on the possibility that the nonlinear parameters can be reasonably estimated.

APPENDIX A

FINITE ELEMENT FORMULATIONS

This section provides the finite element formulations for the soil-pile system governing equations for vertical motion of piles given in chapter 4. The formulations for active and passive piles are considered separately since the latter also involve a support motion input for the soil springs.

A.1 Finite element formulation for an active pile

The governing equation of pile motion in the axial direction is given as:

$$\begin{aligned} &\rho_p A_p \ddot{w}(z,t) - E_p A_p w''(z,t) + \alpha k w(z,t) \\ &\quad + (1-\alpha) k w_0 \zeta(z,t) + c\dot{w}(z,t) = 0 \end{aligned} \tag{A.1}$$

Using the Galerkin method of residuals and discretizing over the pile length, one obtains:

$$\begin{aligned} \sum_{n=1}^{n=nel} \int_0^L [&\rho_p A_p \ddot{w}(z,t)\underline{w}(z,t) - E_p A_p w''(z,t)\underline{w}(z,t) + \alpha k w(z,t)\underline{w}(z,t) \\ &+ (1-\alpha) k w_0 \zeta(z,t)\underline{w}(z,t) + c\dot{w}(z,t)\underline{w}(z,t)]dz = 0 \end{aligned} \tag{A.2}$$

Variable z in the above equation, and in all subsequent equations in this section, is a local coordinate going from 0 to L within each element, distinct from z in equation (A.1). The summation sign represents assembly over neighboring elements. To yield a symmetric formulation for the stiffness matrix, the second term must be integrated by parts once:

$$-\int_0^L E_p A_p w''(z,t)\underset{\sim}{w}(z,t)dz = \int_0^L E_p A_p w'(z,t)\underset{\sim}{w}'(z,t)dz + E_p A_p w'(0,t)\underset{\sim}{w}(0,t) - E_p A_p w'(L,t)\underset{\sim}{w}(L,t) \tag{A.3}$$

Defining the element internal force vector $\{Q(t)\}$ as:

$$\{Q(t)\} = E_p A_p \begin{bmatrix} w'(0,t) \\ w'(L,t) \end{bmatrix} \tag{A.4}$$

and using linear shape functions $\{N(z)\}$ to discretize $w(z,t)$ and $\underset{\sim}{w}(z,t)$ as:

$$w(z,t) = \{N(z)\}^T\{w(t)\} \tag{A.5}$$

$$\underset{\sim}{w}(z,t) = \{N(z)\}^T\{\underset{\sim}{w}(t)\} = \{\underset{\sim}{w}(t)\}^T\{N(z)\} \tag{A.6}$$

with

$$\{w(t)\} = \begin{bmatrix} w(0,t) \\ w(L,t) \end{bmatrix}; \quad \{\underset{\sim}{w}(t)\} = \begin{bmatrix} \underset{\sim}{w}(0,t) \\ \underset{\sim}{w}(L,t) \end{bmatrix} \tag{A.7}$$

the following equation is obtained

$$\sum_{n=1}^{nel}\left(\int_0^L \rho_p A_p\{\underset{\sim}{w}(t)\}^T\{N(z)\}\{N(z)\}^T\{\ddot{w}(t)\}dz + \int_0^L E_p I_p\{\underset{\sim}{w}(t)\}^T\{N'(z)\}\{N'(z)\}^T\{w(t)\}dz - \{\underset{\sim}{w}(t)\}^T\{Q(t)\} + \int_0^L \alpha k\{\underset{\sim}{w}(t)\}^T\{N(z)\}\{N(z)\}^T\{w(t)\}dz + \int_0^L (1-\alpha)kw_0\{\underset{\sim}{w}(t)\}^T\{N(z)\}\zeta(z,t)dz + \int_0^L c\{\underset{\sim}{w}(t)\}^T\{N(z)\}\{N(z)\}^T\{\dot{w}(t)\}dz\right) = 0 \tag{A.8}$$

This reduces to the general form that can be incorporated into a time-integration scheme such as the Hilbert-Hughes-Taylor-α method used in the present model.

$$[M]\{\ddot{w}(t)\} + [C]\{\dot{w}(t)\} + \{F^{\text{int}}(t)\} = \{F^{\text{ext}}(t)\} \tag{A.9}$$

It is to be noted that equation (A.9) is in global coordinates. To incorporate the tip stiffness and damping, the boundary condition at the pile tip is considered:

$$\begin{aligned} -E_p A_p w'(L, t) + \alpha_t k_t w(L, t) + (1 - \alpha_t) k_t w_{0t} \zeta_t(t) \\ + c_t \dot{w}(L, t) = 0 \end{aligned} \tag{A.10}$$

Note that the above equation is in local coordinates for the element at the pile tip (i.e., $n = nel$). Substitution of (A.10) in equation (A.3) gives

$$\begin{aligned} -\int_0^L E_p A_p w''(z, t) \underset{\sim}{w}(z, t) dz = \int_0^L E_p A_p w'(z, t) \underset{\sim}{w}'(z, t) dz \\ + E_p A_p w'(0, t) \underset{\sim}{w}(0, t) + \alpha_t k_t w(L, t) \underset{\sim}{w}(L, t) \\ (1 - \alpha_t) k_t w_{0t} \zeta_t(t) \underset{\sim}{w}(L, t) + c_t \dot{w}(L, t) \underset{\sim}{w}(L, t) \end{aligned} \tag{A.11}$$

The spatial discretization of equation (A.11) now leads to additional terms in the stiffness and damping matrices, and the force vectors:

$$[C] = \sum_{n=1}^{nel} \int_0^L c\{N(z)\}\{N(z)\}^T dz + c_t\{N(L)\}\{N(L)\}^T \delta_{nnel} \tag{A.12}$$

$$[K_s] = \sum_{n=1}^{nel} \int_0^L k\{N(z)\}\{N(z)\}^T dz + k_t\{N(L)\}\{N(L)\}^T \delta_{nnel} \tag{A.13}$$

$$\begin{aligned} \{F^{int}(t)\} = (\{K_b\} + \alpha\{K_s\})\{w(t)\} \\ + \sum_{n=1}^{nel} \int_0^L ((1 - \alpha) k w_0 \{N(z)\} \zeta(z, t) dz) \\ + (1 - \alpha_t) k_t w_{0t} \{N(L)\} \zeta_t(t) \delta_{nnel} \end{aligned} \tag{A.14}$$

δ_{nnel} is the Kronecker-delta, used here to indicate that the additional terms are appended to the matrices and vectors corresponding to element $n = nel$ only. Furthermore:

$$[M] = \sum_{n=1}^{nel} \int_0^L \rho_p A_p \{N(z)\}\{N(z)\}^T dz \tag{A.15}$$

$$\{K_b\} = \sum_{n=1}^{nel} \int_0^L E_p A_p \{N'(z)\}\{N'(z)\}^T dz \tag{A.16}$$

$$\{F^{\text{ext}}(t)\} = \sum_{n=1}^{nel} \{Q(t)\} \tag{A.17}$$

Slippage is introduced by specifying, at the element level, the maximum possible soil-restoring force to be equal to the pile-soil adhesion. The incremental stiffness and damping contributions of that element are set equal to zero once this condition is encountered.

A.2 Finite element formulation for passive pile

The governing equation for pile motion in this case is given as:

$$\begin{aligned} \rho_p A_p \ddot{w}(z,t) - E_p A_p w''(z,t) + \alpha k \varepsilon(z,t) + (1-\alpha) k \varepsilon_0 \zeta(z,t) \\ + c\dot{\varepsilon}(z,t) = 0 \end{aligned} \tag{A.18}$$

$$\text{where} \quad \varepsilon(z,t) = w(z,t) - v(z,t); \tag{A.19}$$

Upon application of the Galerkin method of residuals to (A.18) and subsequent discretization over the pile length, the following equation is obtained:

$$\begin{aligned} \sum_{n=1}^{nel} \int_0^L [\rho_p A_p \ddot{w}(z,t)\underset{\sim}{\varepsilon}(z,t) + E_p A_p w''(z,t)\underset{\sim}{\varepsilon}(z,t) + \alpha k \varepsilon(z,t)\underset{\sim}{\varepsilon}(z,t) \\ (1-\alpha) k \varepsilon_0 \zeta(z,t)\underset{\sim}{\varepsilon}(z,t) + c\dot{\varepsilon}(z,t)\underset{\sim}{\varepsilon}(z,t)]dz = 0 \end{aligned} \tag{A.20}$$

Again, z in the above equation is now a local coordinate within each element of length L.

Introducing linear shape functions

$$w(z, t) = \{N(z)\}^T \{w(t)\} \tag{A.21}$$

$$\varepsilon(z, t) = \{N(z)\}^T \{\varepsilon(t)\} \tag{A.22}$$

$$\underset{\sim}{\varepsilon}(z, t) = \{N(z)\}^T \{\underset{\sim}{\varepsilon}(t)\} = \{\underset{\sim}{\varepsilon}(t)\}^T \{N(z)\} \tag{A.23}$$

$$v(z, t) = \{N(z)\}^T \{v(t)\} \tag{A.24}$$

with

$$\{w(t)\} = \{\varepsilon(t)\} + \{v(t)\} \tag{A.25}$$

$$\{\ddot{w}(t)\} = \{\ddot{\varepsilon}(t)\} + \{\ddot{v}(t)\} \tag{A.26}$$

The boundary condition at the pile tip, written in terms of local coordinates for element $n = nel,.$ is:

$$\begin{aligned} -E_p A_p w'(L, t) + \alpha_t k_t \varepsilon(L, t) + (1 - \alpha_t) k_t \varepsilon_{0t} \zeta_t(t) \\ + c_t \dot{\varepsilon}(L, t) = 0 \end{aligned} \tag{A.27}$$

Upon integrating by parts twice the second term in equation (A.20) and using equation (A.27) one obtains:

$$\begin{aligned} -\int_0^L E_p A_p w''(z, t) \underset{\sim}{\varepsilon}(z, t) dz = \int_0^L E_p A_p w'(z, t) \underset{\sim}{\varepsilon}'(z, t) dz \\ + E_p A_p w'(0, t) \underset{\sim}{\varepsilon}(0, t) + \alpha_t k_t \varepsilon(L, t) \underset{\sim}{\varepsilon}(L, t) \\ + (1 - \alpha_t) k_t \varepsilon_{0t} \zeta_t(t) \underset{\sim}{\varepsilon}(L, t) + c_t \dot{\varepsilon}(L, t) \underset{\sim}{\varepsilon}(L, t) \end{aligned} \tag{A.28}$$

On discretizing equation (A.20) along with (A.28) we get to the same standard form:

$$[M]\{\ddot{\varepsilon}(t)\} + [C]\{\dot{\varepsilon}(t)\} + \{F^{\text{int}}(t)\} = \{F^{\text{ext}}(t)\} \tag{A.29}$$

in which

$$[M] = \sum_{n=1}^{nel} \int_0^L \rho_p A_p \{N(z)\}\{N(z)\}^T dz \tag{A.30}$$

$$[C] = \sum_{n=1}^{nel} \int_0^L c\{N(z)\}\{N(z)\}^T dz + c_t\{N(L)\}\{N(L)\}^T \delta_{nnel} \tag{A.31}$$

$$\{K_b\} = \sum_{n=1}^{nel} \int_0^L E_p A_p \{N'(z)\}\{N'(z)\}^T dz \tag{A.32}$$

$$[K_s] = \sum_{n=1}^{nel} \int_0^L k\{N(z)\}\{N(z)\}^T dz + k_t\{N(L)\}\{N(L)\}^T \delta_{nnel} \tag{A.33}$$

$$\begin{aligned} \{F^{int}(t)\} &= (\{K_b\} + \alpha\{K_s\})\{\varepsilon(t)\} \\ &+ \sum_{n=1}^{nel} \int_0^L (1-\alpha) k \varepsilon_0 \{N(z)\}\zeta(z,t) dz \\ &+ (1-\alpha_t) k_t \varepsilon_{0t} \{N(L)\}\zeta_t(t)\delta_{nnel} \end{aligned} \tag{A.34}$$

$$\{F^{ext}(t)\} = \sum_{n=1}^{nel} \{Q(t)\} - [M]\{\ddot{v}(t)\} - \{K_b\}\{v(t)\} \tag{A.35}$$

REFERENCES

American Petroleum Institute (1986). *Recommended practice for planning, designing and constructing fixed offshore platforms.* API Recommended Practice 2A (RP 2A), Sixteenth edition, pp. 47-53.

Angelides, D. and Roesset, J. M. (1981). "Nonlinear lateral dynamic stiffness of piles," *Journal of Geotechnical Engineering, ASCE*, Vol. 107, pp. 1443-1460.

Badoni, D. (1995). *Nonlinear response of pile foundations under inertia and seismic loading*. Masters Thesis, University of Notre Dame, Indiana.

Badoni, D. and Makris, N. (1996). "Nonlinear response of single piles under lateral inertial and seismic loads," *Soil Dynamics and Earthquake Engineering,* Vol. 15, pp. 29-43.

Badoni, D. and Makris, N. (1997). "Pile-to-pile interaction in the time domain - nonlinear axial group response," *Geotechnique* (in press).

Banerjee, P. K. and Sen, R. (1987). "Dynamic behavior of axially and laterally loaded piles and pile groups." *Dynamic Behavior of Foundation and Buried Structures*, Elsevier Applied Science, New York, pp. 95-133.

Blaney, G. W., Kausel, E. and Roesset, J. M. (1976). "Dynamic stiffness of piles," *Proceedings of the 2nd International Conference on Numerical Methods in Geomechanics*, Blacksburg, VA, Vol. 2, pp. 1001-1012.

Blaney, G. W. and O'Neill, M. W. (1986). "Measured lateral response of mass on single pile in clay," *Journal of Geotechnical Engineering, ASCE*, Vol. 112, pp. 443-457.

Bond, A. J. and Jardine, R. J. (1995). "Shaft capacity of displacement piles in a high OCR clay," *Geotechnique,* Vol. 45, No. 1, pp. 3-23.

Bouc, R. (1967). "Forced vibration of mechanical system with hysteresis," *4th Conference on Nonlinear Oscillation,* Prague.

Brown, D. A., Morrison, C. and Reese, L. C. (1988). "Lateral load behavior of pile group in sand," *Journal of Geotechnical Engineering, ASCE*, Vol. 114, pp. 30-45.

Brown, D. A. Reese, L. C. and O'Neill, M. W. (1987). "Cyclic lateral loading of a large scale pile group," *Journal of Geotechnical Engineering, ASCE*, Vol. 113, pp. 1326-1343.

Ciampoli, M. and Pinto, P. E. (1995). "Effects of soil-structure interaction on inelastic seismic response of bridge piers," *Journal of Structural Engineering, ASCE*, Vol. 121, pp. 806-814.

Clough, R.W. and Penzien, J. (1993). *Dynamics of Structures*, Second Edition, McGraw-Hill, New York.

CNEL-ENEL (1976). *Contribution of the study of the Fruili earthquake of May 1976*, Rome, Italy.

Comartin, C. D., Greene, M. and Tubbesing, S. K. (1995). *The Hyogo-Ken Nanbu earthquake January 17,1995*. Preliminary Reconnaissance Report, EERI 95-04.

Constantinou, M. C. and Adnane, M. A. (1987). *Evaluation of two models for yielding systems*. Report to NSF, Department of Civil Engineering, Drexel University, PA.

Coyle, H. M. and Reese, L. C. (1966). "Load transfer for axially loaded piles in clay," *Journal of Soil Mechanics, Foundation Engineering Division, ASCE* Vol. 93, SM2, pp. 1-26.

Crouse, C. B., Kramer, S. L., Michell, R. and Hushmand, B. (1993). "Dynamic test of pipe in saturated peat," *Journal of Geotechnical Engineering, ASCE*, Vol. 119, pp. 1550-1567.

Dobry, R. and Gazetas, G. (1988). "Simple method for dynamic stiffness and damping of floating pile groups," *Geotechnique*, Vol. 38, No. 4, pp. 557-574.

EL Naggar, M. H. and Novak, M. (1994). "Non-linear model for dynamic axial pile response," *Journal of Geotechnical Engineering, ASCE*, Vol. 120, No. 2, pp. 308-329.

Fan, K., Gazetas, G., Kaynia, A., Kausel, E. and Ahmad, S. (1991). "Kinematic seismic response of single piles and pile groups," *Journal of Geotechnical Engineering, ASCE*, Vol. 117, pp.1860-1879.

Finn, W. D. L., Wu, G. and Thavaraj, T. (1994). "Seismic response analysis of pile foundations," *Soil Dynamics and Earthquake Engineering VII,* Crete, May 1995, pp. 459-46.

Fleming, W. G. K., Wetman, A.J., Randolph, M.F. and Elson, W.K. (1984). *Piling Engineering*. Surrey University Press, Glasgow, UK.

Gazetas, G. (1983). "Analysis of machine foundation vibrations: State of the art," *Soil Dynamics and Earthquake Engineering,* Vol. 2, No. 1, pp. 2-42.

Gazetas, G. (1984). "Seismic response of end-bearing piles," *Soil Dynamics and Earthquake Engineering*, Vol. 3, 82-93.

Gazetas, G. and Dobry, R. (1984). "Horizontal response of piles in layered soils," *Journal of Geotechnical Engineering, ASCE*, Vol. 110, pp. 20-40.

Gazetas, G., Fan, K., Kaynia, A., and Kausel, E. (1991). "Dynamic interaction factors for floating pile groups," *Journal of Geotechnical Engineering, ASCE*, Vol. 117, pp. 1531-1548.

Gazetas, G., Fan, K., Tazoh, T., Shimizu, K., Kavvadas, M., and Makris, N. (1992). "Seismic response of soil-pile-foundation-structure systems: some recent developments," *Piles under Dynamic Loads, Geotech. Special Publ.* No. 34, ASCE, S. Prakash (ed.), pp. 56-93.

Gazetas, G. and Makris, N. (1991). "Dynamic pile-soil-pile interaction. Part I: Analysis of axial vibration," *Earthquake Engineering and Structural Dynamics,* Vol. 20, No. 2, pp. 115-132.

Gradshteyn, I. S. and Ryzhik, I. M. (1980). *Tables of integrals, series and products.* San Diego: Academic Press.

Heuze, F. E. and Swift, R. P. (1991). *Seismic refraction studies at the Painter Street Bridge site, Rio Dell, California.* Report UCRL-ID-108595, Lawrence Livermore National Laboratory.

IMSL Library, (1987). *Fortran library for mathematical applications.* Transform Subroutines FFTCF, FFTCB.

Jennings, D. N., Thurston, S. J. and Edmonds, F. D. (1984). "Static and dynamic lateral loading of two piles," *Proceedings of the 8th WCEE, San Francisco, CA*, Vol. 3, pp. 561-568.

Kagawa, T. and Kraft, L. M. (1982). "Lateral pile response during earthquakes," *Journal of the Geotechnical Engineering Division, ASCE*, Vol. 108, pp. 554-569.

Kaynia, A. M. (1980). *Dynamic stiffness of seismic response of pile groups.* Research Report R82-03, MIT.

Kaynia, A. M. and Kausel, E. (1982). *Dynamic stiffness and seismic response of sleeved piles.* Report R80-12, Department of Civil Engineering, M.I.T.

Kaynia, A. M. and Novak, M. (1992). "Response of pile foundations to Rayleigh waves and to obliquely incident body waves," *Earthquake Engineering and Structural Dynamics*, Vol. 21, pp. 303-318.

Kobori, T., Minai, R. and Baba, K. (1991). "Dynamic behavior of a pile under earthquake type loading." *2nd International Conference on Recent Advancements in Geotechnical, Earthquake Engineering and Soil Dynamics*, St. Louis, pp. 795-800.

Kramer, S. L. (1996). *Geotechnical Earthquake Engineering.* Upper Saddle River: Prentice-Hall.

Kramer, S. L., Satari, R. and Kilian, A. P. (1992). "Evaluation of in situ strength of a peat deposit from laterally loaded pile test results," *Transportation Research Record*, No. 1278, Transportation Research Board, Washington, D. C., pp. 103-109.

Kunnath, S., K., Reinhorn, A. M. and Park, Y. J. (1990). "Analytical modeling of inelastic seismic response of R/C structures," *Journal of Structural Engineering, Vol.* 116, pp. 996-1017.

Lighthill, M. J. (1989). *An introduction to Fourier analysis and generalized functions*, Cambridge University Press, Cambridge, UK.

Lysmer, J. and Richart, F. E. (1966). "Dynamic response of footing to vertical loading," *Journal of the Soil Mechanics and Foundation Engineering Division, ASCE,* Vol. 92, SM1, pp. 65-91.

Makris, N. (1994). "Soil-pile interaction during the passage of Rayleigh waves: An analytical solution," *Earthquake Engineering and Structural Dynamics*, Vol. 23, pp. 153-167.

Makris, N. (1995). "Time domain analysis of generalized viscoelastic models," *Soil Dynamics and Earthquake Engineering*, Vol. 14, pp. 375-386.

Makris, N. (1997a). "Dynamic stiffness, flexibility, impedance, mobility and the hidden delta function," *Journal of Engineering Mechanics* (in press).

Makris, N. (1997b). "The causal hysteretic element," *Journal of Engineering Mechanics* (in press).

Makris, N. and Badoni, D. (1995). "Seismic response of pile-groups during the passage of oblique-shear and Rayleigh waves." *Earthquake Engineering and Structural Dynamics*, Vol. 24, pp. 517-532.

Makris, N., Badoni, D., Delis, E. and Gazetas, G. (1994). "Prediction of observed bridge response with soil-pile-structure interaction," *Journal of Structural Engineering,* Vol. 120, No. 10., pp. 2922-3011.

Makris, N. and Gazetas, G. (1992). "Dynamic pile-soil-pile interaction II: lateral and seismic response,"*Earthquake Engineering and Structural Dynamics*, Vol. 20, pp. 145-162.

Makris, N., Cardosa, J., Badoni, D. and Delis, E. (1993). *Soil--pile-group--superstructure interaction in applications of seismic analysis of bridges*. Report No. NDCE-93-001, Dept. of Civil Engineering and Geological Sciences, University of Notre Dame.

Makris, N. and Gazetas, G. (1992). "Dynamic pile-soil-pile interaction II: lateral and seismic response," *Earthquake Engineering and Structural Dynamics*, Vol. 20, pp. 145-162.

Makris, N. and Gazetas, G. (1993). "Displacement phase differences in a harmonically oscillating pile," *Geotechnique*, Vol. 43, pp. 135-150.

Mamoon, S. M. and Banerjee, P. K. (1992). "Time domain analysis of dynamically loaded single piles," *Journal of Engineering Mechanics,* Vol. 118, No. 1, pp. 140-160.

Mamoon, S. M. and Banerjee, P. K. (1990). "Response of piles and pile groups to travelling SH waves," *Earthquake Engineering and Structural Dynamics*, Vol. 19, pp. 597-610.

Maroney, B., Romstad, K. and Chajes, M. (1990). "Interpretation of Rio Dell freeway response during six recorded earthquake events,"*Proceedings of the Fourth U.S. National Conference on Earthquake Engineering*, Vol. 1, pp. 1007-1016.

Marquardt, D. W. (1963). "An algorithm for least square estimation of nonlinear parameters," *Journal of the Society of Industrial and Applied Mathematics,* Vol. 11, pp. 431-441.

Miramontes, D., Merabet, O. and Reynouard, J. M. (1996). "Beam global model for the seismic analysis of RC frames," *Earthquake Engineering and Structural Dynamics,* Vol. 25, pp. 671-688.

Mizuno, H. (1987). "Pile damage during earthquakes in Japan," *Dynamic response of Pile Foundations (ed. T. Nogami), ASCE, pp.* 53-78.

Morse, P. M. & Ingard, K. U. (1968). *Theoretical Acoustics.* New York: McGraw-Hill.

Muster II, G. L.& O'Neill, M. W. (1986). "Dynamically loaded pile in overconsolidated clay," *Geotechnical Testing Journal*, GTJODJ Vol. 9, No. 4, pp. 189-197.

Nogami, T. (1983). "Dynamic group effect in axial responses of grouped piles," *Journal of the Geotechnical Engineering Division, ASCE*, Vol. 109, pp. 225-243.

Nogami, T., Otani, J., Konagai, K. and Chen, H.-L. (1992). "Nonlinear soil-pile interaction model for dynamic lateral motion," *Journal of Geotechnical Engineering,* Vol. 118, No. 1, pp. 89-106.

Nogami, T. and Konagai, K. (1986). "Time-domain axial response of dynamically loaded single piles", *Journal of Engineering Mechanics, ASCE*, Vol. 112, pp. 1241-1252.

Nogami, T. and Konagai, K. (1987). "Dynamic response of vertically loaded nonlinear pile foundations," *Journal of Geotechnical Engineering, ASCE*, Vol. 113, No. 2, pp. 147-161.

Novak, M. (1974). "Dynamic stiffness and damping of piles," *Canadian Geotechnical Journal,* Vol. 11, pp. 574-598.

O'Neill, M. W., Hawkins, R. A. and Mahar, L. J. (1982). "Load transfer mechanisms in piles and pile-groups," *Journal of the Geotechnical Engineering Division, ASCE*, Vol. 108, No. 12, pp. 1605-1623.

Papoulis, A. (1987). *The Fourier integral and its applications.* New York: McGraw-Hill.

Porcella, R. L., Etheredge, E. C., Mayley, R. P. and Acosta, A. V. (1994). *Accelerograms recorded at USGS National strong-motion network stations during the Ms=6.6 Northridge, California earthquake of January 17, 1994.* Open File Report 94-141, U.S. Geological Survey.

Poulos, H. G. (1968). "Analysis of the settlement of pile groups," *Geotechnique*, Vol. 18, pp. 449-471.

Priestley, M. J. N., Seible, F. and Calvi, G. M. (1996). *Seismic design and retrofit of bridges.* John Wiley & Sons, Inc.

Randolph, M. F. (1977). *A theoretical study of the performance of piles.* Doctoral thesis, Cambridge University, U. K.

Randolph, M. F. (1981). "Response of flexible piles to lateral loading," *Geotechnique*, Vol. 31, pp. 247-262.

Roesset, J. M. (1984). "Dynamic stiffness of pile groups," *Pile Foundations, ASCE*, New York.

Rohrs, C. E., Melsa, J. L. and Schultz, D. G. (1993). *Linear control systems.* New York: McGraw-Hill.

Ross, G. A., Seed, B. H. and Migliaccio, R. (1969). "Bridge foundations in the Alaska earthquake," *Journal of the Soil Mechanics and Foundation Engineering Division, ASCE,* 95.

Roufaiel, M. S. L. and Meyer, C. (1983). *Analysis of damaged concrete frame buildings.* Report No. NSF-CEE81-21359-1, Dept. of Civ. Engrg. Mech., Columbia University, New York, NY.

Roufaiel, M. S. L. and Meyer, C. (1987). "Analytical modeling of hysteretic behavior of R/C frames," *Journal of Structural Engineering,* Vol. 113, No. 3, pp. 429-444.

Sanchez-Salinero, I. (1983). *Dynamic stiffness of pile groups: approximate solutions.* Geotechnical Engineering Report GR83-5, University of Texas at Austin.

Scott, R. F. (1981). *Foundation Analysis.* London: Prentice Hall.

Sheta, M. and Novak, M. (1982). "Vertical vibrations of pile groups," *Journal of the Geotechnical Engineering Division, ASCE,*. Vol. 108, pp. 570-590.

Sweet, J. (1993). *A technique for nonlinear soil-structure interaction.* Report CAI-093-100, CalTrans.

Tajimi, H. (1977). "Seismic effects on piles, state-of-the-art report No. 2," *International Conference on Soil Mechanics and Foundation Engineering,* Proc. Specialty Session 10, pp. 15-27.

Takeda, T., Sozen, M. A. and Nielsen, N. N. (1970). "Reinforced concrete response to simulated earthquakes," *Journal of the Structural Engineering Division, ASCE,* Vol. 96, No. 12, pp. 2557-2573.

Tatsuoka, F., Iwasaki, T., Yoshida, S. and Fukushima, S. (1979). "Shear modulus and damping by drained tests on clean sand specimens reconstructed by various methods," *Soils and Foundations*, Vol. 19, pp. 39-54.

Tika, T. (1989). *The effect of fast shearing on the residual strength of soils.* Ph.D. thesis, Imperial College of Science, Technology and Medicine.

Ting, J. M. (1987). "Full-scale cyclic dynamic lateral pile responses," *Journal of Geotechnical Engineering, ASCE,* Vol. 117, pp. 30-45.

Trochanis, A. M., Bielak, J. and Christiano, P. (1991). "Simplified model for analysis of one or two piles," *Journal of Geotechnical Engineering, ASCE,* Vol. 117, pp. 448-466.

Veletsos, A. S. and Ventura, C. E. (1985). "Dynamic analysis of structures by the DFT method," *Journal of Structural Engineering,* Vol. 111, pp. 2625-2642.

Veletsos, A. S. and Verbic, B. (1974). "Basic response functions for elastic foundations," *Journal of the Engineering Mechanics Division, ASCE,* Vol. 100, EM2, pp. 189-202.

Waas, G. and Hartmann, H. G. (1984). "Seismic analysis of pile foundations including soil-pile-soil interaction," *8th World Conference on Soil Dynamics and Earthquake Engineering,* Vol. 5, pp. 55-62.

Wen, Y-K. (1975). "Approximate method for nonlinear random vibration," *Journal of the Engineering Mechanics Division., ASCE,* Vol. 101, EM4, pp. 389-401.

Wen, Y-K. (1976). "Method for random vibration of hysteretic systems," *Journal of the Engineering Mechanics Division, ASCE,* Vol. 102, EM2, pp. 249-263.

Wolf, J. P. (1988). *Soil-Structure interaction analysis in time-domain.* Englewood Cliffs: Prentice-Hall.

Wolf, J. P. and von Arx, G. A. (1978). "Horizontally travelling waves in a group of piles taking pile-soil-pile interaction into account," *Earthquake Engineering and Structural Dynamics,* Vol. 10, pp. 225-237

Wu, G. and Finn, W. D. L. (1994). "A new method for dynamic analysis of pile groups," *Soil Dynamics and Earthquake Engineering VII,* Crete, May 1995, pp. 467-474.

EERC REPORTS

EERC reports are available from the National Information Service for Earthquake Engineering (NISEE) and from the National Technical Information Service (NTIS). To order EERC Reports, please contact the Earthquake Engineering Research Center, 1301 S. 46th Street, Richmond, California 94804-4698, ph 510-231-9468.

UCB/EERC-97/07: Analysis of the Nonlinear Response of Structures Supported on Pile Foundations, by Badoni, D. and Makris, N., July 1997. $26

UCB/EERC-97/06: Executive Summary on: Phase 3: Evaluation and Retrofitting of Multilevel and Multiple-Column Structures -- An Analytical, Experimental, and Conceptual Study of Retrofitting Needs and Methods, by Mahin, S.A., Fenves, G.L., Filippou, F.C., Moehle, J.P., Thewalt, C.R., May, 1997. $20

UCB/EERC-97/05: The EERC-CUREe Symposium to Honor Vitelmo V. Bertero, February 1997. $26

UCB/EERC-97/04: Design and Evaluation of Reinforced Concrete Bridges for Seismic Resistance, by Aschheim, M., Moehle, J.P. and Mahin, S.A., March 1997. $26

UCB/EERC-97/03: U.S.-Japan Workshop on Cooperative Research for Mitigation of Urban Earthquake Disasters: Learning from Kobe and Northridge -- Recommendations and Resolutions, by Mahin, S., Okada, T., Shinozuka, M. and Toki, K., February 1997. $15

UCB/EERC-97/02: Multiple Support Response Spectrum Analysis of Bridges Including the Site-Response Effect & MSRS Code, by Der Kiureghian, A., Keshishian, P. and Hakobian, A., February 1997. $20

UCB/EERC-97/01: Analysis of Soil-Structure Interaction Effects on Building Response from Earthquake Strong Motion Recordings at 58 Sites, by Stewart, J.P. and Stewart, A.F., February 1997. $57

UCB/EERC-96/05: Application of Dog Bones for Improvement of Seismic Behavior of Steel Connections, by Popov, E.P., Blondet, M. and Stepanov, L., June 1996. $13

UCB/EERC-96/04: Experimental and Analytical Studies of Base Isolation Applications for Low-Cost Housing, by Taniwangsa, W. and Kelly, J.M., July 1996. $20

UCB/EERC-96/03: Experimental and Analytical Evaluation of a Retrofit Double-Deck Viaduct Structure: Part I of II, by Zayati, F., Mahin, S. A. and Moehle, J. P., June 1996. $33

UCB/EERC-96/02: Field Testing of Bridge Design and Retrofit Concepts. Part 2 of 2: Experimental and Analytical Studies of the Mt. Diablo Blvd. Bridge, by Gilani, A.S., Chavez, J.W. and Fenves, G.L., June 1996. $20

UCB/EERC-96/01: Earthquake Engineering Research at Berkeley -- 1996: Papers Presented at the 11th World Conference on Earthquake Engineering, by EERC, May 1996. $26

UCB/EERC-95/14: Field Testing of Bridge Design and Retrofit Concepts. Part 1 of 2: Field Testing and Dynamic Analysis of a Four-Span Seismically Isolated Viaduct in Walnut Creek, California, by Gilani, A.S., Mahin, S.A., Fenves, G.L., Aiken, I.D. and Chavez, J.W., December 1995. $26

UCB/EERC-95/13: Experimental and Analytical Studies of Steel Connections and Energy Dissipators, by Yang, T.-S. and Popov, E.P., December 1995. $26

UCB/EERC-95/12: Natural Rubber Isolation Systems for Earthquake Protection of Low-Cost Buildings, by Taniwangsa, W., Clark, P. and Kelly, J.M., June 1996. $20

UCB/EERC-95/11: Studies in Steel Moment Resisting Beam-to-Column Connections for Seismic-Resistant Design, by Blackman, B. and Popov, E.P., October 1995, PB96-143243. $20

UCB/EERC-95/10: Seismological and Engineering Aspects of the 1995 Hyogoken-Nanbu (Kobe) Earthquake, by EERC, November 1995. $26

UCB/EERC-95/09: Seismic Behavior and Retrofit of Older Reinforced Concrete Bridge T-Joints, by Lowes,

L.N. and Moehle, J.P., September 1995, PB96-159850. $20

UCB/EERC-95/08: Behavior of Pre-Northridge Moment Resisting Steel Connections, by Yang, T.-S. and Popov, E.P., August 1995, PB96-143177. $15

UCB/EERC-95/07: Earthquake Analysis and Response of Concrete Arch Dams, by Tan, H. and Chopra, A.K., August 1995, PB96-143185. $20

UCB/EERC-95/06: Seismic Rehabilitation of Framed Buildings Infilled with Unreinforced Masonry Walls Using Post-Tensioned Steel Braces, by Teran-Gilmore, A., Bertero, V.V. and Youssef, N., June 1995, PB96-143136. $26

UCB/EERC-95/05: Final Report on the International Workshop on the Use of Rubber-Based Bearings for the Earthquake Protection of Buildings, by Kelly, J.M., May 1995. $20

UCB/EERC-95/04: Earthquake Hazard Reduction in Historical Buildings Using Seismic Isolation, by Garevski, M., June 1995. $15

UCB/EERC-95/03: Upgrading Bridge Outrigger Knee Joint Systems, by Stojadinovic, B. and Thewalt, C.R., June 1995, PB95-269338. $20

UCB/EERC-95/02: The Attenuation of Strong Ground Motion Displacements, by Gregor, N.J., June 1995, PB95-269346. $26

UCB/EERC-95/01: Geotechnical Reconnaissance of the Effects of the January 17, 1995, Hyogoken-Nanbu Earthquake, Japan, August 1995, PB96-143300. $26

UCB/EERC-94/12: Response of the Northwest Connector in the Landers and Big Bear Earthquakes, by Fenves, G.L. and Desroches, R., December 1994. $20

UCB/EERC-94/11: Earthquake Analysis and Response of Two-Level Viaducts, by Singh, S.P. and Fenves, G.L., October 1994, PB96-133756 (A09). $20

UCB/EERC-94/10: Manual for Menshin Design of Highway Bridges: Ministry of Construction, Japan, by Sugita, H. and Mahin, S., August 1994, PB95-192100(A08). $20

UCB/EERC-94/09: Performance of Steel Building Structures During the Northridge Earthquake, by Bertero, V.V., Anderson, J.C. and Krawinkler, H., August 1994, PB95-112025(A10). $26

UCB/EERC-94/08: Preliminary Report on the Principal Geotechnical Aspects of the January 17, 1994 Northridge Earthquake, by Stewart, J.P., Bray, J.D., Seed, R.B. and Sitar, N., June 1994, PB94203635(A12). $26

UCB/EERC-94/07: Accidental and Natural Torsion in Earthquake Response and Design of Buildings, by De la Llera, J.C. and Chopra, A.K., June 1994, PB94-203627(A14). $33

UCB/EERC-94/05: Seismic Response of Steep Natural Slopes, by Sitar, N. and Ashford, S.A., May 1994, PB94-203643(A10). $26

UCB/EERC-94/04: Insitu Test Results from Four Loma Prieta Earthquake Liquefaction Sites: SPT, CPT, DMT and Shear Wave Velocity, by Mitchell, J.K., Lodge, A.L., Coutinho, R.Q., Kayen, R.E., Seed, R.B., Nishio, S. and Stokoe II, K.H., April 1994, PB94-190089(A09). $20

UCB/EERC-94/03: The Influence of Plate Flexibility on the Buckling Load of Elastomeric Isolators, by Kelly, J.M., March 1994, PB95-192134(A04). $15

UCB/EERC-94/02: Energy Dissipation with Slotted Bolted Connections, by Grigorian, C.E. and Popov, E.P., February 1994, PB94-164605. $26

UCB/EERC-94/01: Preliminary Report on the Seismological and Engineering Aspects of the January 17, 1994 Northridge Earthquake, by EERC, January 1994, (PB94 157 666/AS)A05. $15

UCB/EERC-93/13: On the Analysis of Structures with Energy Dissipating Restraints, by Inaudi, J.A., Nims, D.K. and Kelly, J.M., December 1993, PB94-203619(A07). $20

UCB/EERC-93/12: Synthesized Strong Ground Motions for the Seismic Condition Assessment of the Eastern Portion of the San Francisco Bay Bridge, by Bolt, B.A. and Gregor, N.J., December 1993, PB94-165842(A10). $26

UCB/EERC-93/11: Nonlinear Homogeneous Dynamical Systems, by Inaudi, J.A. and Kelly, J.M., October 1995. $20

UCB/EERC-93/09: A Methodology for Design of Viscoelastic Dampers in Earthquake-Resistant Structures,

by Abbas, H. and Kelly, J.M., November 1993, PB94-190071(A10). $26

UCB/EERC-93/08: Model for Anchored Reinforcing Bars under Seismic Excitations, by Monti, G., Spacone, E. and Filippou, F.C., December 1993, PB95-192183(A05). $15

UCB/EERC-93/07: Earthquake Analysis and Response of Concrete Gravity Dams Including Base Sliding, by Chavez, J.W. and Fenves, G.L., December 1993, (PB94 157 658/AS)A10. $26

UCB/EERC-93/06: On the Analysis of Structures with Viscoelastic Dampers, by Inaudi, J.A., Zambrano, A. and Kelly, J.M., August 1993, PB94-165867(A06). $20

UCB/EERC-93/05: Multiple-Support Response Spectrum Analysis of the Golden Gate Bridge, by Nakamura, Y., Der Kiureghian, A. and Liu, D., May 1993, (PB93 221 752)A05. $15

UCB/EERC-93/04: Seismic Performance of a 30-Story Building Located on Soft Soil and Designed According to UBC 1991, by Teran-Gilmore, A. and Bertero, V.V., 1993, (PB93 221 703)A17. $33

UCB/EERC-93/03: An Experimental Study of Flat-Plate Structures under Vertical and Lateral Loads, by Hwang, S.-H. and Moehle, J.P., February 1993, (PB94 157 690/AS)A13. $26

UCB/EERC-93/02: Evaluation of an Active Variable-Damping-Structure, by Polak, E., Meeker, G., Yamada, K. and Kurata, N., 1993, (PB93 221 711)A05. $15

UCB/EERC-92/18: Dynamic Analysis of Nonlinear Structures using State-Space Formulation and Partitioned Integration Schemes, by Inaudi, J.A. and De la Llera, J.C., December 1992, (PB94 117 702/AS/A05. $15

UCB/EERC-92/17: Performance of Tall Buildings During the 1985 Mexico Earthquakes, by Teran-Gilmore, A. and Bertero, V.V., December 1992, (PB93 221 737)A11. $26

UCB/EERC-92/16: Tall Reinforced Concrete Buildings: Conceptual Earthquake-Resistant Design Methodology, by Bertero, R.D. and Bertero, V.V., December 1992, (PB93 221 695)A12. $26

UCB/EERC-92/15: A Friction Mass Damper for Vibration Control, by Inaudi, J.A. and Kelly, J.M., October 1992, (PB93 221 745)A04. $15

UCB/EERC-92/14: Earthquake Risk and Insurance, by Brillinger, D.R., October 1992, (PB93 223 352)A03.

UCB/EERC-92/13: Earthquake Engineering Research at Berkeley - 1992, by EERC, October 1992, PB93-223709(A10). $13

UCB/EERC-92/12: Application of a Mass Damping System to Bridge Structures, by Hasegawa, K. and Kelly, J.M., August 1992, (PB93 221 786)A06. $26

UCB/EERC-92/11: Mechanical Characteristics of Neoprene Isolation Bearings, by Kelly, J.M. and Quiroz, E., August 1992, (PB93 221 729)A07. $20

UCB/EERC-92/10: Slotted Bolted Connection Energy Dissipators, by Grigorian, C.E., Yang, T.-S. and Popov, E.P., July 1992, (PB92 120 285)A03. $20

UCB/EERC-92/09: Evaluation of Code Accidental-Torsion Provisions Using Earthquake Records from Three Nominally Symmetric-Plan Buildings, by De la Llera, J.C. and Chopra, A.K., September 1992, (PB94 117 611)A08. $13

UCB/EERC-92/08: Nonlinear Static and Dynamic Analysis of Reinforced Concrete Subassemblages, by Filippou, F.C., D'Ambrisi, A. and Issa, A., August, 1992. $20

UCB/EERC-92/07: A Beam Element for Seismic Damage Analysis, by Spacone, E., Ciampi, V. and Filippou, F.C., August 1992, (PB95-192126)A06. $20

UCB/EERC-92/06: Seismic Behavior and Design of Semi-Rigid Steel Frames, by Nader, M.N. and Astaneh-Asl, A., May 1992, PB93-221760(A17). $33

UCB/EERC-92/05: Parameter Study of Joint Opening Effects on Earthquake Response of Arch Dams, by Fenves, G.L., Mojtahedi, S. and Reimer, R.B., April 1992, (PB93 120 301)A04. $15

UCB/EERC-92/04: Shear Strength and Deformability of RC Bridge Columns Subjected to Inelastic Cyclic Displacements, by Aschheim, M. and Moehle, J.P., March 1992, (PB93 120 327)A06. $20

UCB/EERC-92/03: Models for Nonlinear Earthquake Analysis of Brick Masonry Buildings, by Mengi, Y., McNiven, H.D. and Tanrikulu, A.K., March 1992, (PB93 120 293)A08. $20

UCB/EERC-92/02: Response of the Dumbarton Bridge in the Loma Prieta Earthquake, by Fenves, G.L., Filippou, F.C. and Sze, D.T., January 1992, (PB93 120 319)A09. $20

UCB/EERC-92/01: Studies of a 49-Story Instrumented Steel Structure Shaken During the Loma Prieta Earthquake, by Chen, C.-C., Bonowitz, D. and Astaneh-Asl, A., February 1992, (PB93 221 778)A08. $20

UCB/EERC-91/18: Investigation of the Seismic Response of a Lightly-Damped Torsionally-Coupled Building, by Boroschek, R. and Mahin, S.A., December 1991, (PB93 120 335)A13. $26

UCB/EERC-91/17: A Fiber Beam-Column Element for Seismic Response Analysis of Reinforced Concrete Structures, by Taucer, F., Spacone, E. and Filippou, F.C., December 1991, (PB94 117 629AS)A07. $20

UCB/EERC-91/16: Evaluation of the Seismic Performance of a Thirty-Story RC Building, by Anderson, J.C., Miranda, E., Bertero, V.V. and The Kajima Project Research Team, July 1991, (PB93 114 841)A12. $26

UCB/EERC-91/15: Design Guidelines for Ductility and Drift Limits: Review of State-of-the-Practice and State-of-the-Art in Ductility and Drift-Based Earthquake-Resistant Design of Buildings, by Bertero, V.V., Anderson, J.C., Krawinkler, H., Miranda, E. and The CUREe and The Kajima Research Teams, July 1991, (PB93 120 269)A08. $20

UCB/EERC-91/14: Cyclic Response of RC Beam-Column Knee Joints: Test and Retrofit, by Mazzoni, S., Moehle, J.P. and Thewalt, C.R., October 1991, (PB93 120 277)A03. $13

UCB/EERC-91/13: Shaking Table - Structure Interaction, by Rinawi, A.M. and Clough, R.W., October 1991, (PB93 114 917)A13. $26

UCB/EERC-91/12: Performance of Improved Ground During the Loma Prieta Earthquake, by Mitchell, J.K. and Wentz, Jr., F.J., October 1991, (PB93 114 791)A06. $20

UCB/EERC-91/11: Seismic Performance of an Instrumented Six-Story Steel Building, by Anderson, J.C. and Bertero, V.V., November 1991, (PB93 114 809)A07. $20

UCB/EERC-91/10: Evaluation of Seismic Performance of a Ten-Story RC Building During the Whittier Narrows Earthquake, by Miranda, E. and Bertero, V.V., October 1991, (PB93 114 783)A06. $20

UCB/EERC-91/09: A Preliminary Study on Energy Dissipating Cladding-to-Frame Connections, by Cohen, J.M. and Powell, G.H., September 1991, (PB93 114 510)A05. $15

UCB/EERC-91/08: A Response Spectrum Method for Multiple-Support Seismic Excitations, by Der Kiureghian, A. and Neuenhofer, A., August 1991, (PB93 114 536)A04. $15

UCB/EERC-91/07: Estimation of Seismic Source Processes Using Strong Motion Array Data, by Chiou, S.-J., July 1991, (PB93 114 551/AS)A08. $20

UCB/EERC-91/06: Computation of Spatially Varying Ground Motion and Foundation-Rock Impedance Matrices for Seismic Analysis of Arch Dams, by Zhang, L. and Chopra, A.K., May 1991, (PB93 114 825)A07. $20

UCB/EERC-91/05: Base Sliding Response of Concrete Gravity Dams to Earthquakes, by Chopra, A.K. and Zhang, L., May 1991, (PB93 114 544/AS)A05. $15

UCB/EERC-91/04: Dynamic and Failure Characteristics of Bridgestone Isolation Bearings, by Kelly, J.M., April 1991, (PB93 114 528)A05. $15

UCB/EERC-91/03: A Long-Period Isolation System Using Low-Modulus High-Damping Isolators for Nuclear Facilities at Soft-Soil Sites, by Kelly, J.M., March 1991, (PB93 114 577/AS)A10. $26

UCB/EERC-91/02: Displacement Design Approach for Reinforced Concrete Structures Subjected to Earthquakes, by Qi, X. and Moehle, J.P., January 1991, (PB93 114 569/AS)A09. $20

UCB/EERC-90/21: Observations and Implications of Tests on the Cypress Street Viaduct Test Structure, by Bollo, M., Mahin, S.A., Moehle, J.P., Stephen, R.M. and Qi, X., December 1990, (PB93 114 775)A13. $26

UCB/EERC-90/20: Seismic Response Evaluation of an Instrumented Six Story Steel Building, by Shen, J.-H. and Astaneh-Asl, A., December 1990, (PB91 229 294/AS)A04. $15

UCB/EERC-90/19: Cyclic Behavior of Steel Top-and-Bottom Plate Moment Connections, by Harriott, J.D. and Astaneh-Asl, A., August 1990, (PB91 229 260/AS)A05. $15

UCB/EERC-90/18: Material Characterization of Elastomers used in Earthquake Base Isolation, by Papoulia, K.D. and Kelly, J.M., 1990, PB94-190063(A08). $15

UCB/EERC-90/17: Behavior of Peak Values and Spectral Ordinates of Near-Source Strong Ground-Motion over a Dense Array, by Niazi, M., June 1990, (PB93 114 833)A07. $20

UCB/EERC-90/14: Inelastic Seismic Response of One-Story, Asymmetric-Plan Systems, by Goel, R.K. and Chopra, A.K., October 1990, (PB93 114 767)A11. $26

UCB/EERC-90/13: The Effects of Tectonic Movements on Stresses and Deformations in Earth Embankments, by Bray, J. D., Seed, R. B. and Seed, H. B., September 1989, PB92-192996(A18). $39

UCB/EERC-90/12: Effects of Torsion on the Linear and Nonlinear Seismic Response of Structures, by Sedarat, H. and Bertero, V.V., September 1989, (PB92 193 002/AS)A15. $33

UCB/EERC-90/11: Seismic Hazard Analysis: Improved Models, Uncertainties and Sensitivities, by Araya, R. and Der Kiureghian, A., March 1988, PB92-193010(A08). $20

UCB/EERC-90/10: Experimental Testing of the Resilient-Friction Base Isolation System, by Clark, P.W. and Kelly, J.M., July 1990, (PB92 143 072)A08. $20

UCB/EERC-90/09: Influence of the Earthquake Ground Motion Process and Structural Properties on Response Characteristics of Simple Structures, by Conte, J.P., Pister, K.S. and Mahin, S.A., July 1990, (PB92 143 064)A15. $33

UCB/EERC-90/08: Soil Conditions and Earthquake Hazard Mitigation in the Marina District of San Francisco, by Mitchell, J.K., Masood, T., Kayen, R.E. and Seed, R.B., May 1990, (PB 193 267/AS)A04. $15

UCB/EERC-90/07: A Unified Earthquake-Resistant Design Method for Steel Frames Using ARMA Models, by Takewaki, I., Conte, J.P., Mahin, S.A. and Pister, K.S., June 1990, PB92-192947(A06). $15

UCB/EERC-90/05: Preliminary Report on the Principal Geotechnical Aspects of the October 17, 1989 Loma Prieta Earthquake, by Seed, R.B., Dickenson, S.E., Riemer, M.F., Bray, J.D., Sitar, N., Mitchell, J.K., Idriss, I.M., Kayen, R.E., Kropp, A., Harder, L.F., Jr. and Power, M.S., April 1990, (PB 192 970)A08. $20

UCB/EERC-90/03: Earthquake Simulator Testing and Analytical Studies of Two Energy-Absorbing Systems for Multistory Structures, by Aiken, I.D. and Kelly, J.M., October 1990, (PB92 192 988)A13. $26

UCB/EERC-90/02: Javid's Paradox: The Influence of Preform on the Modes of Vibrating Beams, by Kelly, J.M., Sackman, J.L. and Javid, A., May 1990, (PB91 217 943/AS)A03. $13

UCB/EERC-89/16: Collapse of the Cypress Street Viaduct as a Result of the Loma Prieta Earthquake, by Nims, D.K., Miranda, E., Aiken, I.D., Whittaker, A.S. and Bertero, V.V., November 1989, (PB91 217 935/AS)A05. $15

UCB/EERC-89/15: Experimental Studies of a Single Story Steel Structure Tested with Fixed, Semi-Rigid and Flexible Connections, by Nader, M.N. and Astaneh-Asl, A., August 1989, (PB91 229 211/AS)A10. $26

UCB/EERC-89/14: Preliminary Report on the Seismological and Engineering Aspects of the October 17, 1989 Santa Cruz (Loma Prieta) Earthquake, by EERC, October 1989, (PB92 139 682/AS)A04. $15

UCB/EERC-89/13: Mechanics of Low Shape Factor Elastomeric Seismic Isolation Bearings, by Aiken, I.D., Kelly, J.M. and Tajirian, F.F., November 1989, (PB92 139 732/AS)A09. $20

UCB/EERC-89/12: ADAP-88: A Computer Program for Nonlinear Earthquake Analysis of Concrete Arch Dams, by Fenves, G.L., Mojtahedi, S. and Reimer, R.B., September 1989, (PB92 139 674/AS)A07. $20

UCB/EERC-89/11: Static Tilt Behavior of Unanchored Cylindrical Tanks, by Lau, D.T. and Clough, R.W., September 1989, (PB92 143 049)A10. $26

UCB/EERC-89/10: Measurement and Elimination of Membrane Compliance Effects in Undrained Triaxial Testing, by Nicholson, P.G., Seed, R.B. and Anwar, H., September 1989, (PB92 139 641/AS)A13. $26

UCB/EERC-89/09: Feasibility and Performance Studies on Improving the Earthquake Resistance of New and Existing Buildings Using the Friction Pendulum System, by Zayas, V., Low, S., Mahin, S.A. and Bozzo, L., July 1989, (PB92 143 064)A14. $33

UCB/EERC-89/08: Seismic Performance of Steel Moment Frames Plastically Designed by Least Squares Stress Fields, by Ohi, K. and Mahin, S.A., August 1989, (PB91 212 597)A05. $15

UCB/EERC-89/07: EADAP - Enhanced Arch Dam Analysis Program: Users's Manual, by Ghanaat, Y. and Clough, R.W., August 1989, (PB91 212 522)A06. $20

UCB/EERC-89/06: Effects of Spatial Variation of Ground Motions on Large Multiply-Supported Structures, by Hao, H., July 1989, (PB91 229 161/AS)A08. $20

UCB/EERC-89/05: The 1985 Chile Earthquake: An Evaluation of Structural Requirements for Bearing Wall Buildings, by Wallace, J.W. and Moehle, J.P., July 1989, (PB91 218 008/AS)A13. $26

UCB/EERC-89/04: Earthquake Analysis and Response of Intake-Outlet Towers, by Goyal, A. and Chopra, A.K., July 1989, (PB91 229 286/AS)A19. $39

UCB/EERC-89/03: Implications of Site Effects in the Mexico City Earthquake of Sept. 19, 1985 for Earthquake-Resistant Design Criteria in the San Francisco Bay Area of California, by Seed, H.B. and Sun, J.I., March 1989, (PB91 229 369/AS)A07. $20

UCB/EERC-89/02: Earthquake Simulator Testing of Steel Plate Added Damping and Stiffness Elements, by Whittaker, A., Bertero, V.V., Alonso, J. and Thompson, C., January 1989, (PB91 229 252/AS)A10. $26

UCB/EERC-89/01: Behavior of Long Links in Eccentrically Braced Frames, by Engelhardt, M.D. and Popov, E.P., January 1989, (PB92 143 056)A18. $39

UCB/EERC-88/20: Base Isolation in Japan, 1988, by Kelly, J.M., December 1988, (PB91 212 449)A05. $15

UCB/EERC-88/19: Steel Beam-Column Joints in Seismic Moment Resisting Frames, by Tsai, K.-C. and Popov, E.P., November 1988, (PB91 217 984/AS)A20. $39

UCB/EERC-88/18: Use of Energy as a Design Criterion in Earthquake-Resistant Design, by Uang, C.-M. and Bertero, V.V., November 1988, (PB91 210 906/AS)A04. $15

UCB/EERC-88/17: Earthquake Engineering Research at Berkeley - 1988, by EERC, November 1988, (PB91 210 864)A10. $26

UCB/EERC-88/16: Reinforced Concrete Flat Plates Under Lateral Load: An Experimental Study Including Biaxial Effects, by Pan, A. and Moehle, J.P., October 1988, (PB91 210 856)A13. $26

UCB/EERC-88/15: Dynamic Moduli and Damping Ratios for Cohesive Soils, by Sun, J.I., Golesorkhi, R. and Seed, H.B., August 1988, (PB91 210 922)A04. $15

UCB/EERC-88/14: An Experimental Study of the Behavior of Dual Steel Systems, by Whittaker, A.S., Uang, C.-M. and Bertero, V.V., September 1988, (PB91 212 712)A16. $33

UCB/EERC-88/13: Implications of Recorded Earthquake Ground Motions on Seismic Design of Building Structures, by Uang, C.-M. and Bertero, V.V., November 1988, (PB91 212 548)A06. $20

UCB/EERC-88/12: Nonlinear Analysis of Reinforced Concrete Frames Under Cyclic Load Reversals, by Filippou, F.C. and Issa, A., September 1988, (PB91 212 589)A07. $20

UCB/EERC-88/11: Liquefaction Potential of Sand Deposits Under Low Levels of Excitation, by Carter, D.P. and Seed, H.B., August 1988, (PB91 210 880)A15. $33

UCB/EERC-88/10: The Landslide at the Port of Nice on October 16, 1979, by Seed, H.B., Seed, R.B., Schlosser, F., Blondeau, F. and Juran, I., June 1988, (PB91 210 914)A05. $15

UCB/EERC-88/09: Alternatives to Standard Mode Superposition for Analysis of Non-Classically Damped Systems, by Kusainov, A.A. and Clough, R.W., June 1988, (PB91 217 992/AS)A04. $15

UCB/EERC-88/08: Analysis of Near-Source Waves: Separation of Wave Types Using Strong Motion Array Recordings, by Darragh, R.B., June 1988, (PB91 212 621)A08. $20

UCB/EERC-88/07: Theoretical and Experimental Studies of Cylindrical Water Tanks in Base-Isolated Structures, by Chalhoub, M.S. and Kelly, J.M., April 1988, (PB91 217 976/AS)A05. $15

UCB/EERC-88/06: DRAIN-2DX User Guide, by Allahabadi, R. and Powell, G.H., March 1988, (PB91 212 530)A12. $26

UCB/EERC-88/05: Experimental Evaluation of Seismic Isolation of a Nine-Story Braced Steel Frame Subject to Uplift, by Griffith, M.C., Kelly, J.M. and Aiken, I.D., May 1988, (PB91 217 968/AS)A07. $20

UCB/EERC-88/04: Re-evaluation of the Slide in the Lower San Fernando Dam in the Earthquake of Feb. 9, 1971, by Seed, H.B., Seed, R.B., Harder, L.F. and Jong, H.-L., April 1988, (PB91 212 456/AS)A07. $20

UCB/EERC-88/03: Cyclic Behavior of Steel Double Angle Connections, by Astaneh-Asl, A. and Nader, M.N., January 1988, (PB91 210 872)A05. $15

UCB/EERC-88/02: Experimental Evaluation of Seismic Isolation of Medium-Rise Structures Subject to Uplift, by Griffith, M.C., Kelly, J.M., Coveney, V.A. and Koh, C.G., January 1988, (PB91 217 950/AS)A09. $20

UCB/EERC-88/01: Seismic Behavior of Concentrically Braced Steel Frames, by Khatib, I., Mahin, S.A. and Pister, K.S., January 1988, (PB91 210 898/AS)A11. $26